Springer Theses
Recognizing Outstanding Ph.D. Research

Kirti Prakash

Chromatin Architecture

Advances from High-Resolution Single Molecule DNA Imaging

Springer

Springer Theses

Recognizing Outstanding Ph.D. Research

Aims and Scope

The series "Springer Theses" brings together a selection of the very best Ph.D. theses from around the world and across the physical sciences. Nominated and endorsed by two recognized specialists, each published volume has been selected for its scientific excellence and the high impact of its contents for the pertinent field of research. For greater accessibility to non-specialists, the published versions include an extended introduction, as well as a foreword by the student's supervisor explaining the special relevance of the work for the field. As a whole, the series will provide a valuable resource both for newcomers to the research fields described, and for other scientists seeking detailed background information on special questions. Finally, it provides an accredited documentation of the valuable contributions made by today's younger generation of scientists.

Theses are accepted into the series by invited nomination only and must fulfill all of the following criteria

- They must be written in good English.
- The topic should fall within the confines of Chemistry, Physics, Earth Sciences, Engineering and related interdisciplinary fields such as Materials, Nanoscience, Chemical Engineering, Complex Systems and Biophysics.
- The work reported in the thesis must represent a significant scientific advance.
- If the thesis includes previously published material, permission to reproduce this must be gained from the respective copyright holder.
- They must have been examined and passed during the 12 months prior to nomination.
- Each thesis should include a foreword by the supervisor outlining the significance of its content.
- The theses should have a clearly defined structure including an introduction accessible to scientists not expert in that particular field.

More information about this series at http://www.springer.com/series/8790

Kirti Prakash

Chromatin Architecture

Advances from High-Resolution Single Molecule DNA Imaging

Doctoral Thesis accepted by
Institute of Molecular Biology, Mainz and Heidelberg University, Germany

Springer

Author
Dr. Kirti Prakash
Heidelberg University
Heidelberg
Germany

and

Institute of Molecular Biology (IMB)
Mainz
Germany

Supervisor
Prof. Christoph Cremer
Heidelberg University
Heidelberg
Germany

and

Institute of Molecular Biology (IMB)
Mainz
Germany

ISSN 2190-5053 ISSN 2190-5061 (electronic)
Springer Theses
ISBN 978-3-319-52182-4 ISBN 978-3-319-52183-1 (eBook)
DOI 10.1007/978-3-319-52183-1

Library of Congress Control Number: 2017930653

Printed on acid-free paper

This Springer imprint is published by Springer Nature
The registered company is Springer International Publishing AG
The registered company address is: Gewerbestrasse 11, 6330 Cham, Switzerland

Archimedes will be remembered when Aeschylus is forgotten, because languages die but ideas do not. 'Immortality' may be a silly word, but probably an architect has the best chance of whatever it may mean.

Modified from "A Mathematician's Apology" by G.H. Hardy

Supervisor's Foreword

The discovery of the DNA double helix was probably one of the greatest findings of the last century and advanced many fields of the sciences. A large part of the progress in the field of molecular biology since the time of this discovery has been directed towards a better understanding of DNA structure and function. Advances comprise broad topics such as gene expression and regulation, genome sequencing and methods to study chromatin architecture. In this pictorial thesis, the author describes a new methodology to study the spatial organisation of DNA in the cell nucleus at nanometre resolution with light microscopy, which dramatically improves the overall description of chromatin.

The author first shows how a UV-induced photoconverted form of conventional DNA dyes such as Hoechst and DAPI can be used for single molecule localisation microscopy (SMLM). Using this tool, several new patterns of chromatin in interphase cells or meiosis were found that were never reported previously. The findings brought new evidence to understand the relation between structure and function of chromatin and constitute a very promising set of results for the future of chromatin research.

The work is systematically organised in four chapters. The first one opens the thesis with an interesting overview of the history of chromatin. The next chapter introduces minutes of super-resolution microscopy, with a particular emphasis on the use of photoconversion to image DNA. The third chapter shows an application of the new technique to the study of interphase chromosome organisation, with a detailed overview of the different orders of chromatin complexity that folds DNA from individual molecules to chromosome territories. The final chapter closes the thesis nicely with data on the organisation of meiotic chromatin. By using 'blinking' based super-resolving localisation microscopy, the author shows that specific epigenetically defined stretches of the DNA in the pachytene stage of meiosis are organised into small periodic clusters. Each of these chapters starts with an overview of the field and concludes with a summary. Overall, there are more than 100 figures in this book, and one can learn a lot just glancing over the figures.

In Chap. 1, the author presents a historical overview of chromatin research. This is a very condensed text covering a tutorial description of relevant developments in the chromatin biology field, from the initial work of Walther Flemming to the latest developments in the genomic field. This chapter shows how major works in the fields of microscopy, biochemistry and molecular biology have helped to understand better nuclear DNA organisation little by little and how the last two decades have shown levels of details in this organisation that was widely unexpected. It is interesting to see how the chromatin field has evolved over the years and how new techniques are reconfirming old findings and adding novel information. This chapter also contains personal information about various scientists who contributed to the field of chromatin biology. This chapter is a pleasant read for anyone seeking a quick introduction to the history of the chromatin field.

In Chap. 2, the author describes the set-up and use of a 'blinking'-based single molecule imaging system to study chromatin architecture on the nanoscale with conventional DNA dyes. The phenomenon of photoconversion of such dyes required for this approach is discussed. Basics of single molecule localisation microscopy (SMLM) and various elements involved in the processing and analysis of single molecule data are discussed. The author further outlines various artefacts that one might encounter with this technique. This chapter is a useful read for anyone who wants to have an introduction into this type of super-resolution microscopy of chromatin.

In Chap. 3, the author discusses the spatial and temporal aspects of chromatin organisation from three viewpoints: the most basic level of organisation, which are DNA molecules packed in nucleosomes; functional structures of an intermediate level of organisation, such as chromatin domains; and highest order features such as chromosomes or territories. In particular, recent data from SMLM have shown new details of chromatin nanostructure never imaged in such detail before using light microscopy. One major novel finding presented here is the ring- and rodlike shape of chromosomes that are put under environmental stress typical for ischaemia, characterised by oxygen/nutrition depletion.

In Chap. 4, the author shows novel findings regarding the epigenetic landscape of meiotic chromosomes. The author combined SMLM with direct staining of DNA and immunostaining of post-translational histone modifications to improve the nanoscale description of meiotic chromosomes. Overall, the DNA shows periodic clusters along the axis of the pachytene chromosome. Dissection of chromatin into different compartments using various histone modifications revealed more specific information. The SMLM imaging of transcriptionally active chromatin suggested radial hairlike loop patterns emerging from the axis of the synaptonemal complex (SC). Staining of other selective histone modifications indicated large clusters of transcriptionally inactive chromatin and a prominent cluster of centromeric histone mark at one end of the SC. These findings hint at a helicoidal structure of the mammalian chromosomes with clusters of epigenetically regulated chromatin. Furthermore, the author proposes a fascinating (although so far speculative) hypothesis for the pairing of homologous chromosomes based on the coupling of snakes. This chapter brings forward many interesting ideas for the meiosis field

which should be testable (validated or falsified) by currently available experimental techniques.

In summary, I believe that this work presents several significant innovations in an elegant way and will be an excellent introduction for people (especially students) into the field of super-resolution microscopy of nuclear organisation.

Heidelberg, Germany
August 2016

Prof. Christoph Cremer

Preface

All truth passes through three stages.

First, it is ridiculed.

Second, it is violently opposed.

Third, it is accepted as being self-evident.

Arthur Schopenhauer

The organisation of chromatin is non-random and shows a broad diversity across cell types, developmental stages and cell cycle stages. During G_0 and G_1 phases of interphase, chromatin displays a bivalent status. The condensed chromatin (heterochromatin) at the nuclear periphery is mostly associated with low levels of gene expression, while the loosened chromatin (euchromatin) towards the interior of the nucleus is associated with higher gene expression. This quiescent picture of interphase radically changes when the cell cycle progresses towards cell division. Firstly, during S phase, DNA is replicated, and chromatin progressively condenses. This is followed by the G_2 phase that shows a compact heterochromatin recruited towards the centre of the nucleus. At the beginning of mitosis, the chromosomes condense with a significant topological change in their organisation and are segregated during the next stages of the cell division. Meiotic chromosomes are also highly condensed as mitotic chromosomes but show a particular functional structure, which prepares germ cells to exchange DNA sequences between their homologous chromosomes to generate diversity. To summarise, chromatin experiences dramatic organisational changes during mitosis and meiosis. These changes in chromatin organisation during the lifetime of a cell show that chromatin is not a static entity but highly dynamic in nature.

For a variety of reasons, conventional light and electron microscopy have not been able to fully capture the finer details of chromatin organisation and dynamics. For a long time, description of the interphase nucleus was limited to delineate the euchromatin–heterochromatin dichotomy or describe some specific nuclear elements such as the nucleolus. Advancements in molecular biology during the last

thirty years have brought an immense amount of information about how chromatin is organised and genes are regulated. As a classical example, the globin gene has been shown to display a highly constrained shape forced by chromatin looping that brings the regulatory regions to the promoter of the gene. Nowadays, genomic studies can acquire an immense amount of information regarding chromatin organisation and gene regulation, leaving one with the expectation that structure of individual genes could potentially be described visually if sufficient specificity and resolution were reached. With the advent of various super-resolution methods, in particular, single molecule localisation microscopy (SMLM)-based methods and recently developed strategies for labelling DNA, it is now possible to study chromatin organisation and underlying gene regulatory mechanisms at the nanoscale.

During my Ph.D., I have analysed a broad range of nuclear phenotypes using SMLM. My analyses contribute to the description of a periodic and dynamic structure of chromatin. Moreover, I have described several elementary chromatin structures that I call chromatin domains, both in interphase and in meiosis, that are potentially associated with a local function such as gene activation or silencing.

Firstly with colleagues, I established an experimental set-up to study chromatin organisation with single molecule localisation microscopy. I investigated how UV-induced photoconversion of conventional DNA dyes allows increasing sufficiently the labelling density such that it is possible to study various organisational aspects of chromatin in basal interphase. An adequate imaging protocol has been established to bring DNA minor groove binding dyes such as Hoechst 33258, Hoechst 33342 and DAPI (4′,6-diamidino-2-phenylindole) into an efficient blinking state necessary to record single molecule locations with high precision. This method was applied to several cell types to investigate the chromatin organisation during different stages of the cell cycle at the highest resolution currently achievable with light microscopy.

The results show that the method can capture several hierarchical levels of chromatin organisation. In reverse hierarchical order, I could describe previously known chromatin territories of 1000 nm, subchromosomal domains of 500 nm, chromatin domains of 100–400 nm (and further subcategories of active or repressed domains) and chromatin fibres below 100 nm, mostly between 30 and 60 nm. Individual nucleosomal domains are also described, which tend to cluster in batches of 10–15 nucleosomes, a number close to one found in genomic studies upstream to promoter regions. Next, with colleagues, I studied the dynamics of chromatin using stress as a model system. It was found that short-term oxygen and nutrient deprivation provokes chromatin to shrink to a hollow, condensed ring and rodlike configuration, which reverses back to the initial structure when the stress conditions cease. The condensed network of rods and rings interspersed with large, chromatin-sparse nuclear voids was 40–700 nm in dimension, capturing another level of chromatin organisation not described before.

Finally, I explored the unique properties of chromatin during meiosis, which has escaped analysis at the single molecule level until now. Single molecule analysis revealed unexpected highly recognisable periodic patterns of chromatin. Firstly, I observed that meiotic chromatin shows unique clusters of 250 nm diameter along

the synaptonemal complex, extended laterally by chromatin fibres forming loops. These clusters show a remarkable periodicity of 500 nm, a pattern possible to spot because of the highly deterministic nature of pachytene chromosomes and the resolution of the experimental set-up. Furthermore, guided by genomic data, I selected histone modifications associated with different chromatin states to dissect the morphology of meiotic chromosomes. I could examine the morphology of these chromosomes into three spatially distinct nanoscale subcompartments. Histone mark H3K4me3 associated with active chromatin was found in a lateral position, potentially located at the places of de novo double-strand breaks. Repressive histone mark H3K27me3 was shown to display a surprising medial symmetrical and periodic pattern, putatively associated with recombination. Finally, centromeric histone mark H3K9me3 locates at one of the meiotic chromosome ends and is potentially associated with repression of repeated regions and pairing of homologous chromosomes at early stages. I summarise these findings in a comprehensive final model.

Overall, I have used new information brought by super-resolution technologies to show the dynamics of chromatin in various processes and novel orders of chromatin compaction, which were not reported previously. Among these new levels of chromatin compaction are the interphase hierarchical chromatin domains, the stress pattern of cells upon oxygen and nutrient deprivation and the novel epigenetic domains found at pachytene stage of meiosis. These architectures show that the organisation of chromatin is more complex than that thought before, is dynamic in nature and shows a high order of periodicity. Further investigation is, therefore, necessary to understand how chromatin transits from a 'beads-on-string' model to the intermediary chromatin domains and finally to the commonly observed X-shaped chromosomes.

Heidelberg, Germany
Mainz, Germany
August 2016

Dr. Kirti Prakash

Parts of this thesis have been published in the following journal articles

We have a habit in writing articles published in scientific journals to make the work as finished as possible, to cover all the tracks, to not worry about the blind alleys or to describe how you had the wrong idea first, and so on. So there isn't any place to publish, in a dignified manner, what you actually did in order to get to do the work.

Richard Feynman

In Peer-Reviewed Journals

1. **Single molecule localization microscopy of the distribution of chromatin using Hoechst and DAPI fluorescent probes** (Fig. 1)

   - **Authors**: Szczurek*, Aleksander T, **Prakash***, **Kirti**, Lee*, Hyun-Keun, Żurek-Biesiada, Dominika J, Best, Gerrit, Hagmann, Martin, Dobrucki, Jurek W, Cremer, Christoph and Birk, Udo
     ***first co-authors**
   - **Description**: In this report, we demonstrate that DNA minor groove binding dyes, such as Hoechst and DAPI, can undergo UV-induced photoconversion,

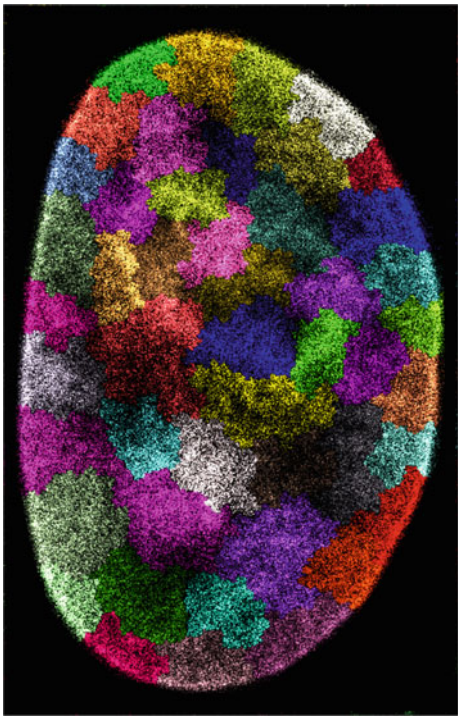

Fig. 1 A simulated chromosome territory model using Hoechst fluorescent probe

to be effectively employed in single molecule localization microscopy (SMLM) with high optical and structural resolution.

- **Journal**: **Nucleus 2014** (*cover page*)
- **Author contributions**: **K.P.**, C.C. and U.B. initiated the project. A.S., H-K.L., **K.P.** and D.Z-B. designed the experiments. A.S. prepared the samples and performed the single molecule measurements. H-K.L., **K.P.**, C.C. and U.B. developed and constructed the microscopy apparatus. **K.P.**, G.B., M.H. and U.B. contributed to the software used for data analysis. D.Z. performed the confocal experiments. **K.P.**, A.S., H-K.L., G.B. and M.H. performed the data analysis. C.C., J.D. and U.B. supervised the work. All authors contributed to writing of the manuscript.
- **Web**: http://www.tandfonline.com/doi/pdf/10.4161/nucl.29564

2. **Superresolution imaging reveals structurally distinct periodic patterns of chromatin along pachytene chromosomes** (Fig. 2)

- **Authors**: **Prakash, Kirti**, Fournier, David, Redl, Stefan, Best, Gerrit, Borsos, Máté, Tiwari, Vijay K, Tachibana-Konwalski, KiKuë, Ketting, René F, Parekh, Sapun H, Cremer, Christoph, Birk Udo J.
- **Description**: In this study, we found that chromatin is non-randomly distributed along the length of the synaptonemal complex (SC) and displays differential condensed clusters. Chromatin structure is further divided into different functional compartments using histone modifications. Taking into account the arrangement and composition of chromatin, as well as the

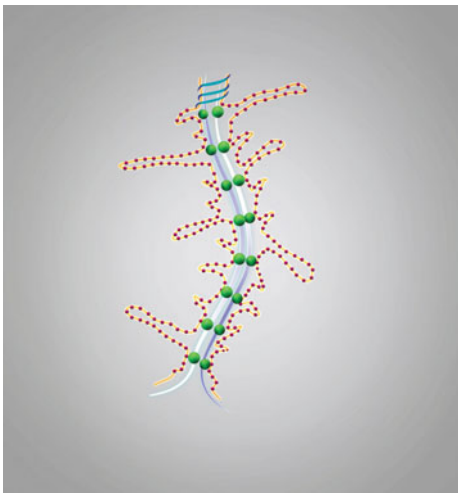

Fig. 2 A model for the epigenetic landscape of meiotic chromosomes. Chromatin (lateral extensions) is constrained by periodic clusters of histone modifications along the synaptonemal complex (SC, *thick axial grey lines*). Active chromatin (H3K4me3) emanates radially in looplike structures (*red dots*), while the repressive chromatin (H3K27me3) is confined to axial regions (*green balls*) of the SC. Centromeric chromatin (H3K9me3) hints at spiralisation of DNA at one of the extremities of SC (*blue lines* at the *top*)

region-specific distribution of post-translational histone modifications, we discuss a model of the chromatin architecture along the length of the SC. This study is a successful application of our newly developed SMLM method applied to DNA dyes.

- **Journal**: **Proceedings of the National Academy of Sciences (PNAS) 2015**
- **Author contributions**: **K.P.** designed research; **K.P.** and S.R. performed research; **K.P.**, S.R., G.B., M.B., V.T., K.T.-K., R.K., S.P., C.C. and U.B. contributed new reagents/analytic tools; **K.P.** and D.F. analysed data; **K.P.** and D.F. wrote the paper with input from all the other authors.
- **Web**: http://www.pnas.org/content/112/47/14635.short

3. **A transient ischemic environment induces reversible compaction of chromatin** (Fig. 3)

   - **Authors**: Kirmes, Ina, Szczurek, Aleksander, **Prakash, Kirti**, Charapitsa, Iryna, Heiser, Christina, Musheev, Michael, Schock, Florian, Fornalczyk, Karolina, Ma, Dongyu, Birk, Udo, Cremer, Christoph and Reid, George

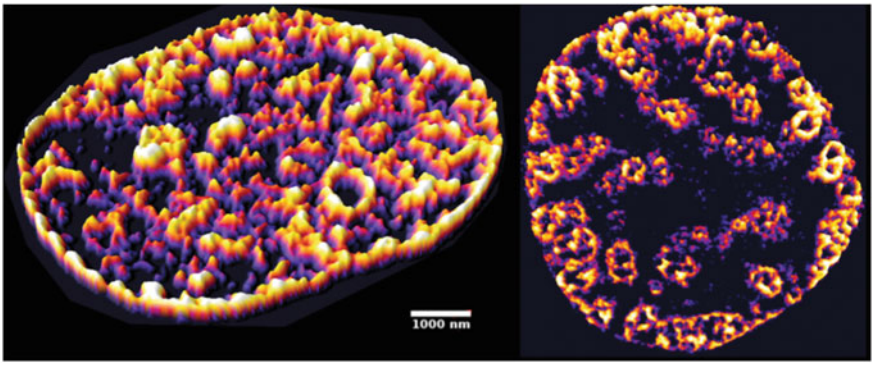

Fig. 3 Deprivation of oxygen and nutrients provokes an entirely novel and previously undescribed chromatin architecture consisting of a condensed network of rods and swirls interspersed between large, chromatin-sparse nuclear voids

- **Description**: Using SMLM, we evaluated the environmental effects of ischemia on chromatin nanostructure. We found short-term oxygen and nutrient deprivation (OND) of the cardiomyocyte cell line HL-1 induces a dramatic and reversible compaction. Chromatin adapts to a previously undescribed subnuclear configuration comprising of discrete, DNA dense, hollow, atoll-like structures, which, upon removal of transient ischemic-like conditions, reverses the open structure in untreated cells.
- **Journal**: **Genome Biology 2015**
- **Author contributions**: C.C. and G.R. conceived of the study and designed the experimental strategy. I.K., A.S., C.H., I.C., M.M., D.M. and K.F. performed experiments. I.K., A.S., **K.P.**, F.S., M.M., U.B. and G.R. analysed data. U.B. prepared the movie. U.B., C.C. and G.R. supervised this project. G.R. wrote the paper and coordinated the supplemental information. All authors discussed the results and contributed to the manuscript. All authors read and approved the final manuscript
- **Web**: http://www.genomebiology.com/2015/16/1/246

4. **Localization microscopy of DNA in situ using Vybrant® DyeCycle Violet fluorescent probe**: **A new approach to study nuclear nanostructure at single molecule resolution** (Fig. 4)

    - **Authors**: Żurek-Biesiada, Dominika, Szczurek, Aleksander T, **Prakash, Kirti**, Mohana, Giriram K, Lee, Hyun-Keun, Roignant, Jean-Yves, Birk, Udo, Dobrucki, Jurek W and Cremer, Christoph

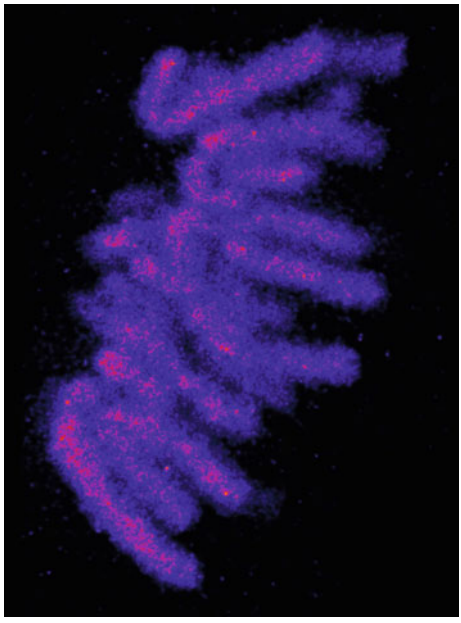

Fig. 4 Mitotic chromosomes stained with Vybrant® DyeCycle Violet fluorescent probe

- **Description**: We report here that the standard DNA dye Vybrant Violet can be used for chromatin imaging using SMLM and helps to describe the nanoscale structure of chromatin. This technique enabled the localisation of a large number of DNA-bound molecules, usually resulting in an excess of 10^6 signals in a $\sim$500-nm optical section of a cell nucleus.
- **Journal**: **Experimental Cell Research 2015**
- **Author contributions**: D.Z-B. and A.S. planned the experiments. D.Z-B. and A.S. performed the experiments, drafted and revised the manuscript. D.Z-B., **K.P.** and A.S. performed image data reconstruction. G.K.M. prepared polytene chromosome samples. J.Y.R., U.B., J.D. and C.C. supervised the work and contributed to writing the manuscript.
- **Web**: http://www.sciencedirect.com/science/article/pii/S001448271530080X

5. **Quantitative super-resolution localization microscopy of DNA in situ using Vybrant® DyeCycle Violet fluorescent probe** (Fig. 5)

- **Authors**: Żurek-Biesiada, Dominika, Szczurek, Aleksander T, **Prakash, Kirti**, Gerrit Best, Mohana, Giriram K, Lee, Hyun-Keun, Roignant, Jean-Yves, Birk, Udo, Dobrucki, Jurek W and Cremer, Christoph
- **Description**: In this manuscript, parameters that influence the quality of SMLM reconstruction using Vybrant DyeCycle Violet, for instance number of frames, wavelength or composition of buffer, are investigated, using quantifications and experimental methods.
- **Journal**: **Data in Brief 2016**
- **Web**: http://dx.doi.org/10.1016/j.dib.2016.01.041

In Conferences

1. **Identify and localise**: **Algorithms for single molecule localisation microscopy** (Fig. 6)

- **Authors**: **Kirti Prakash***, Gerrit Best*, Martin Hagmann, Udo Birk, and Christoph Cremer.
  ***first co-authors**

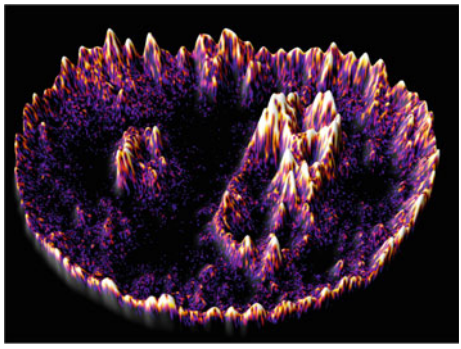

Fig. 5 3D surface plot of DNA

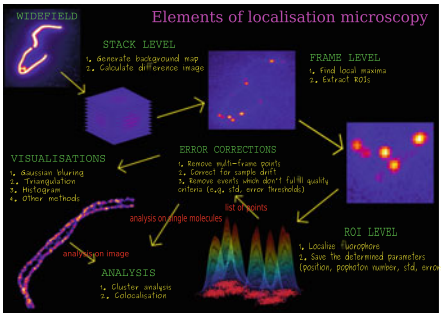

Fig. 6 Algorithm scheme for processing single molecule localisation microscopy data

- **Description**: Here, we present a comparative analysis of a range of available localisation algorithms regarding their complexity, applicability and performance by testing them on both synthetic and experimental data. Experimental data come from both sparse and dense regions, with low and high background levels, to determine which method is suited for a given dataset.
- **Conference**: **International Microscopy Congress (IMC) 2015**
- **Author contributions**: **K.P.** designed and performed research and analysed the data. K.P. and G.B. wrote the code.
- **Web**: http://www.imc2014.com

2. **Drift correction strategies for superresolution imaging modalities** (Fig. 7)

- **Authors**: Martin Hagmann*, **Kirti Prakash***, Rainer Kaufmann, Udo Birk and Christoph Cremer.
  ***first co-authors**
- **Description**: We present two drift correction strategies based solely on acquired data without any fiducial markers. Using both approaches, we successfully corrected localisation microscopy data down to a final drift under 5 nm. We demonstrate that with this procedure, the resolution of the final reconstructions was substantially enhanced.
- **Conference**: **International Microscopy Congress (IMC) 2015**
- **Author contributions**: **K.P.** and M.H. designed and performed research and analysed the data.
- **Web**: http://www.imc2014.com

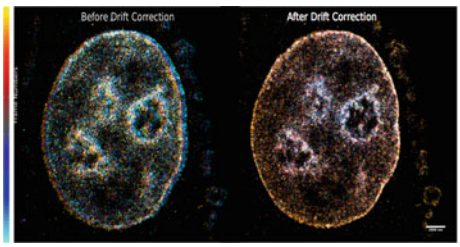

Fig. 7 HeLa cell nucleus stained with Hoechst 33258 photoproduct before and after drift correction

3. **Superresolution imaging of meiosis prophase I chromatin in pachytene stage** (Fig. 8).

   - **Authors**: **Kirti Prakash**, Gerrit Best, Mate Borsos, Stefan Redl, Kikue Tachibana-Konwalski, Rene Ketting, Sapun Parekh, Udo Birk, and Christoph Cremer
   - **Description**: We combined single molecule localisation microscopy with next-generation sequencing data and computer simulations to map and analyse the distribution of chromatin and several of its post-translational modifications along the lateral elements of the SC.
   - **Conference**: **Focus On Microscopy (FOM) 2015**
   - **Author contributions**: **K.P.** conceived the project and planned the experiments. **K.P.** and S.R. performed the experiments. **K.P.** performed image data reconstruction and analysed the data. **K.P.**, S.R., G.B., R.K., S.P., U.B. and C.C. analysed the results.
   - **Web**: http://www.focusonmicroscopy.org/2015/home.html

4. **Lampbrush-like structures in mammalian meiotic chromosomes** (Fig. 9)

   - **Authors**: **Kirti Prakash**
   - **Description**: Lampbrush chromosomes (LBC) are transcriptionally active chromosomes found in meiosis prophase I of most animals, except mammals. In LBC, chromosomes adapt special looplike structures that emanate radially from the axis of the chromosomes, most likely to facilitate transcription. These loops have never been observed previously in mammals, somatic cells or diploid. Here, it is shown for the first time that mammalian chromosomes with clusters of transcriptionally active chromatin show patterns similar to the amphibian LBC.
   - **Conference**: **Nuclear Organization and Function, CSHL 2016**
   - **Web**: https://meetings.cshl.edu/meetings.aspx?meet=NUCLEUS&year=16 year=16

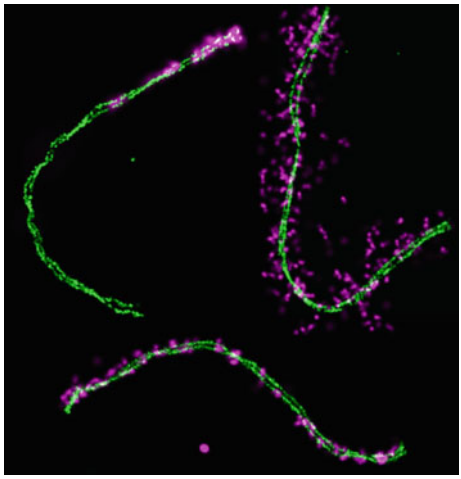

Fig. 8 Distribution of post-translational histone modifications around the synaptonemal complex (SC)

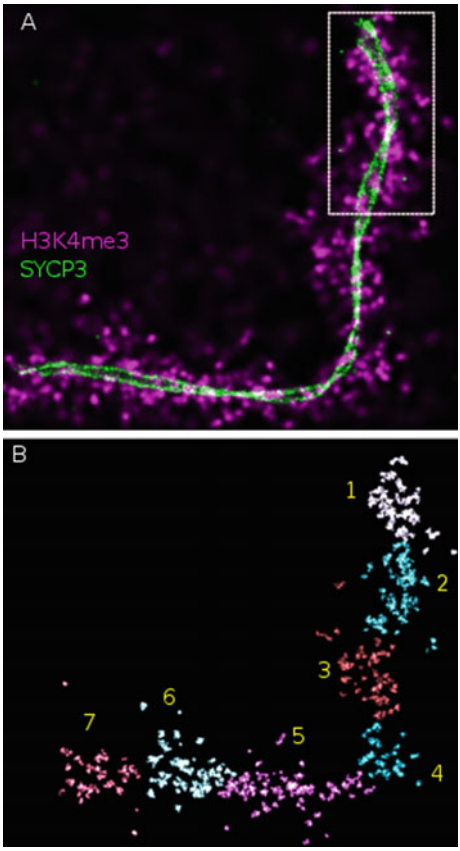

Fig. 9 Distribution of $H_3K_4me_3$ mark around the synaptonemal complex (SC): $H_3K_4me_3$ images revealed lampbrush-like shapes in mammalian chromosomes

Acknowledgements

I thank Christoph Cremer for providing me with the opportunity to enter a new area of research and participate in the establishment of a new laboratory. I would also like to thank him for allowing me to work on my ideas and set up my collaborations. I am further in debt to all Cremer group members. I thank Udo Birk, Martin Hagmann, Gerrit Best, Margund Bach, Hyun-Keun Lee, Florian Schock, Aleksander Szczurek, Amine Gouram and Jan Neumann for the useful discussions.

I thank my friends and colleagues at IMB. Maria Hanulova, Sandra Ritz and Katharina Boese were my unofficial laboratory mates and many thanks for proofreading my thesis. I thank Wolf Gebhardt with whom I had many interesting scientific discussions. During my initial days at IMB, I had the opportunity to work with Heinz Eipel from whom I learnt a lot about science. I would also like to thank George Reid and Jean-Yves Roignant for their support. Finally, I thank Miguel Andrade for the encouragement and many useful pieces of advice.

A lot of algorithms that made way into this thesis were co-written with Martin Hagmann and Gerrit Best. David Fournier, Akshay Prakash, Shashi Bhagat and Wioleta Dudka helped with most of the cartoon figures that made their way into the thesis. I thank my collaborators for the samples. In particular, I thank Wolf Gebhardt, Aleksander Szczurek, Ina Schaefer, Sabine Puetz, Sapun Parekh, Dominika Zurek-Biesiada, Paulina Rybak, Jurek Dobrucki, Giriram Kumar, Jean-Yves Roignant, Ina Kirmes, Dongyu Ma, Mate Borsos, Stefan Redl, Kikue Tachibana-Konwalski, Rene Ketting, George Reid and Wioleta Dudka.

I learnt a lot from some people whom I met during various courses, conferences and laboratory visits. In particular, I would like to thank Thomas Cremer, Marion Cremer, Brad Amos, Jonas Ries and Rainer Heintzmann. I further thank Sapun Parekh and Joseph G. Gall for their support and understanding during the last few months of my thesis writing. Sapun, also thanks for proofreading my thesis.

I am further in debt to Wioleta Dudka for proofreading my thesis multiple times and for providing many valuable criticisms. I have incorporated nearly all of her suggestions which helped in removing a lot of ambiguities and redundancies.

This thesis will not have been through and through without the immense help of David Fournier, who not only critically read and corrected parts of this dissertation but also constantly encouraged and pushed me to write this detailed monograph. David, thank you for being there.

My family has been a constant source of support. My parents always supported my interest in science. Most of all, I thank my friends Wiola and David for the encouragement and for handling my mood swings especially during last 3–4 months of writing, rewriting and re-rewriting experience.

Finally, I hope this thesis provides enough new insights to encourage a young enthusiast to pursue this fascinating field.

August 2016 Kirti Prakash

Contents

Abbreviations

μm	Micrometre
3D	Three dimensional
Ac	Acetylation
AFM	Atom force microscopy
BALM	Binding-activated localisation microscopy
BaLM	Bleaching/blinking assisted localisation microscopy
bp	Base pair
CCD	Charge-coupled device
ChIP	Chromatin immunoprecipitation
ChIP-seq	ChIP-sequencing
CLSM	Confocal laser scanning microscopy
COI	Centre of intensity
CRISPR/Cas9	Clustered regularly-interspaced short palindromic repeats/CRISPR associated protein 9
CTCF	CCCTC-binding factor
Cy3	Cyanine 3
Cy5	Cyanine 5
DAPI	4′,6-diamidino-2-phenylindole
ddNTP	Dideoxynucleotide
DNA	Deoxyribonucleic acid
DSB	Double strand break
EdU	5-ethynyl-2′-deoxyuridine
EM	Electron microscopy
emGFP	Emerald green fluorescent protein
FISH	Fluorescence in situ hybridisation
fPALM	Fluorescence photo-activated localisation microscopy
fps	Frames per second
FRC	Fourier ring correlation
FRET	Fluorescence resonance energy transfer
FWHM	Full width at half maximum

GFP	Green fluorescent protein
H2B	Histone 2B
H3	Histone 3
H3K9ac	Histone 3 lysine 9 acetylation
H3K14ac	Histone 3 lysine 14 acetylation
H3K27ac	Histone 3 lysine 27 acetylation
H3K27me3	Histone 3 lysine 27 tri-methylation
H3K4me1	Histone 3 lysine 4 mono-methylation
H3K4me2	Histone 3 lysine 4 di-methylation
H3K4me3	Histone 3 lysine 4 tri-methylation
H3K9me3	Histone 3 lysine 9 tri-methylation
H4	Histone 4
HAT	Histone acetyl-transferase
HDAC	Histone deacetylase
HL-1	Cardiomyocyte cell line
iPALM	Interference photo-activated localisation microscopy
kb	Kilobase
kDa	Kilodalton
LBC	Lampbrush chromosome
LCR	Locus control region
LM	Light microscopy
LSM	Least-squares method
LTR	Long terminal repeat
Mb	Megabase
Me	Methylation
MEA	Monoethanolamine
MLE	Maximum likelihood estimation
mRNA	Messenger RNA
MSC	Mesenchymal stem cell
NA	Numerical aperture
nm	Nanometre
NND	Nearest neighbour distance
OND	Oxygen and nutrient deprivation
OTF	Optical transfer function
P	Phosphorylation
PALM	Photo-activated localisation microscopy
PBS	Phosphate-buffered saline
PDC	Pixel density classifier
Pixel	Picture element
Pol II	Polymerase II
Pol II Ser2P	Polymerase II serine 2 phosphorylation
PRDM9	PR domain zinc finger protein 9
PSF	Point spread function
PTM	Post-translational modification
R	Arginine

RNA	Ribonucleic acid
ROI	Region of interest
ROS	Reactive oxygen species
rRNA	Ribosomal RNA
S	Serine
S phase	Synthesis phase
SC	Synaptonemal complex
SYCP	Synaptonemal complex proteins
SEM	Scanning electron microscopy
SIM	Structured illumination microscopy
SMLM	Single molecule localisation microscopy
SNR	Signal-to-noise ratio
SPDM	Spectral precision distance microscopy
STED	Stimulated emission depletion
STORM	Stochastic optical reconstruction microscopy
Su	Sumoylation
TAD	Topologically associating domain
TALE	Transcription activator-like effectors
TEM	Transmission electron microscopy
TIRF	Total internal reflection fluorescence
tRNA	Transfer RNA
TSS	Transcription start site
Ub	Ubiquitination
UV	Ultraviolet
VH7	A human fibroblast cell line
VV	Vybrant DyeCycle Violet
Y	Tyrosine
YFP	Yellow fluorescent protein
YOYO-1	A tetracationic homodimer of Oxazole yellow

List of Figures

Chapter 1
A Condensed History of Chromatin Research

The model was so pretty that we wanted to believe it no matter what the data may say.

James D. Watson

The cell nucleus is a discernible cellular compartment, where the expression and regulation of genes take place. Due to limited tools and methods, it remained ignored for a long time (until the late 19th century), however nowadays it is a major research topic. The structure of DNA and in-depth study of the nucleus composition has shown that the DNA is heavily constrained by proteins either modulating gene expression or devoted to shaping DNA into various topological structures such as loops and globules. The DNA with all other associated protein machinery and RNA is referred to as chromatin.

For the most part, chromatin research has highly depended on the advancements of microscopy, from the early days of conventional light and electron microscopy of the cell nucleus to the recent advanced high-resolution and live imaging methods. Much more recently, chromatin research has gained a lot from experiments which have tried to map chromatin in 3D inside the cell nucleus to conclude that it is organised in distinct territories. This, essentially, is the story told in the present chapter.

1.1 The Early Research on the Nucleus and Chromatin

The nucleus was described for the first time as early as the eighteen century by Antonie van Leeuwenhoek[1] in the nucleated blood cells of salmon. For a long time between the late 17th century and the first thirty years of the 18th, it was at best described as a *vesicle* and did not show much complexity than the name suggests.

[1] Antonie van Leeuwenhoek (1632–1723), a Dutch scientist who discovered micro-organisms by developing sophisticated microscopes. Considered to be the *Father of Microbiology.*

K. Prakash, *Chromatin Architecture*, Springer Theses,
DOI 10.1007/978-3-319-52183-1_1

Fig. 1.1 Purkinje drawings of the germinal vesicle of a hen egg. Reproduced from the main set of figures in (Purkyně 1830)

Felice Fontana[2] in 1781 describes the first sub-structure in a nucleus of a skin cell from an eel, probably a nucleolus (Baker 1949). The power of a good drawing is illustrated by Johann Evangelist Purkyně[3] (1830), where he presents the germinal vesicle of the hen egg (see Fig. 1.1). He comments as follows:

"Thus the scar [germinal disk] of the ovarian egg contains a special part, peculiar to itself, a vesicle of the shape of a somewhat compressed sphere. This vesicle is limited by a very delicate membrane and filled with a special fluid, perhaps connected with procreation (for which reason I might call it the germinal vesicle); it is sunk into a white breast-shaped projection composed of globules and perforated in the middle" according to John Baker's translation from Latin (Baker 1949).

As Baker points out, the nuclear envelope and the nucleoplasm are described here for the first time. This first comprehensible picture of a nucleus also brought the first sound hypothesis regarding the function of the nucleus, a "connection with procreatio", exemplifying the need to find quality signals in biology, and so proper

[2] Felice Fontana (1730–1805), an Italian scientist, considered to be the father of modern toxicology.

[3] Johann Evangelist Purkyně (1787–1869), Czech physiologist. His broad contributions touch neurophysiology, reproduction research, physiology of the vision, pharmacological properties of plants and study of cell composition.

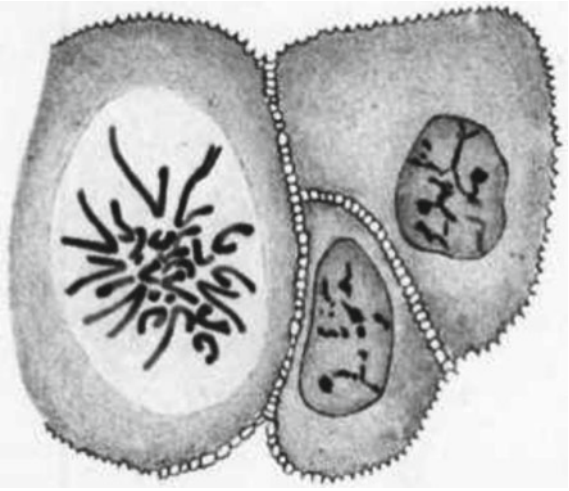

Fig. 1.2 Sketch of a cell: On the *left*, a cell prior to mitosis. On the *right*, two sister cells coming from the same mitotic event (Flemming 1882) (citation inspired by Cremer and Cremer 2009b)

animal or cellular models with extraordinary properties. As a consequence, at one glance, one understands what the structure looks like, and what it can do.

Though the nucleus was observed early, its function remained unexplored for a long time. One of the initial hypothesis (∼1850) stated that nucleus could be the place where new cells emerge (Baker 1949). These studies used optical microscopy and were mainly morphological. Mitotic chromosomes, which are easy to observe under a microscope, captured the focus of many researchers and were the only nuclear component to be studied for a long time. Interphase chromosomes, at that time, were considered only by a handful of scientists, among them Theodor Boveri[4] (1888). The habit to consider only mitosis is also exemplified by modern textbooks, which often present the mitotic chromosomes (highest level in the hierarchy of chromatin compaction) after the initial beads-on-the-string and 30 nm chromatin fibre for the organisation of DNA (Fig. 1.2). Interphase chromatin is obviously not organized in X-shape chromosomes and is much more complex.

In the second part of the 19th century, chromatin research was mainly focused on the chemical quantification of nucleic acids and the fractionation of nuclear proteins. The point of view of chemists was slightly different from that of 18th and early 19th century biologists. Most of them wanted to describe the chemical composition of the cell exhaustively. One of them, Friedrich Miescher,[5] decided to do so for immune cells. In 1869, while studying in Tuebingen, he discovered a substance in pure leukocyte solution which caused the nucleus to swallow and explode upon mild injections of an alkaline solution. He found this substance to have a high phosphate

[4]Theodor Boveri (1862–1915), German biologist, first to propose that chromosomes occupy distinct territories inside of the cell nucleus. Also known for the Boveri-Sutton chromosome theory and the discovery of the centrosome.

[5]Friedrich Miescher (1844–1895), Swiss physician and biologist, most noted for his work on isolation and identification of nucleic acids.

proportion and called it *nuclein*, in reference to its nuclear localization; and later called it *nucleic acid* (Miescher 1871, 1874, 1897; Kossel and Kennaway 1911; Kossel 1883, 1884) (for detail see Dahm 2008). Later, Albrecht Kossel[6] determined the composition of DNA to be a mixture of adenine, cytosine, guanine and thymine, an important step to understand how information is stored in the DNA molecule (Kossel and Kennaway 1911; Kossel 1883, 1884).

1.2 Chromatin Bares Information: The Chromosomes and Genes Era (1870–1945)

Ernst Haeckel[7] proposed that the nucleus contains factors responsible for heredity (1866). Miescher is the first to have postulated a nuclear origin of a cellular functions, the motion of sperm, though without providing hints about the mechanism (Miescher 1874; Dahm 2008).

During the second half of the 19th century, probably the most famous work on nuclear functionality (Hertwig 1875) was conducted by Oscar[8] and Richard[9] Hertwig. Oscar Hertwig, using the sea urchin as a model, showed that a male and a female germ cell merge to form the egg (Hertwig 1875). Moreover, he showed that organisms come from one cell, leaving biologists with the very complex task of explaining the mechanism of development. Oscar Hertwig's observations led to the first proof that a nucleus is a place that stores some information.

An interesting point to note is that the Hertwig brothers carried out their initial work at Jena, where Ernst Abbe[10] was pioneering the work in optics, lens design and microscopy around the same time.[11] As optical technology was still limited at the end of the nineteenth century, knowledge about chromatin function was restricted to the description of the metaphase chromosomes and the characterization of chemical composition. Though chromosomes themselves were observed by several scientists

[6] Albrecht Kossel (1853–1927), German biochemist, who pioneered the work in the field of genetics. He was awarded the Nobel Prize in Physiology or Medicine in 1910 for the discovery of the five fundamental nucleic bases that constitute nucleic acids: adenine, thymine, guanine, cytosine and uracil.

[7] Ernst Haeckel (1834–1919), German biologist known for establishing the first phylogenetic tree of all living forms and for establishing a relation between development and evolution (*ontogeny recapitulates phylogeny*).

[8] Oscar Hertwig (1849–1922),German zoologist, the first to describe fecundation as the merging of a sperm and an egg.

[9] Richard Hertwig (1850–1937), German zoologist known for his work on *protists* and the relationship between the nucleus and the plasma as well as for his work on meiosis and fecundation.

[10] Ernst Abbe (1840–1905), German physicist, a major innovator of modern microscopy. Abbe's innovations in optics led to great improvements in microscope design and understanding of resolution limits of light microscopy.

[11] One wonders to which extent advancements in chromatin biology research have depended on progress in optics and microscopy.

in the first half of the nineteen century, it is only in 1882 that they were associated with mitosis. In a famous work, Walther Flemming[12] described the content of the nucleus under the term chromatin for the first time (Fig. 1.2).

After the works of Flemming and others, the mitosis begins to get the focus of the biologists. The nucleus was rapidly hypothesised to be one of the factors where hereditary information can potentially be stored and transmitted to daughter cells. As such, Wilhelm Roux[13] in 1883 said that there is not only a question of quantity in mitosis (meaning that both daughter cells will inherit the same amount of chromatin), but there is also a question of quality (not all chromatin is equivalent), which supposes that all granules of chromatin have different functions. Around the same time, the work of Oscar Hertwig was prolonged by August Weismann[14] germ plasm theory.[15] Weismann defined chromosome heredity as the process by which information is transmitted from one generation to the other via chromosomes of the germ lines, based on Hertwig observations that sperm + egg = zygote, a sufficient note to claim that one needs information from two different cells to form a new individual, and that information is exchanged during the merging of the cells (Fig. 1.3). Friedrich Miescher, who characterised nucleic acids using nucleus of leukocytes and salmon sperm, hypothesised that information might be stored on this molecule by a change of stereochemistry; during fecundation, each gamete will contribute with a molecule of a different state to combine in the nucleus of the fertilised egg (Miescher 1897).

Theodor Boveri and Walter Sutton[16] were the first scientists to establish a link between chromosomes dynamics during mitosis and Mendel's laws of heredity.[17] According to their theories, there must be entities that are passed differently to the next generation (genes, though the term is coined later in history; see Boveri 1904, 1909).

Later, Thomas Morgan[18] was the leading player in the discovery of genes. As a result, he is considered as the founder of the field of genetics. Along with Hugo De Vries[19] and others, he proved that chromosome regions bare information that is variable in different organisms and can be transmitted to next generation. To achieve this, he provoked mutations in flies using irradiations. After proving that the provoked mutations can be inherited, he found that the transmission of certain

[12] Walther Flemming (1843–1905), German biologist, who discovered mitosis.

[13] Wilhelm Roux (1850–1924), German zoologist, early embryologist, known for studying the outcome of provoked developmental defects.

[14] August Weismann (1834–1914), German evolutionary biologist, known for the germ plasm theory.

[15] According to the theory genetic inheritance takes place via germ cells such as egg and sperm cells. Other cells such as somatic cells do not transmit hereditary information to the next generation.

[16] Walter Sutton (1877–1916), American geneticist, who contributed to discover that chromosomes inheritance follow the laws of Mendel.

[17] Gregor Mendel (1822–1984), German scientist, who discovered fundamental laws of heredity through his experiments on pea plants.

[18] Thomas Morgan (1866–1945), American embryologist, who discovered that traits transmitted to the next generation are coded by certain regions on chromosomes, the so-called genes.

[19] Hugo De Vries (1848–1935), Dutch botanist who introduced the concept of genes and mutation, which he incorporated in an updated theory of evolution.

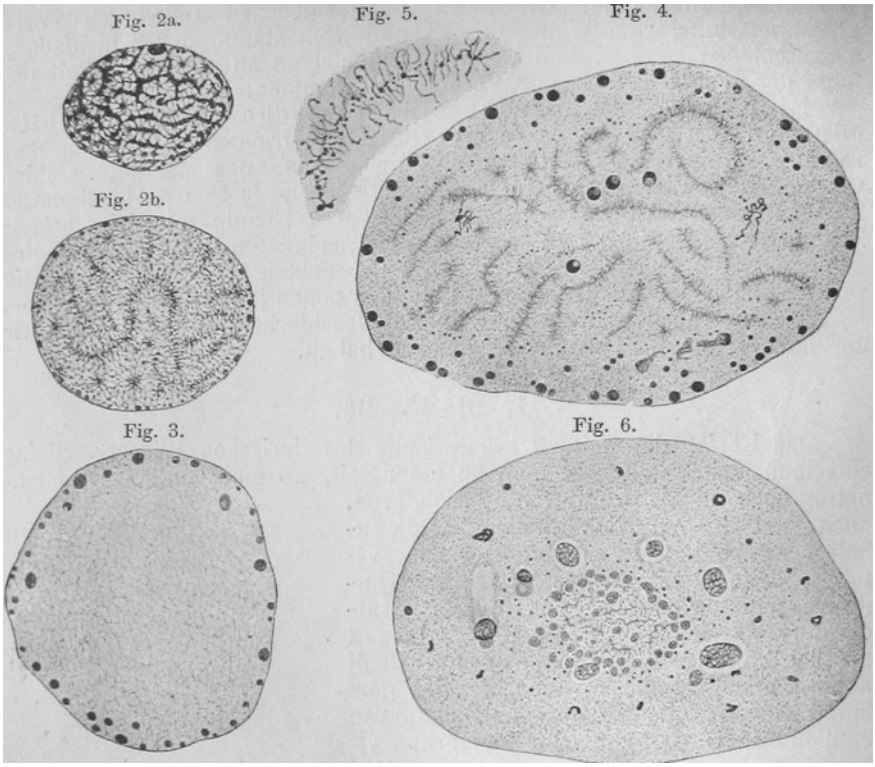

Fig. 1.3 Cell nuclei from the eggs of a Salamander species (adapted from Hertwig 1898)

mutations depends on the gender of the carrier and so, on the presence of the X chromosome. Knowing that the presence of genes on the X chromosome could be shown by this method, Morgan performed appropriate cross-breeding. By examining the phenotypes of the following generations, he could determine if two alleles recombine together more often than predicted by chance, which probably means that the distance between them on the chromosome has an influence on the probability to recombine. The further apart, more likely the recombination of genes will be. This rational was the base for designing experiments leading to a first genetic map, for the X chromosome of Drosophila (Strutevant 1913).

The earliest visualisation of functional sub-chromosomal structures was done on pachytene stage chromosomes by August Weismann in 1913. Images pointed at prominent bulky regions, regularly spread along the chromosomes, which are probably equivalent to chromatin clusters recently observed in meiosis (see Chap. 4 and Prakash et al. 2015). Phoebus Levene [20] in 1929 characterised the composition of DNA and found that DNA contained nucleic bases (already identified previously by

[20] Phoebus Levene (1863–1940), American biochemist who characterized DNA composition as a mixture of nucleic bases, sugars and phosphate groups.

Kossel), deoxyribose, and a phosphate group. It was much later proven by Chargaff that adenine:thymine and cytosine:guanine ratios were 1:1 (Chargaff et al. 1952).

In 1944, one of the most important experiments in molecular biology, known as Avery–MacLeod–McCarty experiment (Avery et al. 1944), was carried out. The experiment proved that DNA and not proteins carry the information i.e. gene. Another major step was also to show that one gene corresponds to one enzyme (see Olins and Olins 2003 for a review).

1.3 Chromatin as a Decision Center of the Cellular Factory: The Golden Age of Molecular Biology and Electron Microscopy (1944–1980)

The fifties and the sixties experienced the emergence of molecular biology and the electron microscopy (EM) as methods to explore the way the nucleus responds to the environment and uses its internal program to maintain the survival of the cell. Before the fifties, the description of chromatin was very shallow. On one hand, chemistry had revealed the composition of the nucleus; on another hand, the optical description of chromatin was limited to individual sub-structures, such as the nucleolus or Cajal bodies. Genes had been described indirectly; polytene chromosomes of Drosophila had been characterised by autoradiography (Ficq and Pavan 1957; Lewis 1945). Nevertheless, beyond the level of basic chemical compounds and the genetic bands of Drosophila, not much was known about the various regulatory processes happening inside the nucleus, especially in the interphase. Molecular biology has emerged in the middle of the 20th century as an attempt to describe this complexity and bridge the gap between basic chemical assays and visual description of chromatin. This will be achieved mostly by experimental evidence but also by modelling. Prompted by research and thoughts from physicians Niels Bohr[21] and Erwin Schrödinger,[22] who saw that the basic laws of physics have to be at the basis of all living forms, many biologists started to use models to address new questions.

The most famous paper of the twentieth century in the field of biology is the 1953 model of DNA by Watson and Crick published in journal Nature (Watson et al. 1953 and Fig. 1.4). According to him, James Watson[23] was inspired by the reading of Schrödinger essay "What is life" (Schrödinger 1945) in choosing his post-doctoral topic which was on the structure of DNA. In the early fifties, many

[21] Niels Bohr (1885–1962), Danish physicist, famous for a model of the atom where electron can transit between orbitals, and for an early quantum theory describing these transitions.

[22] Erwin Schrödinger (1887–1961), Austrian physicist, made fundamental contributions to the field of quantum theory.

[23] James Watson (1928—), American molecular biologist and visionary, co-discoverer of the structure of DNA with Francis Crick, co-discoverer of mRNA and early promoter of the human genome project.

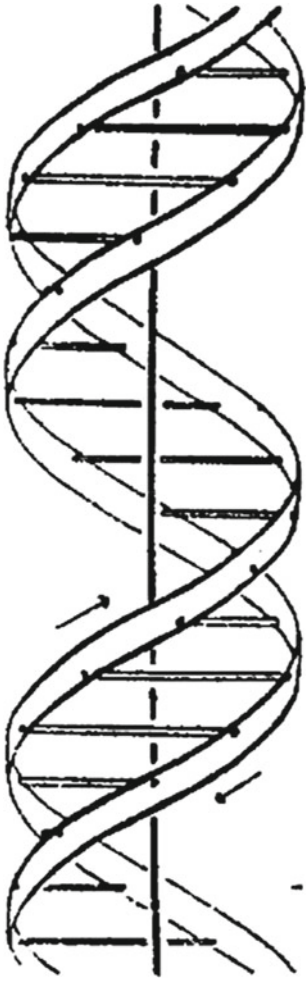

Fig. 1.4 The famous model of the double helix by Watson and Crick published in 1953 (Watson et al. 1953)

people, including Linus Pauling,[24] who had already modelled the alpha-helix of proteins (Pauling et al. 1951), came with the idea that the DNA molecule could be modelled. An earlier hypothesis had claimed that the structure could be a helix, which Pauling falsely thought to be triple (Pauling and Corey 1953). Based on experimental evidence from Franklin, Watson along with his collaborator Francis Crick, designed a double helical structure for DNA (Watson et al. 1953). The model explained how the main components of DNA are placed toward each other: two strands of DNA made of alternating deoxyribose and phosphate, interact via nucleic bases bound to their

[24]Linus Pauling (1901–1994), American chemist who made several important contribution to biochemistry, discovering the structure of the alpha-helix and contributing to the study of genetic diseases.

respective deoxyribose, similarly to the zip of a jacket. The idea of base pairing came from brand new evidence from Erwin Chargaff, who showed that adenine: thymine and cytosine: guanine are 1:1 ratios (Chargaff et al. 1952). The fantastic model of Watson and Crick revealed how a genetic vocabulary is possible by a combination of nucleic bases and how it can be inherited, by duplication of available information. It also showed how modelling is crucial to biology and how the vision is as important as the data themselves.

This finding prompted many subsequent central questions of biology. At that time, where DNA was freshly known to bare information in the cell, the issue that was slowly arising was how information bared by DNA turns into proteins. The correspondence saying that one gene corresponds to one enzyme had just been postulated (Beadle and Tatum 1941). Following Watson and Crick publication, George Gamov[25] postulated that a minimum of 3 nucleotides is necessary to code the 20 amino acids; later experiments by Crick showed that this prediction was true (Crick et al. 1961). Another set of experiments led to the discovery of messenger RNA, mainly characterized by Watson and colleagues (Watson 1963), based on ideas of different discussion groups and seminal reflections by Francois Jacob[26] and Jacques Monod.[27] These investigations led to the conclusion that the nucleus has to be an administrative decision centre of the cell, storing information that can be used to respond to cues. A very remarkable ability of the nucleus is to adapt to the signals from the environment.

The pioneer studies of Salvatore Luria,[28] Alfred Hershey and Max Delbrueck[29] in the 40s, established phage lambda and bacteria models as important platforms to study genes and their regulation. Until the mid-20th century, how genes can be converted to proteins was not understood. Experiments from Jacob and Monod helped to describe such a phenomenon. They showed the existence of activable gene products, proving that genes respond to external cues. Upon presence of sugar, they demonstrated that an intermediary product, moving to the cytoplasm, was transmittable to another bacteria which was not exposed to the initial clue. The famous "operon paper" also hypothesised that these products are RNA (Jacob and Monod 1961). RNA polymerase itself was just discovered in 1960 (Hurwitz 2005). The first quantification of mRNA produced by the nucleus was done in the group of James Watson, who had also been central in thinking about possible intermediary elements to turn genes into proteins. The earliest sketch drawn showing the transformation of DNA

[25] George Gamow (1904–1968), Russian theoretical physicist and cosmologist, who made some fundamental contributions to molecular genetics.

[26] Francois Jacob (1920–2013), French biologist, along with Jacques Monod, came up with the idea that intermediate messengers are needed to make proteins out of genes.

[27] Jacques Monod (1910–1976), French biologist, worked on genetic control of viruses and enzymes together with Francois Jacob.

[28] Salvador Luria (1912–1991), Italian microbiologist, showed that mutations in bacteria are random, and that selection acts on random mutations according to Darwin's theory.

[29] Max Delbrueck (1906–1981), a German-American biophysicist, worked on replication and genetics of viruses.

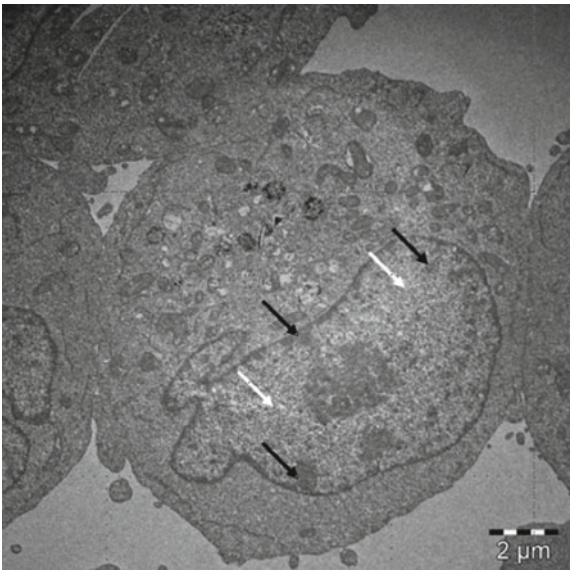

Fig. 1.5 Electron microscopy image showing the classical dichotomy between euchromatin and heterochromatin in a human leucocyte. Most of heterochromatin (*black arrows*) is in the periphery of the nucleus, for the most part tightly attached to the lamina, while euchromatin (space pointed by the *white arrows*) is filling most of the nucleus space, without touching lamina. *Image courtesy* Wioleta Dudka

into RNA to protein is from the hand of Watson, in 1959, according to him (Watson 2012).

Following pioneer works on DNA copying, Frederick Sanger[30] developed a set of techniques to sequence DNA molecules, first published on tRNA (Sanger 1981). This led to more efficient procedures, such as the classical Sanger sequencing protocol, which uses dideoxynucleotides (ddNTP) to interrupt copying of the DNA molecules to sequence at different positions.

Aside from the series of experiments that have led to the 'central dogma' of biology (genes transfer information to messenger RNA which is used to build protein), the development of the electron microscope has been a major advancement of the century. Conceived to record the differential transmission of an electron canon on a sample preparation, this microscope allows viewing cells at the nanometer resolution. Many compartments have been discovered using EM: the endoplasmic reticulum, the Golgi apparatus, the chloroplast (Porter et al. 1945) by Albert Claude.[31] It has also helped to describe the ultrastructure of the interphase nucleus and distinguish euchromatin ('active chromatin') from heterochromatin ('inactive chromatin', see Fig. 1.5), and describe nuclear pores along with other nuclear structures (see Chap. 1 of Busch (1974) for more information). Most importantly, it was crucial to proving that a nascent RNA comes out of pericentric chromatin and that chromosomes in interphase have an inactive region (central) and an active region (pericentric).

[30] Frederick Sanger (1918–2013), British biochemist, known for his work on the structure of proteins, the sequencing of amino acids and for the determination of nucleotide sequences in DNA.

[31] Albert Claude (1899–1983), Belgian cell biologist, who was the first to use electron microscopy for the study of cells and description of various fundamental organelles.

In situ hybridization is another area of research that has been decisive for the description and regulation of a gene. The technique was pioneered by Joseph Gall[32] (Gall 1968a, b), who developed a method to purify rRNA molecules. Gall and Pardue then applied hybridization to the localisation of repeated elements on the chromosomes and could visualise for the first time nanoscale chromatin features in situ (Gall and Pardue 1969). This research shows an early attempt to localise structural and functional pattern on chromosomes, though banding on Drosophila chromosomes had already been shown since long.

Electron microscopy, despite limitations due to the low density of certain cellular components and limited assortment in contrasting compounds, has been an immense advancement in biological research during the 20th century. Radioactive probes used in EM preparation have been slowly replaced by confocal imaging, which allows using fluorescence to stain several types of molecules at the same time, without long, sophisticated EM procedures. Experiments in other areas of research have also shown that the specificity of cells phenotypes (i.e. their function) comes from specific genetic programs executed in the nucleus. For instance, a pioneering experiment has been the successful transplantation of a somatic nucleus to an embryonic stem cell by John Gurdon,[33] which resulted in a healthy production of tadpoles. This proved that the phenotype of a cell depends on the end products of the genetic program, that are mRNA and proteins (Gurdon et al. 1958).

1.4 Chromatin as a Highly Structured System: Genomic Data, Localisation Methods and Modelling (1980 Onwards)

The research of the 60s and 70s had shown many basic principles of the life of a nucleus, the 'administration centre' of the cell. In the following decades, research regarding chromatin function and dynamics has started to take off. The central questions in the field of research on the nucleus were: how many genes does it comprise, and what are they doing? Does the chromatin adopt a given architecture in the nucleus? Are chromosomes, transcription machinery, genes, regulators disposed in a certain way or are things close to stochastic? What about the dichotomy euchromatin/heterochromatin revealed by electronic microscopy? Are there other levels of complexity between the nucleosome level and chromatin dichotomy? Finally, can the nuclear centre store information and change its behaviour using past stimuli which are no longer present? This last question, the question of epigenetics, will be treated in the next section.

Describing the diversity of genes present in a nucleus was certainly not a trivial task. Since Sanger first experiments, sequencing was possible, but at a tiny scale.

[32] Joseph Gall (1928—), American cell biologist, known for developing in situ hybridization and work on repeated genomic regions such as telomeres.

[33] John Gurdon (1933—), a British biologist, the pioneer in the field of cellular reprogramming.

The first automatic sequencer appeared in 1985, with a speed of 3000 nucleotides per day. Knowing that the genome comprises possibly 100,000 genes, with several kilobase pairs long in each case, researchers had to face both an experimental and a computational challenge. Computation would require a high number of very fast processors and was not possible at a decent speed before the 1990s. The first competitive algorithm for high-throughput DNA sequencing, based on graph theory and so on finding the best path to assembling the sequences generated by enzymatic digestion was developed in the early eighties (Kozak 1984). Most importantly, the existence of a vast number of repetitive regions will have to be tackled. A large public consortium started to emerge, on the initiative of several prominent scientists such as James Watson. In the late phase of the project, the public consortium was challenged by an independent project generated by Craig Venter.[34] The two projects published the genome draft by one day of interval (Lander et al. 2001; Venter et al. 2001). The quest was both a biological and a human milestone, revealing the necessity of community effort to produce genome-wide data, a goal achievable in both academics and entrepreneurial environment.

Many insights came from the human genome sequence: a surprisingly low amount of genes (20,000), the prominence of repeated sequences, and the significant number of horizontal transfer events from various organisms, including bacteria. Aside from getting a catalogue of genes, non-coding RNA and repeated elements, information from genomes has also allowed testing many hypotheses at genome-scale, such as identification of genetic mutations, the design of probes to further track sequences or performing site-specific mutations. Following Joseph Gall's pioneer method, fluorescent probes were designed to target specific genes (Fluorescence in situ hybridization or FISH) (Langer-Safer et al. 1982; Schardin et al. 1985; Lengauer et al. 1992). FISH has been extensively used to study the regulation of genes in the genome, at given loci. For instance, interaction between genes has been imaged with this technique ('gene kissing', Cremer and Cremer 2001, 2009a, b). Important applications of FISH include the technique of chromosome painting, which aims at using enough probes to be able to see most of the spatial occupancy of a given chromosome.

Today, it is no doubt that interphase chromatin is a very complex structure that has a relationship with the structure of chromosome during metaphase. For instance, the genes remain in the same order along the cell cycle. Nevertheless, during the early days of chromatin research, it was thought that chromosomes become fragmented at the end of the mitosis and clusters together to reform chromosomes at the end of the interphase. Two scientists explored the alternative hypothesis, Rabl and Boveri, and guessed that chromosomes kept defined positions during interphase, though in a more sophisticated manner as during mitosis (Boveri 1888). This representation of what are now called "chromosome territories" remained marginal for a long time. When the nucleus architecture was better studied using higher levels of magnification, with the advancement of the electron microscopy, interphase nucleus began to be described in terms of condensed and relaxed chromatin, with the idea that the chromosomes

[34] John Craig Venter (1946—), American biochemist and geneticist, known for contributing to the first sequencing of the human genome.

where highly untangled in the nucleus, and that their precise individual localisation did not matter. Some isolated authors described possible models looking closer to the modern view on chromosome territories (Pollister 1952), but the dichotomy hetero/euchromatin prevailed for long. It is only during the late seventies that the idea that interphase chromosomes occupy certain positions or territories in 3D space started to emerge. The concept was in the air but put aside due to experimental limitations for some decades (Comings 1980).

The first demonstration of the existence of chromosome territories was shown by Stack et al. (1977) using specific chemical treatments, to make the DNA mass appear wherever it is located in the nucleus. At the same time, other regions of the nucleus became characterised, such as the perichromatin region, shown to be the zone experiencing most of the transcription, splicing and eventually repair events (Cremer et al. 1982a, b). Recently, more complex models have been proposed to describe the region between the chromosome territories (described in Fakan 2004; Cremer et al. 2004), some hypothesising for separation of chromosomes, other for intermingling (Branco and Pombo 2006). These interchromosomal regions can potentially recruit genes from different chromosomes to transcription machineries (Osborne et al. 2004; Chakalova et al. 2005; Lanctôt et al. 2007; Cremer and Cremer 2009a, b), while some have shown that the number of transcription factories may be very restricted in adult cells (factories are reviewed in Sutherland and Bickmore 2009).

Several levels of chromatin have been modelled in textbook pictures following EM studies (see Uhlmann 2014; Ozer et al. 2015 for a summary). Some regions, '*clumps of chromatin*', presented in Monneron and Bernhard (1969) and visible in other studies, are regions of loose chromatin or euchromatin, though their apparent localisation is only related to the concept of chromosome territory since recently (Albiez et al. 2006). Indeed, for a long time, apart from the euchromatin/heterochromatin dichotomy, high-order chromatin levels have not been considered. Towards the description of potential high-order structures during interphase, in situ hybridization of entire interphase chromosomes is characterised in Schardin et al. (1985). Though chromosome territories are established, and active regions either messy (Branco and Pombo 2006) or confined to specific regions (Cremer and Cremer 2001), trans-associations between chromosomes are now also known to happen (Spilianakis et al. 2005; Lomvardas et al. 2006).

Increasing complexity of the nucleus has been captured recently using techniques cataloguing interactions between DNA sequences (chromosome conformation capture Dekker et al. 2002). Data have shown interchromosomal interactions to happen preferentially in a short range distance, though the two telomeres of a chromosome may be interacting during interphase (Dekker et al. 2002). Interphase sub-chromosomal domains (topologically associating domains, chromatin loops, etc.) have emerged progressively as an intermediate between the beads-on-a-string level (see next section on epigenetics) and the chromosome territory. Ma et al. (1998) attempted to measure these intermediary levels of complexity via optics before the advent of genomics, hinting for chromosome domains in the range of 1 Mb. HiC data (Rao et al. 2014; Lieberman-Aiden et al. 2009) recently helped to refine the picture and describe more complexities in the chromosome territory regions. It only

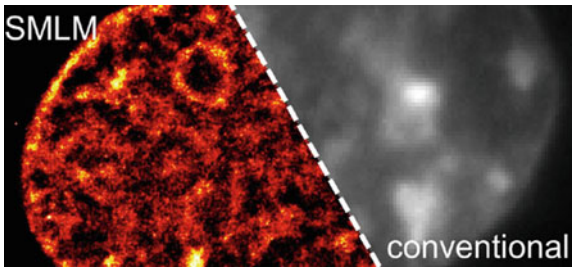

Fig. 1.6 Comparison between recently developed super-resolution microscopy techniques and conventional light microscopy imaging. Chromatin domains are visible on the SMLM only; staining was performed using Vybrant DyeCycle *Violet* DNA dye (Żurek-Biesiada et al. 2015)

recently occurred to scientists that intermediate levels also exist. Before HiC and other techniques, territories of 1 Mb were thought to exist, but only HiC has allowed estimating the distribution of contacts between regions. A more complex picture has come from data showing dynamics of contacts during different phases of the cell cycle (Naumova et al. 2013). Having achieved wide success in generating significant amounts of genomic data, genomics is awaiting validation from microscopy.

Benefiting from advancements in the area of fluorescence microscopy, which include the discovery of properties of the green fluorescent protein (Prasher et al. 1992), and new theoretical frameworks (see Betzig 1995 and Chap. 2 of this work), recent improvements in light microscopy (Hell and Wichmann 1994; Heintzmann and Cremer 1999; Gustafsson 2000; Lidke et al. 2005; Betzig et al. 2006; Rust et al. 2006; Hess et al. 2006; Lemmer et al. 2008; Reymann et al. 2008) have allowed studying the cell nucleus at an unprecedented resolution. These new techniques have been extensively used by Thomas and Christoph Cremer to study chromatin patterns in high resolution (Fig. 1.6), leading to a drastic improvement of chromatin description. Thank to them, chromosome territories are now well described, and a picture of chromatin structure with fundamental functional building blocks of chromatin of about 100–400 nm starts to emerge. These so-called chromatin domains are either associated with high or low transcription, depending on their low or high compaction state, respectively (see Sect. 3.2.3. on this report, Prakash et al. 2015; Boettiger et al. 2016). In case of embryonic cells, these methods have shown that the number of transcription units is much higher than in differentiated cells (i.e. specialized tissues), but surprisingly each of the units contained only one or two molecules (see myoblasts image, Fig. 2 in Smeets et al. 2014), while in non-specialized cells, the machineries in lower number have a broader range of genes to transcribe.

Finally, the dynamics of chromatin during interphase is emerging as a new focus for modelling biological processes. Stimulus-induced chromatin changes have been most of the work on dynamics of chromatin in the pre-genomics area (Jacob and Monod 1961). Stimulation by UV was shown to decrease chromatin extractability, or in more modern words, accessibility (Smith 1962). UV has also shown to induce changes in chromatin localization (Cremer et al. 1982a, b). Movements of chromatin as a possible way to regulate genes has emerged during the seventies, with concepts

such as nuclear matrix[35] (Berezney and Coffey 1976). Understanding the dynamics of nuclear architecture during development has progressed a lot using band painting, to monitor the transition between interphase and mitosis and find relationship between defined chromosome positions in mitosis and the distribution of chromosomes in 3D space during interphase. Contraction and relaxation of chromatin has also captured attention to study the relationship between structure of chromatin and regulation of gene expression (Shilatifard 2006). Recently, application of FRAP has helped to study chromatin dynamics happening in the nucleus (see original method in Axelrod et al. 1976).

1.5 The Substratum of Chromatin Memory: Epigenetic Regulation

The works presented in the previous section have shown that the nucleus contains DNA molecules baring information through a vocabulary of genes, coding for proteins and that this information can be used to respond to external clues. This was a major focus of early molecular biology. In the following decades, up to now, the study of genes and genomes has continuously occupied a prominent place. Nevertheless, researchers have become increasingly aware that genes are not all transcribed at the same time and that the genome needs to modulate their response in space and time. On top of this, it has become more explicit that the spatial disposition of chromatin within the nucleus is essential to modulate the response of the cell to environmental cues. This modulation will be shown to happen through modification of bases of the DNA as well as histone modifications, between other mechanisms summarised under the epithet of epigenetics.

What remains from Jean-Baptiste Lamarck[36] is probably the transmission of information between cells during development, rather than between organisms. Nevertheless, the first statement that can be recognized as an indirect reference to a potential epigenetic regulation of chromatin in a modern sense is the hierarchy of cells during development: “During each cell division on the way from a fertilized egg to an entire organism, each daughter cells obtains one-half of the idioplasm according to mass, but not necessarily according to its quality” (Weismann 1892; Cremer and Cremer 2009b). This is close to the definition of epigenetics. The importance of epigenetics for transcription was taken into account very early in the development of molecular biology. Since the discovery of chromatin and first characterisation of its composition in the nineteenth century, a community of researchers was specifically devoted to study nuclear proteins and their biological importance. Biochemists were nevertheless quite separate from molecular biologists, the latter more focused on high-order processes, while biochemists and chemists by definition focused on the lower scales,

[35] Nuclear matrix: nuclear cytoskeleton thought to be involved in chromatin dynamics.

[36] Jean-Baptiste Lamarck (1744–1829), French naturalist and biologist, most known for his ideas on evolution and inheritance of acquired characteristics.

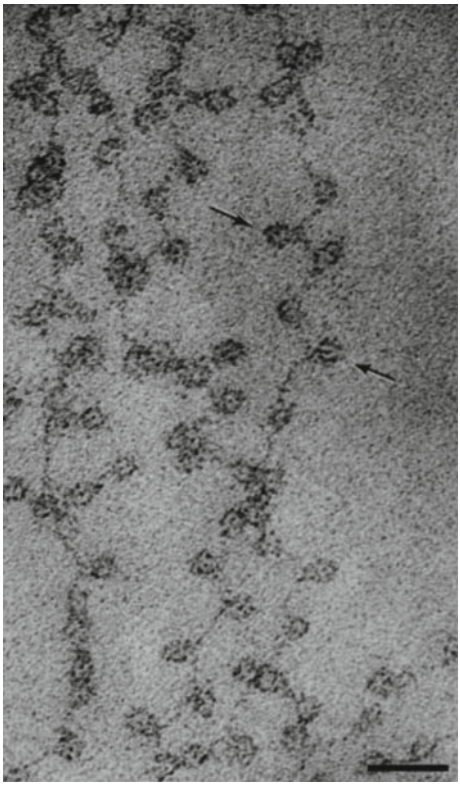

Fig. 1.7 The beads on a string: *in vitro* visualization of nucleosomes punctating DNA. Scale bar: 30 nm. (Olins and Olins 2003)

on entities such as nucleic acids or enzymes (Hurwitz 2005). The composition of histone became characterised in great details by biochemists (Stedman and Stedman 1951). They helped to show that histones can inhibit the work of RNA polymerases, and hypothesised that they have a role in compaction.

Biochemical analysis had shown that histones can be acetylated or methylated, an observation relatively easy to obtain given the small size of the proteins. A relationship between this post-translational modification (both acetylation and methylation) and gene transcription was described very soon after the theorization of messenger RNA (Allfrey et al. 1964). Allfrey and colleagues showed that upon mild acetylation, histone proteins lose their capacity to inhibit the work of RNA polymerase. In the seventies, the first EM images of nucleosomes were published and revealed the nanoscale structure of chromatin (Fig. 1.7).

Histone modifications and DNA methylation were later shown to recruit factors. In this last case, the first proof of DNA methylation binding protein was presented by Meehan et al. (1989), a study showing for the first time a protein binding methylated CG dinucleotides. Another important notion of chromatin architecture and its accessibility stems in the historical dichotomy between euchromatin and heterochromatin. More recent works have proven that epigenetic marks (acetylations or methylations)

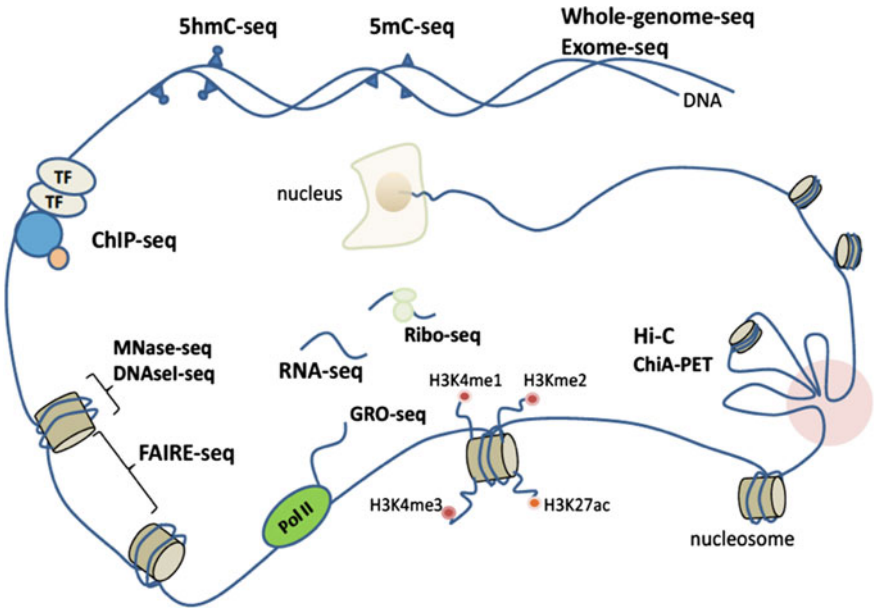

Fig. 1.8 Different genomic methods to study chromatin. The ever expanding range of next-generation sequencing technologies is portrayed. A number of modern sequencing approaches have opened new possibilities to analyse epigenetics at different organisation levels and study various gene regulatory mechanisms. Furthermore, these methods offer numerous opportunities for super-resolution microscopy. *Image courtesy* Wolf Gebhardt

are not evenly distributed in the chromatin and that one can find marks associated with regions visually more condensed and others to regions more relaxed. Findings from recent superresolution experiments have helped to describe epigenetic patterns in interphase for active and inactive X chromosomes, showing that clusters of activating and inactivating histone modifications anti-correlate (Zinner et al. 2007; Cremer et al. 2015). These findings have confirmed patterns already found previously in mitosis or using assays such as ChIP-seq (Barski et al. 2007). What remain to be confirmed are the domains and loops detected with HiC data (Rao et al. 2014). Imaging will aim at confirming the reality of these loops and domains and see if more patterns can be found using pure visual methods. Work from Chandra et al. (2012) and more recently (Boettiger et al. 2016) going in this direction have shown that functional chromatin domains can either display a condensed or relaxed configuration, with different epigenetic signatures associated in each case. An overview of various genomic methods to study chromatin at different length scales is shown in Fig. 1.8.

As the ROM (Random Access Memory) of chromatin, epigenetic regulation is right now one of the hottest topic in biology. While the mechanisms that guide a resting cell have been extensively studied, the way the chromatin architecture adapts to its environment is very little studied. For instance, how long a stress can

be recorded by a cell? Does chromatin learn from previous cues to adapt better to the next situation? Moreover, how chromatin architecture changes from mother to daughter cell during development, based on surrounding environment?

1.6 Fine-Scale Chromatin Architecture: A New Modelling Area

In the last years, a new way of analysing chromatin has emerged, following data from *in situ* hybridization and HiC technique. Biophysicists have started to find patterns and trends in available data to describe possible orders of chromatin that have escaped attention until now. Chromatin is now being viewed as a self-organizing structure (Misteli 2001; Karsenti 2008; Rajapakse and Groudine 2011). Contrary to an object which just folds according to pure Brownian motion and finds its structure by the random association of its separate parts, a self-organised object requires the external intervention of compounds (for instance enzymes) that constrain its parts into adopting a structure not formed by chance. In the case of DNA, these elements could be either transcription factors, epigenetic modifications or their interactors. The key is then to get an overview of the different actors, how they interact with DNA to modify its shape. Though still in its theoretical stage, this research has brought some insights in the recent years.

A recent study defines chromatin states as 'binders' (such as CTCF) and 'strings' (DNA molecules) (Barbieri et al. 2012). In this configuration, binders are in solution and find their targets driven by Brownian movements. Ideally, these binders will target DNA at one unique location. Nevertheless, if a binding site is present at different places in relative close locations on a chromosome, DNA may bind several of them together and form a cluster. The concept matches HiC data, and can explain several known complexity levels of chromatin architecture (chromatin loops, chromatin domains, chromosome territories). Tom Misteli has recently proposed a genome-wide imaging, HIPmap; that is currently being set up to validate HiC contact maps with microscopy (Shachar et al. 2015). Finally, some recent models have also attempted to study the dynamics of chromatin. For instance, a model by Sanborn et al. (2015) describes activation of genes as loops forming through cohesin rings and popping out of chromosome territories to enter a compartment containing transcription machineries (Fig. 1.9).

The existence of the higher level of chromatin compaction, the chromosome territory, has long been oblivious to scientists. Modelling helps to integrate data and see to which kinds of architecture the distributions of contacts could fit (Barbieri et al. 2012). Recent models show a new creativity emerging among biologists to describe chromatin accurately, with the help of concepts from external disciplines such as polymer physics. A lesson from this research is that morphology and structural organisation of mitotic chromosomes might be structurally related to interphasic chromosome territories. One can speculate that there are even more analogies and that

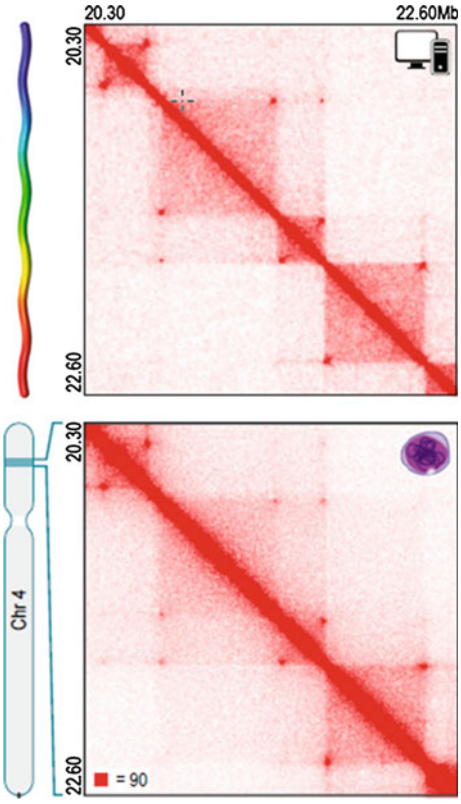

Fig. 1.9 Comparison between predicted data and experimental data in the genomic era. The experimental results (*bottom panel*) were generated using HiC method and show localization of contacts between chromosome regions, an information important to model the 3D structure of the chromatin. The model in the first panel predicts contacts based on dynamic modelling of chromatin folding. In both cases, the *red dots* show the putative contacts. Image modified from Sanborn et al. (2015)

studying either mitotic (or meiotic, as I will discuss later) or interphase stage of the cell cycle will help to get information about the other stages of the cell cycle. In any case, a strong validation of proposed models, both with genomics and microscopy, is urgently needed.

1.7 Conclusion

The history of chromatin research provides numerous lessons for research. One of them is the necessity to put forward theories, even if they prove later wrong. Another lesson is obviously the need to put forward the development of new technologies. Though paradoxically, often, new technical insights come from new questions. For instance, how Morgan decided to study DNA to learn about evolution was a beautiful example of perfect experimental design focused on answering a big theoretical question. Lastly, from Watson and Crick to recent insights in the fields of genome architecture, modelling has emerged as a necessity to describe properly chromatin

structure and behaviour. Direct observation is only useful if it is linked to genomic data, and as such requires the help of physical models to make sense of the complex available information.

Chromatin has been explored using various methods (light microscopy, biochemistry, histochemistry, genomics) but the usage of these methods was blinded by the fact that scientists thought that investigation of interphase chromatin was a dead end, that there was nothing to learn beyond nucleosomes and euchromatin/heterochromatin dichotomy. Later stages of research have shown that the picture was more complex. Firstly, in situ hybridization experiments have shown repeated regions, meaning that there are non-coding regions between genes. Chromosome territories have then revealed a compaction at the high order in the nucleus, which was no longer considered as a spaghetti dish. Moreover, recently, information coming from next-generation sequencing, chromosome capture and hybridization methods have shown even more complexity. New concepts emerge, such as chromatin loops, chromatin domains, which were unknown before. This research is relatively new, and despite thinking of pioneers (Cremer and Cremer 2001, 2009a, b), one has to understand that the idea that chromosome functionalities are compartmentalised in the interphase nucleus is relatively new to biological research.

The questions that challenge the researchers now are: how much of the complexity is still to know? Are there functional domains that one is not aware of yet? And can single-molecule imaging help us in this task? This is the question that I have tried to answer in the work presented here.

Acknowledgments This chapter is an outcome of many discussions with David Fournier, who has helped immensely in formulating and revising the text.

References

Albiez H, Cremer M, Tiberi C, Vecchio L, Schermelleh L, Dittrich S, Küpper K, Joffe B, Thormeyer T, von Hase J et al (2006) Chromatin domains and the interchromatin compartment form structurally defined and functionally interacting nuclear networks. Chromosom Res 14(7):707–733

Allfrey VG, Faulkner R, Mirsky AE (1964) Acetylation and methylation of histones and their possible role in the regulation of rna synthesis. Proc Natl Academy Sci United States Am 51(5):786

Avery OT, MacLeod CM, McCarty M (1944) Studies on the chemical nature of the substance inducing transformation of pneumococcal types induction of transformation by a desoxyribonucleic acid fraction isolated from pneumococcus type iii. J Exp Med 79(2):137–158

Axelrod D, Koppel DE, Schlessinger J, Elson Ei, Webb WW (1976) Mobility measurement by analysis of fluorescence photobleaching recovery kinetics. Biophys J 16(9):1976

Baker JR (1949) The cell-theory: a restatement, history, and critique. Q J Microsc Sci 3(9):87–108

Barbieri M, Chotalia M, Fraser J, Lavitas L-M, Dostie J, Pombo A, Nicodemi M (2012) Complexity of chromatin folding is captured by the strings and binders switch model. Proc Natl Academy Sci 109(40):16173–16178

Barski A, Cuddapah S, Cui K, Roh TY, Schones DE, Wang Z, Wei G, Chepelev I, Zhao K (2007) High-resolution profiling of histone methylations in the human genome. Cell 129(4):823–837

Beadle GW, Tatum EL (1941) Genetic control of biochemical reactions in neurospora. Proc Natl Academy Sci United States Am 27(11):499

Berezney R, Coffey DS (1976) The nuclear protein matrix: isolation, structure, and functions. Advances Enzyme Regul 14:63–100
Betzig E (1995) Proposed method for molecular optical imaging. Opt Lett 20(3):237–239
Betzig E, Patterson GH, Sougrat R, Lindwasser OW, Olenych S, Bonifacino JS, Davidson MW, Lippincott-Schwartz J, Hess HF (2006) Imaging intracellular fluorescent proteins at nanometer resolution. Science 313(5793):1642–1645
Boettiger AN, Bintu B, Moffitt JR, Wang S, Beliveau BJ, Fudenberg G, Imakaev M, Mirny LA, Wu C-T, Zhuang X (2016) Super-resolution imaging reveals distinct chromatin folding for different epigenetic states. Nature 529(7586):418–422
Boveri T (1888) Zellen-Studien: Die Befruchtung und Teilung des Eies von Ascaris megalocephala. Verlag von Gustav Fischer
Boveri T (1904) Ergebnisse über die Konstitution der chromatischen Substanz des Zellkerns. Verlag von Gustav Fischer in Jena
Boveri T (1909) Die Blastomerenkerne von Ascaris megalocephala und die Theorie der Chromosomenindividualität. Engelmann
Branco MR, Pombo A (2006) Intermingling of chromosome territories in interphase suggests role in translocations and transcription-dependent associations. PLoS Biol 4(5):e138
Busch H (1974) The cell nucleus. Academic Press, New York
Chakalova L, Debrand E, Mitchell JA, Osborne CS, Fraser P (2005) Replication and transcription: shaping the landscape of the genome. Nature Rev Genet 6(9):669–677
Chandra T, Kirschner K, Thuret J-Y, Pope BD, Ryba T, Newman S, Ahmed K, Samarajiwa SA, Salama R, Carroll T et al (2012) Independence of repressive histone marks and chromatin compaction during senescent heterochromatic layer formation. Molecular cell 47(2):203–214
Chargaff E, Lipshitz R, Green C (1952) Composition of the desoxypentose nucleic acids of four genera of sea-urchin. J Biol Chem 195(1):155–160
Comings DE (1980) Arrangement of chromatin in the nucleus. Hum Genet 53(2):131–143
Cremer T, Cremer C (2001) Chromosome territories, nuclear architecture and gene regulation in mammalian cells. Nature Rev Genet 2(4):292–301
Cremer T, Cremer C (2009a) Rise, fall and resurrection of chromosome territories: a historical perspective part ii. fall and resurrection of chromosome territories during the 1950s to 1980s. part iii. chromosome territories and the functional nuclear architecture: experiments and m. Eur J Histochem 50(4):223–272
Cremer T, Cremer C (2009b) Rise, fall and resurrection of chromosome territories: a historical perspective. part i. the rise of chromosome territories. Eur J Histochem 50(3):161–176
Cremer T, Cremer C, Baumann H, Luedtke EK, Sperling K, Teuber V, Zorn C (1982a) Rabl's model of the interphase chromosome arrangement tested in chinise hamster cells by premature chromosome condensation and laser-uv-microbeam experiments. Hum Genet 60(1):46–56
Cremer T, Cremer C, Schneider T, Baumann H, Hens L, Kirsch-Volders M (1982b) Analysis of chromosome positions in the interphase nucleus of chinese hamster cells by laser-uv-microirradiation experiments. Hum Genet 62(3):201–209
Cremer T, Küpper K, Dietzel S, Fakan S (2004) Higher order chromatin architecture in the cell nucleus: on the way from structure to function. Biol Cell 96(8):555–567
Cremer T, Cremer M, Hübner B, Strickfaden H, Smeets D, Popken J, Sterr M, Markaki Y, Rippe K, Cremer C (2015) The 4d nucleome: Evidence for a dynamic nuclear landscape based on co-aligned active and inactive nuclear compartments. FEBS Lett
Crick F, Barnett L, Brenner S, Watts-Tobin RJ (1961) General nature of the genetic code for proteins. Macmillan J Ltd
Dahm R (2008) Discovering dna: Friedrich miescher and the early years of nucleic acid research. Hum genet 122(6):565–581
Dekker J, Rippe K, Dekker M, Kleckner N (2002) Capturing chromosome conformation. Science 295(5558):1306–1311
Fakan S (2004) The functional architecture of the nucleus as analysed by ultrastructural cytochemistry. Histochem Cell Biol 122(2):83–93

Ficq A, Pavan C (1957) Autoradiography of polytene chromosomes of rhynchosciara angelae at different stages of larval development
Flemming W (1882) 1: Beiträge zur kenntnis der zelle und ihrer lebenserscheinungen. iii. Teil. Arch. f. mikr. Anat., Bd 20
Gall JG (1968a) Differential synthesis of the genes for ribosomal rna during amphibian oögenesis. Proc Natl Academy Sci United States Am 60(2):553
Gall JG (1968b) The genes for ribosomal rna during oogenesis. Genetics 61 (1): Suppl–121
Gall JG, Pardue ML (1969) Formation and detection of rna-dna hybrid molecules in cytological preparations. Proc Natl Academy Sci 63(2):378–383
Gurdon JB, Elsdale TR, Fischberg M (1958) Sexually mature individuals of xenopus laevis from the transplantation of single somatic nuclei
Gustafsson MGL (2000) Surpassing the lateral resolution limit by a factor of two using structured illumination microscopy. J Microsc 198(2):82–87
Heintzmann R, Cremer C (1999) Laterally modulated excitation microscopy: improvement of resolution by using a diffraction grating. In: international society for optics and photonics BiOS Europe'98, pp 185–196
Hell SW, Wichmann J (1994) Breaking the diffraction resolution limit by stimulated emission: stimulated-emission-depletion fluorescence microscopy. Opt Lett 19(11):780–782
Hertwig O (1875) Beiträge zur kenntniss der bildung, befruchtung und theilung des thierischen eies... W. Engelmann
Hertwig O (1898) Lehrbuch der Entwicklungsgeschichte des Menschen und der Wirbelthiere. G. Fischer
Hess SL, Girirajan TPK, Mason MD (2006) Ultra-high resolution imaging by fluorescence photoactivation localization microscopy. Biophys J 91(11):4258
Hurwitz J (2005) The discovery of rna polymerase. J Biol Chem 280(52):42477–42485
Jacob F, Monod J (1961) Genetic regulatory mechanisms in the synthesis of proteins. J Mol Biol 3(3):318–356
Karsenti E (2008) Self-organization in cell biology: a brief history. Nature Rev Mol Cell Biol 9(3):255–262
Kossel A (1883) Zur chemie des zellkerns. Zeitschrift für physiologische Chemie 7(1):7–22
Kossel A (1884) Ueber einen peptonartigen bestandtheil des zellkerns. Zeitschrift für physiologische Chemie 8(6):511–515
Kossel A, Kennaway EL (1911) Über nitroclupein. Hoppe-Seyler's Zeitschrift für physiologische Chemie 72(5–6):486–489
Kozak M (1984) Compilation and analysis of sequences upstream from the translational start site in eukaryotic mrnas. Nucl Acids Res 12(2):857–872
Lanctôt C, Cheutin T, Cremer M, Cavalli G, Cremer T (2007) Dynamic genome architecture in the nuclear space: regulation of gene expression in three dimensions. Nature Rev Genet 8(2):104–115
Lander ES, Linton LM, Birren B, Nusbaum C, Zody MC, Baldwin J, Devon K, Dewar K, Doyle M, FitzHugh W et al (2001) Initial sequencing and analysis of the human genome. Nature 409(6822):860–921
Langer-Safer PR, Levine M, Ward DC (1982) Immunological method for mapping genes on drosophila polytene chromosomes. Proc Natl Academy Sci 79(14):4381–4385
Lemmer P, Gunkel M, Baddeley D, Kaufmann R, Urich A, Weiland Y, Reymann J, Müller P, Hausmann M, Cremer C (2008) Spdm: light microscopy with single-molecule resolution at the nanoscale. Appl Phys B 93(1):1–12
Lengauer C, Green ED, Cremer T (1992) Fluorescence in situ hybridization of yac clones after alu-pcr amplification. Genomics 13(3):826–828
Lewis EB (1945) The relation of repeats to position effect in drosophila melanogaster. Genetics 30(2):137
Lidke K, Rieger B, Jovin T, Heintzmann R (2005) Superresolution by localization of quantum dots using blinking statistics. Opt Express 13(18):7052–7062

Lieberman-Aiden E, van Berkum NL, Williams L, Imakaev M, Ragoczy T, Telling A, Amit I, Lajoie BR, Sabo PJ, Dorschner MO et al (2009) Comprehensive mapping of long-range interactions reveals folding principles of the human genome. Science 326(5950):289–293

Lomvardas S, Barnea G, Pisapia DJ, Mendelsohn M, Kirkland J, Axel R (2006) Interchromosomal interactions and olfactory receptor choice. Cell 126(2):403–413

Ma H, Samarabandu J, Devdhar RS, Acharya R, Cheng P-C, Meng C, Berezney R (1998) Spatial and temporal dynamics of dna replication sites in mammalian cells. J Cell Biol 143(6):1415–1425

Meehan RR, Lewis JD, McKay S, Kleiner EL, Bird AP (1989) Identification of a mammalian protein that binds specifically to dna containing methylated cpgs. Cell 58(3):499–507

Miescher F (1871) Hoppe-seyler's medicinisch-chemische untersuchungen. Ueber die chemische Zusammensetzung der Eiterzellen 4:441-460

Miescher F (1874) Die Spermatozoen einiger Wirbelthiere: ein Beitrag zur Histochemie. Birkhäuser

Miescher F (1897) Die histochemischen und physiologischen Arbeiten von Friedrich Miescher. Vogel

Misteli T (2001) The concept of self-organization in cellular architecture. J Cell Biol 155(2):181–186

Monneron A, Bernhard W (1969) Fine structural organization of the interphase nucleus in some mammalian cells. J Ultrastruct Res 27(3):266–288

Naumova N, Imakaev M, Fudenberg G, Zhan Y, Lajoie BR, Mirny LA, Dekker J. Organization of the mitotic chromosome. Science 342(6161):948–953

Olins DE, Olins AL (2003) Chromatin history: our view from the bridge. Nat Rev Mol Cell Biol 4(10):809–814

Osborne CS, Chakalova L, Brown KE, Carter D, Horton A, Debrand E, Goyenechea B, Mitchell JA, Lopes S, Reik W et al (2004) Active genes dynamically colocalize to shared sites of ongoing transcription. Nature Genet 36(10):1065–1071

Ozer G, Luque A, Schlick T (2015) The chromatin fiber: multiscale problems and approaches. Current Opin Struct Biol 31:124–139

Pauling L, Corey RB (1953) A proposed structure for the nucleic acids. Proc Natl Academy Sci 39(2):84–97

Pauling L, Corey RB, Branson HR (1951) The structure of proteins: two hydrogen-bonded helical configurations of the polypeptide chain. Proc Natl Academy Sci 37(4):205–211

Pollister AW (1952) Nucleoproteins of the nucleus. Exp Cell Res Suppl II 59–74

Porter KR, Claude A, Fullam EF (1945) A study of tissue culture cells by electron microscopy methods and preliminary observations. J Exp Med 81(3):233–246

Prakash K, Fournier D, Redl S, Best G, Borsos M, Tiwari VK, Tachibana-Konwalski K, Ketting RF, Parekh SH, Cremer C et al (2015) Superresolution imaging reveals structurally distinct periodic patterns of chromatin along pachytene chromosomes. Proc Natl Academy Sci 112(47):14635–14640

Prasher DC, Eckenrode VK, Ward WW, Prendergast FG, Cormier MJ (1992) Primary structure of the aequorea victoria green-fluorescent protein. Gene 111(2):229–233

Purkyně JE (1830) Symbolae ad ovi avium historiam ante incubationem

Rajapakse I, Groudine M (2011) On emerging nuclear order. J Cell Biol 192(5):711–721

Rao SSP, Huntley MH, Durand NC, Stamenova EK, Bochkov ID, Robinson JT, Sanborn AL, Machol I, Omer AD, Lander ES et al (2014) A 3d map of the human genome at kilobase resolution reveals principles of chromatin looping. Cell 159(7):1665–1680

Reymann J, Baddeley D, Gunkel M, Lemmer P, Stadter W, Jegou T, Rippe K, Cremer C, Birk U (2008) High-precision structural analysis of subnuclear complexes in fixed and live cells via spatially modulated illumination (smi) microscopy. Chromosome Research 16(3):367–382

Rust MJ, Bates M, Zhuang X (2006) Stochastic optical reconstruction microscopy (storm) provides sub-diffraction-limit image resolution. Nature Methods 3(10):793

Sanborn AL, Rao SSP, Huang S-C, Durand NC, Huntley MH, Jewett AI, Bochkov ID, Chinnappan D, Cutkosky Ak, Li J et al (2015) Chromatin extrusion explains key features of loop and domain formation in wild-type and engineered genomes. Proc Natl Academy Sci 201518552

Sanger F(1981) Determination of nucleotide sequences in dna. Biosci Report 1(1):3–18
Schardin M, Cremer T, Hager HD, Lang M (1985) Specific staining of human chromosomes in chinese hamster x man hybrid cell lines demonstrates interphase chromosome territories. Hum Genet 71(4):281–287
Schrödinger E (1945) What is life
Shachar S, Voss TyC, Pegoraro G, Sciascia N, Misteli T (2015) Identification of gene positioning factors using high-throughput imaging mapping. Cell 162(4):911–923
Shilatifard A (2006) Chromatin modifications by methylation and ubiquitination: implications in the regulation of gene expression. Annu Rev Biochem 75:243–269
Smeets D, Markaki Y, Schmid VJ, Kraus F, Tattermusch A, Cerase A, Sterr M, Fiedler S, Demmerle J, Popken J, et al. Three-dimensional super-resolution microscopy of the inactive x chromosome territory reveals a collapse of its active nuclear compartment harboring distinct xist rna foci. Epigenet & Chromatin 7 (8), 2014
Smith KC (1962) Dose dependent decrease in extractability of dna from bacteria following irradiation with ultraviolet light or with visible light plus dye. Biochem Biophys Res Commun 8(3):157–163
Spilianakis CG, Lalioti MD, Town T, Lee GR, Flavell RA (2005) Interchromosomal associations between alternatively expressed loci. Nature 435(7042):637–645
Stack SM, Brown DB, Dewey WC (1977) Visualization of interphase chromosomes. J Cell Sci 26(1):281–299
Stedman E, Stedman E (1951) The basic proteins of cell nuclei. Philos Trans Royal Soc London B Biol Sci 235(630):565–595
Strutevant A (1913) The linear arrangement of six sex-linked factors indrosophila as shown by their mode of association. Mol Gen Genet MGG 10(1):293–294
Sutherland H, Bickmore WA (2009) Transcription factories: gene expression in unions?. Nature Rev Genet 10(7):457–466
Uhlmann F (2014) A silent revolution in chromosome biology. Nature Rev Mol Cell Biol 15(7):431–431
Venter JC, Adams MD, Myers EW, Li PW, Mural RJ, Sutton GG, Smith HO, Yandell M, Evans CA, Holt RA et al (2001) The sequence of the human genome. Science 291(5507):1304–1351
Watson J (2012) The double helix. Hachette, UK
Watson JD (1963) Involvement of rna in the synthesis of proteins. Science 140(3562):17–26
Watson JD, Crick FHC et al (1953) Molecular structure of nucleic acids. Nature 171(4356):737–738
Weismann A (1892) Das Keimplasma; eine Theorie der Vererbung. Fischer
Zinner R, Teller K, Versteeg R, Cremer T, Cremer M (2007) Biochemistry meets nuclear architecture: multicolor immuno-fish for co-localization analysis of chromosome segments and differentially expressed gene loci with various histone methylations. Advances Enzyme Regul 47(1):223–241
Żurek-Biesiada D, Szczurek AT, Prakash K, Mohana GK, Lee H-K, Roignant J-Y, Birk U, Dobrucki JW, Cremer C (2015) Localization microscopy of DNA in situ using vybrant dyecycle violet fluorescent probe: A new approach to study nuclear nanostructure at single molecule resolution. Exp Cell Res

Chapter 2
Investigating Chromatin Organisation Using Single Molecule Localisation Microscopy

My intention is not to replace one set of general rules by another such set: my intention is, rather, to convince the reader that all methodologies, even the most obvious ones, have their limits.
Paul Karl Feyerabend

2.1 Introduction

In this chapter,[1] I discuss the technical details of single molecule localisation microscopy (SMLM) to investigate spatial and temporal organisation of DNA. The DNA is hierarchically folded at multiple levels to become more compacted and functionally organise itself inside of the nucleus. This spatial arrangement in turn affects the functionality of DNA. Thus one can characterise the organisation of chromatin into three inter-related categories: (1) the basic building blocks, (2) the functional organisation of chromatin and (3) the spatial arrangement of chromatin inside the cell nucleus.

The two classical building blocks: beads-on-a-string and 30 nm chromatin fibre have been extensively studied by EM (Fig. 2.1, first column). Furthermore, one can view functional chromatin domains (Fig. 2.1, second column) as an emerging building block of chromatin, responsible for its basic functions. I estimate these domains to be about 100–400 nm, according to the literature and my own work (see Chap. 3 on interphase chromatin and Prakash et al. 2015; Boettiger et al. 2016; Rao et al. 2014 for more details). These domains are usually the place of chromatin regulation and can display several configurations, depending on their compaction (Fig. 2.1, second column). These compaction states are often associated with different kinds of

[1]Parts of this chapter, including figures and captions, are based on the following publications: Szczurek et al. 2014; Żurek-Biesiada et al. 2015, 2016; Hagmann et al. 2014; Best et al. 2014.

K. Prakash, *Chromatin Architecture*, Springer Theses,
DOI 10.1007/978-3-319-52183-1_2

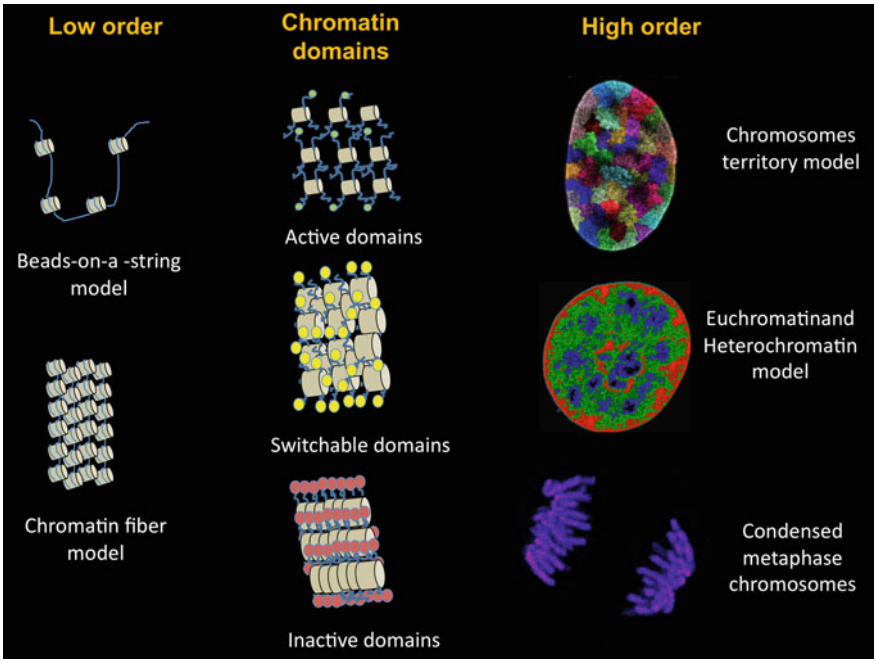

Fig. 2.1 Chromatin spatial organisation: The spatial organisation of chromatin can be studied at three levels: at the lowest orders, which include the beads-on-a-string model and the chromatin fiber, at the level of functional chromatin domains and at high order chromatin patterns. The functional organisation of chromatin domains can be modeled from perspective of various post-translational histone modifications. Depending upon the kind of modification it is enriched with, chromatin can be either highly condensed, in an open conformation or switch between these two extreme forms. The spatial arrangement of chromatin can also be viewed from three points of views: the chromosome territory model of DNA organisation, the bimodal classification condensed and open chromatin in hetero- and eu-chromatin, and finally the highly condensed configuration during metaphase

post-translational histone modifications and can be characterised using information from these modifications (Prakash et al. 2015; Boettiger et al. 2016). Domains can either be highly condensed (usually baring H3K9me3 modification, a mark associated to the presence of transcriptionally inactive repeated regions) or in an open conformation (mostly at gene promoters and intergenic regions, showing enrichment for H3K4me3, a mark associated to active chromatin). Moreover, chromatin can also be in a state where it switches between these two extreme forms as these domains can also coexist very close to each other (see Chandra et al. 2012; for an overview of the different configurations of chromatin domains using microscopy and genomic data, see Fig. 3.16). Higher orders of chromatin folding, above the chromatin domains, include: the rather outdated bimodal classification of chromatin into condensed and open regions (heterochromatin and euchromatin), the chromosome territory model of DNA organisation (Cremer and Cremer 2001) and finally the highly condensed configuration of the metaphase chromosome (Fig. 2.1, last column).

As chromatin has a highly complex shape, theoretical models are limited to describe its functional structure. Moreover, the organisation of its basic building blocks, the functional and spatial domains, lies between what can be achieved by conventional light microscopy (LM) and electron microscopy (EM). Although EM has provided considerable insights into the structure and organisation of chromatin, as it is not DNA specific, it fails at capturing the underlying nature of the patterns observed. Moreover, sample preparation for EM includes harsh chemical cross-linking and vacuum treatment, which also influence the sample. Light microscopy techniques can be used to study protein and chromatin function in live cells but these methods suffer from much lower resolution than EM.

Super-resolution light microscopy provides an interesting alternative to EM that fills the gap between the resolution achieved by a conventional microscope (Abbe 1873; Rayleigh 1896) and the one required to resolve the individual chromatin domains. The first attempts to improve the resolution used confocal (Cremer and Cremer 1978; Sheppard and Wilson 1981) and multiphoton microscopy (Zipfel et al. 2003), allowing for effective background suppression. The advent of various super-resolution methods (Hell and Wichmann 1994; Heintzmann and Cremer 1999; Gustafsson 2000), in particular, Single Molecule Localisation Microscopy (SMLM) based methods (Betzig et al. 2006; Hess et al. 2006; Rust et al. 2006; Lemmer et al. 2008) have allowed to study objects whose structure lies below the diffraction limit.

2.2 Single-Molecule Localization Microscopy: State-of-the-Art

2.2.1 Principle of SMLM

The underlying principle of most SMLM based methods is to label proteins or DNA/RNA with fluorescent molecules that can reversibly switch between a fluorescent state and a stable dark state. This process of switching between states is called 'blinking', and allows for optical isolation of single molecules. Since only a fraction of molecules will switch back to the fluorescent state at a given time, their precise location can be determined. The final accuracy of the position of a molecule depends on the number of detected photons. With a photon count of 10^4 in a single glowing phase, one can achieve a resolution down to a few nanometers (Thompson et al. 2002). In Fig. 2.2, many such molecules are separated by a distance less than $\lambda/(2NA)$ and if all of them are 'on' simultaneously then one cannot resolve them. However, if only a few of them are 'on' while the neighbouring molecules are in dark state, they can be optically isolated and their precise position can be determined (see Fig. 2.2). Subsequently, if one collects a series of such images where only a few of the molecules are 'on' in each image and localise their position, then a final image revealing the structure of the underlying object can be reconstructed (Small and Parthasarathy 2014).

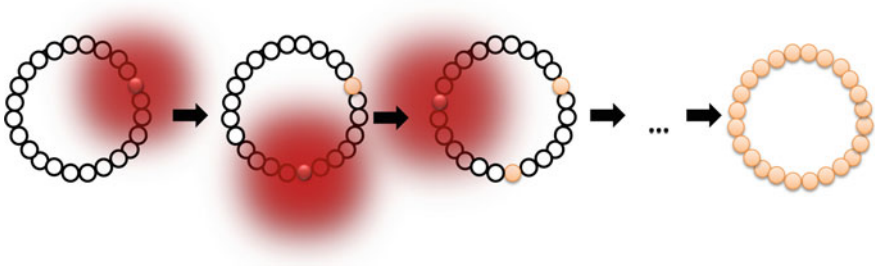

Fig. 2.2 Schematic illustration of the underlying principle of SMLM using a hypothetical object whose building blocks lie below the diffraction limit. This object is made of point sources indicated by *black circles*. Photons emitted by these point sources such as biological molecules or fluorophores are smeared out onto the detector of the imaging system due of the wave nature of light. This distribution of photons is commonly known as the point spread function (PSF) of the imaging system (indicated by the shadow in *red*). PSF has a width of $\lambda/(2NA)$, where λ is the wavelength of the fluorescent light and *NA* is the numerical aperture. Repeated imaging and localisation of indiviual fluorophores provides high resolution image of the diffraction limited object if one approximates the position of the molecule as the center of the spot. The photons in the airy disk, which is the central region of the PSF, are thought to have a repartition that follows a Gaussian distribution if the point source emits a sufficient number of photons (Sengupta et al. 2014; Uno et al. 2014)

2.2.2 The Different SMLM Methods: A Historical Perspective

Optical isolation of individual molecules in order to circumvent the resolution limit by acquiring signals at different times has been first theorized in 1985 (Burns et al. 1985), and later included in a comprehensive framework by Eric Betzig of what is now known under name single molecule localisation microscopy (Betzig 1995). Historically, SMLM was first used outside of the chromatin field. Early design by Betzig was successfully applied in 2006 (Betzig et al. 2006) to study cell architecture in a set-up called Photo-activated localization microscopy (PALM). PALM uses two lasers to provoke the blinking of GFP molecules necessary for single molecule microscopy. The first laser (561 nm) is used as the excitation laser while the second laser (405 nm) is used as the activation laser (see (Sengupta et al. 2014) for a review). The structures imaged showed similar level of resolution as electron microscopy, but helped to mark very precisely the position of given proteins on top of the EM image. Set-ups such as STORM (STochastic Optical Recovery Microscopy) use Cy5–Cy3 dye pair as a switch to optically isolate molecules whose separation is below Abbe's limit. Firstly, all Cy5 molecules are pushed to dark state with a red laser (633 nm) and then a green laser (532 nm) is used to bring a fraction of Cy5 molecules to the florescent state. Though there is no fluorescence from Cy3 itself, a close presence to Cy5 is required for Cy5 to recover from the dark state to a fluorescent emitting state (Rust et al. 2006). dSTORM (direct STORM), a method which extends early observations by (Rust et al. 2006; Lemmer et al. 2008) uses only one laser to push a conventional fluorochrome, for instance Alexa647, between dark and fluorescent

state (Heilemann et al. 2008). Below, I briefly summarize various approaches that led to development of SMLM in its current working form.

- First theoretical approaches: (Burns et al. 1985; Betzig 1995)
- First practical approaches:

  1. Blinking of single molecules (Hirschfeld 1976; Moerner and Kador 1989; Shera et al. 1990; Xie et al. 1994)
  2. Blinking of GFP (Dickson et al. 1997)
  3. Blinking of quantum dots (Lidke et al. 2005)
  4. (fluorescence) Photo-activated localization microscopy (PALM/fPALM, Betzig et al. 2006; Hess et al. 2006)
  5. Stochastic Optical Reconstruction Microscopy (STORM, Rust et al. 2006)

- Methods using standard fluorophores:

  1. Spectral Precision/Position Distance/Determination Microscopy (SPDM, Van Oijen et al. 1998; Lemmer et al. 2008, 2009)
  2. direct Stochastic Optical Reconstruction Microscopy (dSTORM, Heilemann et al. 2008)
  3. Bleaching/blinking assisted localization microscopy (BaLM, Burnette et al. 2011)

- Methods based on binding activation and kinetics: Binding-activated localization microscopy (BALM, Schoen et al. 2011)

Herein, I employed SPDM, the method initiated by (Lemmer et al. 2009) and now known as dSTORM (Heilemann et al. 2008). This method uses a single laser to induce both photoconversion and blinking of a single fluorochrome in one excitation event. This technique was helpful in obtaining a detailed distribution of chromatin, various protein elements and histone modifications, in interphase nuclei (Chap. 3) and during meiosis (Chap. 4). This simple set-up not only enables the analysis of biological samples with the fluorophores used to image DNA molecules in conventional microscopy, but also allows for multi-modal imaging, which can then be used to compare or combine with the results obtained from other microscopic techniques. In this thesis, I discuss various technical aspects of SMLM applied to standard DNA dyes to study chromatin organisation.

2.3 Application of SMLM to Image Chromatin

Chromatin has been a rather recent focus in the field of SMLM. The nano-structure of interphase chromatin was first studied by (Bohn et al. 2010) using SMLM. Statistical methods were combined with SMLM to study the distribution of histone H2B in HeLa and VH7 diploid human fibroblast cells. The main question posed by this study is the possibility of the existence of a recurrent universal chromatin nano-domain and if it can vary across the cell lines and the cell cycle. The author reported

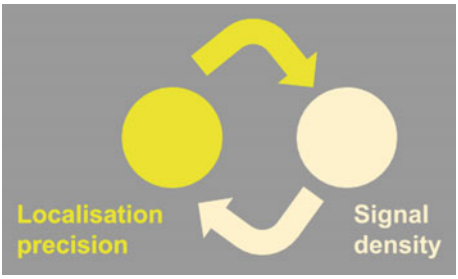

Fig. 2.3 The tao of single molecule microscopy: The two key aspects around which localisation microscopy revolves are localisation precision and signal density. The true representation of the underlying structure is reached when localisation precision and signal density are sufficiently high. Bright fluorophores are required for good localisation precision while for a good signal density, it required to have only a few of them in each frame which is compensated by acquiring a largenumber of frames

that chromatin nano-structure is cell type specific and is dependent on the way the chromatin is labelled. A similar conclusion was reached by a recent study (Ricci et al. 2015). Before I probe further into the limitations of these two studies, I would like to discuss two concepts that are central to localisation microscopy: localization precision and signal density.

2.3.1 The Tao of SMLM

Two key aspects of SMLM imaging are localisation precision and signal density. Figure 2.3 shows the interplay between these factors. While the bright fluorophores i.e. fluorophores with high photon count are good for localization precision ($\propto \frac{1}{\sqrt{N}}$, where N is the number of photons), it is highly desired to have only a subset of them 'on' in each frame (amount of localized events per unit area). To achieve low signal density for each frame, the lifetime of the dark state needs to be significantly longer than the lifetime of the bright state. The overall high signal density (amount of localized events per unit area) is achieved by acquiring a large number of frame so that the theoretical density of the underlying sample is matched.

2.3.2 Importance of a Good Localization Precision in Order to Improve Resolution

The resolution of a final reconstructed image in localisation microscopy can be attributed to two separate causes. The first is the fact that like any measurement of a physical quantity, the true value to be measured is only approached at an infinite

number of measurements. Since the photon count of the localization of a fluorophore is limited, the precision with which the fluorophore location can be predicted is limited too. In this analogy a single measurement corresponds to telling which pixel on the light sensitive array was struck by one single photon. Only with the ensemble comprising many photons spread over the adjacent pixels, a highly precise location of the signal can be determined. The precision can be calculated using the Cramér–Rao Lower Bound (Neice 2010; Small and Parthasarathy 2014) and is always above $\lambda/(2NA \cdot \sqrt{N})$, with λ the wavelength of the fluorescent light, NA the numerical aperture (Hagmann et al. 2016) and N the number of photons.

The second cause for resolution reduction results directly from the first (the measurement uncertainty): The fact that the uncertainty of a localized event is isotropic makes it literally impossible to tell in which direction the measured position has to be displaced in order to set it to the true location of the fluorophore (Hagmann et al. 2016). It is important to be aware that the measured position of a fluorophore is not its true position but only the one with the highest probability. The quality of this position estimate is reflected by the localization precision (or uncertainty). In other words, if the same measurement would be carried out several times under the exact same conditions, the acquired locations would be slightly displaced for each measurement. The scale of displacement for every single fluorophore is reflected by its individual localization precision, given by

$$\sigma^2 = \frac{s^2 + a^2/12}{N} + \frac{8\pi s^4 b^2}{a^2 N^2}$$

where s is the width of PSF, N is the number of detected photons, b is the background intensity and a is the size of pixels on the camera.

In Fig. 2.4, I demonstrate that with an increasingly poor localisation precision (from 2 to 100 nm), the point-like-object start to overlap resulting in a blurred image where fine features cannot be resolved. Another point worth noting is that while the first image has the lowest uncertainty (2 nm), the images with 10 and 20 nm uncertainty appear the best. This is due to the fact that higher uncertainty covers for the missing signals by blurring with a bigger radius (see Fig. 2.5)

2.3.3 Importance of High Signal Density to Improve Signal-to-Noise Ratio

One of the key to SMLM is its ability to provide structural information at the highest possible resolution among various super-resolution methods. The structural resolution in localisation microscopy depends upon the localisation precision $\bar{\sigma}_{xy}$ of the individual molecules and the local density of the detected molecules is given by the following formula:

$$\sigma_{xy} = \sqrt{(2.35\bar{\sigma}_{xy})^2 + (2\bar{d}_{NN})^2}$$

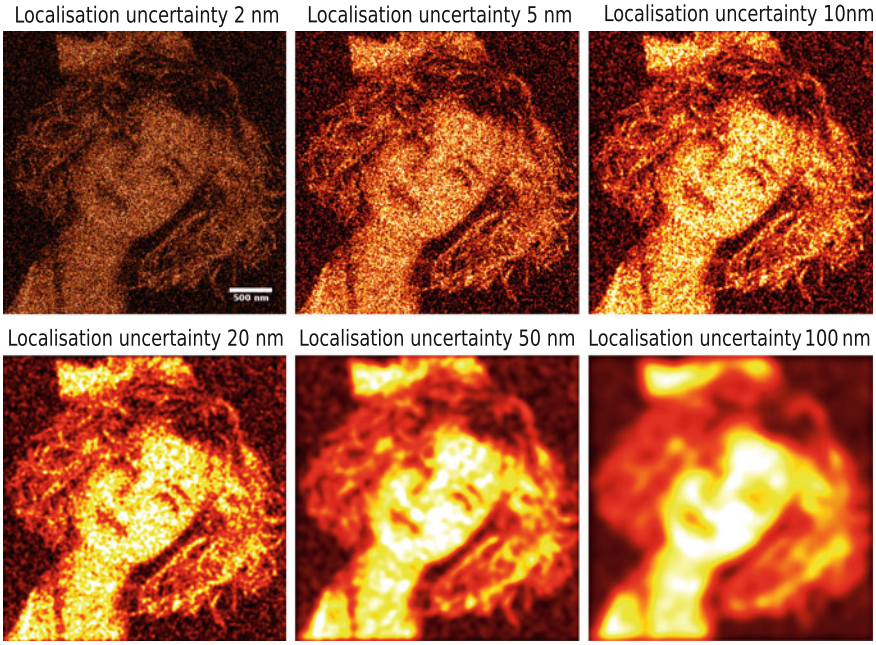

Fig. 2.4 Importance of good localization precision: The measured position of a fluorophore is not its true position but only the one with the highest probability. As the photon budget of a fluorophore is limited, so is the precision with which its position can be localised. In this simulation, I compared the effect of increasing the localisation uncertainty gradually from 2 to 100 nm

$\bar{\sigma}_{xy}$ is the mean lateral localisation accuracy;
$\bar{d}_{NN}$ is the mean distance to the next neighbouring molecules.

The final number of localised signals depends on a number of factors such as labelling efficiency, activation and re-activation frequency and detection efficiency. For example, only a certain percentage of molecules gets labelled and only a subset of these molecules get activated and detected. Furthermore, even a smaller subset of these remaining molecules get reactivated again. This means that only a small subset of the molecules forming the original structure get activated, detected and localised, making it hard to distinguish signals from background. In Fig. 2.5, with 120,000 points one can resolve fine features of Erika's lips (yellow box), while 1000 points are insufficient to draw any satisfactory conclusions. Thus a minimum critical density of signals of at least $\frac{1}{10}$ of the original structure is often required especially if the underlying structure is unknown, a common case for most super-resolution methods. If this is not possible then an intelligent estimate must be made from the prior knowledge based on other studies (for example, EM).

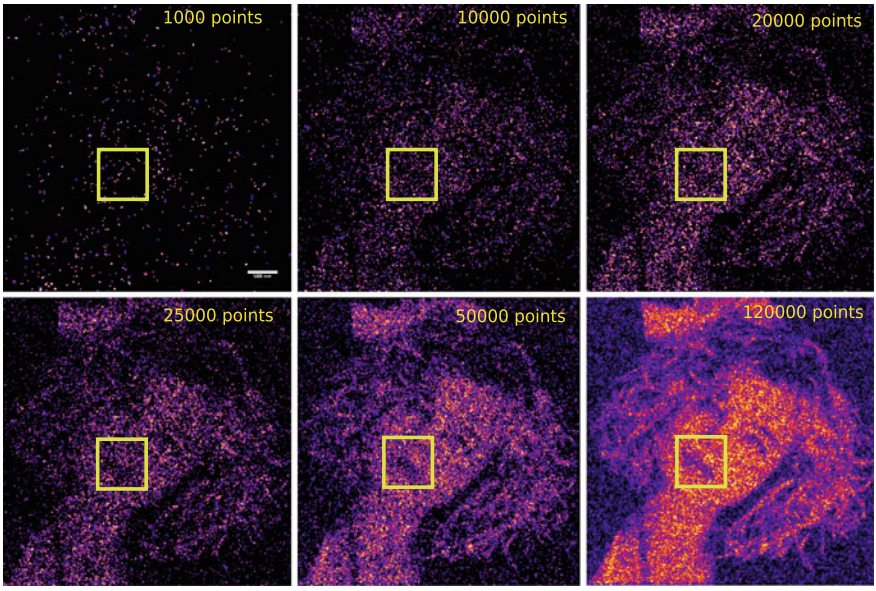

Fig. 2.5 Importance of high signal density: In localisation microscopy, molecules emit fluorescent bursts multiple times before they are bleached (i.e. they stay permanently in dark state), so I use the term 'signals' rather than 'molecules' here. In all 6 images, the signals were sampled with a localisation uncertainty of 10 nm and the number of signals were gradually increased from 1000 to 120,000 points for a 25 μm^2 area. A minimum signal density (signal density means the amount of localized events per area) is required to make a first assessment about the underlying structure

2.3.4 Limitations of Previous Approaches to Study Chromatin Organisation

Human genome has roughly 10^9 base pairs and a spherical nucleus ($\frac{4}{3}\pi r^3$) of 10 μm radius will have an overall volume of approximately 4000 μm^3. Since the cells in culture are relatively flat, one can assume that they show an ellipsoid shape ($\frac{4}{3}\pi r^2 a$) with the axial thickness ($a = 2 - 3\,\mu m$) smaller than the lateral radius ($r = 10\,\mu m$). This would bring down the nuclear volume to roughly 1000 μm^3. Since the observation volume is only a fraction of the total volume, I assume that the final volume of the nuclei imaged would be around 200 μm^3 with an optical section of 500–600 nm axially). So, overall one expects to have around 10^8 putative binding sites/signals in the nuclei. As only a subset of molecules get labelled and are finally detected, the final number of the expected signals is still quite lower. Thus a minimum of 10^7–10^8 signals should be detected in order to get a first accurate representation of chromatin distribution inside the cell nucleus (Szczurek et al. 2014).

In one of the previous studies on chromatin organisation, emGFP conjugated histone protein H2B was expressed (Bohn et al. 2010) while in another similar study (Ricci et al. 2015), H2B was immunostained using Alexa Fluor 647. At present,

both of these studies report a labelling density of 100–500 signals per μm^2 and total identified signals in order of 10^4–10^5. At present, both these studies lack sufficient labelling density to make good estimates about the distribution of chromatin inside the cell nucleus.

Here, I focus on improving the method so that the overall signal density and labelling efficiency of DNA molecules is closer to expected binding sites. In the next section, a simple method which uses direct DNA binding dyes and fulfils the above criteria is presented.

2.4 A Method to Reach High Labelling Density of Chromatin with SMLM

Previous studies of chromatin distribution inside of the cell nucleus have relied on a fluorophore conjugated with antibodies targeting chromatin via core histone proteins (Bohn et al. 2010; Ricci et al. 2015) but none has used direct staining of DNA. Recently it was found that DNA minor groove binding dyes, such as Hoechst and DAPI, can undergo UV-induced photo-conversion, to be effectively employed in single molecule localization microscopy (SMLM) with high optical and structural resolution. A proposed mechanism is that these minor groove DNA dyes undergo intra-molecular proton transfer between the phenol group and the bisbenzimide nitrogen under UV illumination (Cosa et al. 2001; Carvalho 2010). This UV induced photo-conversion leads to a red shift from the blue emitting form to a green emitting form; a second excitation at a higher wave length will push the fluorochrome to a dark state. This situation eventually induces multiple cycles from dark-state to fluorescent state and back to dark state. Fluorescence of these stochastically blinking molecules is registered by illumination with high intensity 491 nm laser, until bleached (i.e. the molecules are permanently in the dark state). It is worth to note that green-emitting forms of both, Hoechst 33,258 and DAPI occur rather sparsely, facilitating the optical isolation of individual dye molecules bound to DNA (Szczurek et al. 2014). To test if the molecules are really photoconverted, SMLM measurements were performed without any prior illumination with 405 nm line. Subsequently, a significantly lower blinking rate in green-yellow channel was observed, resulting in a poor final reconstruction (data not shown). In the reconstruction from these datasets, fine structures of chromatin could not be resolved. However, with low UV excitation (405 nm), a significant increase in number of molecules in blinking state was observed allowing acquisition of more signals. A 630/90 band pass filter was used to record these signals.

Figure 2.6 shows an optimised adjustment of 405/491 nm laser intensities to study the distribution of chromatin inside a HeLa cell nucleus. Compared with previous studies of histone H2B stably expressed with GFP (Bohn et al. 2010), 50 times more signal density was recorded (124 signals per μm^2 for H2B labelling as compared to 5000 signals per μm^2 here). The nucleus stained with Hoechst (Fig. 2.6a) shows

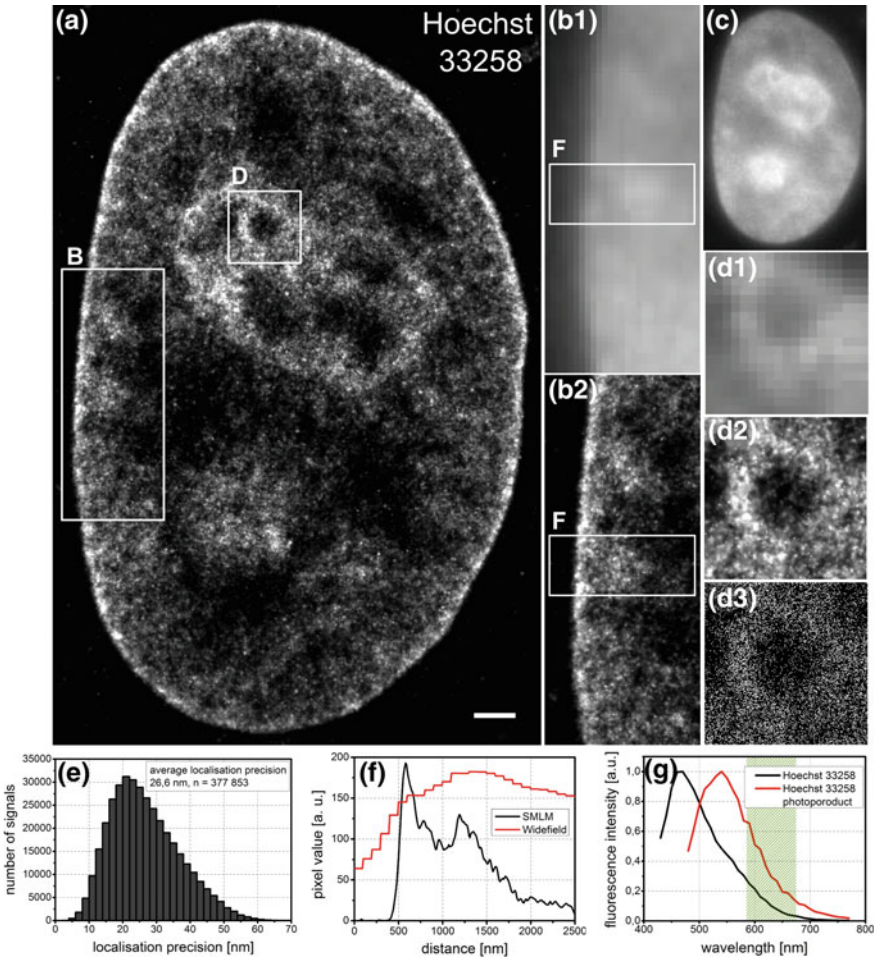

Fig. 2.6 Figure and caption modified from (Szczurek et al. 2014). **a** SMLM image of a HeLa cell nucleus stained with Hoechst 33258. Scale bar: 1 μm. **b1**, **b2** Widefield and SMLM magnifications of the heterochromatin region highlighted in inset (**b**). **c** Complete nucleus in the widefield mode. **d1–d3** Magnified sections of widefield, SMLM and point representation of nucleolus in (**d**). **e** Histogram of localization precision with average precision around 26.6 nm. **f** Profiles of the heterochromatic region in the boxes of insets B1 and B2, comparing widefield and localisation images. **g** Hoechst 33258 excitation spectrum and the emission spectrum shift of its photoproduct. The green interval is the detection band of the photoproduct

higher density of chromatin around the nucleolus and at the periphery of the nucleus likely associated with hetero-chromatin. Furthermore, a lower density of chromatin is observed towards the interior of the nucleus, in line with previous studies (Cremer et al. 2004; Albiez et al. 2006; Cremer et al. 2015).

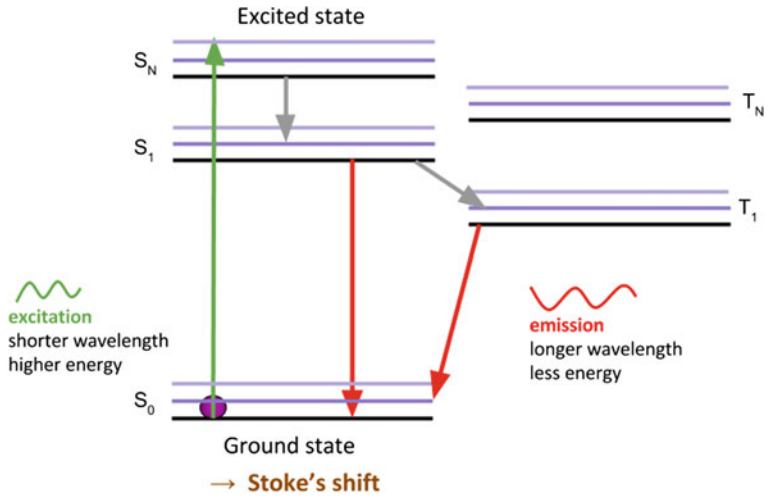

Fig. 2.7 Transitions between excitation states during the fluorescence process. Fluorescence depends on the rapid and lasting rotation between a ground state (electron of low energy) and an excited state (electron of high energy). During relaxation process of the cycle (*red arrow*), a photon is emitted that produces light. With time, electron can reach other intermediate states called triplets (T_1 and T_N here) that can lead to the deteriorative oxidation of the fluorochrome, resulting in bleaching

2.4.1 Theory of DNA Dye Fluorescence

Molecules with multiple aromatic cycles which bind the small groove of DNA, such as DAPI, can potentially emit fluorescence. In solution, the structure of the molecules shows a high flexibility, but while interacting with DNA, they become stabilized and display a planar structure, which enhances the degrees of freedom of circulating electrons across aromatic cycles or other features of the molecule. This situation has both effects of increasing the probability of capturing incident photons, as the surface of the molecule increases, and the probability to observe an electron hit by a photon, as an electron occupies more space at a given time (Biancardi et al. 2013 and Fig. 2.7).

2.4.2 Adapting Study of DNA Dyes Fluorescence to SMLM

Application of blinking properties of DNA dyes to SMLM stems in the photoconversion of individual molecules followed by their excitation to the dark state, a concept pioneered by Betzig using GFP (Dickson et al. 1997; Betzig et al. 2006). The method has two steps:

1. Optimization of photo-conversion, to ensure that the pattern of photo-converted molecules is optimal to generate blinking patterns.
2. Optimization of buffers, to push a higher number of fluorochrome molecules to photo-conversion and delay bleaching of molecules.

2.4.3 *Optimization of the Photoconversion Process*

This step optimizes the amount of molecules photo-converted to obtain high density of signals. The signals are optimally spread in time so that one does not acquire too many signals in a single frame, otherwise one gets unresolved points and poor resolution. To achieve this, the intensity and the timing of photo-conversion, via a 405 nm wave length excitation pushing DAPI or Hoechst to a green form, has to be calibrated properly. If photo-conversion is absent, the final number of detected signals is low and the final reconstruction is impaired (Fig. 2.8).

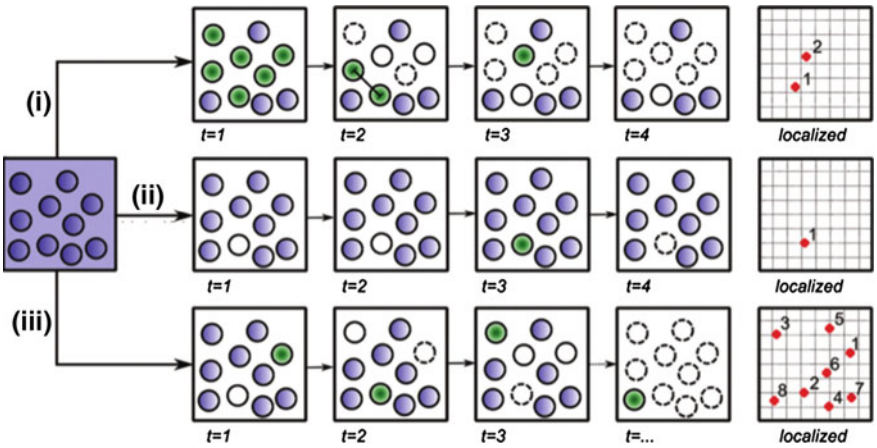

Fig. 2.8 Optimization of the photoconversion process to obtain good resolution and signal density. Obtaining a good blinking pattern is dependent on mild photoconversion. Excessive photoconversion (i) leads to large number of molecules photoconverted and will not be detected along the different frames, preventing optical isolation of single molecules (poor resolution, average density of points). (ii) Insufficient photoconversion separates molecules properly, but does not generate enough signals to reconstruct the initial object (high resolution, low density of points). (iii) An optimized set-up will generate homogenous photoconversion of molecules in time, resulting in both good separation of signals across time points and a high final signal density, allowing a more accurate reconstruction of the initial object (high resolution, high density of points). Figure modified from (Szczurek et al. 2014)

2.4.4 Optimization of the Buffer Conditions

A strong element in the optimization of the protocol to employ conventional DNA dyes for imaging of DNA molecules is the usage of an effective buffer. Usage of mixes with high concentrations of glycerol seems to be the best option according to recent benchmarks (Żurek-Biesiada et al. 2016). Beside preserving the nuclear morphology, glycerol prevents the generation of reactive oxygen species (ROS) from the reaction between the fluorochrome and surrounding dioxide molecules. This reaction releases oxygen atoms with a free radical, which are very hostile for biological molecules such as DNA (Bernas et al. 2004). Glycerol can compete with the fluorochrome for interaction with the free radical, preserving the fluorochrome from degradation (Hussels and Brecht 2011). This results in a better photoconversion than if the DNA dye was subjected to more Brownian movements (Biancardi et al. 2013).

2.4.5 Multicolor Imaging with DNA

To analyse the spatial arrangement of different nuclear proteins with respect to DNA, optimization of various conventional dyes was studied along with DNA dyes and summarised in Fig. 2.9. It is further hoped that the dyes presented in Fig. 2.9 will be optimised to allow the visualization of more fluorochromes within one experiment. This will further enable the analysis of spatial arrangements of various other components of the nucleus in conjunction with chromatin at the level of individual nuclei.

2.4.6 A Summary of Various Approaches Used to Study DNA with SMLM

The strategies to study chromatin inside the cell nucleus can be divided into two broad categories: (1) Direct labelling of DNA and (2) indirect labelling of DNA. Below I provide a brief summary on various approaches that have been used to study chromatin/DNA with SMLM which is pictorially summarised in Fig. 2.10.

- **Direct Staining Methods**

1. **YOYO-1** is a DNA intercalating dye binding between the two strands of DNA. YOYO-1 and PicoGreen (which binds to the major groove) were previously used to study the organisation of bacterial chromosomes with SMLM (Schoen et al. 2011). The authors called this method binding-activated localization microscopy (BALM) because both YOYO-1 and PicoGreen bind directly to the DNA and these molecules only get activated when bound to the DNA. This is a good way to improve both labelling efficiency and localisation accuracy as DNA binding

Fluorophores:		Qualityof blinking in buffer composed of GOX/CAT/Glycerol/10% glucose	Excitation Wavelengths required [nm]:
DNA dyes	DAPI*	++	405 + 491
	Hoechst 33258*	+++	405 + 491
	Hoechst 33342*	+++	405 + 491
	Vybrant dyecycle Violet*	+++	491
Other	Alexa 488	++	491
	Atto 488	+++	491
	Alexa 546	+	561
	Alexa 555$	++	561
	Alexa 568$	+++	561
	Alexa 647*	++++	647 + 491
	Atto 655	+++	647
	Alexa 660*	++	647 + 561
	Alexa 680*	++	671 + (405 / 491 / 561)

Fig. 2.9 Comparison of various DNA dyes and other fluorescent probes. Quality of blinking as well as suitable wave lengths are indicated. Asterisks indicate that blue shift needs only a low excitation to happen. Dollars indicate that dual color imaging can be performed without correction of chromatic shift. Table is reprinted from (Żurek-Biesiada et al. 2016)

increases specificity and is closer to the actual target than antibodies are. These dyes have been shown to work for lambda phage DNA stretches but not for structures which have much higher chromatin density, for example, mammalian cell nuclei. A report of a successful application of YOYO-1/SMLM to staining of eukaryotic nuclei will be presented in Chap. 3.

2. **Hoechst, DAPI and Vybrant Violet (VV)**. Conceptually this is similar to the binding-activated localization microscopy (BALM). DNA minor groove binding dyes such as DAPI or Hoechst do not 'blink' in their standard form. However, with low dose of 405 nm laser, a small proportion of molecules can be photo-converted to green form and start to blink, a property applicable to localisation microscopy. It is proposed that upon UV illumination, these dyes, which either undergo protonation or become photoconverted from blue to green emitting form, might also be driven by hydrogen peroxide (Piterburg et al. 2012). It

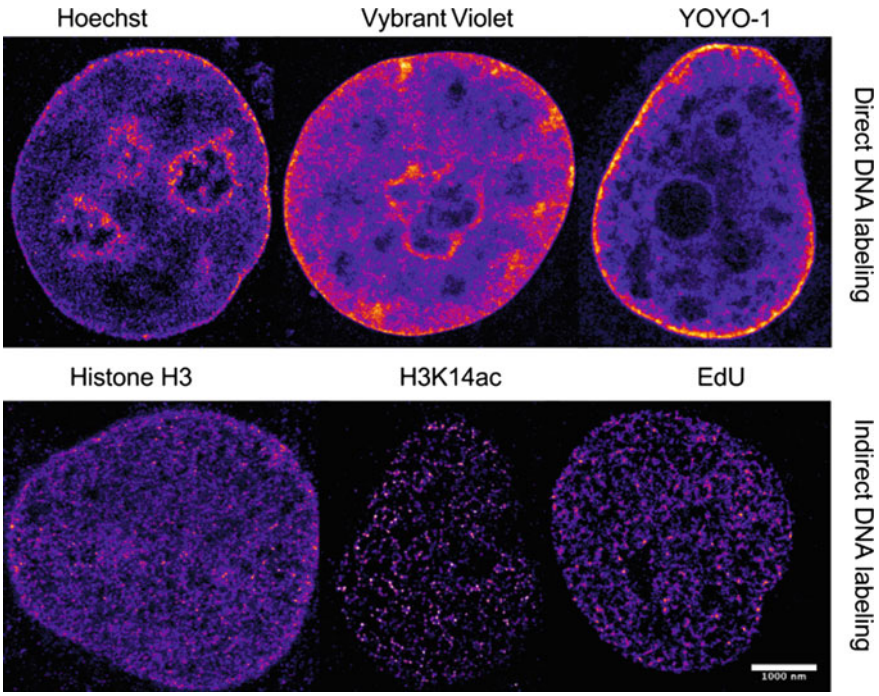

Fig. 2.10 Comparison of direct and indirect DNA labelling. Top block shows various DNA minor groove binding dyes that can be used to study the distribution of the chromatin inside the cell nucleus. *Bottom* block shows examples of indirect methods (immunostaining and EdU incorporation) to study the distribution of chromatin inside the cell nucleus

must be noted that only one wavelength (491 nm) is required for activation and excitation in the case of VV.

3. **Propidium Iodide or DRAQ5** are non-cyanine intercalators that also bind directly to DNA. However, their applicability in superresolution microscopy has yet to be demonstrated.

- **Indirect Staining Methods**

1. **EdU incorporation**: Zessin et al. 2012 were the first to describe a high resolution structure of DNA using precursor incorporation. The authors used EdU (5-ethynyl-2'-deoxyuridine) labelling using click chemistry to image nascent DNA produced during DNA replication. Click-chemistry is a copper-induced covalent binding between an alkyne group of EdU and an azide present in the chemically modified fluorophore (Grammel and Hang 2013). This method has two main advantages. Firstly, it is highly specific. The alkyne-azide bond is not commonly found in any biological system and the method is very specific and sensitive. Because of this specificity, the method produces almost no

background. Secondly, it is less harmful compared to other popular precursors such as BrdU (Baskin et al. 2007; Grammel and Hang 2013).

2. **Core histone proteins**: Bohn et al. 2010 studied chromatin organisation inside the cell nucleus by fusing one of the core histone proteins (H2B) with GFP. In this study, H2B was either stably integrated (H2B-GFP) or over-expressed (H2B-emGFP) in the HeLa cells. In other studies, either immuno-labelling against core histone proteins (H3, H2B) was used or cells were transfected with H2B-mEos2 or H2B-PAmCherry for live cell imaging (Ricci et al. 2015).
3. **Histone modifications**: To study functional chromatin and its compartmentalization, histone modifications were recently used to describe chromatin organisation (Prakash et al. 2015; Boettiger et al. 2016). These two studies were based on antibody labelling of specific histone modifications. The main problem with such labelling methods is the huge size of primary and secondary antibody (molecular weight around 150–200 kDa) and the linker length i.e. the distance between the true position of the molecule and the position where the signal is detected, which can be in the order of 7.5 nm for a primary antibody and in the order of 15 nm for a secondary antibody.

- **Sequence specific imaging of DNA**: It is often desired to study specific loci of gene or other DNA sequences instead of the entire chromatin. This specific staining can be performed using Fluorescence *In Situ* Hybridization (FISH) (Weiland et al. 2011), oligonucleotide probes (Cremer and Cremer 2001; Müller et al. 2010) or via genome editing techniques such as transcription activator-like effectors (TALE), (Miyanari et al. 2013; Thanisch et al. 2013) CRISPR/Cas9 techniques (Anton et al. 2014; Chen et al. 2013; Wood et al. 2011; Hsu et al. 2014; Doudna and Charpentier 2014) or SNAP-tag fusion proteins (Klein et al. 2011).

Figure 2.10 compares the overall staining of the cell nucleus with direct and indirect staining. One can observe that direct staining of DNA leads to a more continuous distribution of chromatin as compared to indirect staining, where the distribution seems to be in a speckle-like patterns (see also Bohn et al. 2010; Ricci et al. 2015 for recent examples of low labelling density). This happens because in specific staining only the functional compartments, usually associated to specific histone modifications, are revealed. For example, H3K14ac is associated with active transcription and hence only sites where chromatin is in a more open conformation fluoresce. Similarly, in EdU incorporation (Fig. 2.10, bottom right) only the freshly replicated sites from S-phase are detected (see Chap. 3 for more examples of these two cases).

2.5 SMLM Microscope Design and Imaging Pipeline

The basic set-up for SMLM imaging is very similar to the configuration of a wide-field microscope. In the following sections, various aspects of the SMLM such as sample preparation, data acquisition, data reconstruction, data visualisation and data analysis are discussed.

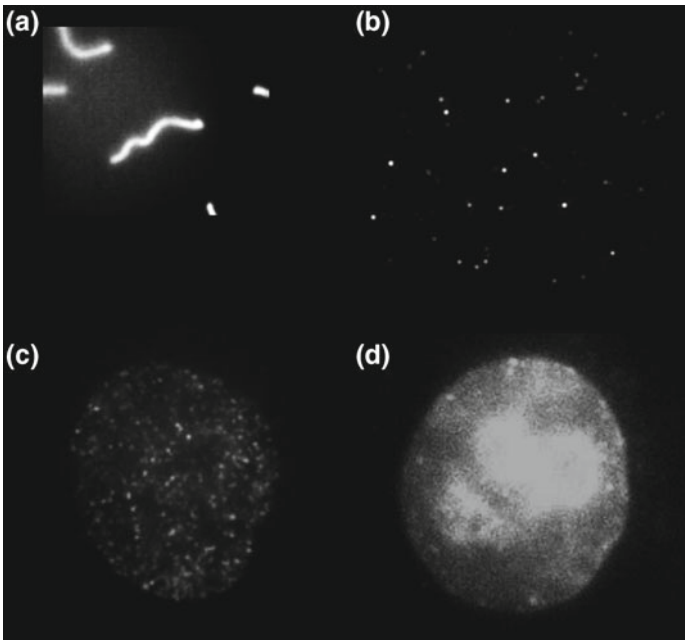

Fig. 2.11 Different kinds of background in a SMLM measurement: **a** No blinking. All signals are considered as background. **b** No background, a typical PALM set-up in TIRF mode with only blinking molecules. **c** Uniform background. **d** Highly spatial and temporal non-uniform background

2.5.1 Sample Preparation for SMLM

A good SMLM sample follows three criteria. (1) The nano-structure is preserved. (2) A high number of fluorophores bind to the target. (3) Non-specific labelling and background are minimised (Bates et al. 2013). For preservation of nanostructure, optimised fixation protocols from EM can be used. Optimization of buffer is key and usage of reactive oxygen species competitors which prevent fluorochrome from degradation can help. Background/non-specific signal can severely decrease the quality of a superresolution reconstruction (Betzig et al. 2006). A comparison of different background scenarios is shown in Fig. 2.11. Use of thin samples in addition to an appropriate imaging buffer can help to minimize the background.

2.5.2 Imaging Medium

Usage of photo-convertible DNA dyes (Hoechst, DAPI and VV) requires certain components to be present in the 'switching buffer'. In particular, the switching buffer should contain 0.5 mg/ml Glucose oxidase, 0.04 mg/ml Catalase, 0.1 g/ml glucose in

PBS. The use of MEA, one of main components of the STORM/dSTORM imaging buffer diminishes the rate of switching in the case of DNA dyes. The switching buffer facilitates the switching of the steady fraction of spontaneously blinking molecule in each frame. The switching buffer is the same as the oxygen scavenger system in STORM/dSTORM, which mainly reduces photo-bleaching fluorescent dyes. More details on imaging medium can be found in (Szczurek et al. 2014; Żurek-Biesiada et al. 2015, 2016).

2.6 Data Acquisition for SMLM

For imaging DNA with photoconvertible DNA dyes, several important aspects have to be considered. Firstly, low power 405 nm illumination in conjunction with a 491 nm laser should be used to increase the number of detected molecules. Similar ideas were previously described in (Heilemann et al. 2008) for photoswitchable fluorescent dyes. However, these dyes have no affinity for DNA. The SMLM measurements were performed with a vertical/upright microscope set-up (see Fig. 2.12). The set-up has four laser sources with excitation wavelengths at 405, 491, 561 and 647 nm and can be dissected into 3 modules described below.

1. **The illumination module**: The laser beam enters the microscope via mirrors (M) and dichroic mirrors (DM) [M1–M4, DM1–DM4], a collimator arrangement (5x expansion of beam diameter) and neutral density filters (if required). This collimator is made up of two achromates with focal lengths of 30 and 150 mm which expand the beams by a factor of 5 to get an homogeneous illumination of the sample.

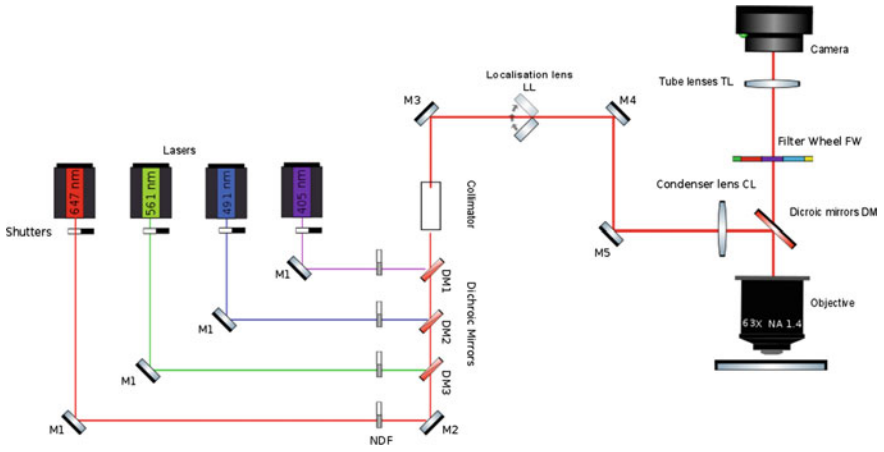

Fig. 2.12 A schematic of the SMLM microscope. For description of optical parts, refer to the text

2. **The localisation module**: To achieve the high laser intensity for the localization mode, a lens [LL] is inserted in the optical pathway, leading to a smaller illuminated area of higher intensity in the object region of interest. The beam is focused by this lens into the back focal plane of an oil immersion objective lens (63x, NA = 1.4). The sample is actuated by a piezoelectrical stage [PS] for focusing.
3. **The detection module**: The emitted fluorescent light goes through the DM and is focused by a tube lens [TL] (1.0x, f = 200 mm) onto the CCD chip of a highly sensitive 12 bit black-and-white camera. A set of appropriate blocking filters is mounted in a filter wheel [FW] in front of the camera chip.

Before acquiring data, certain parameters have to be optimised. For example, bleaching gradient, blinking and their relation to integration time must be studied prior to the measurement and the final number of acquisition frames should be chosen accordingly. One should try to optimise the integration time of the camera as this determines signal-to-noise ratio and eventually the background of the sample. Acquisition of wide-field images before and after measurement helps to compare the structure of the sample with the final reconstruction. Illumination of the sample should be homogeneous. Furthermore, to fasten the acquisition time and save disk space, the sample area can be restricted to a region of interest.

2.7 Data Reconstruction for SMLM

Figure 2.13 presents various steps required to reconstruct a highly resolved image from single molecule coordinates. The operations can be characterized at various levels which are described below.

- **Stack level**: A high number of frames with each frame containing only a few optically isolated molecule must be generated. This data stack can be used to analyse the position of the fluorophore across multiple frames and characterise the fluorophore. Furthermore, a background map for each frame must be calculated and subtracted to get the difference image. This step can be really critical depending on the type of background in the sample (refer Fig. 2.13.)
- **Frame level**: Local maxima in each frame are determined and the corresponding regions-of-interest (ROI) are extracted.
- **ROI level**: Each fluorophore is localised and an estimate about the localisation precision for each molecule based on the parameters of the model function should be calculated. An estimation about the number of photons per molecule is then calculated, an important parameter to study the characteristics of the fluorophores used in the experiments.
- **Error corrections**: Signal from a particular fluorophore occurs more than once during an acquisition and subsequent frames. Removal of signals in multiple consecutive frames is important, so that the same fluorophore is not counted twice. If the sample moved significantly during acquisition, the drift in the sample must be corrected, a common procedure for measurements of long duration. Finally, the events that do not fulfil other quality criteria are removed.

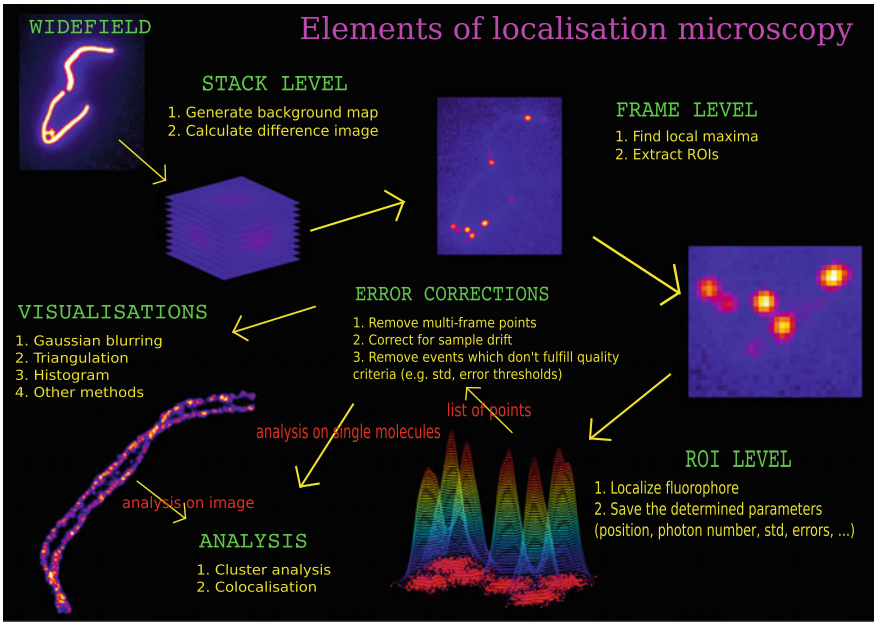

Fig. 2.13 SMLM data reconstruction and analysis flowchart. ROI: Region of interest. See text for details

- **Visualisation**: The position of the single molecules should then be visualised to get a nanoscale representation of the biological object. Visualisation methods include for example, Gaussian blurring, triangulation and histogram methods. A visualisation method is selected based on the labelling density and/or the prior knowledge about the underlying structure from other methods such as EM.
- **Analysis**: Finally, different kinds of analysis such as co-localisation, cluster analysis, nearest neighbour, density analysis can be performed on either high resolution images or coordinates of single molecules.

2.7.1 Spot Finding for SMLM

Algorithms used to precisely identify the locations of fluorophores can be broadly classified into two categories, fitting based and non-fitting based (usually Centroid) methods. While iterative fitting-based methods can usually provide fitted parameters equal or close to the maximum likelihood estimate, *ad hoc* centroid based methods are usually very fast. However, any localisation method will struggle if the underlying model poorly represents the observed data e.g. in case of a high background level, presence of out of focus signals or noise, etc. A particular challenge for the exact fluorophore determination is posed by both spatially and temporally

fluctuating background intensities arising from out-of-focus blinking fluorophores. This can happen if the structure is not *per se* 2-dimensional (e.g. PALM using TIRF illumination, see Fig. 2.11). In the following sections, I discuss these two broad categories of localisation methods.

Fitting Based Methods

Photons emitted by point sources are smeared out onto the detector of the imaging system due of the wave nature of light. This smear or blur is described by the point spread function (PSF) of the imaging system. The intensity distribution of a photon at the detector follows an Airy function but for practical purposes is approximated with a Gaussian function. The overall model function consists in a 2D Gaussian describing the PSF, a function describing the background level and one more term to describe the noise. The model function is represented by:

$$I(x, y) = \frac{A}{2\pi\sigma_x\sigma_y} \exp\left[-\frac{1}{2}\left(\frac{(x-x_0)^2}{\sigma_x^2} + \frac{(y-y_0)^2}{\sigma_y^2}\right)\right] + B + N$$

where x, y are the coordinates of the point emitters, σ_x, σ_y are the width of the distribution, A the peak intensity value of the distribution, $2\pi\sigma_x\sigma_y$ the normalisation factor, x_0, y_0 the coordinates of the real center of the distribution, B the background level and N the noise parameter.

The next task is to optimise the parameter values in order to minimise the error between the signal and the model. The optimisation can be done on all the parameters or just on the coordinates of the emitter positions. Two common methods to optimise the parameters are the least squares method (LSM) and the maximum likelihood estimation (MLE). The principle behind both methods is the same. In LSM, the difference between the signal and model on each pixel is calculated and the error is then squared and added. Based on the error sum, new parameter estimates are made and the sum of the squared errors is calculated again to check if the updated parameter values reduce the error. This process is iterated until the least summed errors are obtained.

In the MLE, the overall process is the same except that detailed information about the experimental conditions such as knowledge about the PSF, noise, background is required. Similarly to LSM, the difference between the signal and the model is calculated and statistics of noise are then used to predict how likely the difference between the model and the signal is. The parameters are tuned to maximise the likelihood of the data. Cramer–Rao Lower Bound (CRLB) states that MLE makes more precise estimates compared to LSM or other parameter optimisation methods (Small and Stahlheber 2014; Small and Parthasarathy 2014).

Non-fitting Based Methods

The fitting methods are often computationally intensive and difficult to handle when the sample is inhomogeneous. Another approach is to find the coordinates of the

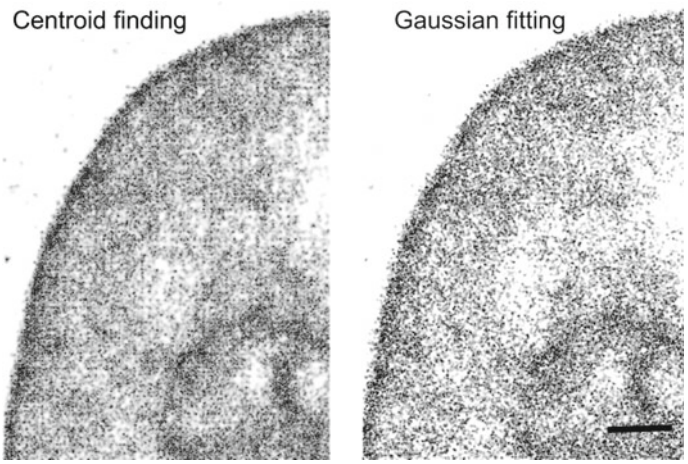

Fig. 2.14 Various reconstruction algorithms for SMLM: Fitting (Gaussian) and non-fitting (centroid) reconstruction algorithms are compared. While non-fitting algorithms are fast, fitting algorithms are more accurate. The grid-like patterns are frequently observed when high density data are reconstructed with centroid method (see text for more details and Best et al. 2014). Scale bar: 1 μm

centroid of the fluorescent spot or in the case of isotropic emitters to take advantage of their radially symmetric shape to estimate the coordinates. When the background is non-uniform and so localisation density is high, due to the additive nature of background noise at regions with high localisation density, the coordinate estimates are biased towards the center of the ROI, often resulting in a grid like patterns (Fig. 2.14 and Best et al. 2014). Various filtering methods should be used to reduce the background intensity and improve the coordinate estimation. For more details on various algorithms estimating the emitter coordinates, please refer to (Small and Stahlheber 2014; Small and Parthasarathy 2014; Chenouard et al. 2014).

2.7.2 Drift Correction Algorithms for SMLM

The correct position determination of fluorescent molecules is crucial for the interpretation of the localisation microscopy data, e.g. to understand the biological structure investigated. The position of fluorophores is highly sensitive to environmental disturbances (e.g. acoustic vibrations) and to mechanical instabilities of the microscope hardware (e.g. thermal expansion, stage drift). These disturbances can cause distortion in the recorded image, significantly affecting the achieved localisation accuracy, especially when it is in the order of tens of nano-meter or better. Previously, on line drift correction methods have been described, which estimate and correct the drift experienced during recording of the experiments. Predicting the drift for future frames is a hard task, as behaviour of vibrations can not be predicted. This can easily be done after measurement.

With colleagues, I developed a drift correction strategy based solely on already acquired data without any fiducial markers (Hagmann et al. 2014). It was found that in some SMLM set-ups (PALM, STORM), most of the biological samples exhibit enough permanent (photostable) structure that can be used at several time points to gain information about the sample. This information was used to correct the lateral drift based on the underlying structure visible in a raw image sequence (averaged over 10 subsequent frames for one sample image), to then calculate the auto-correlation between sample images. Then two (for x and y) eighth order Fourier series were fitted to the acquired data in order to obtain the drift vectors. Figure 2.15a, b shows HeLa cell nucleus stained with Hoechst 33258 photo-product before and after drift correction. The long acquisition times resulted in considerable mechanical drift of the stage. In

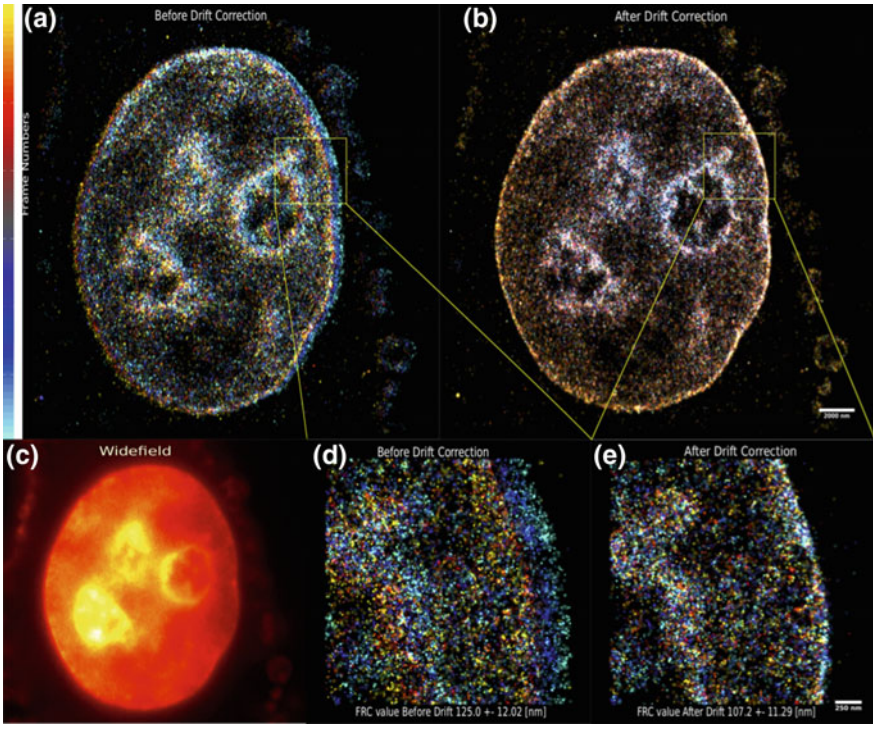

Fig. 2.15 Structed based drift correction strategies for localisation microscopy: Some variants of localisation microscopy exhibit enough permanent (photostable) structure that can be used to correct the lateral drift based on the underlying structure visible in a raw image sequence. HeLa cell nucleus stained with Hoechst 33258 photoproduct before (**a**) and after drift correction (**b**) are shown. **c** Widefield image of the same nucleus. Due to long measurements, the initial drift was found to be in the order of 500–1000 nm. **d**–**e** After application of structured based drift correction algorithm drift improved to less than 20 nm, well within the localisation precision. The magnified sections (D and E) show significant improvement in resolution (computed using FRC method (Nieuwenhuizen et al. 2013)). The resolution before drift correction was 125 nm and improved down to 107 nm after (Hagmann et al. 2014)

the Fig. 2.15, the frames of the data stack are color coded to demonstrate the drift in the sample. The initial frames are coloured blue, while the final frames range from yellow to white. The sample can be seen to drift from top right to bottom left. For the SMLM microscope used for the measurement, the drift was in order of 100–1000 nm (Fig. 2.16a) and was determined by image phase correlation. A polynomial or Fourier series (equation below) was fitted through the data, from which the dislocation of every event was subtracted.

$$y = a_0 + \sum_{i=1}^{n} a_i cos(iwx) + b_i sin(iwx)$$

where a_0 is the intercept term in the data (associated with $i = 0$ cosine term), w the frequency of the signal and n the number of harmonics (8 in our case).

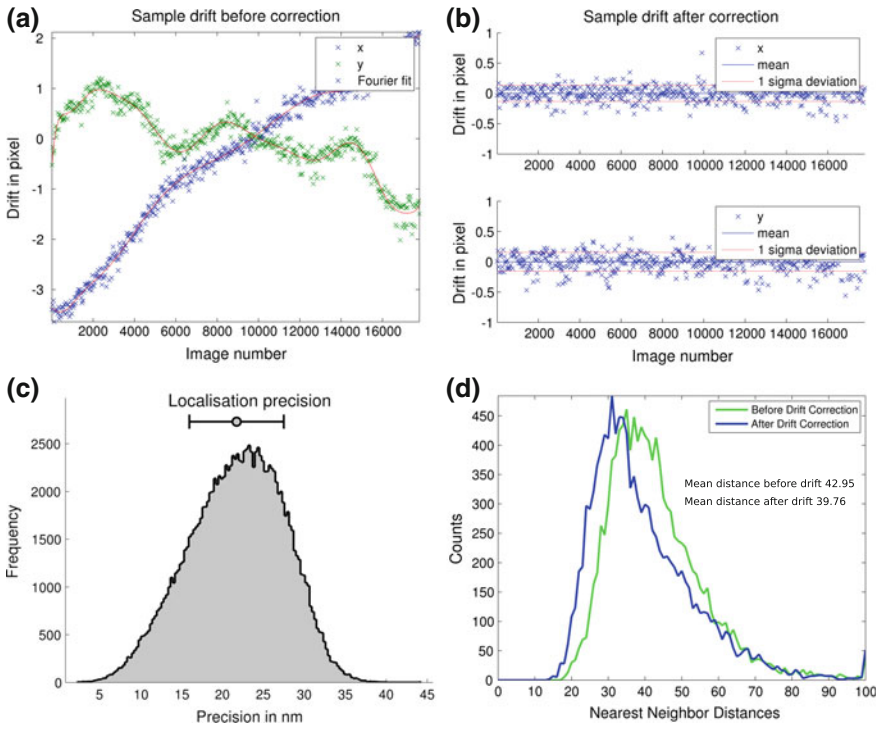

Fig. 2.16 Quantification of sample drift. **a** The drift along x axis was less than 200 nm, however the drift along y axis was in order of 500 nm. **b** After application of structured based drift correction algorithm, the overall drift in both x and y directions was less than 20 nm, well within the localisation precision (**c**). **d** shows the nearest neighbor distances before and after drift correction. The mean nearest neighbour distance before drift was 42 nm while it improved to 39 nm after correction

In the present case of a cell nucleus with high background, the data were corrected to a final drift under 20 nm (Fig. 2.16b), which was reasonable given the high localisation precision (average 25 nm, Fig. 2.16c). Furthermore, the resolution computed based on Fourier ring correlation (Nieuwenhuizen et al. 2013) showed a significant enhancement in resolution before (125 ± 12 nm) and after (107 ± 11 nm) drift correction. The drift correction also resulted in significant improvement of neighbour distances. The mean nearest neighbour distances before and after drift correction were approximately 42.95 nm and 39.76 in the zoomed sections of the cell nucleus (Fig. 2.15d, e and Fig. 2.16d).

Overall, the drift correction resulted in increased local density of chromatin at the nuclear periphery, which is in accordance with nuclear architecture. It is believed that with appropriate drift correction strategies, one can observe true structural features which are often accompanied with a decrease in nearest neighbour distances. Structure based drift correction demonstrates high background and that the underlying structure of datasets can be used to correct drift. Using this approach, one can successfully correct the localisation microscopy data down to a final drift under 5 nm. The results are comparable to fiducial markers based strategies. Moreover, the resolution of the final reconstructions is substantially enhanced and the natural limit of localisation precision is achieved.

2.7.3 Data Visualisation for SMLM

While most imaging modalities generate an image, SMLM provides coordinates single molecules in addition to the image common to the other superresolution methods (STED and SIM). Previously, scatter-gram of point positions (Hess et al. 2006; Van Oijen et al. 1998), 2D histogram of point positions (Heilemann et al. 2008; Lemmer et al. 2008; Fölling et al. 2008; Egner et al. 2007), localisation precision based Gaussian blurring (Betzig et al. 2006; Rust et al. 2006), nearest neighbour blurring of molecule positions (Kaufmann et al. 2012) and triangulation of localisations (Baddeley et al. 2010) have been the most popular visualisation methods.

In Fig. 2.17, localisation precision based Gaussian blurring, triangulation and nearest neighbour blurring of individual molecule are compared. When enough number of nearest neighbour molecules are taken into consideration (20 in the present case), the underlying structure becomes increasingly visible. This happens because blurring locations with a Gaussian is not the best choice when the labelling density is low. In such a case the pointillist appearance of the emitters resurfaces in the final image. Moreover, there is a resolution loss factor of $\sqrt{2}$ as stated in (Baddeley et al. 2010). However, nearest neighbour blurring is helpful at revealing structures especially if the sample suffers from a low density of points. Moreover, the points that are not part of a structure are suppressed. Finally, the visualisation method is chosen based on the labelling density and the characteristics of the structure to visualise (1D, 2D or 3D).

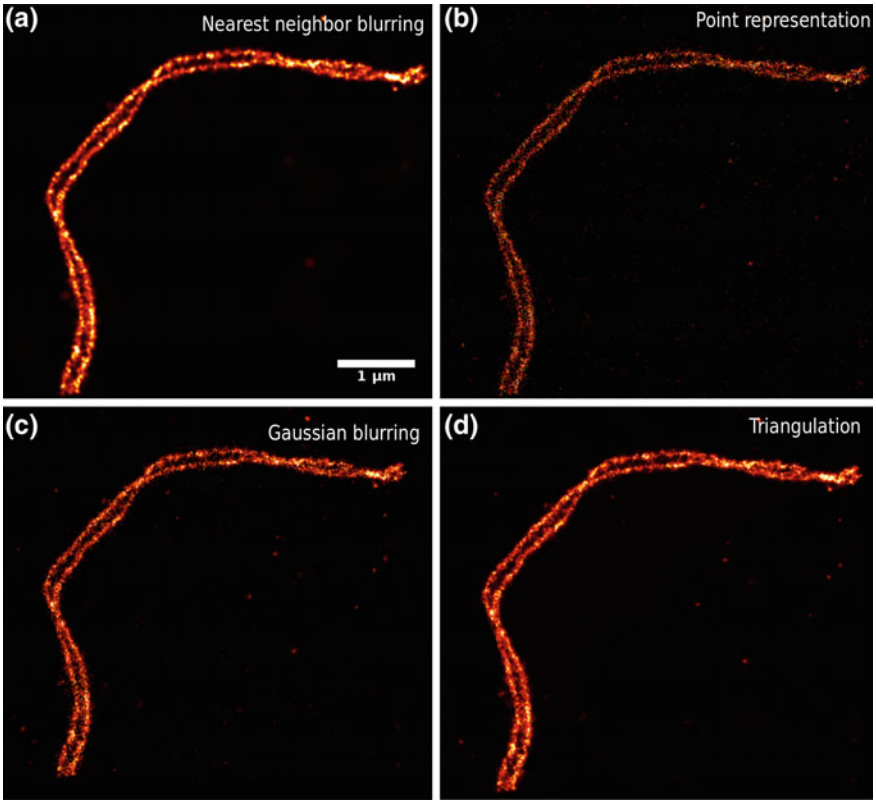

Fig. 2.17 Comparison of various visualisation algorithms: Comparison of Gaussian blurring based localisation precision, triangulation and nearest neighbour blurring of individual molecules is shown. When enough nearest neighbour points are taken into account, the underlying structures can be better observed. Nearest neighbour blurring can help to bring out the underlying structure in images lacking proper labelling density. Moreover, the points that are not part of the structure are suppressed. Figure and caption modified from (Prakash et al. 2015)

2.7.4 Data Analysis for SMLM

Advent of various super-resolution microscopy methods have brought to light various diffraction limited biological objects, revealing periodic patterns (Prakash et al. 2015; Früh et al. 2015; Xu et al. 2013) under better resolution. The analysis of periodicity in these studies (Früh et al. 2015; Xu et al. 2013) was based on the intensity information of the images. In addition to pixel intensity information, SMLM provides information about the single molecule coordinates which can also be used for autocorrelation and periodicity analysis.

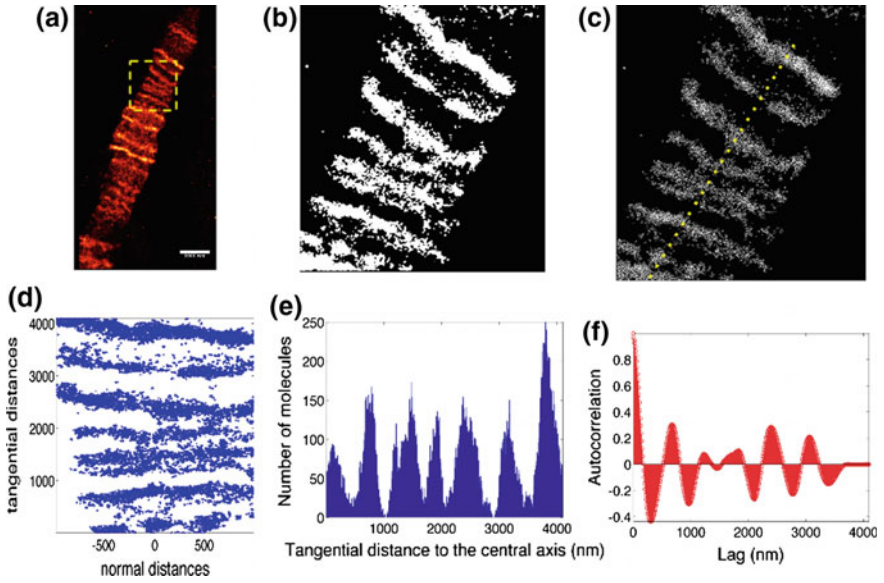

Fig. 2.18 Various steps involved in single molecule autocorrelation. **a** Firstly, each molecule is blurred using the value of the mean distance to 20 nearest neighbour points. **b** Secondly, a binary mask is generated based on the nearest neighbor image and **c** only the signals within the binary mask are considered for further analysis. **d** Each molecule position is then translated to Cartesian coordinates for the ease of analysis. **e** A histogram of the tangential and normal positions is generated. **f** Finally the bins of the histogram are auto-correlated to estimate the periodicity

Single Molecule Autocorrelation

For single molecule autocorrelation, each localisation was blurred with 20 nearest neighbours and a binary mask was generated (see Fig. 2.18) using a global threshold described elsewhere (Prakash et al. 2015; Jianzhuang et al. 1991). The single molecules within this binary mask were extracted for further analysis. This resulted in keeping only the molecules which belong to the structure or the clusters considered. For the autocorrelation analysis, a line was fitted manually to pass through the center of the object. The coordinates were then translated and rotated to get a more linear orientation. Finally, the autocorrelation values were calculated on the histogram of the tangential distances along the central axis. The algorithm is described in detail in (Prakash et al. 2015).

2.8 Some Further Considerations for Localisation Microscopy

There are a number of artefacts that can arise due to sample preparation mainly due to fixation conditions, permeabilization conditions, antibody concentration and the type of buffer used. These are described in detail in (Whelan and Bell 2015). Here, I discuss three more kinds of artefacts that can arise from the way microscope is set up and the coordinates of single molecules are estimated post-acquisition.

2.8.1 Artefacts in Localisation Microscopy

Figure 2.19 shows negative of wide-field and localisation image of a HL-1 cell nucleus stained with Hoechst. Due to the non-homogeneous illumination of the sample (Fig. 2.19a), the lower left of the cell nucleus is more illuminated than the upper right part of the nucleus. This leads to a non-uniform detection of molecules across the sample. For example, the chromatin density at the nuclear periphery (the upper right part of the image in (Fig. 2.19a, b) is higher than the lower left part of the image. The same pattern of density can also be observed around the nucleolus (black arrows). Another factor that can lead to a non-homogeneous illumination of the sample is the Gaussian profile of the excitation beam. In such a case, the central regions are more illuminated than the regions toward the periphery of the nucleus.

Another type of artefact can arise due to the data reconstruction when there is a high number of signals in each frame (Fig. 2.19c). The high density leads to the overlap of the signal resulting in a grid-like patterns. If the centroid fitting algorithm or center-of-intensity (COI) is used to localise the signals then the signal is biased toward the center of the pixel resulting in grid-like patterns (see Sect. 2.7.1). However, no grid-like pattern is observed with Gaussian fitting, which is more accurate but slower when compared to centroid fitting. One solution to solve this problem is to make sure only few signals blink in each frame so signals do not overlap and can be optically isolated. Then one has to take a high number of frames to get a high density super-resolved image. This can be achieved by initial reversible photo-bleaching of the sample before acquisition and waiting until the uniform blinking of the signals is achieved.

A third type of artefact is experienced when biological objects under study are poorly labelled. The pattern which are obvious in wide-field image are missed in the high resolution images. Such an example can be seen in Fig. 2.20. Pol II is known to form barrel-like elongated shapes in polytene chromosomes (Zhimulëv 1996) which are apparent in wide-field image (Fig. 2.20a, inset a1). However, SMLM imaging does not reconstruct these apparent patterns of Pol II (Fig. 2.20b), following the well-known alternation patterns of dense and light regions of polytene chromosomes (Zhimulëv 1996). Pol II-rich regions are enriched for genes, and correspond to the dense regions of electron microscopy images, while Pol II-poor regions

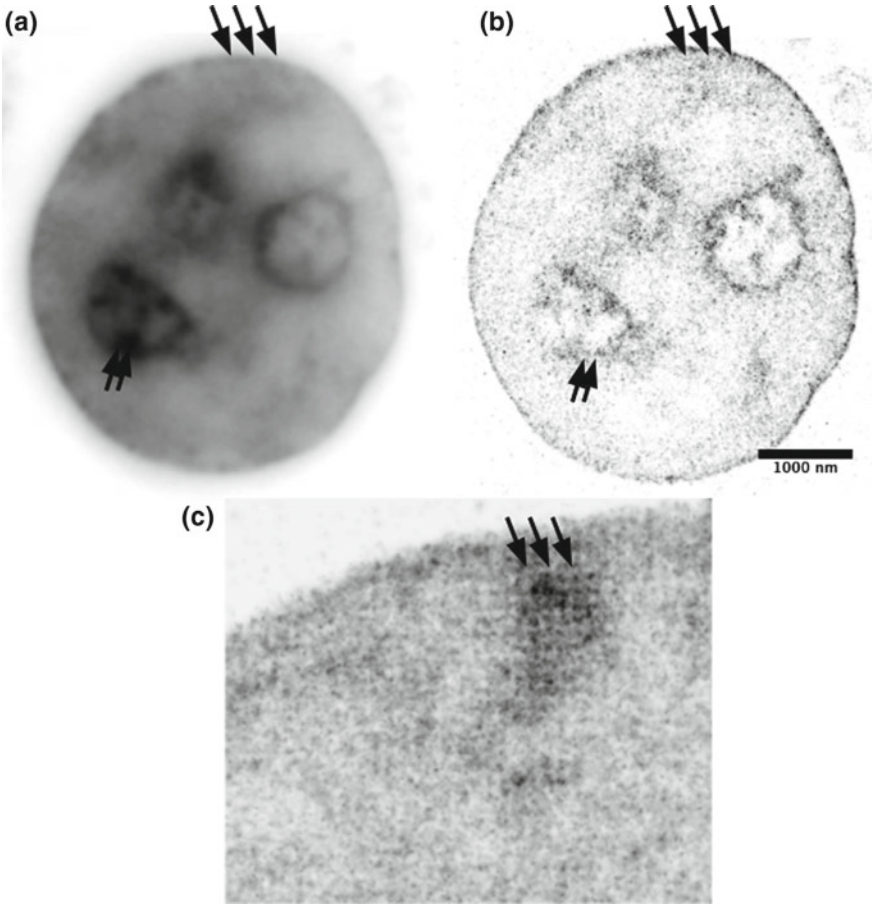

Fig. 2.19 Artifacts in localisation microscopy: **a** Negative of a widefield image of HL-1 cell nucleus stained with Hoechst. **b** Negative of high resolution reconstruction of the same cell. Dense chromatin blob is observed around the nucleolus (black arrows inside the nucleus) in (**a**) but is missing in (**b**). Moreover, no dense chromatin is observed at the nuclear periphery in (**a**) but is present in the high resolution reconstruction in (**b**). This is usually due to non-homogenous illumination of the sample. One factor that can generate non-homogenous illumination is the Gaussian profile of the high intensity excitation beam that causes the central region in widefield mode to be illuminated more than the peripheral regions. **c** A section of the nucleus showing a grid-like pattern. Such patterns usually arise in high density single molecule reconstructions when the Center-Of-Intensity (COI) algorithm is used. COI biases the localisation towards the center of the CCD camera pixel, giving rise to such grid-like patterns

correspond to light regions, deprived of genes. This example shows a major pitfall of super-resolution imaging, particularly prominent when the underlying structure is unknown and poor or insufficient labelling of the biological object might lead to a wrong interpretation of the data. This also reflects the importance of a good in-depth

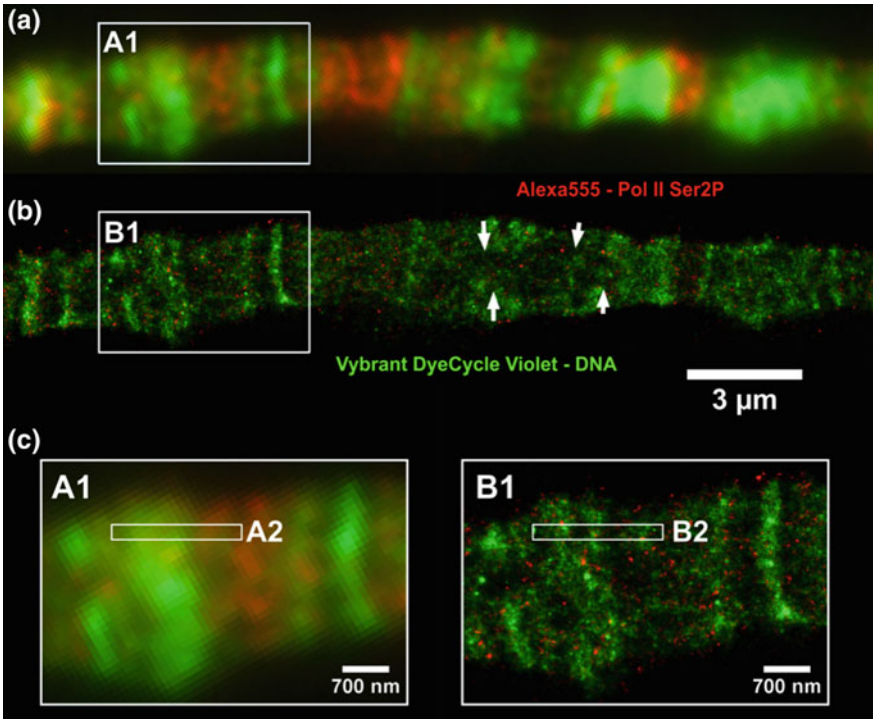

Fig. 2.20 Dual color SMLM image of Drosophila polytene chromosome stained with VV (*green*) and Pol II Ser2P-Alexa Fluor 555 (*red*). **a** Widefield image of a fragment of a polytene chromosome. **b** SMLM images of the fragment as in (**a**). *Arrows* indicate regions of loose chromatin inside the polytene chromosome. **c** Enlarged fragment of the images shown in A and B, embracing dense heterochromatic and lower density eu-chromatic regions of DNA. Figure and caption modified from (Żurek-Biesiada et al. 2015)

literature survey about the biological object and the importance of blurring when the labelling density is limited.

2.8.2 *Difference Between Localisation Precision and Accuracy*

The terms localisation precision and accuracy are often used interchangeably. Localisation precision is the exactness with which the position of a signal can be predicted, which can be slightly off the true position of the molecule. This distance between the true position of a molecule and the detected signal is the localisation accuracy. Figure 2.21a, shows a detected signal slightly off from the true position of the molecule. As the signals are not spread, the localisation precision will be good but the

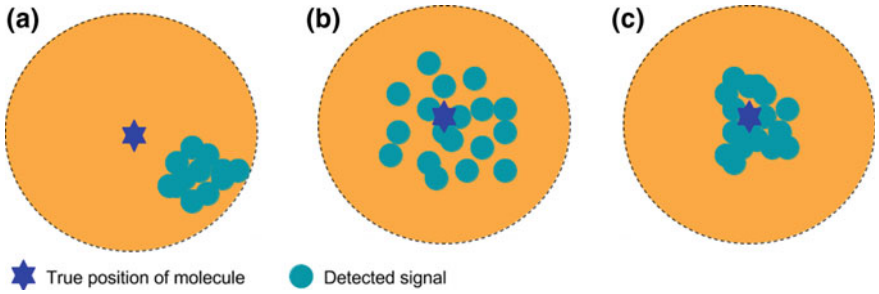

Fig. 2.21 Localisation precision Vs localisation accuracy: **a** Good localisation precision but poor localisation accuracy. **b** Good localisation accuracy but poor localisation precision. **c** Good localisation accuracy and localisation precision. The true position of a fluorophore is indicated by a *blue star* while turquoise blobs indicate the detected signal

localisation accuracy will be poor. In the second case (Fig. 2.21b) the detected signals are spread over a large region resulting in a poor localisation precision but an increased localisation accuracy as the detected signals are close to the true position of the molecule. In the third case (Fig. 2.21c), localisation accuracy and precision are both high, a typical case for Hoechst and DAPI which directly bind to DNA (high localisation accuracy) and display a high photon count (high localisation precision).

2.9 Summary

Single Molecule Localisation Microscopy (SMLM) is one of the major emerging tools for the analysis of biological structures at approximately 10 nm spatial resolution. The procedure relies on sequential detection of (a subset of) individual fluorophores. For dense regions (fluorophores with significant overlap), a compromise between labelling density and the photoswitching behaviour of fluorophores is needed to optically isolate molecules in each acquired frame. The last 10 years have seen a significant progress in fluorescence imaging with the development of new fluorescent probes and the discovery of new properties of existing fluorochromes (Szczurek et al. 2014; Żurek-Biesiada et al. 2015), making them applicable for super-resolution imaging.

Until recently, description of chromatin was limited to immunostaining of histone proteins, which does not provide enough labelling efficiency and density for chromatin imaging (Bohn et al. 2010; Ricci et al. 2015). Nevertheless, usage of conventional dyes dramatically increases the amount of signals recorded, opening avenues for the description of chromatin architecture at all levels of magnification. This is the matter of the next two chapters; Chap. 3 discusses many structural features of chromatin found in interphase, while Chap. 4 presents recent results regarding the chromatin architecture of the pachytene chromosome. Both these aspects of chro-

matin organisation grandly benefit from the developments presented in the current chapter. In this chapter, I discussed the theory and concepts of SMLM, as well as sample preparation, hardware implementation, data reconstruction, visualisation and quantifications. I closed the chapter with a note about localisation accuracy, precision, resolution and some of other technical pitfalls.

With more efficient fluorophores (i.e. with higher photon counts), highly sensitive camera, high NA objective lenses, an even higher spatial resolution can be expected in the future. A particular important challenge is live cell imaging, which requires both high spatial and temporal resolution though efforts in this direction are already being made (Biteen et al. 2008; Shroff et al. 2008). Single particle tracking is another area where photo-switchable fluorescent probes will facilitate tracking of high-density particle in live cells (Manley et al. 2008). Finally, I hope that together with SIM, SMLM can be broadly applied to chromatin biology and other areas of cell biology to provide insights into the nuclear architecture at nanoscale.

References

Abbe E (1873) Beiträge zur Theorie des Mikroskops und der mikroskopischen Wahrmehmung. Archiv für Mikroskopische Anatomie 9:413–420. doi:10.1007/BF02956173

Albiez H, Cremer M, Tiberi C, Vecchio L, Schermelleh L, Dittrich S, Küpper K, Joffe B, Thormeyer T, von Hase J et al (2006) Chromatin domains and the interchromatin compartment form structurally defined and functionally interacting nuclear networks. Chromosom Res 14(7):707–733

Anton T, Bultmann S, Leonhardt H, Markaki Y (2014) Visualization of specific dna sequences in living mouse embryonic stem cells with a programmable fluorescent crispr/cas system. Nucleus 5(2):163–172

Baddeley D, Cannell MB, Soeller C (2010) Visualization of localization microscopy data. Microsc Microanal 16(01):64–72

Baskin JM, Prescher JA, Laughlin ST, Agard NJ, Chang PV, Miller IA, Lo A, Codelli JA, Bertozzi CR (2007) Copper-free click chemistry for dynamic in vivo imaging. Proc Natl Acad Sci 104(43):16793–16797

Bates M, Jones SA, Zhuang X (2013) Stochastic optical reconstruction microscopy (storm): a method for superresolution fluorescence imaging. Cold Spring Harbor Protoc 2013(6):pdb–top075143

Bernas T, Zarebski M, Cook RR, Dobrucki JW (2004) Minimizing photobleaching during confocal microscopy of fluorescent probes bound to chromatin: role of anoxia and photon flux. J Microsc 215(3):281–296

Best G, Prakash K, Hagmann M, Cremer C, Birk U (2014) Identify and localise: algorithms for single molecule localisation microscopy. In: Hozák P (ed) 18th international microscopy congress, number ISBN 978-80-260-6720-7

Betzig E (1995) Proposed method for molecular optical imaging. Opt Lett 20(3):237–239

Betzig E, Patterson GH, Sougrat R, Wolf Lindwasser O, Olenych S, Bonifacino JS, Davidson MW, Lippincott-Schwartz J, Hess HF (2006) Imaging intracellular fluorescent proteins at nanometer resolution. Science 313(5793):1642–1645

Biancardi A, Biver T, Secco F, Mennucci B (2013) An investigation of the photophysical properties of minor groove bound and intercalated dapi through quantum-mechanical and spectroscopic tools. Phys Chem Chem Phys 15(13):4596–4603

Biteen JS, Thompson MA, Tselentis NK, Bowman GR, Shapiro L, Moerner WE (2008) Super-resolution imaging in live caulobacter crescentus cells using photoswitchable eyfp. Nature Methods 5(11):947–949

Boettiger AN, Bintu B, Moffitt JR, Wang S, Beliveau BJ, Fudenberg G, Imakaev M, Mirny LA, Wu C-T, Zhuang X (2016) Super-resolution imaging reveals distinct chromatin folding for different epigenetic states. Nature 529(7586):418–422

Bohn M, Diesinger P, Kaufmann R, Weiland Y, Müller P, Gunkel M, Von Ketteler A, Lemmer P, Hausmann M, Heermann DW et al (2010) Localization microscopy reveals expression-dependent parameters of chromatin nanostructure. Biophys J 99(5):1358–1367

Brooks Shera E, Seitzinger NK, Davis LM, Keller RA, Soper SA (1990) Detection of single fluorescent molecules. Chem Phys Lett 174(6):553–557

Burnette DT, Sengupta P, Dai Y, Lippincott-Schwartz J, Kachar B (2011) Bleaching/blinking assisted localization microscopy for superresolution imaging using standard fluorescent molecules. Proc Natl Acad Sci 108(52):21081–21086

Burns DH, Callis JB, Christian GD, Davidson ER (1985) Strategies for attaining superresolution using spectroscopic data as constraints. Appl Opt 24(2):154–161

Chandra T, Kirschner K, Thuret J-Y, Pope BD, Ryba T, Newman S, Ahmed K, Samarajiwa SA, Salama R, Carroll T et al (2012) Independence of repressive histone marks and chromatin compaction during senescent heterochromatic layer formation. Mol cell 47(2):203–214

Chen B, Gilbert LA, Cimini BA, Schnitzbauer J, Zhang W, Li G-W, Park J, Blackburn EH, Weissman JS, Qi LS et al (2013) Dynamic imaging of genomic loci in living human cells by an optimized crispr/cas system. Cell 155(7):1479–1491

Chenouard N, Smal I, De Chaumont F, Maška M, Sbalzarini IF, Gong Y, Cardinale J, Carthel C, Coraluppi S, Winter M et al (2014) Objective comparison of particle tracking methods. Nature Methods 11(3):281

Cosa G, Focsaneanu KS, McLean JRN, McNamee JP, Scaiano JC (2001) Photophysical properties of fluorescent dna-dyes bound to single-and double-stranded dna in aqueous buffered solution. Photochem Photobiol 73(6):585–599

Cremer C, Cremer T (1978) Considerations on a laser-scanning-microscope with high resolution and depth of field. Microsc Acta 81:31–44

Cremer T, Cremer C (2001) Chromosome territories, nuclear architecture and gene regulation in mammalian cells. Nature Rev Genet 2(4):292–301

Cremer T, Küpper K, Dietzel S, Fakan S (2004) Higher order chromatin architecture in the cell nucleus: on the way from structure to function. Biol Cell 96(8):555–567

Cremer T, Cremer M, Hübner B, Strickfaden H, Smeets D, Popken J, Sterr M, Markaki Y, Rippe K, Cremer C (2015) The 4d nucleome: Evidence for a dynamic nuclear landscape based on co-aligned active and inactive nuclear compartments. FEBS Lett 589:2931–2943

Diana C, Carvalho PC (2010) Supramolecular biomimetic binding of the DNA-dye Hoechst 33258 by a synthetic macrocycle. Ph.D. thesis

Dickson RM, Cubitt AB, Tsien RY, Moerner WE (1997) On/off blinking and switching behaviour of single molecules of green fluorescent protein. Nature 388(6640):355–358

Doudna JA, Charpentier E (2014) The new frontier of genome engineering with crispr-cas9. Science 346(6213):1258096

Egner A, Geisler C, Von Middendorff C, Bock H, Wenzel D, Medda R, Andresen M, Stiel AC, Jakobs S, Eggeling C et al (2007) Fluorescence nanoscopy in whole cells by asynchronous localization of photoswitching emitters. Biophys J 93(9):3285–3290

Fölling J, Bossi M, Bock H, Medda R, Wurm CA, Hein B, Jakobs S, Eggeling C, Hell SW (2008) Fluorescence nanoscopy by ground-state depletion and single-molecule return. Nature Methods 5(11):943–945

Früh SM, Schoen I, Ries J, Vogel V (2015) Molecular architecture of native fibronectin fibrils. Nature Commun 6:7275

Grammel M, Hang HC (2013) Chemical reporters for biological discovery. Nature Chem Biol 9(8):475–484

Gustafsson MGL (2000) Surpassing the lateral resolution limit by a factor of two using structured illumination microscopy. J Microsc 198(2):82–87

Hagmann M, Prakash K, Best G, Kaufmann R, Birk U, Cremer C (2014) Drift correction strategies for single molecule localisation microscopy. In: Hozák P (ed) 18th international microscopy congress, number ISBN 978-80-260-6720-7

Hagmann M, Prakash K, Cremer C (2016) Visualisation enhancement for single molecule reconstructions using wigner–seitz cells (in preparation)

Heilemann M, Van De Linde S, Schüttpelz M, Kasper R, Seefeldt B, Mukherjee A, Tinnefeld P, Sauer M (2008) Subdiffraction-resolution fluorescence imaging with conventional fluorescent probes. Angew Chem Int Edition 47(33):6172–6176

Heintzmann R, Cremer C (1999) Laterally modulated excitation microscopy: improvement of resolution by using a diffraction grating. In: BiOS Europe'98. International Society for Optics and Photonics, pp 185–196

Hell SW, Wichmann J (1994) Breaking the diffraction resolution limit by stimulated emission: stimulated-emission-depletion fluorescence microscopy. Opt Lett 19(11):780–782

Hess ST, Girirajan TPK, Mason MD (2006) Ultra-high resolution imaging by fluorescence photoactivation localization microscopy. Biophys J 91(11):4258

Hirschfeld T (1976) Optical microscopic observation of single small molecules. Appl Opt 15(12):2965–2966

Hsu PD, Lander ES, Zhang F (2014) Development and applications of crispr-cas9 for genome engineering. Cell 157(6):1262–1278

Hussels M, Brecht M (2011) Effect of glycerol and pva on the conformation of photosystem i. Biochemistry 50(18):3628–3637

Jianzhuang L, Wenqing L, Yupeng T (1991) Automatic thresholding of gray-level pictures using two-dimension otsu method. In: 1991 international conference on circuits and systems, 1991. Conference proceedings, China, pp 325–327. IEEE

Kaufmann R, Piontek J, Grüll F, Kirchgessner M, Rossa J, Wolburg H, Blasig IE, Cremer C (2012) Visualization and quantitative analysis of reconstituted tight junctions using localization microscopy. PloS One 7(2):e31128

Klein T, Löschberger A, Proppert S, Wolter S, van de Linde S, Sauer M (2011) Live-cell dstorm with snap-tag fusion proteins. Nature Methods 8(1):7–9

Lemmer P, Gunkel M, Baddeley D, Kaufmann R, Urich A, Weiland Y, Reymann J, Müller P, Hausmann M, Cremer C (2008) Spdm: light microscopy with single-molecule resolution at the nanoscale. Appl Phys B 93(1):1–12

Lemmer P, Gunkel M, Weiland Y, Müller P, Baddeley D, Rainer Kaufmann A, Urich HE, Amberger R, Hausmann M et al (2009) Using conventional fluorescent markers for far-field fluorescence localization nanoscopy allows resolution in the 10-nm range. J Microsc 235(2):163–171

Lidke K, Rieger B, Jovin T, Heintzmann R (2005) Superresolution by localization of quantum dots using blinking statistics. Opt Express 13(18):7052–7062

Manley S, Gillette JM, Patterson GH, Shroff H, Hess HF, Betzig E, Lippincott-Schwartz J (2008) High-density mapping of single-molecule trajectories with photoactivated localization microscopy. Nature Methods 5(2):155–157

Miyanari Y, Ziegler-Birling C, Torres-Padilla M-E (2013) Live visualization of chromatin dynamics with fluorescent tales. Nature Struct Mol Biol 20(11):1321–1324

Moerner WE, Kador L (1989) Optical detection and spectroscopy of single molecules in a solid. Phys Rev Lett 62(21):2535

Müller P, Schmitt E, Jacob A, Hoheisel J, Kaufmann R, Cremer C, Hausmann M (2010) Combofish enables high precision localization microscopy as a prerequisite for nanostructure analysis of genome loci. Int J Mol Sci 11(10):4094–4105

Neice A (2010) Chapter 3 - methods and limitations of subwavelength imaging. In: Hawkes PW (ed) Advances in imaging and electron physics, vol 163. Elsevier, pp 117–140. doi:10.1016/S1076-5670(10)63003-0

Nieuwenhuizen RPJ, Lidke KA, Bates M, Puig DL, Grünwald D, Stallinga S, Rieger B (2013) Measuring image resolution in optical nanoscopy. Nature Methods 10(6):557–562
Piterburg M, Panet H, Weiss A (2012) Photoconversion of dapi following uv or violet excitation can cause dapi to fluoresce with blue or cyan excitation. J Microsc 246(1):89–95
Prakash K, Fournier D, Redl S, Best G, Borsos M, Tiwari VK, Tachibana-Konwalski K, Ketting RF, Parekh SH, Cremer C et al (2015) Superresolution imaging reveals structurally distinct periodic patterns of chromatin along pachytene chromosomes. Proc Natl Acad Sci 112(47):14635–14640
Rao SSP, Huntley MH, Durand NC, Stamenova EK, Bochkov ID, Robinson JT, Sanborn AL, Machol I, Omer AD, Lander ES et al (2014) A 3d map of the human genome at kilobase resolution reveals principles of chromatin looping. Cell 159(7):1665–1680
Rayleigh L (1896) Xv. on the theory of optical images, with special reference to the microscope. Lond Edinb Dublin Philos Mag J Sci 42(255):167–195
Rust MJ, Bates M, Zhuang X (2006) Stochastic optical reconstruction microscopy (storm) provides sub-diffraction-limit image resolution. Nature Methods 3(10):793
Ricci MA, Manzo C, García-Parajo MF, Lakadamyali M, Cosma MP (2015) Chromatin fibers are formed by heterogeneous groups of nucleosomes in vivo. Cell 160(6):1145–1158
Schoen I, Ries J, Klotzsch E, Ewers H, Vogel V (2011) Binding-activated localization microscopy of dna structures. Nano Lett 11(9):4008–4011
Sengupta P, van Engelenburg SB, Lippincott-Schwartz J (2014) Superresolution imaging of biological systems using photoactivated localization microscopy. Chem Rev 114(6):3189–3202
Sheppard CJR, Wilson T (1981) Effects of high angles of convergence on v (z) in the scanning acoustic microscope. Appl Phys Lett 38(11):858–859
Shroff H, Galbraith CG, Galbraith JA, Betzig E (2008) Live-cell photoactivated localization microscopy of nanoscale adhesion dynamics. Nature Methods 5(5):417–423
Small AR, Parthasarathy R (2014) Superresolution localization methods. Ann Rev Phys Chem 65:107–125
Small A, Stahlheber S (2014) Fluorophore localization algorithms for super-resolution microscopy. Nature Methods 11(3):267–279
Sunney Xie X, Dunn RC et al (1994) Probing single molecule dynamics. Science 265:361
Szczurek AT, Prakash K, Lee H-K, Żurek-Biesiada DJ, Best G, Hagmann M, Dobrucki JW, Cremer C, Birk U (2014) Single molecule localization microscopy of the distribution of chromatin using hoechst and dapi fluorescent probes. Nucleus 5(4):331–340
Thanisch K, Schneider K, Morbitzer R, Solovei I, Lahaye T, Bultmann S, Leonhardt H (2013) Targeting and tracing of specific dna sequences with dtales in living cells. Nucleic Acids Res, gkt1348
Thompson RE, Larson DR, Webb WW (2002) Precise nanometer localization analysis for individual fluorescent probes. Biophys J 82(5):2775–2783
Uno SN, Kamiya M, Yoshihara T, Sugawara K, Okabe K, Tarhan MC, Fujita H, Funatsu T, Okada Y, Tobita S et al (2014) A spontaneously blinking fluorophore based on intramolecular spirocyclization for live-cell super-resolution imaging. Nature Chem 6(8):681–689
Van Oijen AM, Köhler J, Schmidt J, Müller M, Brakenhoff GJ (1998) 3-dimensional super-resolution by spectrally selective imaging. Chem Phys Lett 292(1):183–187
Weiland Y, Lemmer P, Cremer C (2011) Combining fish with localisation microscopy: super-resolution imaging of nuclear genome nanostructures. Chromosom Res 19(1):5–23
Whelan DR, Bell TDM (2015) Image artifacts in single molecule localization microscopy: why optimization of sample preparation protocols matters. Sci Rep 5:7924
Wood AJ, Lo T-W, Zeitler B, Pickle CS, Ralston EJ, Lee AH, Amora R, Miller JC, Leung E, Meng X et al (2011) Targeted genome editing across species using zfns and talens. Science 333(6040):307–307
Xu K, Zhong G, Zhuang X (2013) Actin, spectrin, and associated proteins form a periodic cytoskeletal structure in axons. Science 339(6118):452–456
Zessin PJM, Finan K, Heilemann M (2012) Super-resolution fluorescence imaging of chromosomal dna. J Struct Biol 177(2):344–348

Zhimulëv IF (1996) Morphology and structure of polytene chromosomes. Academic Press, New York

Zipfel WR, Williams RM, Webb WW (2003) Nonlinear magic: multiphoton microscopy in the biosciences. Nature Biotechnol 21(11):1369–1377

Żurek-Biesiada D, Szczurek AT, Prakash K, Mohana GK, Lee H-K, Roignant J-Y, Birk U, Dobrucki JW, Cremer C (2015) Localization microscopy of dna in situ using vybrant dyecycle violet fluorescent probe: a new approach to study nuclear nanostructure at single molecule resolution. Exp Cell Res 343:97–106

Żurek-Biesiada D, Szczurek AT, Prakash K, Best G, Mohana GK, Lee H-K, Roignant J-Y, Dobrucki JW, Cremer C, Birk U (2016) Quantitative super-resolution localization microscopy of dna in situ using vybrant dyecycle violet fluorescent probe. Data Brief 7:157–171

Chapter 3
Structure, Function and Dynamics of Chromatin

Stress is the shortest distance between two homologous chromosomes. Searching for a soul-mate?

3.1 Introduction

Chromatin is a DNA-protein polymer, which consists of DNA, structural proteins, non-structural proteins and RNA. During interphase, chromatin encodes the information necessary to maintain the primary functions of the cells. At the same time, the cell holds in a relatively small volume (roughly 4000 μm^3 of diameter for the nucleus) the entire genome, which is billions of base pairs long and roughly 3 m in length when completely unfolded. Moreover, information needs to be retrieved from this highly condensed structure when a gene needs to be expressed at a fast pace. To achieve this, chromatin arranges itself in a highly ordered and compact structure. This compaction has several hierarchical levels of folding, similar to fractals, which show similar patterns at multiple length scales. DNA helix represents the lowest level of the hierarchy while the metaphase chromosome represents the highest level. Before the advent of EM studies, research on the nucleus was mainly focused on (1) its chemical composition and (2) the structure of highly condensed chromosomes. The status of chromatin during interphase was oblivious and limited to the description of punctuated elements such as nucleoli. Recently, the overall view of interphase chromosomes has become very detailed, and several intermediate orders have been shown to exist, though the importance of these orders is still unknown.

The main feature of interphase chromatin that has been extensively studied is the bead-on-string like structure called nucleosome. A nucleosome is a structure of 11 nm diameter consisting of DNA and histone proteins (Kornberg 1974; Richmond et al. 1983; Luger et al. 1997; Kornberg and Lorch 1999). The DNA molecule wraps around an octamer of four histones with a linker histone (H1) at the base leading to compaction of nucleosome clusters. Nucleosome clusters deprived of linker histone

K. Prakash, *Chromatin Architecture*, Springer Theses,
DOI 10.1007/978-3-319-52183-1_3

(H1) decondense and rearrange themselves into 'beads-on-a-string' configurations (Thoma et al. 1979). The DNA sequence has a highly consistent length of 147 base-pairs across nucleosomes. Overall, there is a very good understanding about the chromatin organisation at the DNA and nucleosomal level, but the way chromatin is compacted at higher levels is still oblivious, despite the recent evidence from genomic and microscopy studies.

Due to its significantly higher resolution, previously EM has been a very powerful method to study organisation of chromatin at various length scales. EM could distinguish structural elements such as heterochromatin, nuclear pores or mRNA. Experimental destruction of chromosomes (Cremer et al. 1982b; Cremer and Cremer 2001) showed that chromosomes barely intermingle inside of the nucleus and for the most part are organized in distinct territories (Zorn et al. 1976, 1979; Stephen et al. 1977). Nevertheless, between these two contrasting levels of chromatin organisation: the nano level (DNA double helix, nucleosome level) and the micron level (chromosome territory level), how chromatin is organized is not well understood. Recent experiments from high resolution microscopy, genetics and genomics have brought new observations to light regarding the apparent hidden complexity of interphase chromatin (Fig. 1.8). Methods such as nucleosome profiling or HiC have provided valuable information, but at the same time convoluted the picture of nuclear processes and structural features. As a consequence, there is still not a consensus regarding the way interphase chromatin is organised. Genomics has brought some strong clues, but this information is mostly population-based and suffers from strong cell to cell heterogeneity. As a result, it is hoped that single-cell information coming from microscopy and also from single-cell genomics provides the missing information required to understand chromatin architecture. Figure 3.1 presents various methods from microscopy or genomics to study chromatin architecture.

In this chapter and Chap. 4 on the organisation of meiotic chromosomes, I tried to gather some evidence regarding the organisation of chromatin at multiple levels that I could capture during my PhD studies. I will show how microscopy at single molecule resolution can be a useful tool to identify the different levels of chromatin compaction, from the nucleosome level up to the level of the metaphase chromosome. One of the challenges is the scarcity of data. Here, using newly established SMLM applied to conventional DNA dyes, I highlight the different levels of chromatin compaction. In reverse hierarchical order, I will start by the concept of chromatin territory, which states that chromosomes have defined regions within the cell (Sect. 3.2.1, scale of 1–2 μm). I will then present subchromosomal domains, which are bulky parts of the chromosome territory with potential functionality (Sect. 3.2.2, scale of 500 nm). I will show how chromatin domains now emerge as fundamental building blocks of chromatin, at least from the point of view of a biologist (Sect. 3.2.3, scale of 100–400 nm). These regulatory domains have a strong potential to be functional units of chromatin and their detection here is backed up by recent data from genomics. I will finish by describing lower orders of chromatin folding, including nucleosomes and chromatin fibres (Sects. 3.2.4 and 3.2.6). I hope that these findings will help to define a framework for the further investigation of chromatin structure and function.

Technique	Chromatin feature	Resolution	Comments
Confocal microscopy	Chromatin domains, nucleoli	200 nm	3D structure of chromatin features
In situ hybridization	Genomic positions, repeat elements		Localisation of specific of DNA sequences
Electron microscopy	Euchromatin, heterochromatin, nucleoli	10 nm	High resolution but unspecific & denaturated
Scanning electron microscopy	Chromatin domains, chromocenters, nucleoli, surface aspect of chromatin	0.5 nm	Highest resolution images of chromatin
Structure illumination microscopy (SIM)/3D-SIM	Chromatin territories, chromatin domains, chromocenters, nucleoli	50-100 nm	Fast generation of 3D nanoscale structures
Stimulated emission depletion (STED)	Chromatin domains, DNA fibers	80 nm	
SMLM: DNA dyes (Vibrant Violet, DAPI, Hoechst, YOYO)	Chromatin territories, chromatin domains, chromocenters, nucleoli, nucleosome clusters, DNA fibers	50-100 nm	High specificity and signal density
SMLM: standard fluorophores (histone modifications or other proteins)	Chromatin domains (H2B, emGFP), classification into active, inactive and repressed chromatin domains	10-50 nm	High precision compared to SMLM of DNA dyes
SMLM: Click chemistry (EdU)	Chromatin territories, nucleosome clusters, replication regions, chromatin domains, nucleosomes	10-20 nm	Almost no background in the reconstructed images
Genomic accessibility methods (DNAse, ATAC, FAIRE-seq)	Chromatin compaction	100 bp	Accessible sites at base pair resolution
ChIP-seq for histone modifications	Chromatin feature and associated function	100 bp	Functional description of chromatin at base pair resolution
Chromosome conformation capture, ChIA-PET	Chromatin domains, chromosome territories	1 kb	Systemic genomic position of co-localization events

Fig. 3.1 Methods from microscopy and genomics to capture chromatin structural patterns

3.2 The Hierarchical Organisation of Chromatin

There are two classical views about how the interphase chromatin is organised at the highest level of hierarchy. The first is the compartmentalization of nucleus into distinct and functional chromosome territories and the other is the classical bimodal euchromatin and heterochromatin model. In this section, I will provide recent evidences from single molecule localisation microscopy to get a more detailed structure of interphase chromosomes and how their hierarchical nature might result from association of fundamental building blocks of chromatin.

3.2.1 Chromosome Territories (Scale: 1000–2000 nm)

As mentioned in the first chapter, interphase chromatin has long been described as an alternation of dense and loose chromatin, i.e. heterochromatin and euchromatin, with no further complexity. With time, the idea that chromosomes follow a territorial organisation slowly became established (Cremer and Cremer 2001). Later, it was shown that chromosome territories do exist and are well conserved between different cell types (Mayer et al. 2005). The paradox between the existence of chromosome territories and the lack of visible territories in electron microscopy has recently been solved by the emergence of super-resolution microscopy. By relying on the detection of single molecules rather than on the capability of the sample to transmit an electron flux, these methods have drawn a clearer picture of the organisation of DNA and associated proteins in the interphase nucleus (Cremer et al. 2006). Interphase chromatin is presently described as chromatin networks and foci, separated by caveats, as exemplified by EM images (Branco and Pombo 2007; Markaki et al. 2010). It is thought that most of these caveats are the place of protein machineries such as transcription factories (Iborra et al. 1996; Sexton et al. 2007) and alternative splicing complexes known as speckles (Zirbel et al. 1993; Puvion and Puvion-Dutilleul 1996). Transcription factories co-localise in DNA void regions while the speckles have been shown to anti-localize with DNA elements (Zirbel et al. 1993; Cremer and Cremer 2001; Markaki et al. 2010). In this first section, I will show how SMLM can be used to get information about chromatin and reveal some structural properties of CT and other nuclear features belonging to a high-order level of structure.

Nearest Neighbour Clustering Identifies Chromosome Territories and Inter Chromosomal Compartments

Nearest neighbour molecules information was used to predict territories of different chromosomes. The algorithm generates a hierarchical cluster tree of localization data using the MATLAB built-in function *linkage*. This function links pair-wise fluorophores in order to form clusters, then links the clusters again pair-wise and so on. The process is iterated until only one cluster is found. A parameter threshold that helps to decide when to separate territories, was set to fit the number of expected regions (39 territories here). The resulting image is a mosaic of clusters that are predicted to be chromosome territories (Fig. 3.2). Further validation is required to prove whether the prediction of territories positions is correct. This could be done using FISH or additional labelling techniques.

Interestingly, the picture also reveals regions of lower density (dark regions) which are overlapping two to four chromosomes. This pattern is a putative interchromosomal territory, a region of the nucleus thought to be the place of active transcription, while the core of the territory displays a more condensed chromatin (Cremer and Cremer 2001) (yellow territory in Fig. 3.2, see also Appendix A.1). The alternation between light and dark regions of Fig. 3.2 further validates the CT/IT model proposed in (Cremer and Cremer 2001).

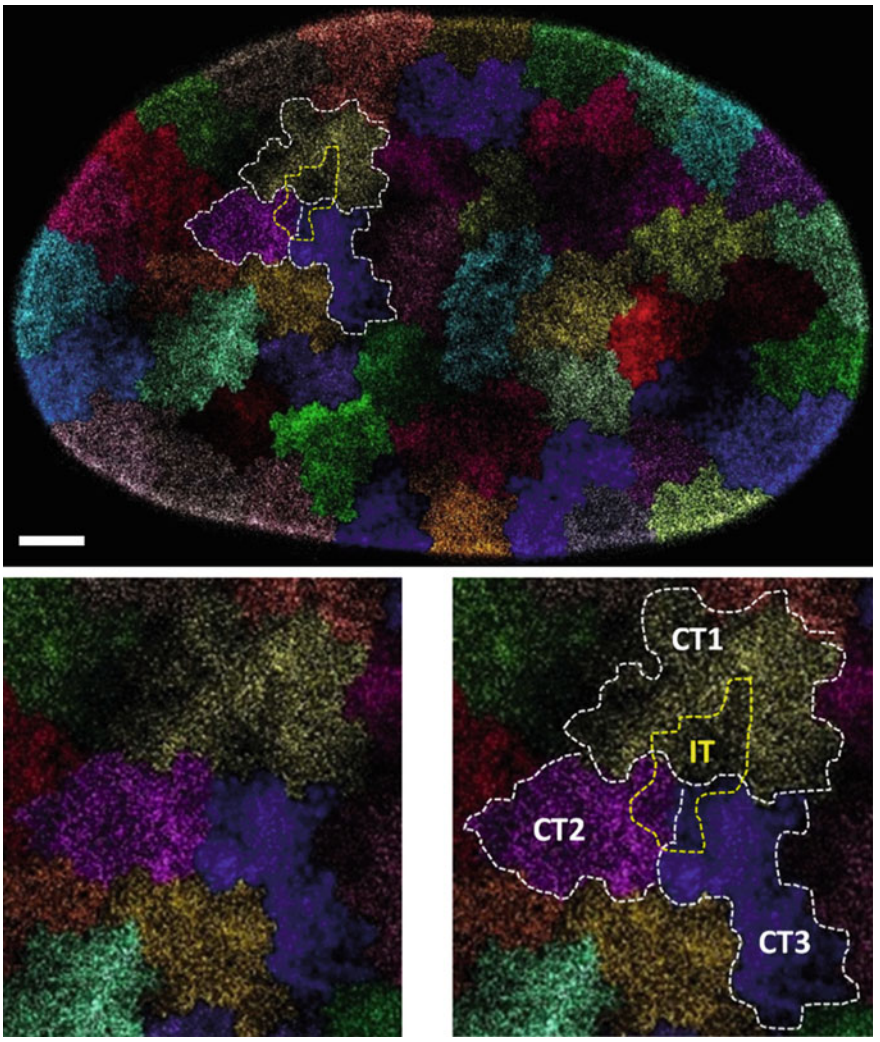

Fig. 3.2 A simulated chromosome territory map (*CT*) based on SMLM data. *Top panel* The nearest neighbour based clustering is used to segregate chromatin into 46 distinct clusters representing individual chromosomes and marking their individual territories. *White lines* show the delimitations of three chromosome territories. *Yellow line* highlights a putative active inter-chromosomal territory (*IT*). *Bottom panels* Magnifications of top panel. In *white* are depicted three chromosome territories and an hypothetical region of active chromatin is displayed in *yellow*. Scale bar: 2 μm

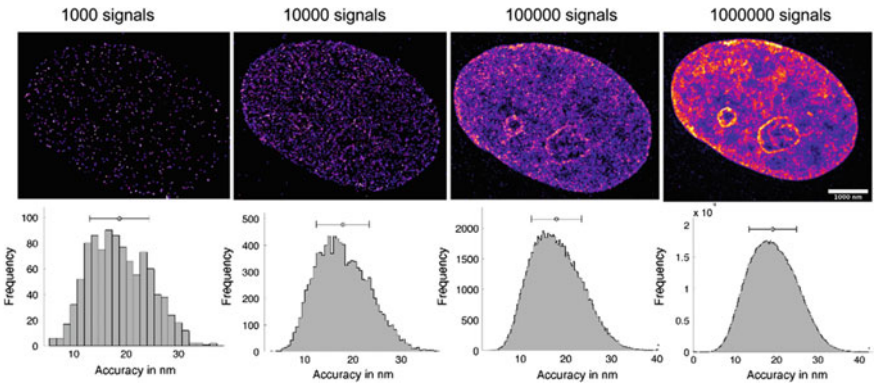

Fig. 3.3 Identification of sub-chromosomal territories. *Top panel* The number of signals is gradually increased from 10,000 to 1,000,000 to reconstruct the final image. *Bottom panel* corresponding values of localisation precision. Irrespective of the increase in number of signals, the average localisation precision is found to be around 20 nm in each case. However, increasing the number of signals acquired helps to identify sub-chromosomal territories (*top right panel*)

Good Labelling Density is Required to Distinguish Chromosome Territories and Sub-chromosomal Compartments

Single molecule microscopy is highly useful to identify the precise location of molecules and distinguish signals whose relative position with respect to the neighbouring molecules is not distinguishable in conventional microscopy. Moreover, by gradually increasing the number of detected molecules, one is able to refine the description of various nuclear structures. Figure 3.3 shows the minimum number of signals required to distinguish various nuclear compartments. For instance, the nucleolus is only visible for 100,000 signals detected. Conversely, a much higher number of signals is required to distinguish individual chromatin domains and the dense chromatin at the nuclear periphery commonly seen in EM images (Fig. 3.3). Another thing worth noting is that localisation precision remains around 20 nm throughout our analysis.

SMLM Reveals Putative Sites for Transcription

Our SMLM setup is useful at probing chromatin structures without prior knowledge about the underlying DNA topology or sequence. One such interesting structure revealed is the discrete sites of gene expression called transcription machineries (Sutherland and Bickmore 2009) different from the nucleolus. The nucleolus is known to be a large nuclear compartment devoted to constant transcription of ribosomal RNA (see the seminal study of nucleolus RNA by Gall and Pardue 1969), found in both widefield and confocal images. The representation is globally the same at microscopic level using SMLM even with a low number of frames, for instance 5000. Nevertheless, when augmenting the number of frames to 20,000, new structures start to emerge, of round shape, similar in nature to nucleoli structure, but 50 times smaller (Fig. 3.4, right image, see also Fig. 3.29). It is hypothesized

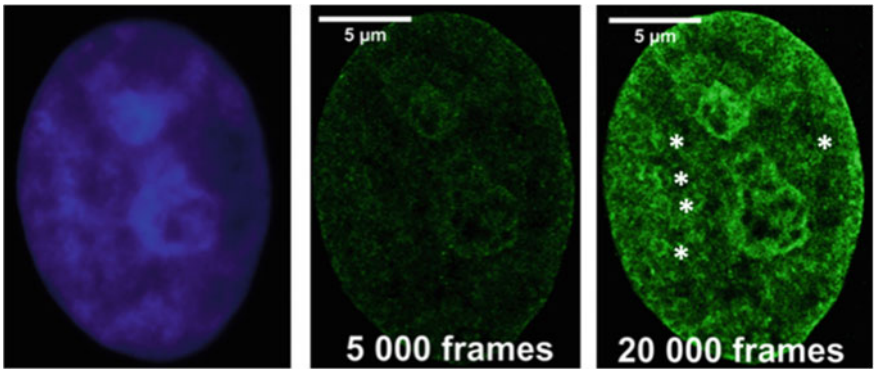

Fig. 3.4 Sub-chromosomal regions corresponding to potential transcription machineries distinct from nucleolus are revealed by SMLM with a high frame number. On the *left*, a widefield image of a sample. On the middle panel, a picture with 5000 frames. In both widefield and low frame number, only two giant nucleolus foci are visible. On the *right*, a high number of frames reveals emerging structures corresponding to potential transcription factories (Figure and caption modified from Żurek-Biesiada et al. 2015)

that these are the sites of machineries transcribing a cluster of genes. One can relate these patterns to a possible low diversity of genes transcribed at single cell level.

3.2.2 Sub-chromosomal Domains (Scale: 500–1000 nm)

Conventional light microscopy (LM) has already shown some sub-chromosomal structures of chromatin (Mora-Bermúdez and Ellenberg 2007; Dietzel et al. 2004), but due to the resolution limitations of LM (∼200 nm), the precise organisation of chromatin during interphase is barely described. Though transmission electron microscopy has been spectacular at describing the nanoscale structure of cellular objects (Haggis 1992; Dehghani et al. 2005) (see comparison to high resolution microscopy in Betzig et al. 2006), superresolution methods have been a real advancement in localising individual molecules inside the nucleus.

Here, SMLM was used to image the chromosome territories of an interphase nucleus of a primate fibroblast (Fig. 3.5). Magnification and manual segmentation of chromatin structure helps at describing sub-regions of chromosome territories, as proposed in Cremer and Cremer (2001). Between different dense regions, one can easily distinguish corridors, which are likely to give freedom for transcription machinery to function (Fig. 3.5, top inset), though only staining for RNA Pol II or messenger RNA would allow to confirm this hypothesis. The pattern observed follows the model of chromosome territories described previously (Cremer and Cremer 2001), with chromosome territories showing the shape of grapes, each of the grains representing a sub-chromosomal domain (Fig. 3.6a).

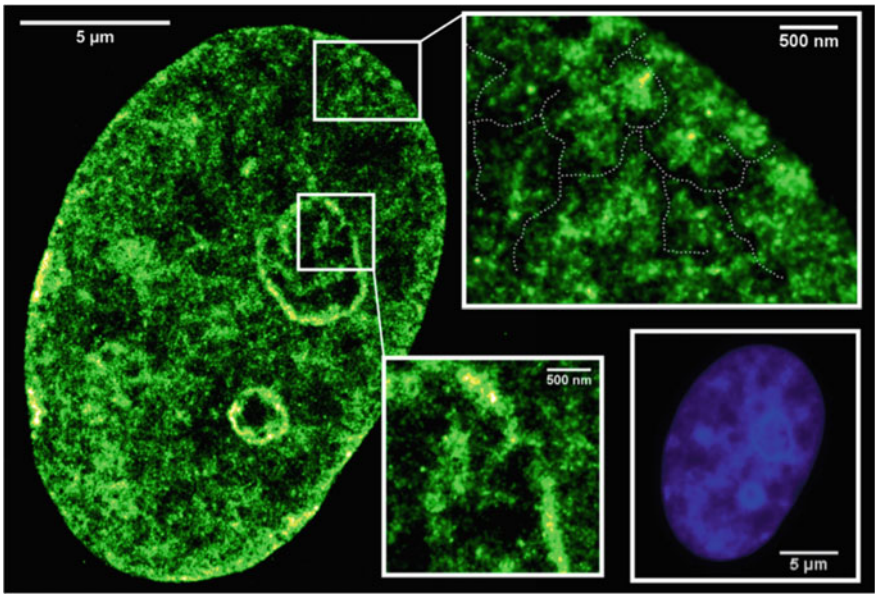

Fig. 3.5 Inter chromatin compartments observed by SMLM (Figure and caption modified from Żurek-Biesiada et al. 2015). A Vero-B4 monkey kidney fibroblast-like cell stained with 500 nM Vybrant DyeCycle Violet is shown. The blowup (*top right*) shows the interchromatin compartments, which possibly provide a path for mRNA to escape into the cytoplasm. The *blue* nucleus (*bottom right panel*) is the non-photo converted widefield image. The periphery of the nucleolus is associated to heterochromatin (*bottom inset*). The signal density is of approximately 5000 single molecules/μm^2

3.2.3 Chromatin Domains (Scale: 100–400 nm)

Recent Proof of a Universal Chromatin Domain Morphology in Mammalian Systems

Genomics has recently generated exciting maps of chromosome interactions within the nucleus, via chromosome capture technologies (3C, HiC and others, see Fig. 1.8). These maps have allowed to identify structural regions called Topologically Associating Domains (TAD). Functionally, this kind of structure comprises genes and remote regulatory regions, and correlate strongly with replication domains (Ibn-Salem et al. 2014; Pope et al. 2014). Structurally, a TAD is an element of about 185 kb in mammals, ranging from 100 kb to 1 Mb (Rao et al. 2014). Low-throughput experiments have been made to validate these structures using DNA probes, however no study has tried to give these genomic data a visual perspective. Thus, a detailed description of fundamental building blocks of chromatin, beyond nucleosome and chromosome territory scale linking genomic data to microscopy data is of immediate importance. For example, how do one-dimensional genome browser or HiC plots (from sequencing

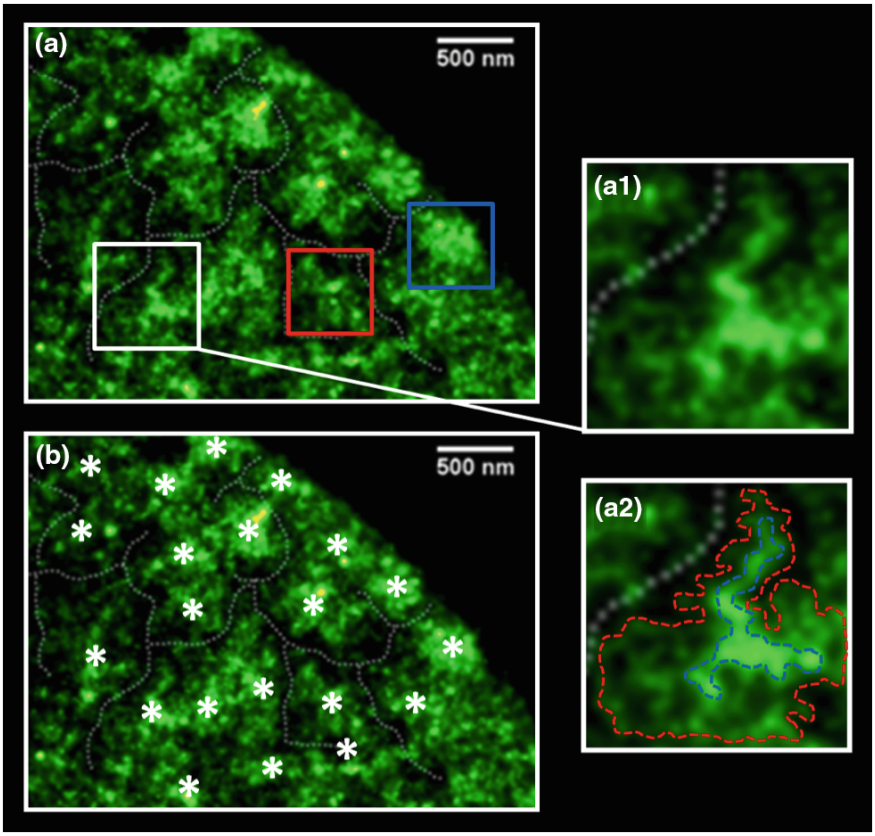

Fig. 3.6 SMLM reveals several levels of chromatin compaction, among them functional chromatin domains: **a** View of a single chromosome territory already presented in Fig. 3.5. *White broken lines* delimit the different sub-chromosomal domains. The boxes show chromatin domains of about 400 nm inside each sub-chromosomal domain. *Red box* active domain. *Blue* repressed domain. *White* intermediate pattern, zoomed in insets (**a1**) and (**a2**). **a1** magnification of mildly compacted domain. **a2** dissection of domain into repressed chromatin (delimited by *blue broken line*) and loose chromatin (*red broken line*). **b** Same picture as **a**, with positions of putative functional chromatin domains shown with white stars. Note that each sub-chromosomal territory has several chromatin domains

data) correlate to microscopy data? Say one observes 100 nm clusters containing 40 signals of activating mark H3K4me3 on microscopy images and finds several peaks on the same region in a ChIP-seq dataset for H3K4me3 (in a similar cell line). How can one relate the two kinds of data? Some models have been described, that attempt to address this problem, but these are mostly theoretical without experimental basis (Fig. A.2).

Recent studies based on FISH and super-resolution microscopy have estimated the sizes of clusters to be between 50 and 400 kbps and around 100–500 nm spatially

(Prakash et al. 2015; Boettiger et al. 2016, and Chap. 4 of this thesis). The regions probed were selected based on combination of histone modifications, distinguishing active, inactive and repressed regions. Overall, the studies provide evidence that there is a functional fundamental building block of chromatin around 100–400 nm confirmed by microscopy data (see Fig. 3.6, the different categories of active and repressed chromatin, red and blue boxes in panel A, respectively). From the center of a domain to the periphery, a gradient is observed, from highly dense chromatin, which is likely compacted, to chromatin of low density, which is loose and probably an active place of transcription (Fig. 3.6b), white box). In a different analysis, chromatin at the periphery of a domain was associated to intense DNA transcription and stress-dependent gene activity (see Sect. 3.4 for more details).

In a recent study (Boettiger et al. 2016), active, inactive and repressed chromatin domains were studied based on ChIP-seq data of histone modifications from Filion et al. (2010). The authors chose H3K4me2 (which marks both enhancers and promoters Barski et al. 2007; Wang et al. 2008) as the mark to study active chromatin domains. H3K27me3 was chosen to mark the repressed and condensed chromatin. It must be noted that H3K9me3 is the mark of the most condensed chromatin while H3K27me3 often localises at the periphery of H3K9me3 and is slightly smaller in size than H3K9me3 clusters (Prakash et al. 2015). Nonetheless, in the study from Boettiger et al. (2016), the active regions based on H3K4me2 could roughly be divided into two categories: short active regions, around 50 kb and of 100–200 nm of radius, and long active regions, around 100–200 kb and of 200–400 nm. Repressed regions based on H3K27me3 designated as regions of most condensed chromatin (corresponding probably to the early concept of 'heterochromatin'), were restricted to a 100–200 nm size.

SMLM Identifies Chromatin Domains Without Prior Knowledge About the Function or Sequence

The data from Boettiger et al. (2016) were generated using DNA probes coupled to fluorochromes and directed toward specific DNA sequences. Interphase chromatin using our SMLM setup that uses conventional DNA binding dyes or EdU coupled to a fluorochrome was also explored. The image of interphase chromatin (Fig. 3.6) identifies different chromosome territories, sub-chromosomal domains (panel a, white broken lines), chromatin domains (panel b, white stars), categories of chromatin domains (panel a, blue and red for repressed and active domain, respectively), and loci with different levels of compaction (inset a1 and a2, with denser region in the center in blue and active region in the outer region in red).

In order to highlight the hierarchical levels of chromatin folding, EdU was coupled to a fluorochrome, showing the positions of freshly replicated DNA molecules within the nucleus. As the targets are theoretically unbiased, a complete view of chromatin distribution within the nucleus was possible (Fig. 3.7). Domains are found to be in the range of 100–500 nm, as predicted by other methods (see Fig. 3.16 for comparison, red rows). Moreover, magnification of the domains reveals smaller highly identifiable spots, likely to be individual loci, possibly nucleosomes (Fig. 3.7a1, a2).

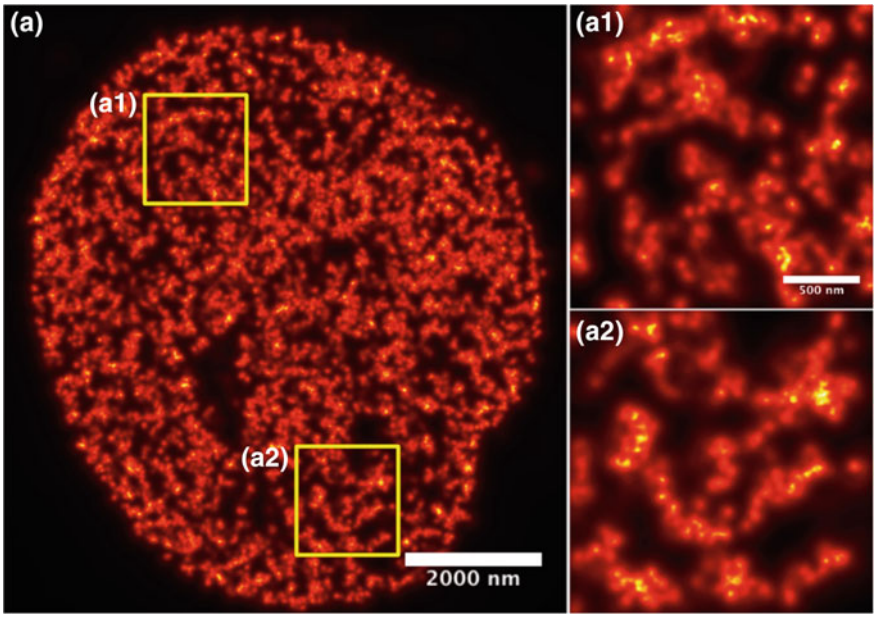

Fig. 3.7 A549 human lung cancer cells were incubated with EdU (DNA base pair precursor) for 15 min and fixed with formaldehyde. Incorporated DNA basepairs were detected using click-it reaction with Alexa 555 leading to staining of freshly synthesised DNA. These samples provide a higher resolution with SMLM as there is very little influence of signals from the background

Universality and Functionality of Chromatin Domains

With respect to recent literature, chromatin domains have started to emerge as the units of genetic regulation, with two important characteristics:

1. **Universality of the patterns**: In HiC experiments, chromatin domains (the term used in genomics is topologically associating domain, or TAD) were found to be about 90% cell-type independent (2763/3000 conserved boundaries between two assayed cell types (Dixon et al. 2012)). The 100–400 nm scale is confirmed in recent studies (Prakash et al. 2015; Boettiger et al. 2016), indicating a very high consistency and possibly universality of chromatin domains. However, one should be cautious in comparing the data, because most of HiC data come from mammals while the work of Boettiger et al. (2016) was conducted in Drosophila. Moreover, the relevance of the patterns found in HiC data is challenged by the low amount of reads (poor sequencing depth) generated by this type of analysis (Fig. A.3).
2. **Functionality of the patterns**: Chromatin domains facilitate function by bringing genes and their regulatory elements closer to each other, with an optimum at 50 kb distance (Doyle et al. 2014). The first comprehensible equivalence between genomic and physical distance provided by Boettiger et al. (2016) confirms this

value. A pure threading pattern of fibres would never allow these sorts of patterns, which hints at folding for both active and inactive regions of the genome at TAD, following models from Rao et al. (2014). In terms of functionality of chromatin domains, Prakash et al. (2015), Boettiger et al. (2016) show that these chromatin domains come from epigenetically characterized regions. Thus, the results presented in Figs. 3.6 and 3.7 further show the potential to find different morphologies of compaction among these patterns.

3.2.4 Chromatin Fibres (Scale: 30–100 nm)

Measurements of DNA is key to describe chromatin accurately. Describing a heterogeneous polymer as complex as chromatin requires to identify its most fundamental elements. Early studies of chromatin spectrum showed several peaks at 110, 55, 37, 27 and 22 Å, shown to be in the direction of the axis of the helix (values highlighted in Finch and Klug 1976). Later this proved to be corresponding to a beads-on-a-string pattern with a width of 8 nm, below an expected 11 nm diameter. The value of 11 nm was confirmed later (see Luger et al. 1997 for instance). First measurements of DNA and DNH (nucleohistone) led to an early incorrect model of chromatin. The molecules of DNA were thought to be in the center of the structure, and the histones at the periphery, though diameter was correctly predicted to be 10 nm (Luzzati and Nicolaieff 1963). Later experiments proved that the real structure follows a different configuration, with DNA molecules wrapping around an octamer of 4 histone proteins. In-vitro evidences from Olins (1974) have described strings of nucleosomes more or less packed and have provided solid evidence for the existence of fibres, but this, only in in vitro studies.

Seminal study from Finch and Klug led to the description of a higher compacted state of chromatin, that was named ‘chromatin fibre’ with a width of 300 Å. Nevertheless, a close look at pictures reveals that there is an intrinsic variability and that the width of elementary chromatin size spans from 30 to 70 nm (Finch and Klug 1976). Though Maeshima et al. (2014) argue that this finding is highly depending on salt concentration, these pictures are likely to capture some elementary features of chromatin. The study also showed that each transversal section of chromatin comprises about 4–7 nucleosomes, leaving a first estimation of correspondence between distances in nm and kb. As found, 12 (visible) nucleosomes of about 200 bp each (if compaction is maximum) multiplied by a factor 2 (to take into account nucleosomes that may not visible), compaction is estimated to be 5-fold. As will be seen later, that is largely an underestimation. An earlier finding from Joseph Gall estimates the diameter of a chromatin fibre around 40–60 nm (Gall 1963).

Different patterns have been seen for chromatin fibres, with more or less nucleosomes visible across transversal plane but this is explained by different relaxation levels of the fibre, highly depending on environmental conditions (Bassett et al. 2009). Opponents to chromatin fibres have proposed a solenoid model (Dubochet et al. 1986), though possible in theory, does not threaten the concept of fibre and the

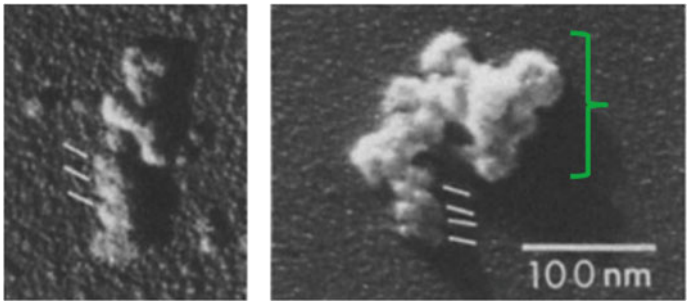

Fig. 3.8 Transition between the 30 nm chromatin fibre and a small chromatin domain of 100 nm from Woodcock et al. (1984). *White* bars show several turns of the fibre, whose width can be appreciated with the scale to be around 30 nm, while the *green* domain is a complex folding of the chromatin fibre with possible regulatory function, a putative chromatin domain. Chromatin domains are presented in Sect. 3.2.3

possibility to build higher order building blocks. Enlightening study from Woodcock and collaborators (1984) has shown how a fibre-like (or solenoid-like) chromatin of 30 nm diameter leads to higher orders of chromatin folding. A very revealing image from their report is reproduced here showing the transition between three turns of the 30 nm chromatin fibre and a more compacted pattern of about 100 nm diameter, a putative chromatin domain (Fig. 3.8). It is a rare case of pattern showing transition between two levels of chromatin compaction, giving a hint about the way structure builds itself hierarchically.

This direct proof of evidence of hierarchy between the fibre and chromosomal domains has not been highlighted in literature, to a point that some researchers now question the existence of fibres. Scarcity of evidence led some authors to recently dispute the concept of chromatin fibre (Fussner et al. 2011), but the question remains open as the article failed at disproving the notion and based its assumption on a spectrum, which can be very well disturbed by the multilevel complexity of chromatin. More evidences account for the high conservation of a level of chromatin compaction in order 40–60 nm across cell types and species (Mayer et al. 2005; Harmon and Sedat 2005). Generally accepted is the idea that fibres can display several levels of compaction and diameter ranges between 30 and 60 nm (Fig. 3.16).

Various groups have experimented new optical devices in order to get insight into fundamentals of chromatin architecture. Most of direct images of in vivo chromatin have been low resolution, and so far only Scanning Electron Microscopy (SEM) and Atom Force Microscopy (AFM) have been able to give a good idea of the actual shape of chromatin. Spectacular images of chromatin from 3T3 cells taken with SEM by Haggis and Pawley (1988), Haggis (1992) show chromatin architecture as a combination of bulky ('balls') and elongated regions connecting 'balls' together, the 'linker' domains (see Fig. 3.9). Measurements of the two categories reveal a configuration of fibres compatible with previous findings of Gall (1963):

- 'balls' display an apparent size of 42 nm.

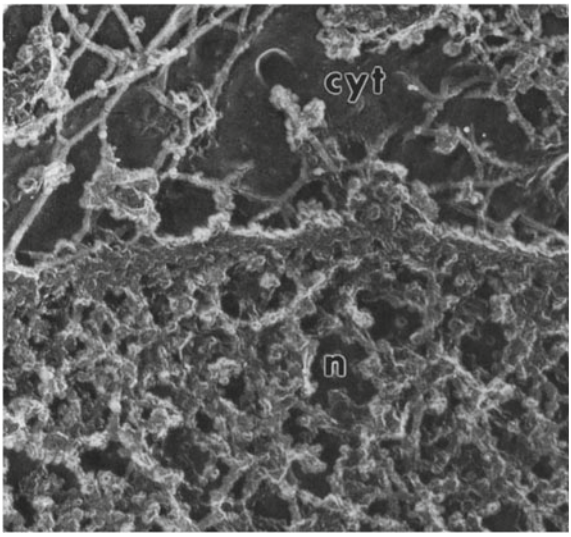

Fig. 3.9 Differential topology of nuclear and cytoplasmic molecular set up revealed by SEM. Cytoplasmic compartment (cyt) is made mostly from highly elongated structures, the cytoskeleton, while nuclear compartment (n) is a web of threads (linkers) connecting bulky regions (balls). Magnification x45,000. From Haggis (1992)

- 'linkers' which bind the 'balls' of length 100 nm on average. Width is close to 40 nm.

The compaction here is not a thread, but a rather cluster on a string. Each cluster or 'ball' is a product of compaction of many nucleosomes (size: 7 nm), possibly several hundreds, for about 50 kb of DNA length. Besides, AFM has been used by Ushiki and Hoshi (2008) to image mitotic chromosomes. Authors find similar 'ball and stick' patterns, whose sizes are approximately 50–60 nm (see the comprehensive scale in Hoshi and Ushiki 2001 and Fig. 4c in Ushiki and Hoshi 2008).

To summarize, history of chromatin research in the last decades has demonstrated the existence of at least two levels of DNA compaction, beyond nucleosomes. One is the 30 nm chromatin fibre, which has been demonstrated beyond shadow of a doubt in several instances. The picture can be a little refined by saying that this element is in most cases not elongated, but rather shrinks to form higher order structures, questioning the epithet 'fibre'. Nevertheless, in several instances (relaxed interphase chromatin, pachytene loops), the term fibre is highly appropriate. One should forget the picture of chromatin as a thread of fibres and replace it by a more complex fibre, which gives birth after folding to a second level of DNA compaction, which is the building block of chromatin regulation (the chromatin domain, whose size is of 100–400 nm).

Finally, I mention the accepted idea that chromatin fibres are one level of ordered compaction of DNA during mitosis (see Ushiki and Hoshi 2008 for nice AFM pictures showing both fibres and chromosome domains; see also Fig. A.4). Beautiful imaging of condensin proteins together with DNA have helped build one of the best models of chromatin architecture proposed until today, with a condesin core holding chromatin around in a regular pattern (Maeshima et al. 2014, Fig. 6).

3.2.5 A Cluster-on-a-String Model to Describe the Fibre/Domain Transition

In order to describe transition between fibres to chromatin domains, one could imagine chromatin domains as clusters on a string. The chromatin fibres of 30 nm would be the string that link two or more domains together. On Fig. 3.9, one can see the white peanut-shape regions as the clusters, while fibres could be the darker grey regions between them. This model is one level higher compared to the bead-on-a-string model in the hierarchy of chromatin compaction and is a sort of intermediate chromatin organisation between the lowest levels of compaction and chromosome or sub-chromosome territories. Imaging of chromosome in meiosis shows that this type of structure is maintained during meiosis and is potentially even more visible on SMLM preparations of meiotic chromosomes if staining against histone modifications such as H3K4me3 is used Prakash et al. (2015).

3.2.6 Nucleosome Domains (Scale: 10–30 nm)

A number of studies have dealt with chromatin fibres at a scale of 30 nm and have tried to establish fibres as the basic structures of chromatin both in inter- and metaphase (Frenster et al. 1963; Hay and Revel 1963). A few studies (Davies 1968; Davies and Small 1968) have pointed out that chromatin is more or less distributed randomly towards the interior (mostly euchromatin) while periodic lumps of chromatin are attached to the nuclear periphery (mostly heterochromatin). In the following section, I revisit this idea from single molecule co-ordinate information and try to explore it further.

Nearest-Neighbour Method Identifies Worm-Like Patterns

In order to study the structure of chromatin at the lowest order, I analysed images of fibroblasts (Fig. 3.10). On the magnified image, the distribution of bead sizes shows an average diameter of 10 nm, in line with the historical measurements of these structures (Oudet et al. 1975; Olins and Olins 2003). In order to give more weight to these beads and strings associations and validate the patterns, I used blurring of nearest-neighbours. Applied to HeLa cells, this technique resulted in finding worm-like patterns of roughly 5–10 nm of periodicity (Fig. 3.11), close to the magnitude of the theoretical nucleosome size (Oudet et al. 1975). On the magnification presented in this figure, one can note some highly identifiable shapes in the decondensed chromatin, which form circles and crosses.

Comparison of the Worm-Like Pattern to Simulated Random Patterns

To understand if the worm-like pattern or beads on the string pattern is a real structure, I simulated the same type of data using a stochastic distributed process to produce the locations. Surprisingly, I could find similar and comparable worm-like structure with overlaid density variation (Fig. 3.12).

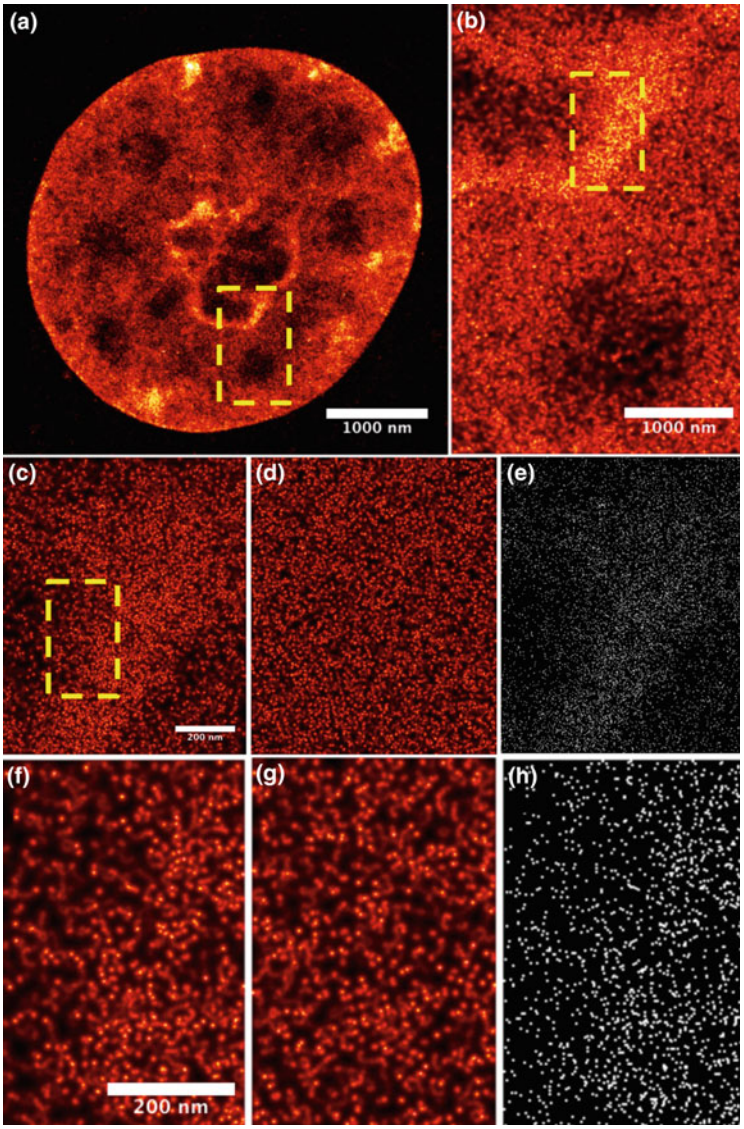

Fig. 3.10 Bead on a string model. Monkey kidney fibroblast-like cell stained with Vybrant Violet to reveals positions of chromatin with several levels of magnification (**a**), (**b**), (**c**) and (**f**). In the magnified section (**c**), it is interesting to note the beads-on-a-string-like patterns that are commonly seen in EM images of 10 nm in vitro nucleosome structures, which fit with the scale bar (200 nm in the inset). The average density is around 3000–4000 molecules per μm^2. The localization image was acquired with a high intensity laser excitation 491 nm, detecting more than 1,300,000 signals in an optical plane through section of approx. 500–600 nm. The mean localisation precision was 15 nm with a standard deviation of 4 nm. In **d** random distribution of **c** is presented, in **g** random distribution of **f**. In **e** and **h** the positions of the single molecules are displayed

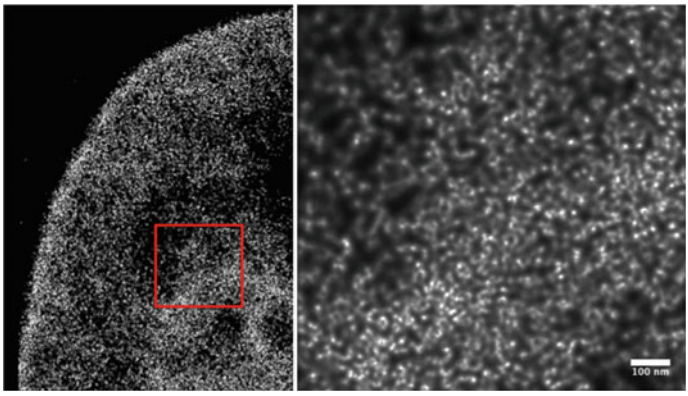

Fig. 3.11 Inverse distance map of pixels based on the next 5 neighbours. The distance of the center of a pixel *i* to the next 5 locations is measured and averaged. 1/meandistance is then assigned as a **grey** value to pixels *i*. The procedure is iterated over all pixels in the image (even those where no fluorophore resides in). The image is then scaled to 8 bit. Is the worm-like pattern a real structure? The cell imaged is a HeLa cell stained with Hoechst 33258

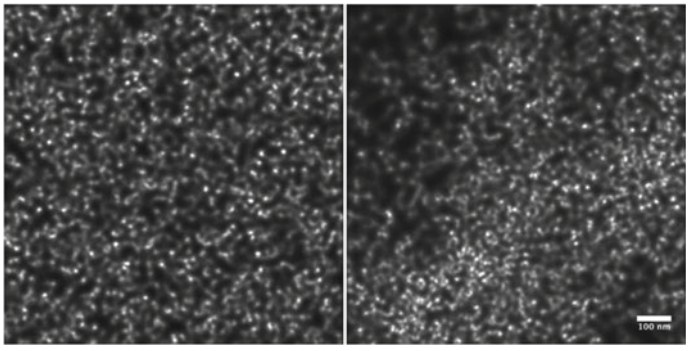

Fig. 3.12 Comparison of chromatin patterns in random and experimental data. (*Left*) Simulation. An image was generated with locations produced by a stochastic gaussian distributed process. (*Right*) Measurement. Comparable worm-like structure with overlaid inverse distance variation are observable. The cell is the same as the one on Fig. 3.11. For the simulated image, the density map is based on the list of localisations or single molecule coordinates. For every pixel in the image the local density is measured based on the mean distance to the next 5 neighbours in the list of localisations. The reciprocal value of this mean distance is then mapped to the corresponding pixel

If the building block is real, the shapes created at scale of 100 nm on this picture could be potential artefacts and the result of a random superimposition of basic patterns. Though one cannot conclude on the relevance of the shape of the chromatin patterns seen around 100 nm, one can still observe more accurate patterns that can be seen at higher scale by using nearest-neighbour methods.

Nearest Neighbour Method Helps to Capture Further Chromatin Complexity Using Combinations of Building Blocks

I then increased the number of nearest neighbours taken for calculation of mean distance and I observed that in the random data worm-like structures were visible at all length scales. According to the theoretical definition, random data is one which is not correlated and therefore does not change under scaling. Interestingly, the worm-like structures vanished when enough next neighbours were taken into account (see Fig. 3.13).

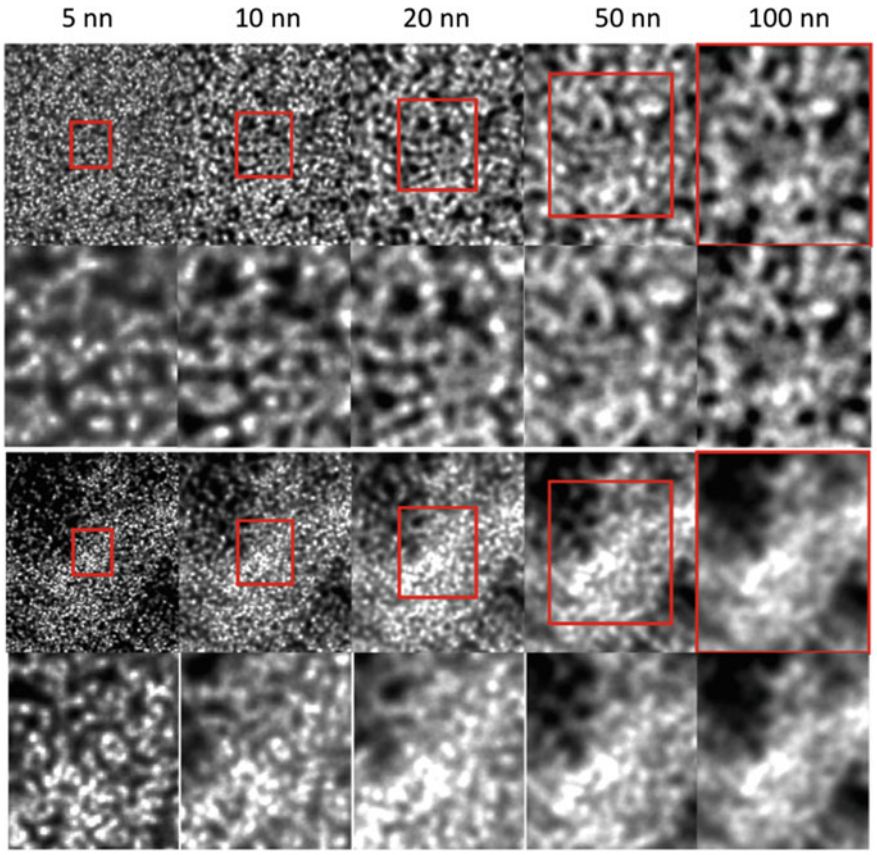

Fig. 3.13 Comparison of chromatin patterns generated with random simulated data to experimental data when different number of nearest-neighbours are taken into account. *Top block* Random case. *Bottom block* SMLM Measurement. From *left* to *right*, influence of the number of next neighbours is considered. In each block, the *second row* shows the region highlighted with a *red box* in the *first row*. In the case of the random configuration, worm-like structures are visible at all scales. In the case of the real data, the worm-like structure vanishes when enough next neighbours are taken into account. Same cell as in Fig. 3.11

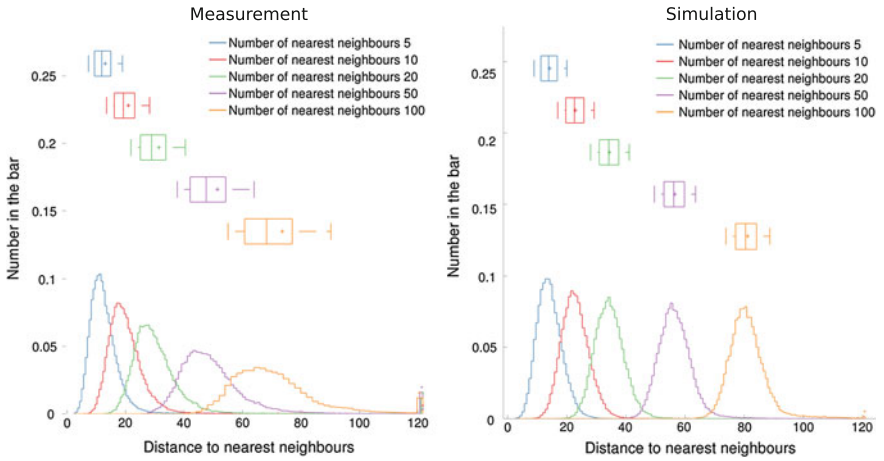

Fig. 3.14 Quantification of chromatin condensation. Distances to 5, 10, 20, 50, 100 nearest neighbours are compared between measurements and simulations. While the distribution of 5 and 10 nearest neighbours are similar between simulation and measurement, there is a significant drop in neighbouring molecules when 20 nearest neighbours are taken into account. For 100 nearest neighbours, a big drop is observable with a very broad distribution, as an indication of over smoothing. The line inside each coloured box-plot in the graph indicates the median, '+' denotes the mean, the boxes delimit the 25 and 75% quartiles, while the whiskers show bounding of 9 and 91% of the data

While the low scale patterns found using nearest neighbour are likely to correspond to topologically associating domains of low scale of around 100 kb ('chromatin domain 2'), the higher order elements defined here correspond to the 'chromatin domain 1' and TAD of about 1 Mb (see Fig. 3.16 for nomenclature). The former are around 100 per chromosome, while the latter are 10 per chromosome and may be equivalent to active genomic regions of high gene content.

Quantification of Chromatin Condensation

I next quantified chromatin compaction in SMLM images by analyzing distances to 5, 10, 20, 50, 100 nearest neighbours (Fig. 3.14). Considerable differences were observed between the experimental data and randomly simulated data. First, the nearest neighbour distances (NND) in the experimental measurements were considerably less than the random simulated when enough number of nearest neighbour was taken into account. Significant differences started to emerge using 20–100 nearest neighbours (65 vs 80 nm). This fact was indicative of local condensation in the experimental data and also provided the expected degree of condensation. Secondly, the distribution of NND in the experimental started to broaden up as the number of nearest neighbour molecule increased. The broadening of peaks can be attributed to the fact that the sparser distributions of chromatin might be represented at the boundary of condensed chromatin, a common feature of chromatin organisation (please refer to Fig. 3.6).

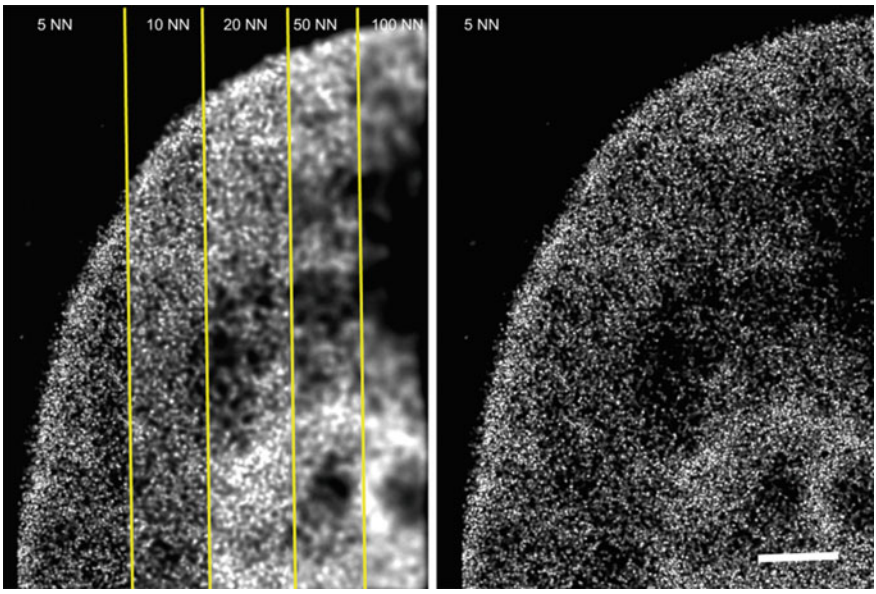

Fig. 3.15 Inference of pattern from local chromatin density maps. *Left* A composite image shows the impact of blurring and condensation enhancement when different number of nearest neighbour (NN) are taken into account. *Right* Same cell with 5 nearest neighbour blurring. The far *left* block in both images (5 NN) are identical. Scale bar: 1 μm

3.2.7 Inference of Further Intermediate Chromatin Structures Using Local Chromatin Density Maps

Images of isolated molecules appear to be similar to the beads-on-a-string-like patterns that are commonly seen in EM images of folded chromatin in vitro (Fig. 3.15). To further investigate this hypothesis, the experimental data were compared with the random simulated data. Comparison of the local inverse distance maps with the distance maps generated by a random process shows that at a larger scale there is a local condensation of the fluorophores whereas at a finer scale the structure becomes random. In the case of real data, the large structures are different from the structures that one observes at a finer scale - which are *'wormlike'* shape. In random data, the worm-like pattern is visible at all scales. This result shows that one cannot resolve the fine substructure because there is none. The molecule signals are real, but the patterns at low scale are not meaningful. Only at a larger scale structure becomes dominant. Hence, organisation of chromatin is clustered at large scales but distributed randomly at fine scales. If our result is confirmed in the future by complementary experiments, our method will prove competence at detecting beads-on-a-string patterns in situ, which is not possible with other current methods so far.

Study	Chromatin feature	radius (nm)	Length (bp)	Method
Olins and Olins 1974	Nucleosome fiber	8 nm	147 bp	EM
Finch and Klug 1976	Chromatin fiber (thin)	30 nm	?	EM
Haggins 1992	Kinks and thick fibers	Kinks: 40-60 nm Linkers: 40 nm	?	SEM
Heng et al. 1996	Meiotic chromatin fibers	50 nm	110 kb	EM
Woodcock et al. 1984	Transition chromatin fiber to chromatin domain	Fibers: 30 nm Domains: 100 nm	?	SEM
Cremer et al. 2000, Cremer and Cremer 2001	Chromatin domain type 1 Chromatin domain type 2	Type 1: 500 nm – 1 µm Type 2: 100 nm – 300 nm	Type 1: 1 Mb Type 2: 100kb	Chromatin treatment and LM (for Type 1)
Lieberman-Aiden et al. 2009, Pope et al. 2014 Rao et al. 2014	Chromatin domains (TADs)	250 nm (approximation from Rao et al. FISH image)	from 50kb to 2Mb median: 185kb	HiC
Boettiger et al. 2016 Prakash 2016 (this report)	Chromatin domains	100-400 nm	From 50 kb to 400 kb	SMLM
Prakash et al. 2015	Meiotic chromatin domains	50-100nm	?	SMLM
Stack et al. 1977 Cremer et al. 2000 Cremer et al. 2001 Bolzer et al. 2005	Chromosome territories	1 µm	?	EM, chromatin treatment, LM, FISH
Lieberman-Aiden et al. 2009 Kalhor et al. 2011	Fractal globule	?	From 50 kb to whole chromatin	HiC

Fig. 3.16 Different milestones of chromatin architecture research, with color classification related to scale investigated. *Yellow* region at the *top* shows milestones toward discovery of chromatin fibre architecture and similar scale fibre patterns (30–60 nm). *Red* region shows main data regarding sizes of chromatin domains (range 100–500 nm). *Orange* region shows a remarkable study of the transition between the two kinds of chromatin architecture that are fibres and domains. Finally, *blue* region at the *bottom* lists the studies which epitomize higher order compaction level of chromatin, including chromosome territories

3.2.8 Hierarchical Organisation of Chromatin Structure

I finally summarize information from literature and personal findings regarding chromatin architecture and its different levels of hierarchical compaction in Fig. 3.16. The table shows the hierarchy of chromatin organisation from nucleosome to chromosome territory, including the building block of a size around 50 nm. In Sect. 3.2.6,

a 50 nm pattern is visible with superresolution microscopy performed on interphase cells. Similar configurations are further shown in stem cells and confirm the existence of functional chromatin clusters around 50–100 nm using the meiotic chromosome as a model, and histone modifications H3K27me3 and H3K4me3 as targets, instead of DNA itself (see the Chap. 4 on meiotic chromatin).

3.3 The Dynamics of Chromatin

Only recently, gene regulation has started to be seen as the result of chromatin dynamics inside of the cell nucleus. A way for chromatin to be dynamically regulated is to switch between heterochromatin and euchromatin states. Electron microscopy, though of high resolution, is poor at identifying regions of low density, such as euchromatin (Cremer et al. 2006), though usage of an expended protocol for Giemsa staining has been shown to turn euchromatin denser and so reveal chromosome territories (Stack et al. 1977). In any case, for a long time, the description of chromatin was confined to distinguish dense and clear regions as compact chromatin (heterochromatin) and relaxed chromatin (euchromatin) respectively, the latter being the place of transcription. Besides, other nuclear components such as the nucleolus were also identified.

For historical purpose, I have showed in the first chapter a photograph of a classical euchromatin/heterochromatin dichotomy, generated from a human leukocyte (Fig. 1.5). A characteristic very thin layer of heterochromatin is present close to the nuclear envelope, while most of the center of the nucleus is the place of a loose chromatin (white arrows). The nucleolus, which is the place of active transcription of ribosomal RNA, is the large dense cluster in the middle. Some stem cells show a contrasting phenotype with euchromatin in the exterior and hetero-chromatin toward the interior. This is discussed in the following section.

3.3.1 Contrasting Arrangement of eu- and Hetero-Chromatin Inside the Cell Nucleus

Previously, chromatin was broadly divided into classical bimodal model i.e. euchromatin and heterochromatin regions. Euchromatin is the open and transcriptionally active compartment of chromatin, mostly found in the interior of the cell, and mostly associated with histone acetylation and certain histone variants. Heterochromatin is condensed and is mostly found at the nuclear and nucleolar periphery. It is also usually referred to as ‘silent DNA’. Repressive histone marks and hyper-methylated DNA are characteristics of heterochromatin.

A comparison of fibroblast cells and mesenchymal stem cells shows that this textbook picture is rather the characteristic of the pattern observed in the fibroblast. Images show a clear contrast between compact and relaxed chromatin, as well as a

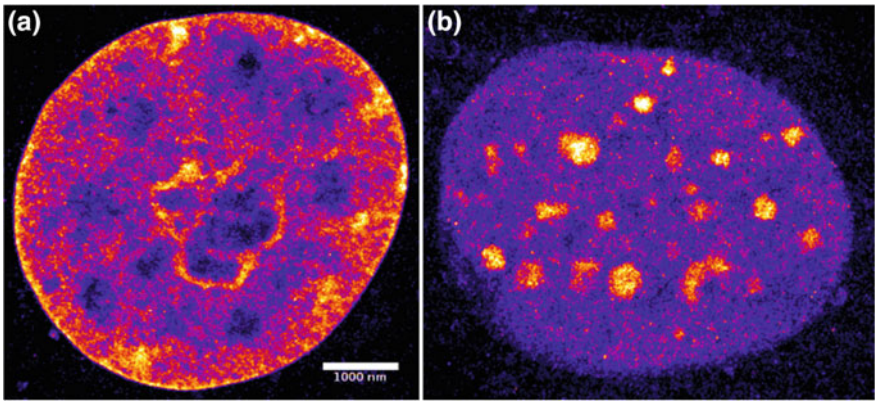

Fig. 3.17 Contrasting phenotype of interphase chromatin. Different cell lines can display very different chromatin phenotypes. The standard belief **a** is that dense chromatin sits at the nuclear periphery while sparse chromatin is located in the interior (here, a monkey fibroblast cell). In **b** one can observe that in Mesenchymal Stem Cells (MSC, mouse), the dense chromatin is absent at the nuclear periphery but is rather found in the interior of the nucleus, in places commonly known as chromocenters. These are rich in H3K9me3, a mark of centromeric chromatin (Smeets et al. 2014; Cremer et al. 2015)

predominant nucleolus (Fig. 3.17a, monkey fibroblast). On the opposite side, stem cells have a broader spectrum of gene expression and show several foci of heterochromatin in the middle, possibly by migration of heterochromatin away from the lamina (Fig. 3.17b), from a mouse mesenchymal stem cell).

3.3.2 Classifier Identifies Intermediate States Between eu- and Heterochromatin Regions in Differentiated Cells

I developed a new method called Pixel Density Classifier (PDC) to classify localisation microscopy data into regions with different spatial densities and structural features. I applied PDC to select different levels of chromatin compaction on SMLM images (Fig. 3.18). Setting the parameter to three different levels of chromatin compaction, I could define three compartments with different densities: one is associated to a loosened state of chromatin, present in the nucleus as large foci (Fig. 3.18c) and corresponding most likely to transcription machinery compartments (which bare chromatin speckles, place of splicing machinery; see similar patterns stained with antibodies against speckles on Fig. 6 in Cremer and Cremer 2001). The second degree of compaction (Fig. 3.18d) is the surrounding area of these foci; this category has the largest distribution of the three and mostly corresponds to euchromatin, that is, the part of chromatin deployed out of the chromosome to be transcribed. Finally, dense chromatin (heterochromatin) is found at the outer part of the nucleus (Fig. 3.18e).

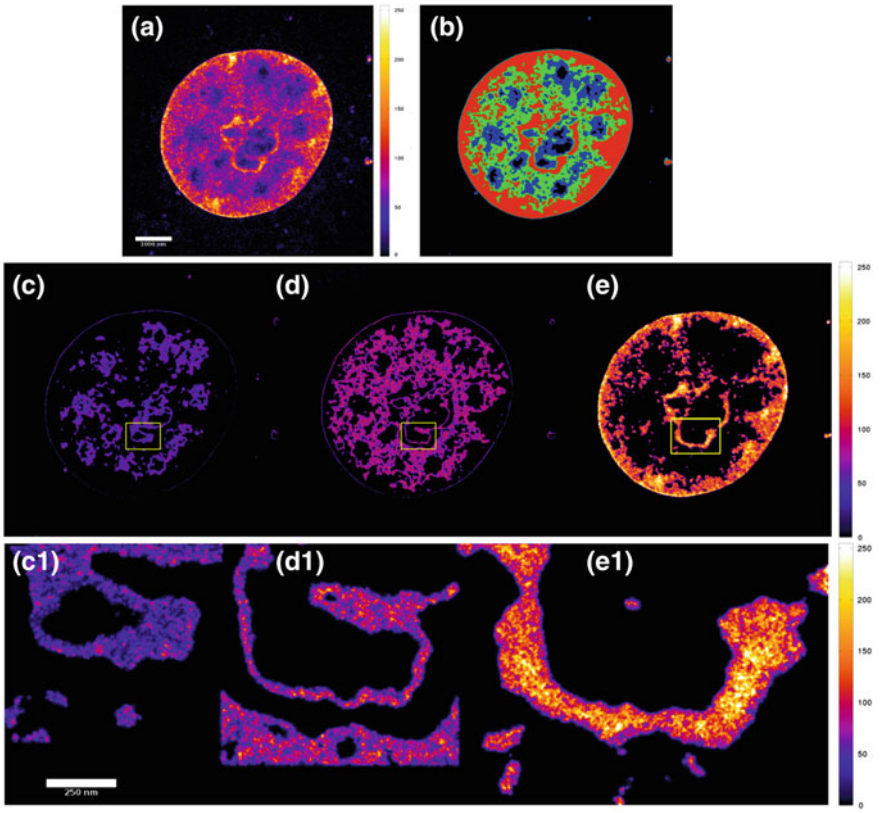

Fig. 3.18 Pixel density classification of chromatin. **a** Monkey fibroblast cell in SMLM using photoconversion of DNA dyes. **b** Decomposition of chromatin into three density states (pixel density of 2, 5 and 9 molecules/100 nm^2 for *blue*, *green*and *red* regions respectively). **c**–**e** Image decomposition shows at least three different status of chromatin of increasing compaction, from **c** to **e**. Intermediate levels are actually the most abundant (**d**) and cannot be classified strictly into eu- or heterochromatin state. (**c1**–**e1**) Magnifications of (**c**–**e**)

3.3.3 Chromatin Dynamics During Differentiation of Mesenchymal Stem Cells

In order to study dynamics of chromatin, I present an example in Fig. 3.19 which shows two images of differentiated and undifferentiated mesenchymal stem cells. From this data, one can draw scenarios regarding the timing of chromatin dynamics during differentiation, even if refined synchronization is needed to capture the entire dynamics.

Step captured in Fig. 3.19a slightly precedes Fig. 3.19b. The chromatin has almost the same level of compaction. Nevertheless, binning the level of compaction into three levels shows that first figure displays elongated patterns of chromatin of intermediate

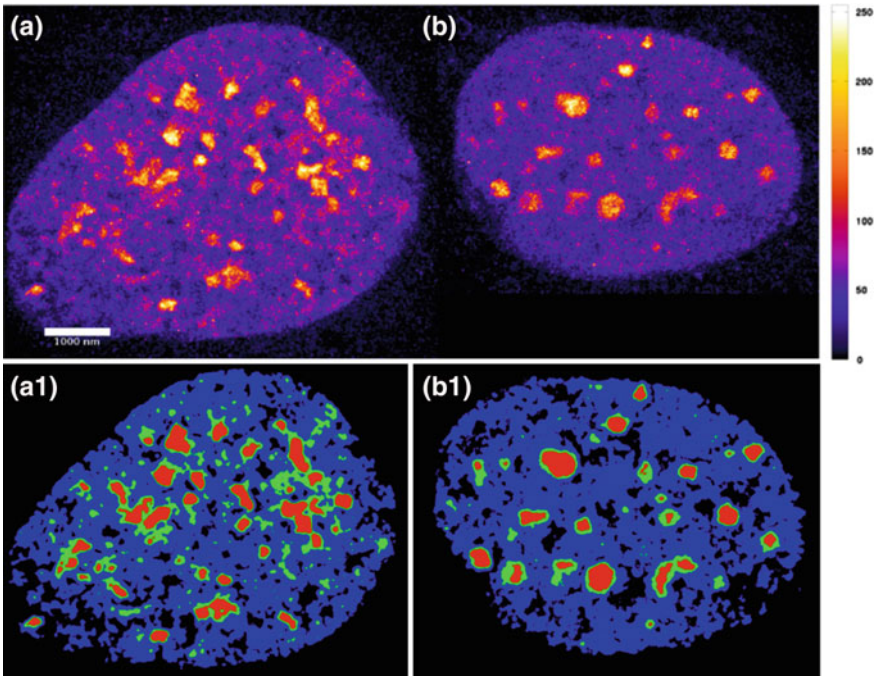

Fig. 3.19 Compaction increases during early differentiation of mesenchymal stem cells. **a** Undifferentiated cell. **b** Differentiated cell. **a1** and **b1** show the different categories of chromatin compaction with number of categories set to three. *Red* is the most condensed chromatin, *blue* the least condensed and *green* is an intermediate level

compaction level, forming threads, showing the progression of chromatin towards condensation in the middle. Figure 3.19b is a slightly later time point, when the compaction is maximum.

Such particular patterns have been also observed previously in Popken et al. (2015). The intermediate stages of the stem cells associated with central heterochromatin islands are reported. Differences between ESC versus differentiated cells chromatin status have been also exemplified in Mikkelsen et al. (2007), confirming the model.

3.3.4 Dynamics of Chromatin upon Stress

Stress as a Good Model to Study Chromatin Dynamics[1]

In order to capture the changes that chromatin can experience during a dynamic process, cardiomyocytes under a cellular stress mimicking infarctus, ischemia, were

[1]This section is partially based on Kirmes et al. (2015).

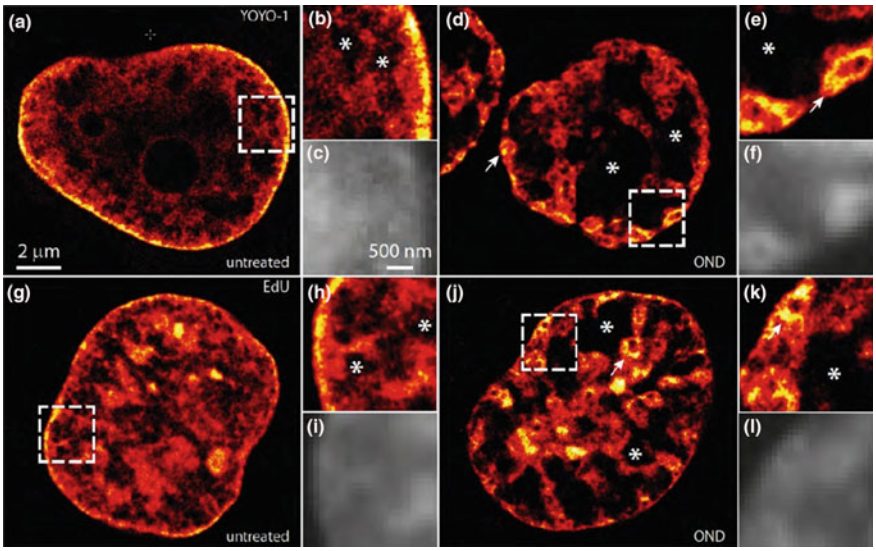

Fig. 3.20 Chromatin compaction upon stress, stained with YOYO-1 (**a**–**f**) or Edu (**g**–**l**) and imaged via SMLM (figure and caption modified from Kirmes et al. 2015). YOYO-1 staining. **a**–**c** untreated cells; **d**–**f** cell subjected to one hour of OND. **g**–**l** 24 h of 10 µM EdU labeling. **g**–**i** untreated cells; **j**–**l** after one hour of OND. After fixation, EdU was fixed to AlexaFluor 488 via click chemistry in situ (see Zessin et al. 2012 for method). Regions devoided of chromatin are indicated by an asterisk, atolls are indicated by a *white arrow*. **c**, **f**, **i** and **l** wide-field images corresponding to (**b**), (**e**), (**h**) and (**k**), respectively

imaged using SMLM. Stress has been shown to remodel chromatin (Johnson and Barton 2007; Hargreaves and Crabtree 2011) and seems to be a good source to study dynamics of chromatin. Extreme patterns of stress highlighting specific ring-shape patterns, likely for mechanistic protection, were previously reported in Everid et al. (1970). This study shows compaction patterns of chromatin following citrate treatment of chicken erythrocytes.

In the present study, the effect of environment on chromatin nanostructure with SMLM and 3D structured illumination microscopy (SIM) was evaluated. Following a short-term oxygen and nutrient deprivation (OND) of the cardiomyocyte cell-line HL-1, chromatin architecture experiences a dramatic changes, adapting to large ring patterns, of 1–5 µm in diameter, with sparse voids inside. These rings most likely correspond to individual chromosomes, hinting at an intense chromatin compaction. The findings show a dramatic adaptation of chromatin to environment, probably due to a major change of energy status.

Distinct Changes of Nuclear Morphology upon Stress

In order to mimic ischemia, SMLM was employed on HL-1 cells transiently exposed to OND. OND procedure was performed by collaborators as follows: cells were put in a hypoxia chamber (Whitley Hypoxystation, see Kirmes et al. 2015 for details) during one hour without any nutrient (ion solution with no organic molecules), to

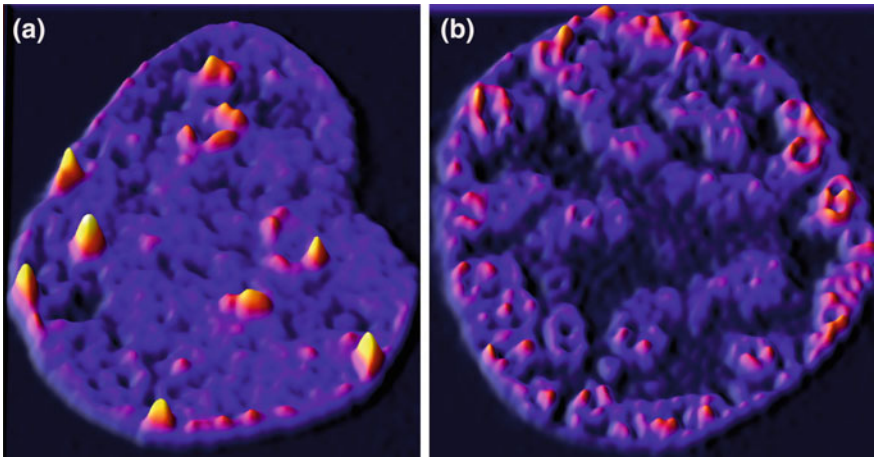

Fig. 3.21 3D surface plot of chromatin nanostructure under ischemia conditions. **a** Untreated cell. **b** Cell subjected to 1 hr of OND. The height represents the density of signal in the reconstructed image

then recover by restoration of normal oxygen concentration and nutrients (Claycomb media). Localization maps were generated in minimum nine replicates for each condition, by integrating 30,000 observations capturing photons re-emitted by the samples after 50 ms of exposure. The images generated spots at the positions of molecules under the diffraction limit, at a structural resolution of 103 nm, which is actually above the theoretical resolution of 67 nm that can be expected.

HL-1 cells treated one hour with OND displayed a major change of their nuclear architecture. Chromosomes shifted from classical interphase territory distribution to a characteristic ring-shape. Most of the chromosomes are attached to one another, mostly at the periphery of the nucleus (Fig. 3.20d, j). Certain chromosomes are bound to the lamina, with elongated patterns nicely exemplified by 3D surface plot in Fig. 3.21. Almost all chromosomes are bound together and form a sort of continuous chain. No part of chromatin shows the diffuse chromatin pattern observed in untreated condition.

3.3.5 Reversible Compaction of Chromatin Under Stress

Next, a time course of chromatin organisation upon hypoxia (Fig. 3.22) was evaluated. Stress induced posture happens within the one hour of induction, while relaxation takes up to four hours to reach complete normal state (Fig. 3.22). The typical stress induced pattern is already vanished after 5 min, leaving the cell with a few caveats that disappear totally after 4 hour of relaxation. Additional images of the time course can be found in appendix (Fig. A.5).

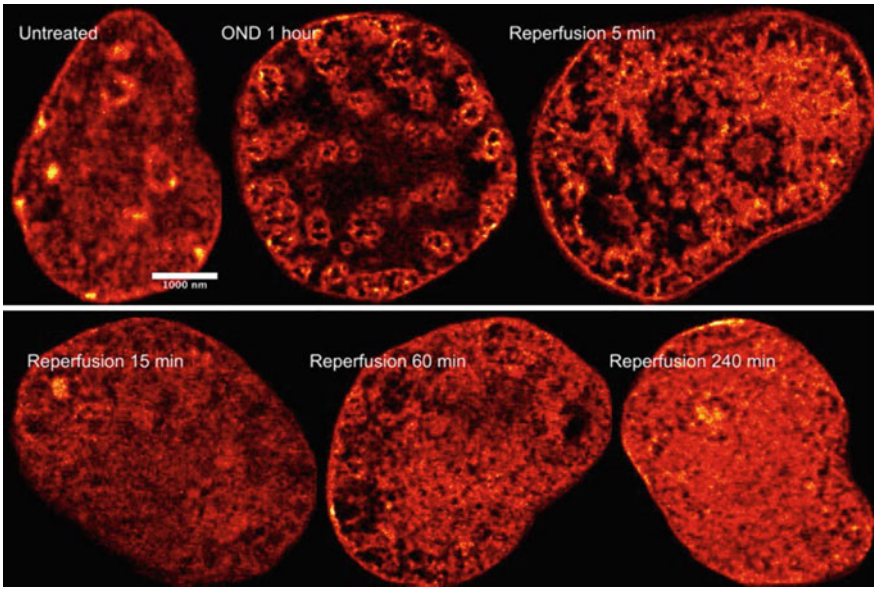

Fig. 3.22 Reversible compaction of chromatin (figure and caption modified from Kirmes et al. 2015). Representative SMLM images of Vybrant Dyecycle Violet-stained nuclei, either untreated, subjected to 1 h of OND or 5, 15, 60 and 240 min after release from OND are shown to demonstrate the reversible compaction of chromatin

This pattern has been related by collaborators to H3K14ac signal during the same hypoxia process; result from confocal imaging shows that H3K14ac is reversibly vanishing during hypoxia (Fig. 3.27 and Kirmes et al. 2015, Supplementary Fig. 4). This result hints at the restoration of the normal phenotype of the cell. Overall, the patterns observed upon stress demonstrate a protective rearrangement mechanism of chromosomes, associated with a reduction of transcription-related histone modifications.

Nearest Neighbour Analysis to Describe the Extent of Chromatin Reversibility

I then tried to describe comprehensively the dynamics of chromatin and its reversible characteristic by computing the distance distribution of the nearest neighbour molecules to regions of interest (ROI) and see how molecules are forming clusters during stress. I find that molecules clustering upon 1 hr of hypoxia tend to be kept away to each other at approximately 100 nm (Fig. 3.23). The normal distribution is broader, showing a more diffuse pattern of chromatin, while the OND-induced condition is narrower and shows further distance, describing the observed clusters. The pattern shifts back to normal upon return to normal environmental conditions, with nearest neighbour distance showing broader distribution again, describing the diffuse pattern (Fig. 3.23, 240 min).

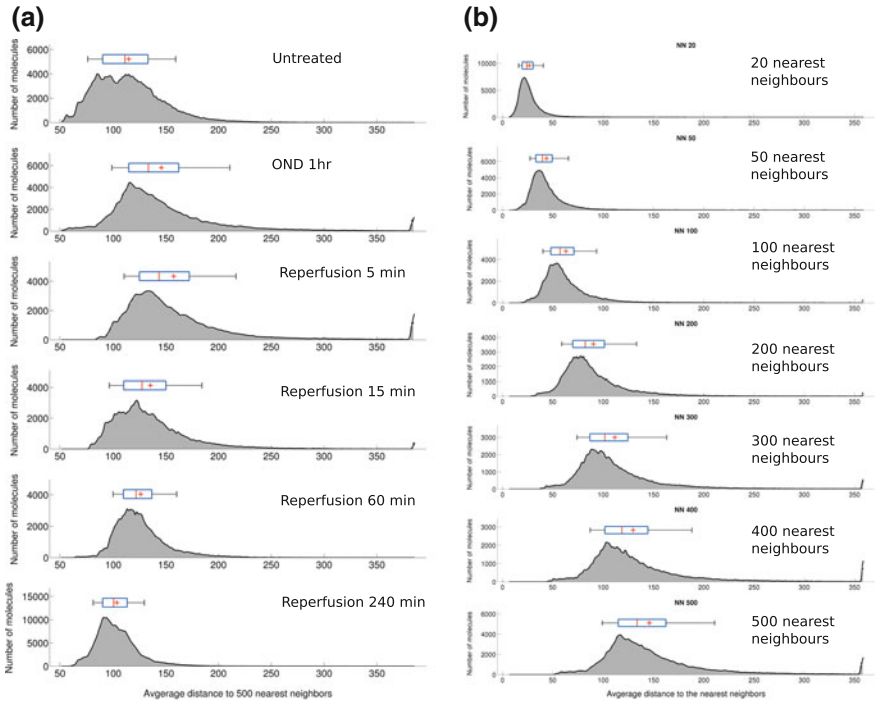

Fig. 3.23 Nearest neighbour characterization to describe the extent of chromatin reversibility. **a** 500 next nearest molecules were used to describe the extent and reversibility of chromatin compaction upon one hour of OND. **b** The effect of different numbers of nearest neighbours (20, 50, 100, 200, 300, 400, 500) was evaluated on the analysed position shown in (**a**) for OND 1 h condition. X-axis: unit is the nanometer

To parametrise the method, I had previously tested the influence of the number of nearest neighbours to calculate the average distance to neighbours (Fig. 3.23b). In the case of 1 h OND, both median distance and breadth of distribution increase with the number of nearest neighbours, showing that low sampling favours neighbours from the same cluster while high sampling captures more complexity and more distant patterns.

I further plotted the distance to nearest neighbours for the different conditions (Fig. 3.24). Interestingly, patterns show that the distribution of distances tends to have an exaggerated normal phenotype upon 4 hr of relaxation, with a mean distance lower for 4 h relaxation than normal condition, and a narrower peak. This result hints at an even lower amount of caveats in the cell under relaxation, caused by an even higher diffusion than for normal state (as the distribution is shifted to the left in Fig. 3.23a), associated potentially with small clustering difficult to observe by sight, of slightly granular shape (as the distribution is narrower, a characteristic of clustering behaviour seen in Fig. 3.23a).

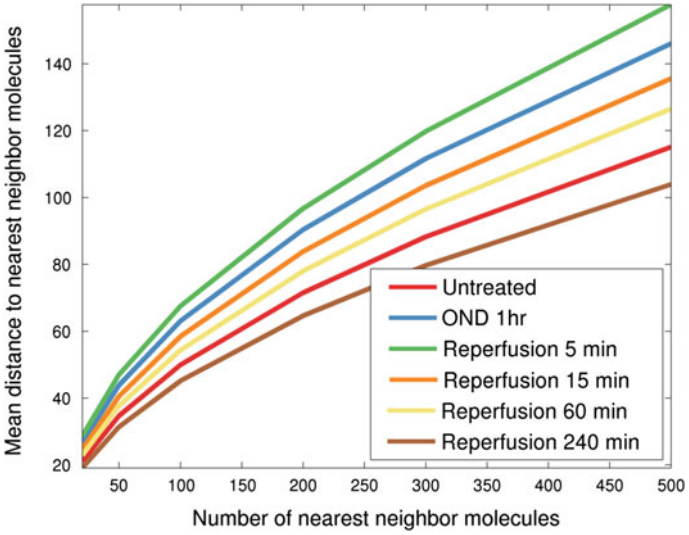

Fig. 3.24 Mean nearest neighbour distance characterisation for different moments of the OND stress experiment. The relationship between the number of nearest neighbours used in the analysis to the mean distance to the nearest neighbour molecules is shown for untreated, 1 h OND or 5, 15, 60 and 240 min relaxation. It is observed that chromatin adapts to a more closed configuration after 240 min of relaxation

Such a pattern may be necessary for the cell to recover from damage, or is a sign of permanent DNA damage. Finally, the recovering pattern after 4 h of relaxation may account for an anarchical distribution of chromatin, resulting in a random pattern of signal position.

Resolution Estimation of DNA Data

Monitoring the resolution for the different steps of the experimental procedure shows that resolution is better for the normal and post OND-induced conditions, while the OND states are more difficult to resolve (Fig. A.6), probably due to condensation and formation of highly dense chromatin. This can come from a poor localisation precision of the signals in the case of the OND state (Fig. 3.25).

3.3.6 Conclusion

I have shown in this section that our super-resolution setup is able to capture the dynamics of chromatin upon biological processes, using hypoxia as model. Such observations would be very difficult to observe using lower resolution methodologies as exemplified by comparisons of our results with widefield images and confocal images. Dynamics of chromatin under stress have shown exceptional patterns rarely

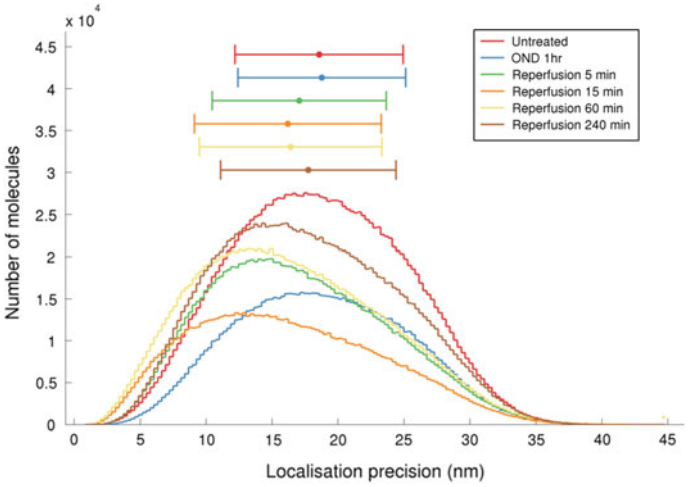

Fig. 3.25 Localisation precision of untreated cells, subjected to 1 h of OND or 5, 15, 60 and 240 min after release from OND

described before (see early study by Everid et al. 1970 on influence of citrate on chicken erythrocytes, which created foci of stress in chromatin). Our set up can also be used for biomedicine in order to further describe the consequence of ischemia for myocardiac cells.

Regarding cellular differentiation, chromatin dynamics is a drastic change in gene expression management. Differentiated cells show clear contrast of compact and relaxed chromatin, with an active region corresponding to the nucleolus which shows that translation is preponderant compared to transcription, leading to betting all nuclear energy on transcribing rRNA (Fig. 3.17a from an adult mouse fibroblast). On the opposite side, stem cells have a broader spectrum of gene expression and show several foci of heterochromatin in the middle, by migration of heterochromatin away from the lamina (right picture on Fig. 3.19, from a mouse mesenchymal stem cell).

From these basic morphologies, one can hypothesize that some kinds of cells do not need to transcribe a lot of genes, but ribosomal RNA; while cells with a stem capacity have to transcribe many specialized genes associated to differentiation and maximize transcription by migrating their dense regions toward the center, to increase the available space for genes to deploy their transcription machinery. Similar patterns have been also observed previously (Popken et al. 2015). In this article, authors report intermediate stages of cells differentiation associated to central heterochromatin islands.

Findings presented in this chapter show both that cells have an intrinsic capacity to condense chromatin (the basis of all developmental processes) and that a cell about to die maximizes its protection mechanism by showing an extreme condensation phenotype. I do not claim here that the model of compaction holds true for every

kind of cells, but that it could rather be a specific properties of certain stem cells which have a high potential of compaction (compatibility) as the genome is not completely folded yet and can be assumed in a 'naive' state.

A Model for Chromatin Dynamics

In the analysis of the differentiation of mesenchymal stem cells and more importantly of the reaction to hypoxia of HL-1 cells, a similar pattern is found: reprogramming of the cell, whether it is for enhancing gene expression at genome scale, or condensing chromatin for protecting DNA integrity, requires condensation or reshuffling in the center of the nucleus. DNA is still present at the lamina, though in little amount compared to classical euchromatin/heterochromatin dichotomy; in the case of mesenchymal stem cells, mostly all over the lamina, while in the case of HL-1 cells, at certain foci which possibly play the role of anchors. In a situation of massive gene regulation as early differentiation events, a big part of the genome can be bound to lamina and so be silenced. The situation for highly stressed cells is different: the entire chromatin has to be packed. In order to facilitate the process, the amount of chromatin attached to the lamina, a process necessary for maintaining coherence of chromatin, has to be as little as possible, so the packing can be done on most of the chromatin.

3.4 The Function of Chromatin

Chromatin was initially defined as a nuclear material composed of histone proteins (Kossel 1884), other proteins (Mirsky and Ris 1951) and possibly RNA (Busch 1974). In order to refine the description of chromatin structure and correlate structure to function, information from histone modification and other nuclear components were employed. This information helped to further identify compartments in SMLM images, something which was not possible with EM previously (Haggis 1992). In this section, different labelling strategies are used in order to understand how the dynamic architecture of chromatin relates to function. Importantly, I show that the periphery of chromatin domains (see Sect. 3.2.3 for a thorough description of these domains) is associated with active transcription and related enhanced replication activity.

3.4.1 Periphery of Chromatin Domains is Associated with High DNA Synthesis

Early replication is associated to regions of high transcription (Boulos et al. 2015). To further describe chromatin domains, I decided to test where replication sites localise in the nucleus. If the outer part of chromatin domains is the place of more active transcription, then replication sites should also localise at the periphery of the domains.

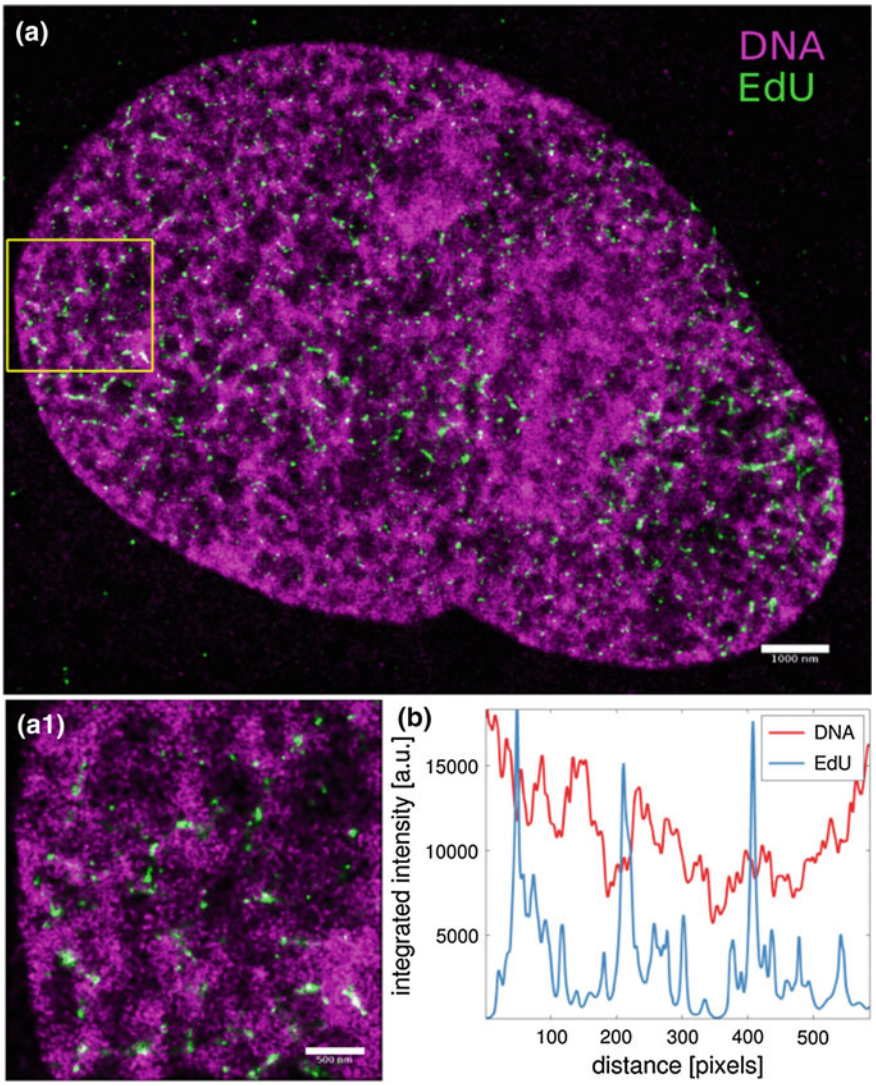

Fig. 3.26 **a** DNA synthesis occuring at the periphery of chromatin domains in a monkey kidney fibroblast cell. *Purple* channel shows chromatin and *green* regions of newly synthesized DNA. White represents the regions overlapping. **a1** Zoomed-in section corresponding to yellow box in (**a**). The vast majority of EdU signals anti-colocalize with chromatin and is observed at the periphery of chromatin domains (**b**). Scale bar in **a** is 1000 nm while in **a1** is 500 nm

To investigate this hypothesis, sites of DNA replication were targeted by incorporating EdU, an DNA-basepair analogue (Fig. 3.26). Alexa 647 was conjugated with Cu(I)-induced 'click chemistry'. Intensity of pixels coming from DNA or EdU signals were recorded on an homogeneous section of the preparation. It is observed that

in newly synthesized DNA sites, the signal locates at the periphery of the chromatin domains (chromatin domain 1 or sub-chromosomal domains, of about 1 μm, in the classification presented in Fig. 3.16), confirming that this region of the nucleus is the site of new synthesised DNA and active transcription, while the center of chromatin domains is a place of repressed transcription, due to condensation of chromatin.

3.4.2 *Stress-Dependent Transcription at the Periphery of Chromatin Domains*

As previously discussed chromatin can protect itself via contraction (Sect. 3.3.4). HL-1 cells were transiently exposed to OND and stained for both DNA and H3K14ac, a histone modification known to be associated to active promoter state (Karmodiya et al. 2012). Cells were fixed, immunostained with AlexaFluor647 conjugated anti-H3K14ac antibody and counter-stained with Vybrant DyeCycle Violet (Żurek-Biesiada et al. 2015). The dynamics of histone modification H3K14ac was monitored during stress. Result shows that this mark experiences a great regression (Fig. 3.27).

Resting state of the nucleus is associated with a classical diffuse pattern of chromatin, with denser regions observable close to the nuclear periphery (Fig. 3.27). The threading network is complex and is interspaced by small inter-nuclear compartments. Staining for an active mark H3K14ac shows punctuate distribution throughout the nucleus (Fig. 3.27). Foci of H3K14ac are found to be present at the edge of chromatin regions (Fig. 3.27b) and in very few places inside of the mass, a result in agreement with theory on nuclear compartmentalization, which identifies interchromatin regions as places of transcription and transport of messenger RNAs (Cremer et al. 2015). Wide-field images are not sufficient to show the tight relationship between chromatin and histone modifications (Fig. 3.27c). As H3K14ac is related to active promoters, it is hypothesized that the cells imaged here are subjected to a high reduction of transcription. This clearly advocates for a physical mechanism of self-protection of chromatin by contraction, which leads to the shut-down of transcription in order to preserve the physical integrity of the DNA.

3.4.3 *Histone Modifications Allow to Further Dissect Chromatin into Active and Inactive Domains*

In order to gain insight into the epigenetic landscape of the interphase nucleus, and study how its structure may be regulated by histone modifications, several histone modifications were stained (Fig. 3.28). A fluorophore density per 100 nm^2 of 0.0125 for H3K9me3; 0.0119 for H3K27me3 and 0.0089 for H3K14ac was found (Fig. 3.28). Globally, this identifies centromeric mark (H3K9me3) as a mark of high density, active chromatin mark (H3K14ac) as the least dense, and the repressive

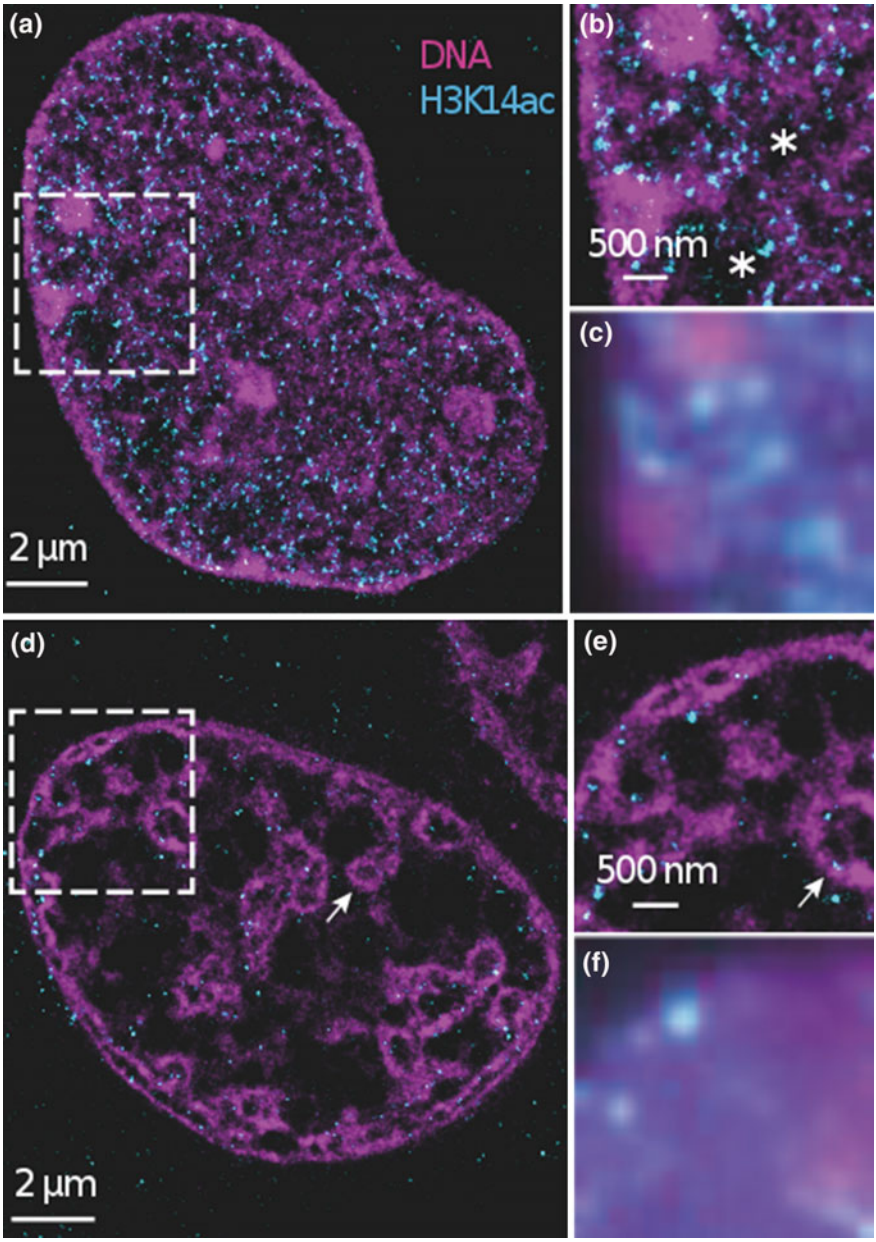

Fig. 3.27 OND induces compaction of chromatin to mechanistically reduce transcription (Figure and caption modified from Kirmes et al. 2015). HL-1 cells were subjected to both anti-H3K14 immunostaining and counter-staining with Vybrant DyeCycle Violet. Signals were analysed using a SMLM set up. **a**–**b** untreated cells; **d**–**e** cells after one hour of OND stress. **b**–**e** magnifications of white boxes in **a** and **d**, respectively. **c**–**f** wide-field images corresponding to **b** and **e**, respectively. Regions deprived of chromatin are highlighted with an asterisk and atolls are shown with a *white arrow*

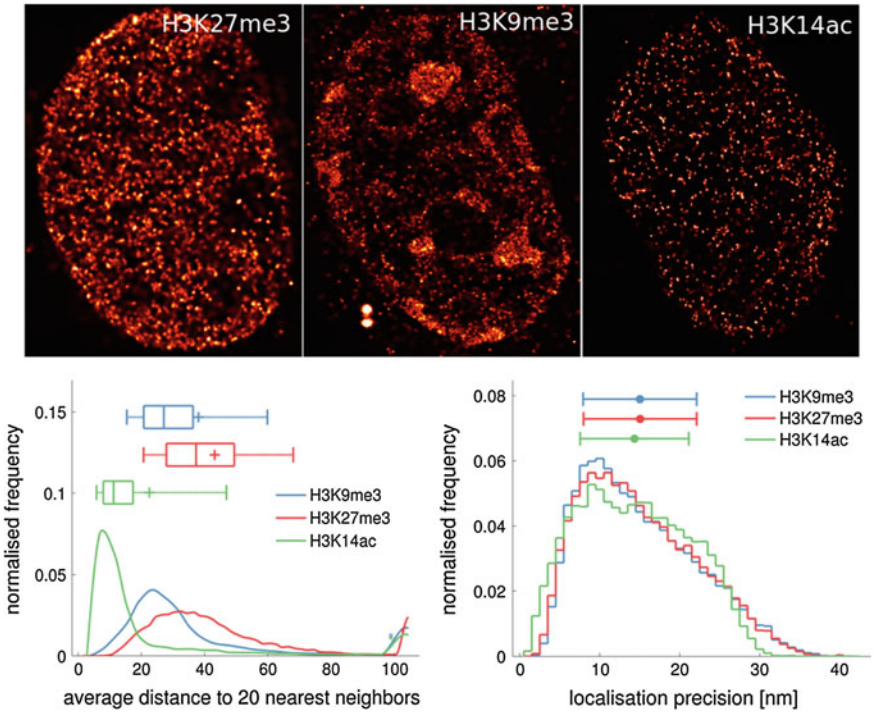

Fig. 3.28 Various histone modifications identify different functional compartments of the nucleus. The figure aside describes the distribution of various post-translational histone modifications in interphase. Often histone modifications have distinct molecular signature suggesting different functional roles in gene regulatory mechanisms. While H3K9me3 is mostly enriched at chromocenters as expected, H3K27me3 is distributed more in a speckle-like patterns. The acetylation patterns (H3K14ac) vary in density and are more diverse in distribution. For functional histone modification patterns during meiosis, see Chap. 4. The nearest neighbour plot gives a measure of the spread of 20 closest signals. Localisation precision plots show that the different sizes of the clusters are not due to the fluorophore i.e. the fluorophore behaves the same in all three cases in terms of photon counts

chromatin mark (H3K27me3) as having the best balance between strength of signal and overall repartition. Comparison between H3K14ac and H3K27me3 marks reveals that the former has a distribution shifted to the left (Fig. 3.28, bottom left image). This shows that the H3K27me3 clusters are broader than the H3K14ac and so are less dispersed. Overall, these findings confirm the highest density of chromatin associated to repressive histone marks.

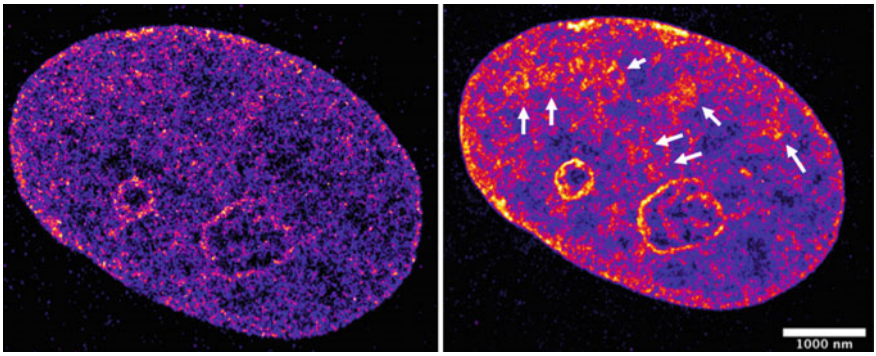

Fig. 3.29 Possible functional compartments emerge from increasing the number of signals on a given figure. *Left panel* 100,000 signals, *right panel* 1,000,000 signals. *White arrows* structures that are not visible with 100,000 signals but are with 1,000,000 signals

3.4.4 SMLM Identifies Potential Sites of Transcription Machineries in the Mammalian Nucleus

Transcription factories are self organising discrete sites where polymerases and other transcription factors are concentrated (Cook 2010). Similarly to Sect. 3.2.1, transcription machineries are identified using SMLM. As shown in Fig. 3.29, while nucleoli are visible with a low number of signals, certain central structures start to appear when enough number of signals are accumulated (white arrows). The organisation of the structures is thought to be an active region of transcription because their round shape is analogical to nucleoli and they are likely to be a collection center of chromatin coming from several chromosomes, similar to the territories/inter-territories model presented in Sect. 3.2.2.

3.5 Summary and Discussion

SMLM was successfully applied to conventional DNA dyes (Hoechst and DAPI) to describe different levels of chromatin organisation, from nucleosome to chromosome territories. High labelling density (more than 10^7 signals per 500–600 nm optical section) of these minor groove binding DNA dyes helped to infer structural features and density variations in chromatin organisation at the nanoscale. It was found that chromatin is clustered at large scales but distributed randomly at the finest scale. At a lower order of organisation, statistical analysis of chromatin distribution revealed distinct differences from a random density distribution. At an intermediate order, 100–400 nm domains emerged as the functional building blocks of chromatin architecture, with differential condensation states. The outer side of these domains being less condensed as compared to the more condensed inner domains.

Furthermore, some examples of dynamic processes that chromatin undergoes were shown, with special emphasis on stress. The compaction of chromatin observed upon stress conditions indicates that it might be experiencing a phase separation process. At its core 'phase separation' means 'like dissolves like and unlike separates/phases out'. For example, GC-rich might separate out from AT-rich regions. From a polymer physics perspective, monomers of the same species phase separate from monomers of a different species. At a chemical level, a polymer composed of hydrophilic and hydrophobic components may arrange itself differentially in order to maximise or minimise interactions with the surroundings medium. In OND conditions, one observes large and dense ring/rod like structures. It is known that most AT-rich region are heterochromatic due to the presence of 2 hydrogen bonds (less active) and that GC-rich regions are euchromatic due to the presence of 3 hydrogen bonds (more active). Since Hoechst and DAPI have high specificity for AT-rich sequences, the GC-rich block of the chromosomes phase separates to form non overlapping micelles (Ostashevsky 1998). Staining of DNA using different oligonucleotide probes specific for simple repetitive DNA sequences might provide further clues.

Finally, using multicolour staining, the structure-to-function relationship of chromatin was studied with focus on metrics that could hint at chromatin activity. The active chromatin regions were on exterior and in decondensed regions (Sect. 3.4.1 and 3.4.2.) while the inactive regions in the interior of the domain (Sect. 3.4.3), with an increase of chromatin density. EdU and several histone modifications helped in identifying novel chromatin compartments. Histone modifications associated with active chromatin were always on the periphery of a chromatin while histone modification associated with repressed chromatin were more toward the interior of a chromatin domain. Also, several new orders of chromatin domains were reported in this chapter.

Overall, it is hoped that the data presented in this chapter will help acknowledging that chromatin folds at various length scales and that domains in the range 100–400 nm constitute the fundamental functional elements of nucleus organisation. Focus on understanding the biology of these domains will be of great help to understand the mechanisms behind chromatin folding and organisation.

References

Barski A, Cuddapah S, Cui K, Roh TY, Schones DE, Wang Z, Wei G, Chepelev I, Zhao K (2007) High-resolution profiling of histone methylations in the human genome. Cell 129(4):823–837

Bassett A, Cooper S, Wu C, Travers A (2009) The folding and unfolding of eukaryotic chromatin. Current Opinion Genet Dev 19(2):159–165

Betzig E, Patterson GH, Sougrat R, Lindwasser OW, Olenych S, Bonifacino JS, Davidson MW, Lippincott-Schwartz J, Hess HF (2006) Imaging intracellular fluorescent proteins at nanometer resolution. Science 313(5793):1642–1645

Boettiger AN, Bintu B, Moffitt JR, Wang S, Beliveau BJ, Fudenberg G, Imakaev M, Mirny LA, Wu C-t, Zhuang X (2016) Super-resolution imaging reveals distinct chromatin folding for different epigenetic states. Nature 529(7586):418–422

Boulos RE, Drillon G, Argoul F, Arneodo A, Audit B (2015) Structural organization of human replication timing domains. FEBS Lett 589(20PartA):2944–2957

Branco MR, Pombo A (2007) Chromosome organization: new facts, new models. Trends Cell Biol 17(3):127–134

Busch H (1974) The cell nucleus. Academic Press, New York

Cook PR (2010) A model for all genomes: the role of transcription factories. J Mol Biol 395(1):1–10

Cremer T, Cremer C (2001) Chromosome territories, nuclear architecture and gene regulation in mammalian cells. Nat Rev Genet 2(4):292–301

Cremer T, Cremer C, Schneider T, Baumann H, Hens L, Kirsch-Volders M (1982b) Analysis of chromosome positions in the interphase nucleus of chinese hamster cells by laser-UV-microirradiation experiments. Hum Genet 62(3):201–209

Cremer T, Cremer M, Dietzel S, Müller S, Solovei I, Fakan S (2006) Chromosome territories-a functional nuclear landscape. Current Opinion Cell Biol 18(3):307–316

Cremer T, Cremer M, Hübner B, Strickfaden H, Smeets D, Popken J, Sterr M, Markaki Y, Rippe K, Cremer C (2015) The 4D nucleome: evidence for a dynamic nuclear landscape based on co-aligned active and inactive nuclear compartments. FEBS Lett

Davies HG (1968) Electron-microscope observations on the organization of hetero-chromatin in certain cells. J Cell Sci 3(1):129–150

Davies HG, Small JV (1968) Structural units in chromatin and their orientation on membranes. Nature 217:1122–1125

Dehghani H, Dellaire G, Bazett-Jones DP (2005) Organization of chromatin in the interphase mammalian cell. Micron 36(2):95–108

Dietzel S, Zolghadr K, Hepperger C, Belmont AS (2004) Differential large-scale chromatin compaction and intranuclear positioning of transcribed versus non-transcribed transgene arrays containing β-globin regulatory sequences. J Cell Sci 117(19):4603–4614

Dixon JR, Selvaraj S, Yue F, Kim A, Li Y, Shen Y, Hu M, Liu JS, Ren B (2012) Topological domains in mammalian genomes identified by analysis of chromatin interactions. Nature 485(7398):376–380

Doyle B, Fudenberg G, Imakaev M, Mirny LA (2014) Chromatin loops as allosteric modulators of enhancer-promoter interactions. PLoS Comput Biol 10(10):e1003867

Dubochet J, Adrian M, Schultz P, Oudet P (1986) Cryo-electron microscopy of vitrified SV40 minichromosomes: the liquid drop model. EMBO J 5(3):519

Everid AC, Small JV, Davies HG (1970) Electron-microscope observations on the structure of condensed chromatin: evidence for orderly arrays of unit threads on the surface of chicken erythrocyte nuclei. J Cell Sci 7(1):35–48

Filion GJ, van Bemmel JG, Ulrich B, Wendy T, Jop K, Ward LD, Wim B, de Castro IJ, Kerkhoven RM, Bussemaker HJ et al (2010) Systematic protein location mapping reveals five principal chromatin types in drosophila cells. Cell 143(2):212–224

Finch JT, Klug A (1976) Solenoidal model for superstructure in chromatin. Proc Natl Acad Sci 73(6):1897–1901

Frenster JH, Allfrey VG, Mirsky AE (1963) Repressed and active chromatin isolated from interphase lymphocytes. Proc Natl Acad Sci 50(6):1026–1032

Fussner E, Ching RW, Bazett-Jones DP (2011) Living without 30 nm chromatin fibers. Trends Biochem Sci 36(1):1–6

Gall J (1963) Chromosome fibers from an interphase nucleus. Science 139(3550):120–121

Gall JG, Pardue ML (1969) Formation and detection of RNA-DNA hybrid molecules in cytological preparations. Proc Natl Acad Sci 63(2):378–383

Haggis GH (1992) Sample preparation for electron microscopy of internal cell structure. Microsc Res Tech 22(2):151–159

Haggis GH, Pawley JB (1988) Freeze-fracture of 3T3 cells for high-resolution scanning electron microscopy. J Microsc 150(3):211–218
Hargreaves DC, Crabtree GR (2011) ATP-dependent chromatin remodeling: genetics, genomics and mechanisms. Cell Res 21(3):396–420
Harmon B, Sedat J (2005) Cell-by-cell dissection of gene expression and chromosomal interactions reveals consequences of nuclear reorganization. PLoS Biol 3(3):e67
Hay ED, Revel JP (1963) The fine structure of the DNP component of the nucleus: An electron microscopic study utilizing autoradiography to localize DNA synthesis. J Cell Biol 16(1):29–51
Hoshi O, Ushiki T (2001) Three-dimensional structure of G-banded human metaphase chromosomes observed by atomic force microscopy. Arch Histol Cytol 64(5):475–482
Ibn-Salem J, Köhler S, Love MI, Chung H-R, Huang N, Hurles ME, Haendel M, Washington NL, Smedley D, Mungall CJ, et al (2014) Deletions of chromosomal regulatory boundaries are associated with congenital. Genome Biol 15(9):423
Iborra FJ, Pombo A, Jackson DA, Cook PR (1996) Active RNA polymerases are localized within discrete transcription factories in human nuclei. J Cell Sci 109(6):1427–1436
Johnson AB, Barton MC (2007) Hypoxia-induced and stress-specific changes in chromatin structure and function. Mutation Res/Fundam Mol Mech Mutagen 618(1):149–162
Karmodiya K, Krebs AR, Oulad-Abdelghani M, Kimura H, Tora L (2012) H3K9 and H3K14 acetylation co-occur at many gene regulatory elements, while H3K14AC marks a subset of inactive inducible promoters in mouse embryonic stem cells. BMC genomics 13(1):424
Kirmes I, Szczurek A, Prakash K, Charapitsa I, Heiser C, Musheev M, Schock F, Fornalczyk K, Ma D, Birk U et al (2015) A transient ischemic environment induces reversible compaction of chromatin. Genome Biol 16(1):1–19
Kornberg RD (1974) Chromatin structure: a repeating unit of histones and DNA. Science 184(4139):868–871
Kornberg RD, Lorch Y (1999) Twenty-five years of the nucleosome, fundamental particle of the eukaryote chromosome. Cell 98(3):285–294
Kossel A (1884) Ueber einen peptonartigen bestandtheil des zellkerns. Zeitschrift für physiologische Chemie 8(6):511–515
Luger K, Mäder AW, Richmond RK, Sargent DF, Richmond TJ (1997) Crystal structure of the nucleosome core particle at 2.8 å resolution. Nature 389(6648):251–260
Luzzati V, Nicolaieff A (1963) The structure of nucleohistones and nucleoprotamines. J Mol Biol 7(2):142–163
Maeshima K, Imai R, Tamura S, Nozaki T (2014) Chromatin as dynamic 10-nm fibers. Chromosoma 123(3):225–237
Markaki Y, Gunkel M, Schermelleh L, Beichmanis S, Neumann J, Heidemann M, Leonhardt H, Eick D, Cremer C, Cremer T (2010) Functional nuclear organization of transcription and DNA replication a topographical marriage between chromatin domains and the interchromatin compartment. Cold Spring Harbor Symp Quant Biol 75:475–492; Cold Spring Harbor Laboratory Press (2010)
Mayer R, Brero A, Von Hase J, Schroeder T, Cremer T, Dietzel S (2005) Common themes and cell type specific variations of higher order chromatin arrangements in the mouse. BMC Cell Biol 6(1):44
Mikkelsen TS, Ku M, Jaffe DB, Issac B, Lieberman E, Giannoukos G, Alvarez P, Brockman W, Kim T-K, Koche RP et al (2007) Genome-wide maps of chromatin state in pluripotent and lineage-committed cells. Nature 448(7153):553–560
Mirsky AE, Ris H (1951) The desoxyribonucleic acid content of animal cells and its evolutionary significance. J General Physiol 34(4):451
Mora-Bermúdez F, Ellenberg J (2007) Measuring structural dynamics of chromosomes in living cells by fluorescence microscopy. Methods 41(2):158–167
Olins AL, Olins DE (1974) Spheroid chromatin units (ν bodies). Science 183(4122):330–332
Olins DE, Olins AL (2003) Chromatin history: our view from the bridge. Nat Rev Mol Cell Biol 4(10):809–814

Ostashevsky J (1998) A polymer model for the structural organization of chromatin loops and minibands in interphase chromosomes. Mol Biol Cell 9(11):3031–3040
Oudet P, Gross-Bellard M, Chambon P (1975) Electron microscopic and biochemical evidence that chromatin structure is a repeating unit. Cell 4(4):281–300
Pope BD, Ryba T, Dileep V, Yue F, Wu W, Denas O, Vera DL, Wang Y, Scott Hansen R, Canfield TK et al (2014) Topologically associating domains are stable units of replication-timing regulation. Nature 515(7527):402–405
Popken J, Graf A, Krebs S, Blum H, Schmid VJ, Strauss A, Guengoer T, Zakhartchenko V, Wolf E, Cremer T (2015) Remodeling of the nuclear envelope and lamina during bovine preimplantation development and its functional implications. PLoS One
Prakash K, Fournier D, Redl S, Best G, Borsos M, Tiwari VK, Tachibana-Konwalski K, Ketting RF, Parekh SH, Cremer C et al (2015) Superresolution imaging reveals structurally distinct periodic patterns of chromatin along pachytene chromosomes. Proc Natl Acad Sci 112(47):14635–14640
Puvion E, Puvion-Dutilleul F (1996) Ultrastructure of the nucleus in relation to transcription and splicing: roles of perichromatin fibrils and interchromatin granules. Exp Cell Res 229(2):217–225
Rao SSP, Huntley MH, Durand NC, Stamenova EK, Bochkov ID, Robinson JT, Sanborn AL, Ido M, Omer AD, Lander ES et al (2014) A 3D map of the human genome at kilobase resolution reveals principles of chromatin looping. Cell 159(7):1665–1680
Richmond TJ, Finch JT, Rushton B, Rhodes D, Klug A (1983) Structure of the nucleosome core particle at 7 a resolution. Nature 311(5986):532–537
Sexton T, Umlauf D, Kurukuti S, Fraser P (2007) The role of transcription factories in large-scale structure and dynamics of interphase chromatin. Semin Cell Dev Biol 18:691–697 (Elsevier)
Smeets D, Markaki Y, Schmid VJ, Kraus F, Tattermusch A, Cerase A, Sterr M, Fiedler S, Demmerle J, Popken J et al (2014) Three-dimensional super-resolution microscopy of the inactive X chromosome territory reveals a collapse of its active nuclear compartment harboring distinct Xist RNA foci. Epigenetics Chromatin 7:8
Stack SM, Brown DB, WC Dewey (1977) Visualization of interphase chromosomes. J Cell Sci 26(1):281–299
Sutherland H, Bickmore WA (2009) Transcription factories: gene expression in unions? Nat Rev Genet 10(7):457–466
Thoma F, Koller Th, Klug A (1979) Involvement of histone H1 in the organization of the nucleosome and of the salt-dependent superstructures of chromatin. J Cell Biol 83(2):403–427
Ushiki T, Hoshi O (2008) Atomic force microscopy for imaging human metaphase chromosomes. Chromosom Res 16(3):383–396
Wang Z, Zang C, Rosenfeld JA, Schones DE, Barski A, Cuddapah S, Cui K, Roh TY, Peng W, Zhang MQ et al (2008) Combinatorial patterns of histone acetylations and methylations in the human genome. Nat Genet 40(7):897–903
Woodcock CL, Frado L-LY, Rattner JB (1984) The higher-order structure of chromatin: evidence for a helical ribbon arrangement. J Cell Biol 99(1):42–52
Zessin PJM, Finan K, Heilemann M (2012) Superresolution fluorescence imaging of chromosomal DNA. J Struct Biol 177(2):344–348
Zirbel RM, Mathieu UR, Kurz A, Cremer T, Lichter P (1993) Evidence for a nuclear compartment of transcription and splicing located at chromosome domain boundaries. Chromosom Res 1(2):93–106
Zorn C, Cremer T, Cremer C, Zimmer J (1976) Laser UV microirradiation of interphase nuclei and post-treatment with caffeine. Hum Genet 35(1):83–89
Zorn C, Cremer C, Cremer T, Zimmer J (1979) Unscheduled DNA synthesis after partial UV irradiation of the cell nucleus: distribution in interphase and metaphase. Exp Cell Res 124(1):111–119
Żurek-Biesiada D, Szczurek AT, Prakash K, Mohana GK, Lee H-K, Roignant J-Y, Birk U, Dobrucki JW, Cremer C (2015) Localization microscopy of DNA in situ using vybrant dyecycle violet fluorescent probe: a new approach to study nuclear nanostructure at single molecule resolution. Exp Cell Res

Chapter 4
Periodic and Symmetric Organisation of Meiotic Chromosomes

Only a structure built on profound symmetry and periodicity can possibly fit 3 meters of DNA inside 10 micron wide nucleus.

In this chapter,[1] single molecule localization microscopy (SMLM) is combined with analytical tools to describe the chromatin organisation of the pachytene chromosomes. DNA is found to be non-randomly distributed along the length of chromosome proteinaceous backbone, the synaptonemal complex (SC), in condensed clusters. Furthermore, chromatin is organized in spatially distinct functional clusters associated to specific epigenetic marks (Fig. 4.1). For functional characterization, various post-translational histone modifications were selected based on information from genomic data and the three following chromatin compartments were identified in the pachytene chromosome:

1. *Radial chromatin* identified by trimethylation of histone H3 at lysine 4 (H3K4me3) — indicative of actively transcribed chromatin.
2. *Polar chromatin* identified by trimethylation of histone H3 at lysine 9 (H3K9me3) — indicative of centromeric chromatin.
3. *Tangential chromatin* identified by trimethylation of histone H3 at lysine 27 (H3K27me3) — indicative of repressed chromatin. This compartment is remarkably associated to the backbone of the chromosome, showing a putative implication in the regulation of recombination.

Periodic clusters of H3K27me3 are found at 500 nm intervals along the SC, while H3K9me3 mark is associated with a large and dense cluster at one of the ends of SC. H3K4me3 is arranged in a radial hair-like loop pattern emerging laterally from the SC, observed for the first time in mammals, especially in context of post-translational

[1] Parts of this chapter, including figures and captions, have been published as Prakash et al. (2015), Prakash (2012).

K. Prakash, *Chromatin Architecture*, Springer Theses,
DOI 10.1007/978-3-319-52183-1_4

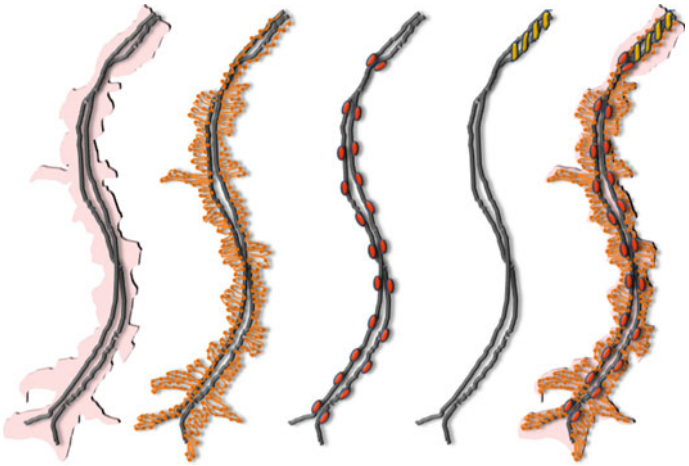

Fig. 4.1 A model for spatial distribution of chromatin at pachytene stage of meiosis prophase I (figure and caption modified from Prakash et al. 2015): Based on localisation maps of post-translational histone modifications, I can dissect the meiotic chromosome structure into at-least three distinct morphologies, highlighted by the differential, nanoscale organization: (1) Radial chromatin identified by trimethylation of histone H3 at lysine 4 (H3K4me3): indicative of actively transcribed chromatin, (2) Tangential chromatin identified by trimethylation of histone H3 at lysine 27 (H3K27me3): indicative of repressed chromatin and (3) Polar chromatin identified by trimethylation of histone H3 at lysine 9 (H3K9me3): indicative of centromeric chromatin. *Image courtesy* David Fournier

histone modifications. For the first time, SMLM is combined with immunostainings and DNA stains to map the global epigenetic landscape of pachytene chromosomes. In this study, single molecule localisation microscopy protocol was optimised to combine direct staining of SC proteins either with DNA molecules or modified histones. This work can be used as a rational to explore the chromatin organization of any cell nucleus, giving both an overview of DNA molecules and refine the picture with meaningful functional annotations.

Finally, taking into account the arrangement and composition of chromatin, as well as the region-specific distribution of post-translational histone modifications, a model of the chromatin architecture along the SC is discussed in this chapter. It is tempting to speculate on a possible super-coiling of meiotic chromosomes, not seen in mitosis or interphase, possibly needed to mechanically simulate chromosome pairing and recombination.

4.1 Introduction

Meiosis is an essential event in the life cycle of sexual organisms, as it creates new genetic combinations at each generation. The two consecutive major events that participate in generating genetic diversity during meiosis are chromosome segregation

and genetic recombination. Chromosome segregation is the sorting of each chromosome of a pair into a different two daughter cell, an event happening in the two cell divisions of meiosis, which results in a major shuffling of alleles. Recombination also participates to diversity by exchanging sequences of 1–2 kb of two homologous chromosomes during an event called crossing-over. This event is more likely to generate innovation as the portion involved are smaller and can potentially edit gene scaffolds, regulatory intergenic regions, or non-coding genes. The places of recombination are not random and are heavily constrained by DNA sequence (mainly GC content, see Clément 2012) and chromosome structure.

Figure 4.2 (inspired by Lichten 2001; Baudat et al. 2013 and other studies mentioned below) details the mammalian meiotic process, preceded by DNA duplication, as described previously in mouse. Particularity of mouse chromosomes compared to human is the location of the centromere at one telomere, resulting in one-arm chromosomes exclusively. During interphase, chromosomes are complex objects consisting of one chromatid and the telomeric centromere (Fig. 4.2, Step 1). After DNA replication, the chromosomes display two chromatids, associated at certain locations via cohesin protein. During early meiosis, cohesin spots dramatically increase, leading chromosomes to form typical chain of loops, called axial element (Fig. 4.2, Step 2, inset). The chromosomes are unpaired and elongated. Moreover, chromosomes start to attach to the nuclear envelopes via their two extremities (Fig. 4.2, Step 3). During zygotene stage, two-chromatids chromosomes start to pair, most likely using extruding DNA generated by double strand breaks (DSB) as probes to find the partner (see pairing in Fig. 4.2, Step 4 represented with light green). The search for the partner chromosome is essentially a random process. Chromosomes move along the lamina until they find another chromosome; if the two chromosomes match, they will start pairing (see dynamics in Sato et al. 2009). Pairing shows formation of a giant protein scaffold, the SC, which holds the two homologous chromosomes at a distance of between 150–200 nm from each other, which is a prerequisite for recombination to happen consistently in a 3D space. The pairing usually starts close to the centromere, as the DSB are more likely in this region (Pratto et al. 2014). Pachytene stage shows the most constrained DNA, with complete pairing all along the chromosome (Fig. 4.2, Step 5). Chromosome pairs at this time are all attached around the same spot of the nuclear envelope that is called the bouquet (Berríos et al. 2014; Gall and Pardue 1969; Sato et al. 2009). During pachytene, recombination happens via the resolution of chromatid DSB from the homologous chromosome and creating a chimera chromosome with extensive portion of both original chromosomes (Fig. 4.2, Step 6, black arrows). Diplotene is a relaxation of chromatin, with unzipping starting from centromeres, leaving progressively the pair attached only at the location of the recombination site (Fig. 4.2, Step 7). Meiosis I ends with the migration of chromosomes to the two asters along microtubules, an event that entangles the recombined chromosomes and leads to migration of the two chromosomes of each pair to different sides of the cell (Fig. 4.2, Step 8). Meiosis I generates two cells with 2n chromosomes (Fig. 4.2, Step 9), while meiosis II completes gametogenesis by generating overall four gametic cells with n chromosomes (Fig. 4.2, Step 10).

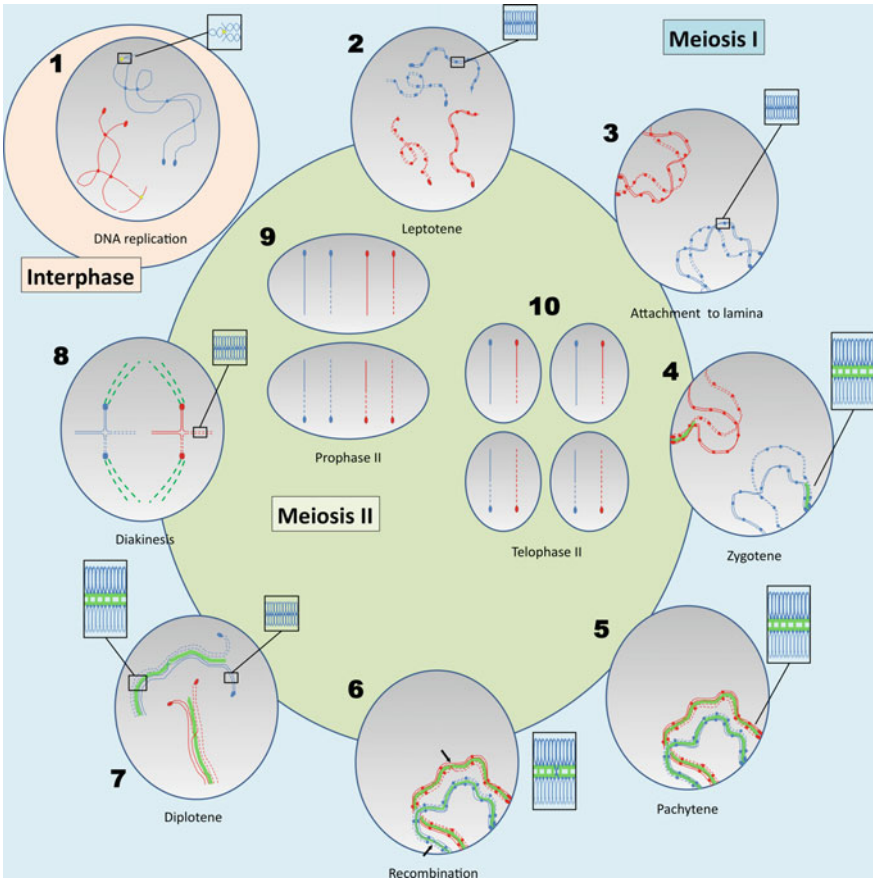

Fig. 4.2 Stages of meiosis: During leptotene, the duplicated chromosomes condense. In zygotene, the SC starts to form the synapsis of homologous chromosomes. During pachytene, homologous chromosomes are completely synapsed and crossing-overs occur. In diplotene, SC starts to disappear. In diakinesis, nuclear envelope starts to fragment and the bivalent chromosomes are ready for subsequent divisions. Blue and red distinguish chromosome pairs. Continuous or broken lines distinguish the two chromosomes of a given pair. *Dots* Cohesin. *Ovals* Centromeres. *Light green* SC. *Black arrows* Recombination sites. *Dark green broken lines* Microtubules. *Image courtesy* David Fournier

In this description of meiosis, synapsis is an essential event for recombination of the homologous chromosomes. Though advances of genomics have proven that recombination can be studied by DNA sequence analysis, getting the detailed structure of the pachytene chromosome is essential to understand the mechanistic steps that have to take place in order to make recombination happen. Here, I propose a detailed description of meiotic chromosomes at pachytene stage. I start by exploring the organization of SYnaptonemal Complex Proteins (SYCPs), which form the SC, the backbone of pachytene chromosome, and then I describe the spatial distribution

of chromatin, including some of its functional compartments associated to certain histone modifications, in relation to SYCP.

4.2 Organisation of the Synaptonemal Complex (SC)

4.2.1 Superresolution Imaging of the SC Substructures

The synaptonemal complex (SC) is an important structural component of meiosis that is used to localise pachytene chromosomes in routine experiments (Baudat et al. 2013). Two important components of SC, namely SYCP3 (the lateral element, Fig. 4.3a) and SYCP1 (the central element, Fig. 4.3b) were first characterised in order to study the architecture of meiotic chromosomes.

Chromosome spreads from oocytes were obtained from collaborators (for details see Prakash et al. 2015). SYCP3 and SYCP1 C-terminus were labelled on separate preparations using antibodies coupled with Alexa Fluor 555. On average, 2500 photons per cycle were detected for Alexa Fluor 555 and localization maps of the two proteins were generated by integrating roughly 20,000 observations. Each frame captured photons acquired during 100 ms of integration time. Individual localisations were blurred using the mean distance to the 20 nearest molecules (method described in detail in Kaufmann et al. 2012). This particular blurring method was chosen for clarity of the visuals and comparison to other visualisation methods is done in Chap. 2, Sect. 2.7.3.

Main images of SC proteins are shown in Fig. 4.3. The colours show a density map, with denser regions close to yellow and regions with low density close to red. Qualitatively, one can see the double-strand nature of both proteins, which is not apparent in wide-field mode of the same image (Fig. 4.3, inset a1 and b1). A dual color image showing relative organisation of SYCP1 and SYCP3 is shown in Fig. B.1 and confirms the double-stranded patterns (Fig. 4.4).

4.2.2 Quantification of SC Substructures

Quantifications confirmed the general structural features of the synaptonemal complex. Profiles of pixel density show the improvement of the superresolution setup compared to a wide-field image of the same object, the double-stranded SYCP3 and SYCP1 scaffold (Fig. 4.4a): clearly, the two strands cannot be distinguished with conventional microscopy (for confocal microscopy images, see Baudat et al. 2013). Distribution of SYCP1 and SYCP3 signals along the SC shows a clear separation of the two lateral elements, and a more central localisation for SYCP1 (Fig. 4.4b). By computing the distance from the maxima of each individual strand of SYCP3, I estimated the distance between the two strands of SYCP3 to be around 181 nm

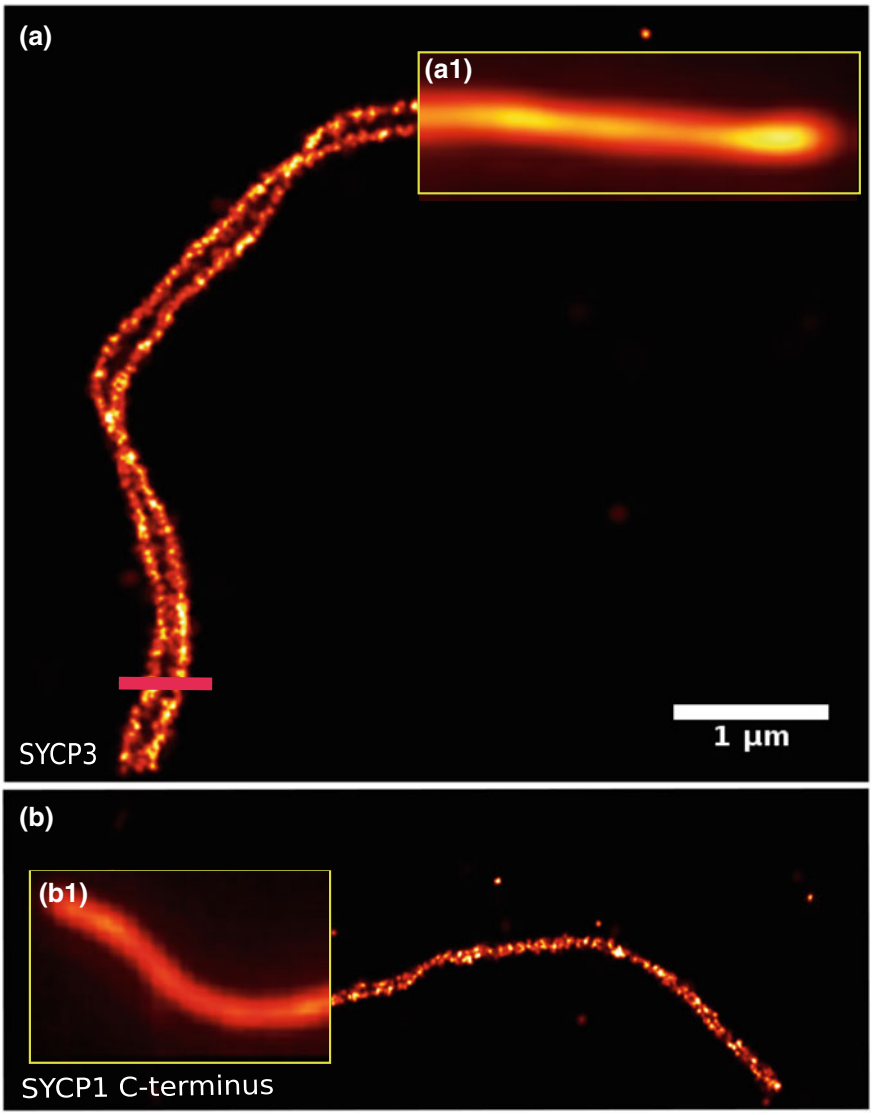

Fig. 4.3 Organisation of the synaptonemal complex proteins (figure and caption modified from Prakash et al. 2015): SYCP3 (**a**) and C-terminus of SYCP1 (**b**) protein are imaged using antibodies coupled with Alexa Fluor 555. Insets **a1** and **b1** show the widefield equivalents of the underlying localization image

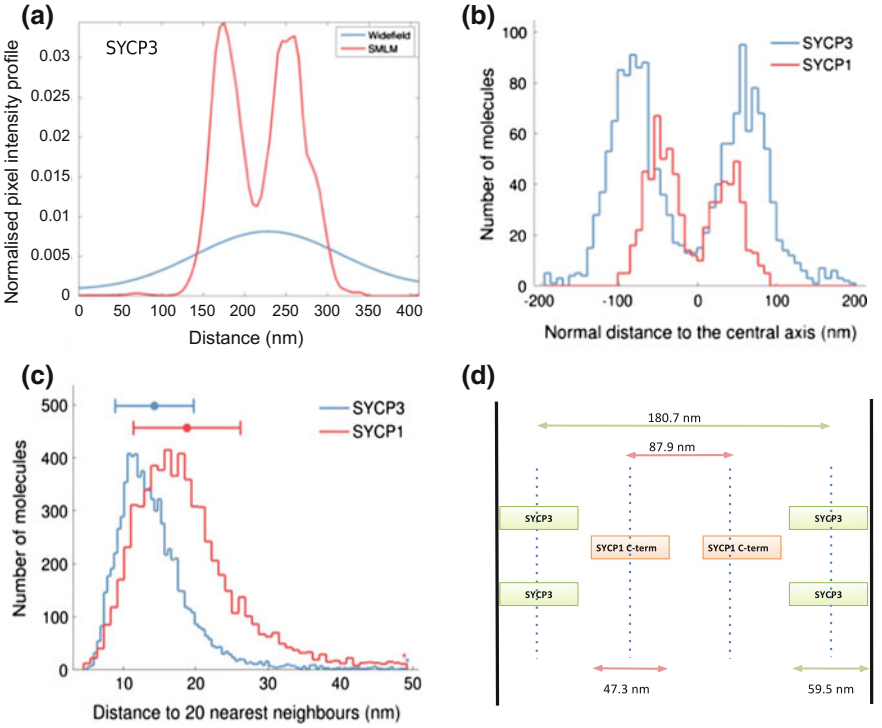

Fig. 4.4 Quantification of SC substructures (figure and caption modified from Prakash et al. 2015): **a** Distribution of SYCP3 along the transversal plane of the SC (i.e. perpendicular to main axis) in SMLM (*red*) versus wide-field configuration (*blue*). **b** Distribution of C-terminal end of SYCP1 and SYCP3 along the transversal plane (*red* and *blue plots* respectively). The distance between the positions with highest molecule occupancy is 180.7 nm for SYCP3 and 87.9 nm for the C-terminus of SYCP1. **c** Average distance to the 20 nearest neighbors was used to calculate the extension of blurring of the individual molecules. For SYCP3, the distance used was 14.31 nm +/− 5.43 nm and 18.81 +/− 7.40 nm for SYCP1. **d** A schematic diagram illustrating the thickness and the interstrand distance of SYCP3 and SYCP1

and the width of an individual strand to be 60 nm (Fig. 4.4b). Moreover, analysis of SYCP3 patterns at the ends of the chromosomes shows that the SC is narrower at the telocentric end compared to the other end (Figs. 4.11 and B.8). I used the same approach for SYCP1, whose distance between the strands was found to be 88 nm and the width of the strands themselves 47 nm.

The inter-distance between strands was calculated by taking the position with the maxima of molecule distribution on each strand. Individual fluorophores were detected with a precision of 11 nm for SYCP3 and 16 nm for SYCP1. Moreover, a Fourier Ring Correlation (FRC) resolution of 43 and 56 nm was found for SYCP3 and SYCP1 C-terminus, respectively. For SYCP3, the nearest neighbour distance was 14 +/− 5 nm and for SYCP1, this distance was 19 +/− 7 nm (Fig. 4.4c). These distances were used as the standard deviation of the Gaussian distribution applied

to the individual molecule position for blurring, a slight modification of Gaussian blurring (see Fig. 2.17 of methods chapter for comparison of visualisation methods using the SC data as example).

Furthermore, in a two colour experiment both SYCP3 and SYCP1 C-terminus were stained. Immunostainings were performed using either Alexa 555 coupled to an antibody against SYCP3 or Alexa 488 coupled to an antibody against the C-terminal of SYCP1 (Fig. B.1). The merged image clearly shows that SYCP1 is located inside of SYCP3 (Fig. B.1c), of similar double-strand nature (insets). I roughly summarize the findings in a visual that shows SYCP3 proteins on the outside of the SC and SYCP1 on the inside (Fig. B.1d). These results are in line with observations from other studies (Gustafsson et al. 2008; Syrjänen et al. 2014; Schücker et al. 2015). A recent SMLM study reported the width of individual strands of SYCP3 to be around 56 nm while the distance between strands to be around 165 nm (Schücker et al. 2015). The width of SYCP1 C-terminus was reported to be 45 nm with overall width of central region (composed of transverse filaments (TF) and the central element (CE)) to be around 148 nm, similar to the values found in my analysis (Fig. B.1d).

4.2.3 A Model for Organisation of SC

In this section, I suggest a model for the SC incorporating further information from Syrjänen et al. (2014). As the antibodies are directed toward the C-terminal of SYCP1 proteins, information obtained from localization of these molecules confirms the inner position of the SYCP1 C-terminal domain (Fig. 4.5), with N-terminal sides of SYCP3 molecules directed toward the center of the SC. SYCP1 dimers could interact to form a ladder-like structure, while SYCP3 molecules link neighbour DNA loops, as demonstrated in the model of Syrjänen et al. (2014). The figure shows the two chromosomes modelled with two sister chromatids shown in light and dark blue. SYCP3 triads can act to bring distant locations on a chromosome together by self assembly (Syrjänen et al. 2014). This would eventually lead to the shortening of the chromosome axis longitudinally while lengthening or looping out of chromatin radially. The chromatids for both homologs are separated by a distance of roughly 150–200 nm i.e. the distance between the two strands of SYCP3 (green box). The inter-loop DNA is figured with a black line. This region is likely to be the site of repetitive DNA sequence and may be enriched with histone marks that condense chromatin like H3K27me3 (Pauler et al. 2009). SYCP1 is depicted as a blue box. Similarly to SYCP3, SYCP1 might play an important role in the final assembly of the pachytene chromosomes.

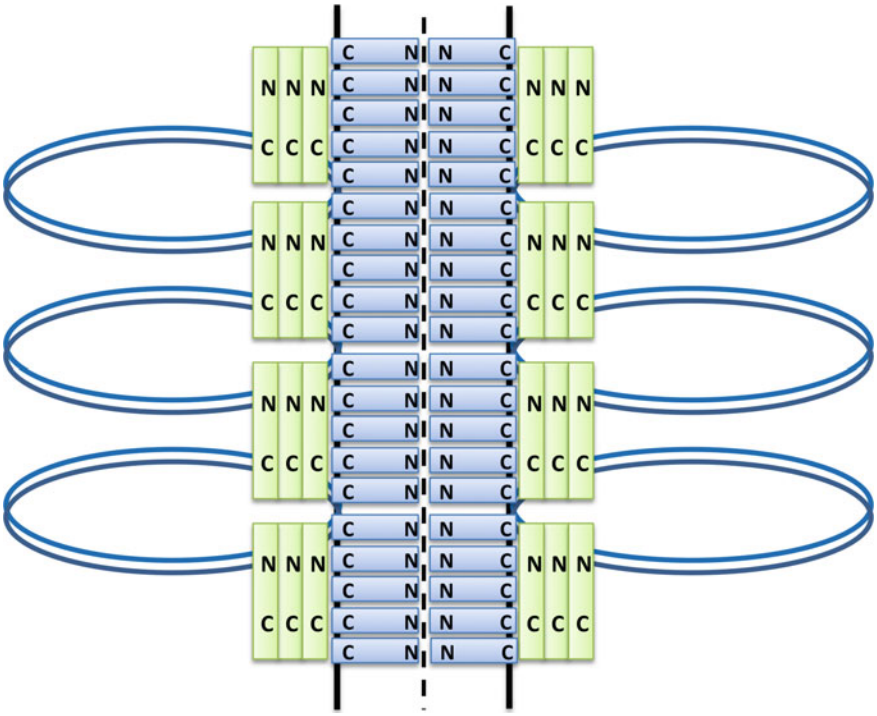

Fig. 4.5 A model for the synaptonemal complex explaining the results presented in this chapter with evidences and models from Syrjänen et al. (2014) is shown. The view shows the two chromosomes modeled with two sister chromatids in *light and dark blue*; the inter-loop DNA is figured with a *black line*. SYCP1 is depicted as a *blue box* and SYCP3 with a *green box*; both show their N and C terminal domains

4.3 Periodic Organisation of Pachytene Chromosomes

The pachytene chromosomes have a very constrained pattern in 3D space (Schücker et al. 2015), which is highly identifiable on mammalian chromosome spreads. This is due to the fact that recombination process requires two chromosomes of a pair to be kept apart 100 nm of each other in order exchange of chromatids to happen (Petronczki et al. 2003). As a result, both the highest order of chromatin complexity and density is attained at pachytene stage of meiosis, the moment when recombination takes place. Pachytene chromosomes are visible in EM (for instance in Moses et al. 1977) and SEM (Fig. B.3) preparations of mouse samples and display a typical caterpillar shape. Though EM and SEM are among the most powerful techniques to probe nanoscale structures, they do not stain efficiently and specifically particular proteins. High resolution light microscopy based measurements of pachytene chromosome are therefore necessary and occupy the next section of the present chapter.

4.3.1 Superresolution Imaging of Pachytene Chromosomes Reveals Periodic Clusters of Chromatin

Experimental procedure was close to the one described for the characterization of SC proteins. The protocol for imaging DNA has been described in Żurek-Biesiada et al. (2015). Briefly, samples were immunostained using Alexa 555 conjugated anti-SYCP3 and DNA with Vybrant DyeCyble Violet (Life Technologies), a dye with similar properties as Hoechst and DAPI (Szczurek et al. 2014; Żurek-Biesiada et al. 2015). Blinking efficiency was stimulated using our custom switching buffer consisting of glycerol with 10% (wt/vol) imaging buffer (stock comprising 0.25 mg/mL glucose oxidase, 0.02 mg/mL catalase, 0.05 g/mL glucose in PBS). For SYCP3, localisation maps were generated integrating roughly 20,000 observations and about 100,000 observations for DNA. A two-color image was generated after application of nearest-neighbour blurring to the raw single molecule data (Fig. 4.6a). Density map of the DNA channel reveals periodic clusters of chromatin, characterized by a central high density region (Fig. 4.6b). Elongated extensions of the DNA are localised laterally, possibly involved in recombination (Gall 2012; Callan 2012). General shape of chromatin is reproducible (Fig. B.6) and is validated by SEM experiments (see Fig. B.3).

4.3.2 Quantification of Periodic Chromatin Clusters

Quantification helped to further describe the density distribution and the periodicity of the chromatin clusters. Pixel density classification (Fig. B.4) reveals that the clusters have two major regions: a central region which bares the highest density (3.5 signals/nm^2) and an outer region of lower density (1.5 signals/nm^2 see Fig. B.4, purple and green regions, respectively).

In order to characterize the periodicity of the clusters and distinguish them from background, I first applied auto-correlation, an algorithm to find similarity of signals (Fig. 4.6c). Periodicity lies in the range 550–700 nm tangentially along the SC axis (Figs. 4.6e and B.6a3). The average diameter of the clusters is found to be in range of 170–225 nm (Fig. B.9). Later, a new algorithm was developed to further characterize the clusters (Fig. 4.7). First, a binary mask was generated based on distance to 20 nearest neighbour and signals within this mask were taken for further analysis. A randomly generated image with the same number of localisations is presented for comparison (Fig. B.2b). The random distribution served as a control to be compared to the SMLM data. Nearest neighbour distances were used to characterise the local condensation in SMLM and randomly simulated data (Fig. B.2c). In the experimental data, the mean distance to 500 nearest neighbours was around 86 nm while in the simulated random data, it was 110 nm (see Prakash et al. 2015), supplementary data). This non-random distribution of DNA was indicative of the fact that the clustering observed in SMLM images of DNA is a consequence of structural packing of DNA.

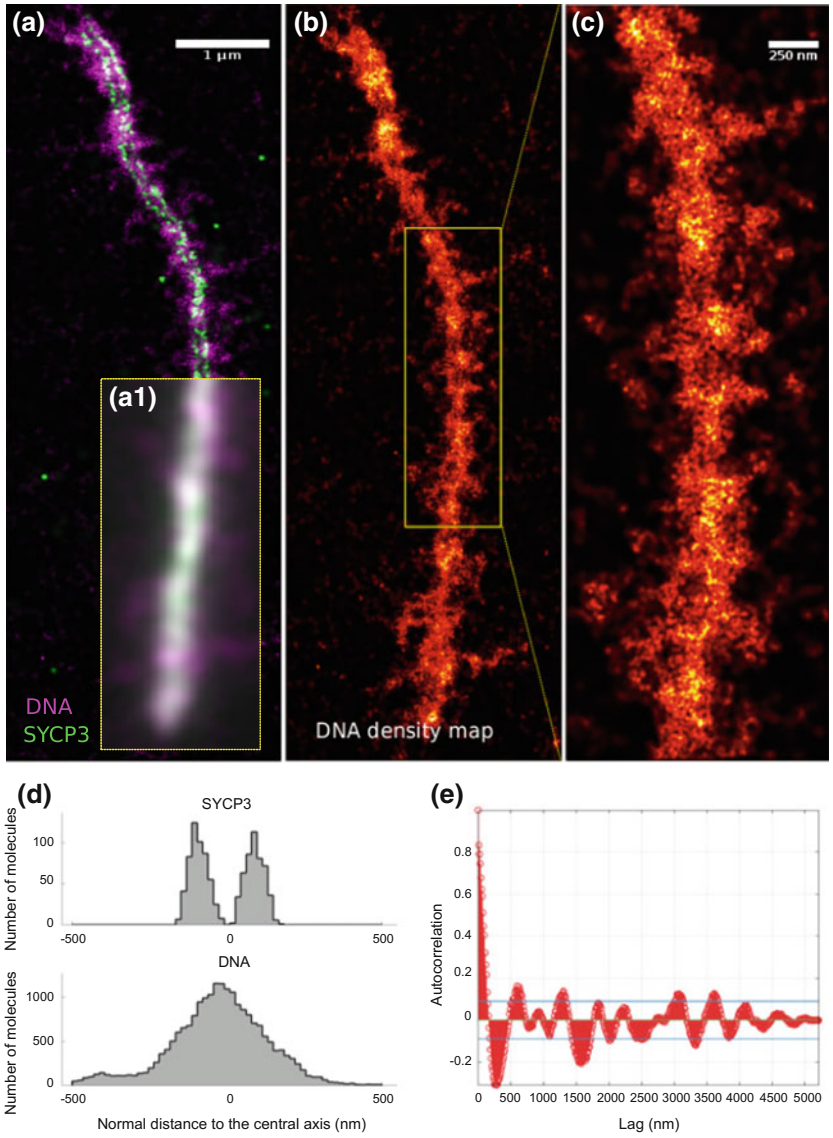

Fig. 4.6 Super resolution microscopy reveals higher order clusters of chromatin patterns along the pachytene chromosome (figure and caption modified from Prakash et al. 2015): **a** Samples immunostained using Alexa 555 conjugated anti-SYCP3 and counter-stained with Vybrant Violet, a photocovertible DNA dye (see Chap. 2 for more details). Inset **a1** shows the wide-field image for comparison. **b** DNA density map of the pachytene chromosome. Scale bar same as in **a**. **c** Magnified section corresponding to yellow box in **b**. Scale bar: 250 nm. **d** Distributions of SYCP3 and DNA molecules around central axis of SYCP3. **e** Autocorrelation plot of chromatin patterns along the SC axis based on chromosome section displayed in panel **c**. Periodicity is found to be 550–700 nm tangentially and the cluster diameter is estimated to be in the range 170–225 nm. *Blue lines* show the 95% confidence bounds (+/−0.08) of the autocorrelation function

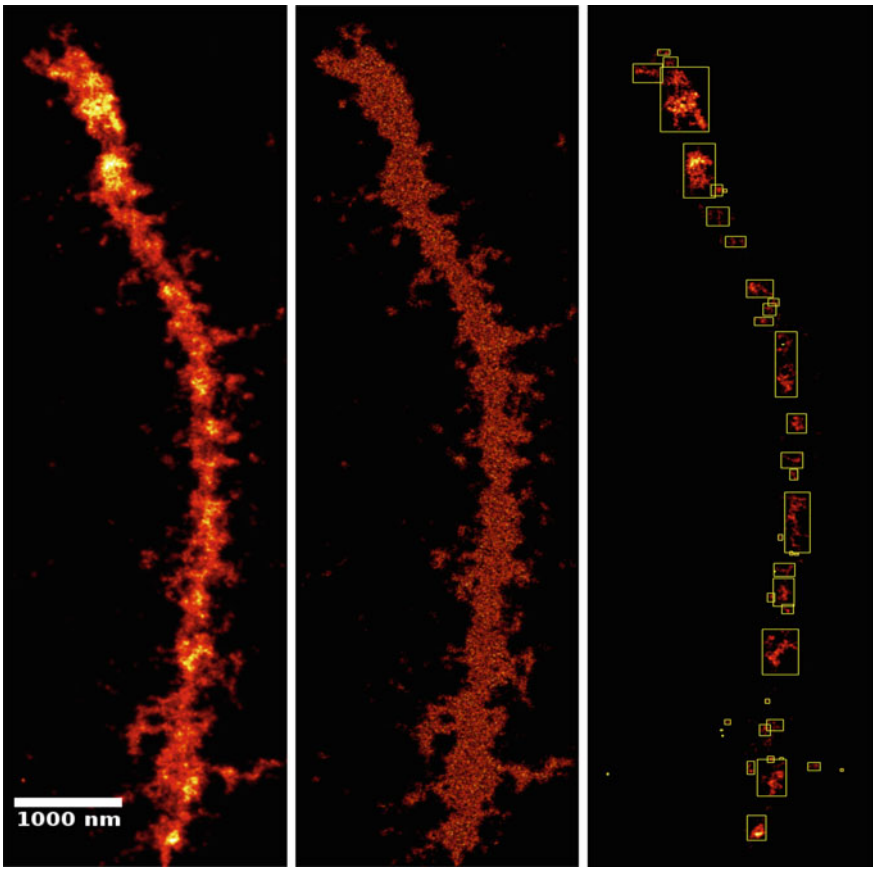

Fig. 4.7 Characterization of pachytene chromosome clusters: **a** Pachytene chromosomes stained with Vybrant Violet. **b** Randomly simulated dataset. **c** Location of clusters above a threshold is indicated with *yellow boxes*

4.4 Functional Organisation of Pachytene Chromosomes

4.4.1 Rational

The power of high resolution light microscopy over electron microscopy is to specifically label particular structures on a given sample (for comparison on same sample refer to Lippincott-Schwartz and Patterson 2009, Fig. 5). With SMLM, one can not only observe nano-scale structures but is also able to describe them in molecular terms. For example, individual functional compartments of chromatin whether active, inactive, or repressed can be described and categorised independently. Each

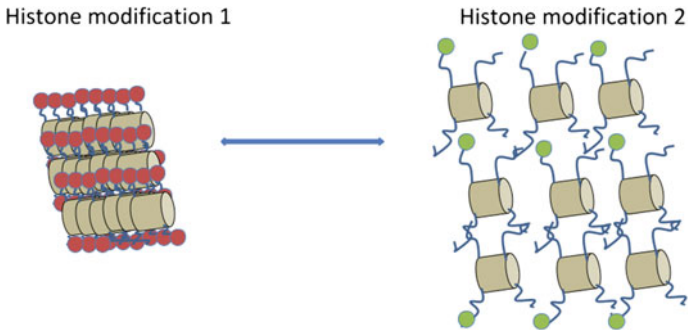

Fig. 4.8 Chromatin compaction as a function of histone modifcations: Chromatin is not an inert structure and its compaction and relaxation can be modulated by many external and internal factors, among them post-translational modifications of histones. A few of these modifications and their impact on chromatin structure has been characterised, however, the list of these modifications is constantly growing. Some histone modification cause chromatin to be more compact while others can make chromatin to take a more relaxed and open configuration (Bannister and Kouzarides 2011).

of these categories experiences a different epigenetic regulation and is enriched with various combinations of epigenetic modifications.

I was curious to investigate the contribution of epigenetics, more specifically histones post-translational modifications (PTM) associated to the structure of pachytene clusters observed in SMLM experiments (Fig. 4.7). In interphase, PTM are known to regulate gene expression by modifying DNA accessibility (see example on Fig. 4.8 and Chap. 1, Sect. 1.5). In meiosis, apart from de novo H3K4me3, which is thought to be a major regulator of meiotic recombination by promoting double strand breaks (Mihola et al. 2009; Sommermeyer et al. 2013), not much is known about the epigenetic regulation of chromatin. As a result, I tried to define a rational to select meaningful histone modifications in order to investigate and better characterise the chromatin architecture of the pachytene chromosomes.

I decided to take a naive approach to systematically select relevant histone marks for the study. Assuming that chromatin states such as gene activation or gene repression are often defined by combinations of post-translational histone modifications (also known as the 'histone code'), it is likely that positions of several histone marks, having similar function, may co-localise throughout the genome. Finding these clusters of marks would tell what is the minimal number of marks to study in order to get a rough picture of chromatin functionality. Therefore, I studied the co-occurrences of histone marks and derived meaningful functional clusters. As the data is sparse for mouse oocytes meiotic chromosome, I used data from classical studies of Barski et al. (2007), Wang et al. (2008) in human immune cells to benchmark histone mark associations. This method is described in detail in Prakash (2012). The Boolean model helped to select genomic positions which have strong ChIP-seq signals to study the association of histone marks at these sites. This resulted in a table where associations between histone modifications are marked with a coloring scheme (Fig. 4.9).

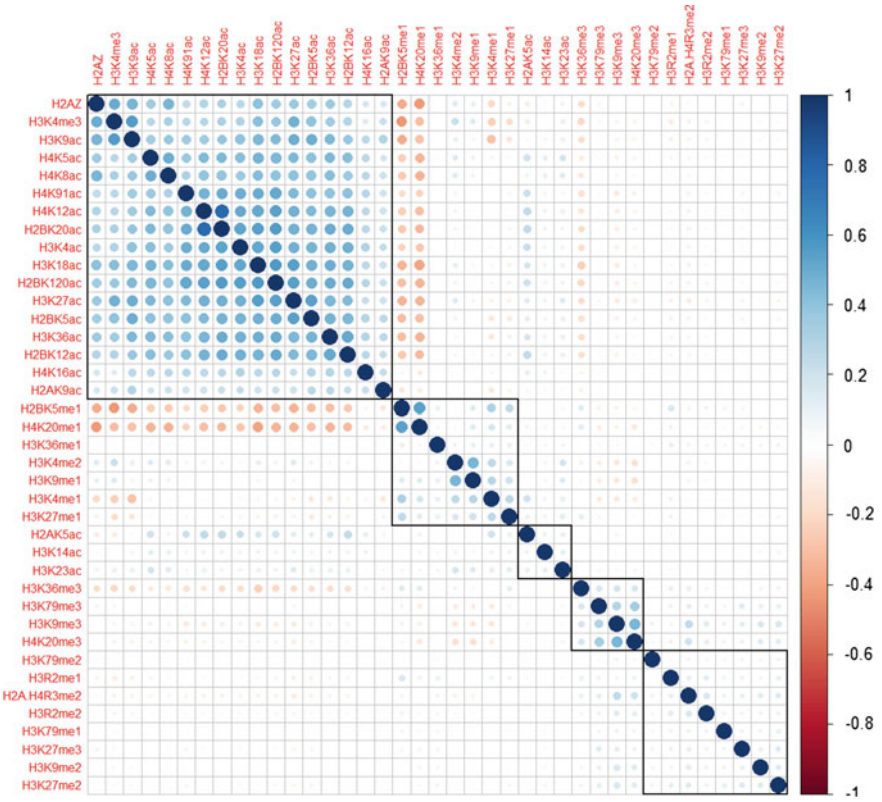

Fig. 4.9 Co-occurrences and clustering of histone post-translational modifications in CD4 T cells: *Blue circles* represent positive correlations between histone modifications while *red circles* represent negative correlations. Size and color depth indicate the measure of the correlations. Histone modifications with no significant correlation are left blank. The *dark blue rectangles* along the diagonal of the correlation matrix represent clusters of histone modifications and are based on the results of hierarchical clustering. The cluster on the *top left corner* shows H3K4me3 correlating with several acetylation marks. The *bottom right cluster* shows positive correlation of H3K27me3 with H3K79me1, H3K9me2 and H3K27me2. The fourth cluster along the diagonal shows strong correlation between H3K9me3, H4K20me3 and H3K79me3

4.4.2 Clustering Method Sorts Chromatin into Functional Epigenetic Compartments

Hierarchical clustering of 39 different histone modifications led to identification of five functional clusters. The first cluster was found to be associated with gene activation, comprising acetylation marks and H3K4me3, a well-known mark associated to initiation of double strand breaks during recombination (Fig. 4.9, top-left cluster displayed as a blue box); a second cluster was found to be associated to H3K9me3, a mark involved in constitutive heterochromatin of centromeres, struc-

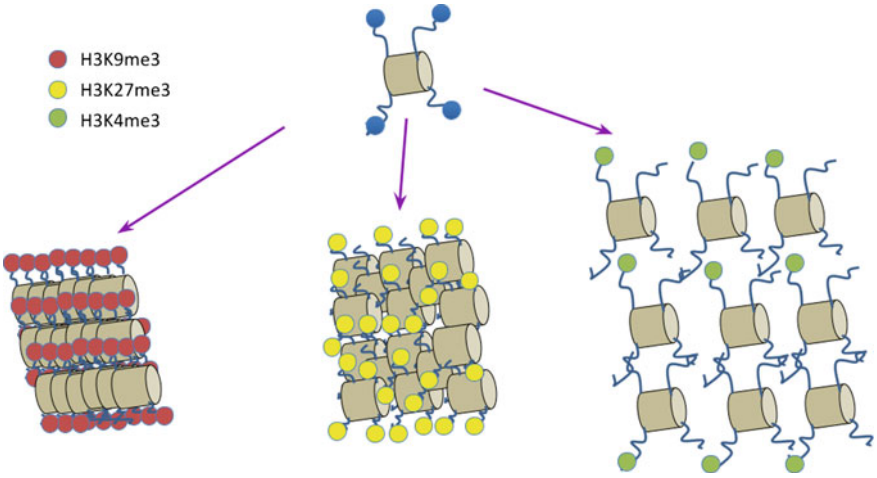

Fig. 4.10 Functional chromatin states: Chromatin can be broadly classified into 3 functional chromatin states and these states are characterised by three different histone modifications. The constitutive heterochromatin is found in centromeres, telomeres and repetitive sequences. Constitutive chromatin is highly condensed, transcriptionally silent and is marked by H3K9me3. Facultative heterochromatin is relatively less condensed, transcriptionally reversible and marked by H3K27me3. Euchromatin, which is rich in genes and transcriptionally active is marked by H3K4me3

tures which have a strong importance in synaptonemal complex initiation (Fig. 4.9, fourth cluster from the left); lastly, I identified a cluster of repressive marks (Fig. 4.9, fifth cluster from the left), from which H3K27me3 has been previously identified as anti-correlated to meiotic DSBs (Buard et al. 2009). Genomic data confirm the anti-correlation of H3K9me3 and H3K27me3 clusters during germ cell differentiation (Liu et al. 2014). On the other hand, H3K27me3 and H3K4me3 are shown by genomics to anti-correlate genome-wide (Hammoud et al. 2014). As a result of this analysis, I decided to stain the following 3 representative marks to further characterize chromatin organisation: H3K4me3, H3K9me3 and H3K27me3. The function and genomic regions where these marks are known to be enriched is summarised in Fig. 4.10.

4.4.3 Centromeric Histone Mark (H3K9me3) Labels One End of the SC

H3K9me3 is associated to centromeres and to the initiation of double-strand breaks at the early stages of SC formation (Hernández-Hernández et al. 2012; Mikkelsen et al. 2007). In mouse chromosomes, centromeres localise at one of the telomeres (often referred to as telocentres), resulting in chromosomes having only one arm. Chromatin staining of the pachytene chromosome shows a huge cluster of DNA at

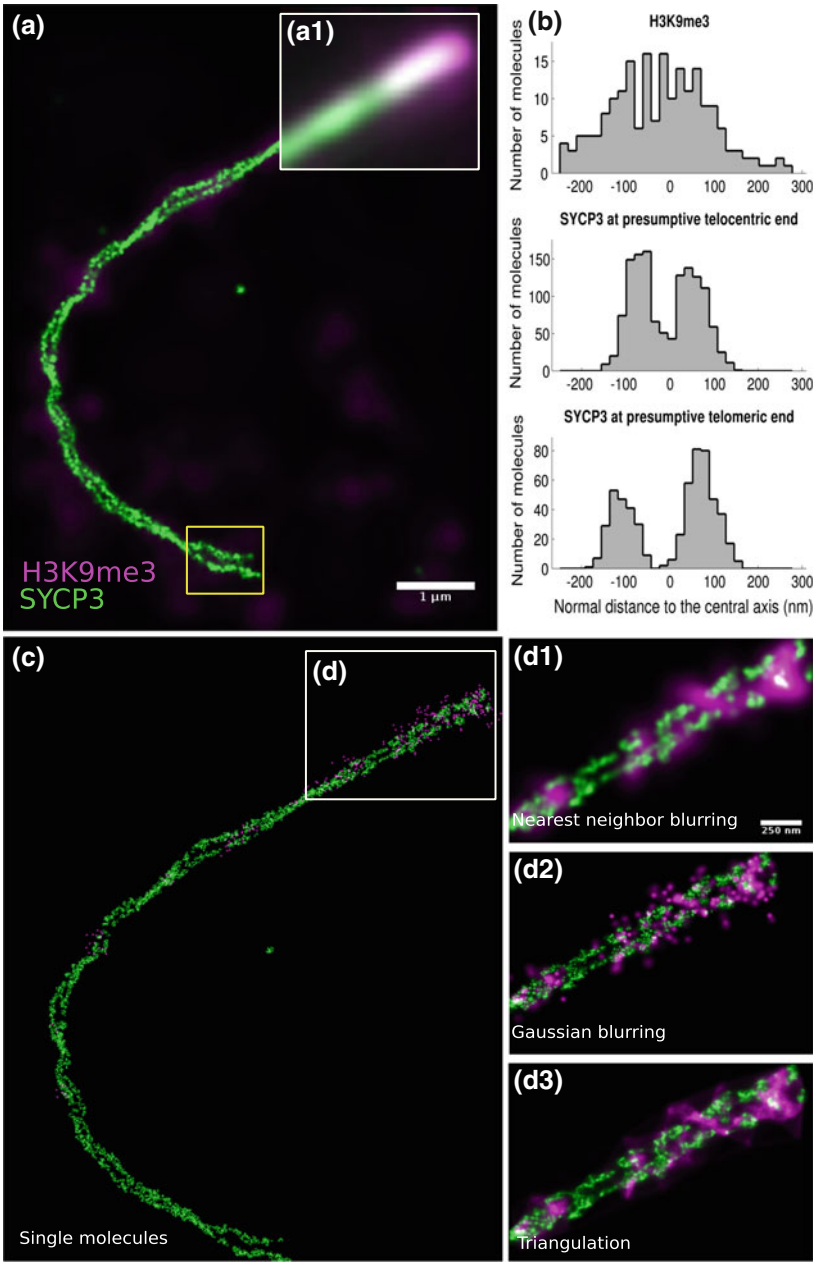
(a)
(a1)
H3K9me3
SYCP3
1 µm
(b)
H3K9me3
Number of molecules
SYCP3 at presumptive telocentric end
SYCP3 at presumptive telomeric end
Normal distance to the central axis (nm)
(c)
(d)
Single molecules
(d1)
Nearest neighbor blurring
250 nm
(d2)
Gaussian blurring
(d3)
Triangulation

Fig. 4.11 H3K9me3 displays a centromeric position along the SC (figure and caption modified from Prakash et al. 2015): Two-color SMLM image **a** immunostained with anti-SYCP3 (Alexa 555) and anti-trimethylated histone H3K9 (Alexa 488). Inset **a1** shows the underlying wide-field image. Large dense clusters of repressive centromere mark H3K9me3 can be seen at the presumptive telocentric end of the pachytene chromosomes. High H3K9me3 density at the telocentric ends of SYCP3 is concomitant with high chromatin density at the top axial end in Fig. 4.6b. **b** The strands of SYCP3 where H3K9me3 co-localises (presumptive telocentric end) are found to be closer (∼135 nm) than at the presumptive telocentric end (∼180 nm). **c** H3K9me3 distribution hints for spiralization of DNA at the centromeric end of the SC. Point of representation of single molecules of SYCP3 and H3K9me3 is shown in **c**. **d** compares different visualization strategies. Spiralization of DNA was observed at one of the extremities of synapsed chromosomes (**d1**–**d3**), probably working as an anchor for the two chromosomes to start synapsis. This spiralization exemplifies the relevance of blurring methods for visualisation, nevertheless, feature is visible in all three visualisation methods

one end of chromosomes (Fig. 4.6b). I used SMLM to probe if these dense chromatin regions were enriched with the centomeric mark H3K9me3. Images obtain show that one of the ends of SYCP3 is highly enriched with H3K9me3 (Fig. 4.11), compared to the other end of SYCP3. Moreover, the centromeric end is remarkably distinguishable by a narrower SYCP3 structure compared to the other end (Fig. 4.11b). This observation is further presented in replicates (Figs. B.7 and B.8a–b). Furthermore, at the telocentric end of the chromosome (Fig. 4.11c), H3K9me3 co-localizes with a high chromatin density. The top cluster on chromatin image (Fig. 4.6b) has a similar average axial spread of 1–1.5 μm as in case of H3K9me3 (Fig. 4.11a) image.

4.4.4 Repressive Histone Mark (H3K27me3) Shows Characteristic Periodic Clusters Along the SC

H3K27me3 is associated to repeat regions of the genome and some of them can be deleterious for the proper transmission of information to the next generation (Pauler et al. 2009). Next, I wondered if H3K27me3 might possibly contribute to the periodic clusters seen in Fig. 4.6c. In agreement with previous findings (Hernández-Hernández et al. 2010), H3K27me3 post-translational modification was found to be localised close to the SC, directly at the outside of the regions occupied by SYCP3 proteins (Fig. 4.12). The important overlap between H3K27me3 and SYCP3 was also visible in wide-field (Fig. 4.12a). However, the SMLM image revealed an unexpected pattern. H3K27me3, instead of spanning the entire length of the chromosome, displayed large periodic clusters, disposed in pairs (Fig. 4.12b), found every 450–650 nm along the SC according to auto-correlation analysis (Fig. 4.12d). Size of clusters was found in the 90–130 nm range (Fig. B.9) and the average lateral distance from the strands of SYCP3 in the 40–50 nm range (Fig. 4.12c), though there is an overlap with SYCP3 in several instances, possibly due to twisting of SYCP3. The proximity of H3K27me3 and SYCP3 on the SMLM cliches explains why the two features seem to co-localise with confocal images (∼200 nm resolution of the imaging system).

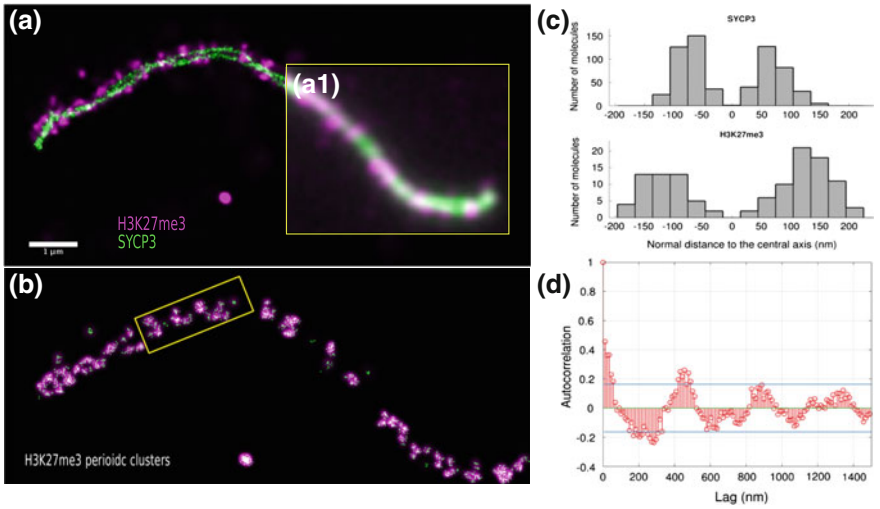

Fig. 4.12 H3K27me3 displays periodic paired clusters in proximity to the SC (figure and caption modified from Prakash et al. (2015). Two color SMLM image **a** immunostained with anti-SYCP3 (Alexa Fluor555) and anti-trimethylated histone H3K27 (Alexa Fluor488). Inset **a1** shows a wide-field version of the image for comparison. Overlaps between H3K27me3 and SYCP3 channels are shown in *white*. **b** The periodic and symmetric clusters of H3K27me3 mark shown as raw data (single molecules in *green* or after blurring procedure in *purple*). **c** Differential distribution of SYCP3 (*top*) and H3K27me3 clusters (*bottom*). Both distributions are symmetrical, but H3K27me3 are found slightly outside of the SYCP3 strands, laterally 50 nm apart from the SC, with a 90–130 nm diameter. **d** Autocorrelation on *yellow section* of **panel b** reveals the tangential distance of the clusters from the central axis of SYCP3 to be 40–50 nm and reveals a periodicity of approximately 500 nm (see also Prakash et al. 2015), supplementary data). *Blue lines* correspond to the 95% confidence bounds (+/−0.1633) of the autocorrelation function

The patterns shown on Fig. 4.12 were reproducible on all chromosomes (see Prakash et al. 2015) supplementary data). The periodicity of H3K27me3 and chromatin clusters found in Fig. 4.6c seem to match and I hypothesize that the larger chromatin clusters with lateral extensions have strong enrichment for H3K27me3 mark at their base, an information that I incorporate in a model of the pachytene chromosome (see Sect. 4.6.1).

The pattern of the clusters itself indicates their high functional nature. Symmetry and perfect pairing means that deposition of this repressive mark is dependent on the genomic content of chromosomal regions and is reproducible between chromosomes. What is the function of these regions? The present analysis does not provide any answer, but one speculates that these periodic clusters might correspond to the silent repeated regions of genomes, such as long interspersed elements (LINE) or long-terminal repeat (LTR), as H3K27me3 is often found to be associated to this kind of element (Pauler et al. 2009). This repressive feature is key to prevent the mobility of jumping elements during meiosis, whose movements can have consequence for the progeny.

4.4.5 Histone Mark (H3K4me3) Associated with Active Transcription Emanates Radially from the Axis of the SC

Finally, I present here the distribution of H3K4me3, a mark known to be highly involved in generation of double strand breaks, along the pachytene chromosome. Instead of localising at the axis, H3K4me3 showed localisation in the lateral to the central axis of SYCP3 (Fig. 4.13), possibly corresponding to the extensions identified with DNA staining (Fig. 4.6). H3K4me3 extensions were found to be 500 nm wide which were in accordance with chromatin protrusions (Fig. 4.6d). Similarly to H3K27me3, H3K4me3 forms clusters of 50 nm diameter (Fig. B.9). The average spread of the radial emanations of H3K4me3 ranged from 300 to 500 nm, with the overall distribution of H3K4me3 qualitatively similar to the chromatin distribution (Figs. 4.6d and 4.13a1). By applying autocorrelation to the tangential distances from the central axis of SYCP3 (Fig. 4.13a3), I estimated the average spread (approx. 500 nm) of the protrusions to be larger than their spacing (approx. 200 nm).

4.5 Structure and Dynamics of Meiotic Chromosomes

4.5.1 Lampbrush-Like Structures in Mammalian Meiotic Chromosomes

Lampbrush chromosomes (LBC) are giant chromosomes found in oocytes of diverse organisms, both vertebrate and invertebrate. They are characterized by paired loops of transcriptionally active chromatin that extend laterally from an axis of inactive chromatin. Among vertebrates, they have been extensively studied in amphibians, reptiles, fish, and birds, but have not been convincingly demonstrated in mammals (Gall 2012; Callan 2012).

Though known to be necessary for the pachytene chromosome to function normally, presence of loops in mammals has not been so far optically demonstrated (Heng et al. 1996), does not show convincing images). Data in this thesis are a good step in this direction, as some of the images show H3K4me3-marked processes forming circular patterns (Fig. 4.14) resembling SEM (Fig. B.3) and EM data of pachytene chromosomes observed in amphibians (Rattner et al. 1980). Some putative looping structures are found on our chromatin SMLM pictures (Fig. 4.6) but it is possible that the pattern is the result of contact of two adjacent extensions of the chromatids. Nevertheless, the size of lateral chromatin extensions (500 nm) (Fig. 4.6d) is similar to the size of H3K4me3 extensions (Fig. 4.14d). H3K4me3 is better at spotting possible loops because the labelling density is lower than DNA (DNA staining: 5,000 single-molecule signals per square micrometer (Szczurek et al. 2014), histone staining: 100 single-molecule signals per square micrometer (Bohn et al. 2010), which

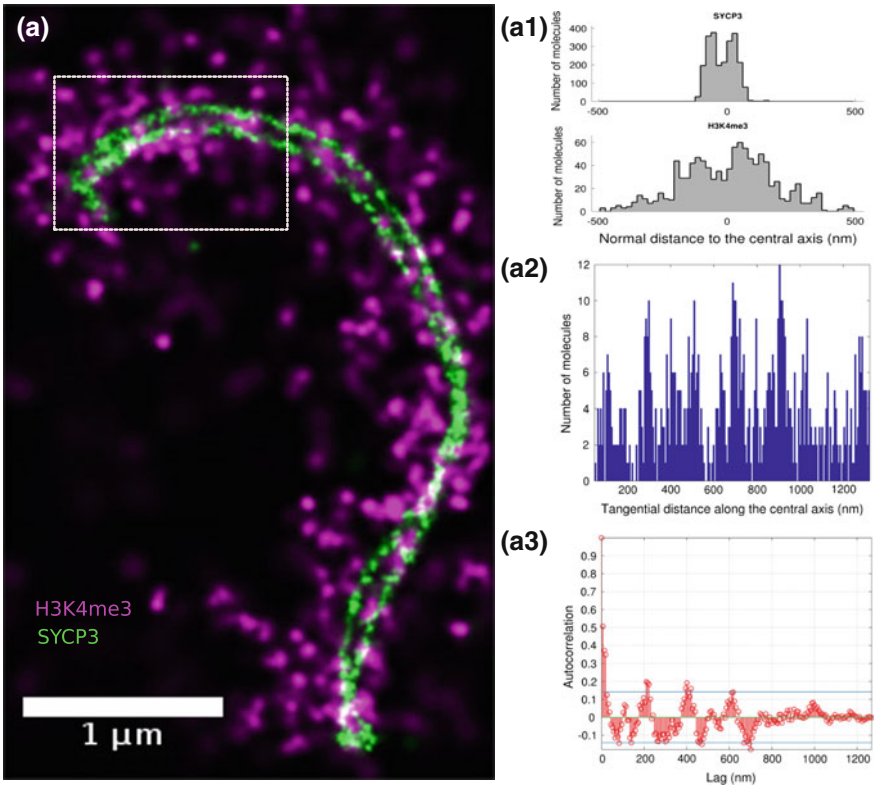

Fig. 4.13 Lower orders of chromatin domains characterised by H3K4me3: Two color SMLM image **a** immunostained with anti-SYCP3 (Alexa Fluor 555) and anti-trimethylated histone H3K4 (Alexa Fluor 488). H3K4me3 clusters reveal lower orders of chromatin domains along the pachytene chromosomes (figure and caption modified from Prakash et al. 2015). The average spread of H3K4me3 shows periodicity along the lateral direction to the central axis of SYCP3, possibly indicating individual H3K4me3 clusters (**a1**). The average cluster diameter in **a** was found to be 47 nm (see also Fig. B.9). **a2** shows the histogram of the tangential distances taken along the central axis of SYCP3 in the *white box* indicated in **a**. **a3** shows the periodicity of clusters of H3K4me3. The periodicity in **a** was found to be around 216 nm. The *blue lines* in the A3 plot correspond to the 95% confidence bounds (A3, $+/-0.1414$)

creates more opportunity to distinguish thin or subtle structures. This point is another example of the importance of staining chromatin with both DNA dyes and histone modifications.

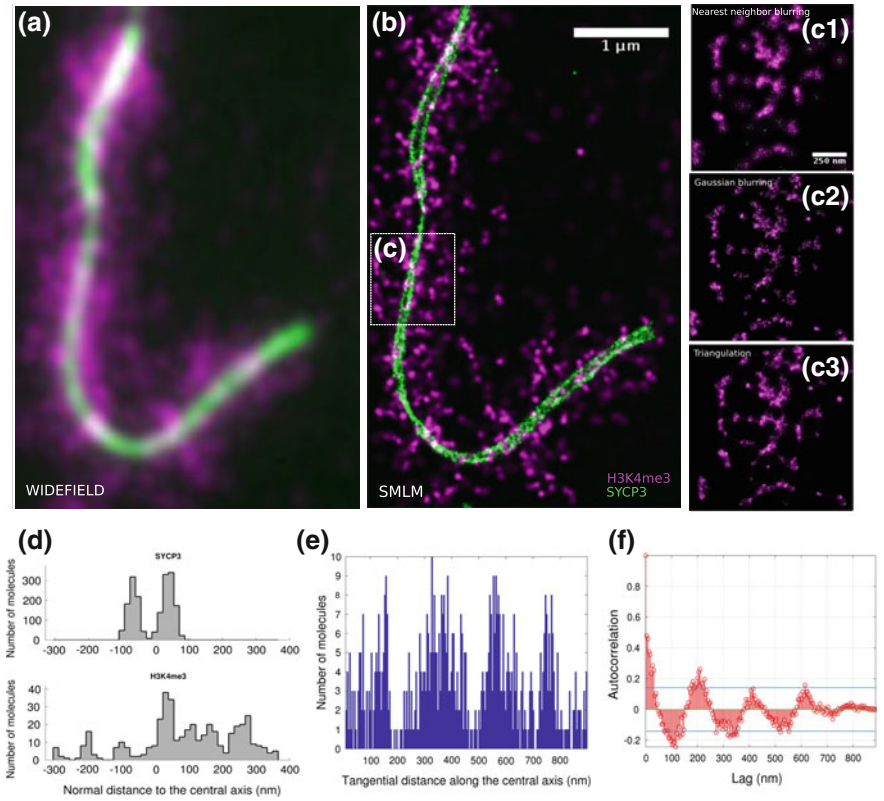

Fig. 4.14 Distribution of transcriptionally active chromatin (figure and caption modified from Prakash et al. 2015): Radially emanating chromatin loops are punctuated with transcriptionally active histone mark (H3K4me3): Two color wide-field image **a** immunostained with anti-SYCP3 (Alexa Fluor 555) and anti-trimethylated histone H3K4 (Alexa Fluor 488) with **b** showing the corresponding SMLM image. **c** shows radial loop like patterns emerging laterally compared to SYCP3, with **c1**–**c3** showing **c** with different visualisation methods. **d** The distribution of H3K4me3 around SYCP3 is characteristically similar to chromatin distribution stained with Vybrant DyeCycle Violet (Fig. 4.6d). The average spread (∼300 nm) of radially emanating chromatin loops perpendicular to the lateral elements of SC is uneven across the SYCP3 strands punctuated with periodic patterns of H3K4me3. **e** shows the histogram of the tangential distances taken along the central axis of SYCP3 in **c**. Using an autocorrelation function **f**, the estimated average spread of the radial loops was found to be larger than their spacing (∼200 nm)

4.5.2 A Model for SC Spiralisation During the Zygotene/Pachytene Transition

The above data provide important information regarding the organisation of pachytene chromosomes. They also provides some hints regarding the dynamics of pachytene chromosomes during meiosis. Though presently there is no time series data of meio-

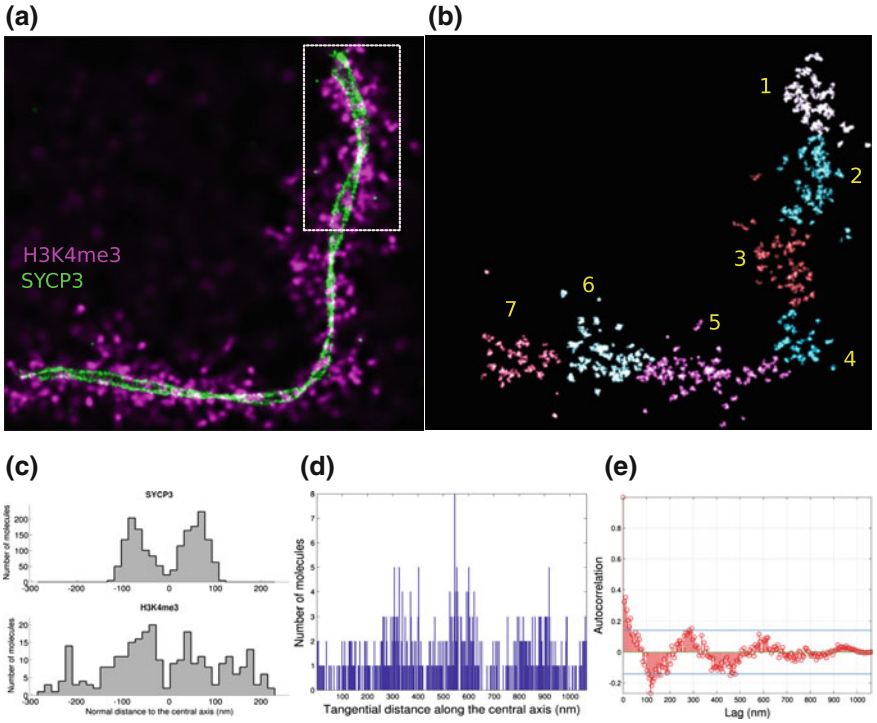

Fig. 4.15 Helical structure of the pachytene chromosomes: General pattern of H3K4me3 confirms hypothesis of helical structure of the pachytene chromosomes. **b** The distribution of H3K4me3 hints for potential rotation of chromatin along the entire length of SC. The clusters of H3K4me3 are color-coded based on nearest neighbor distances to indicate that the rotation follows the rotation of SYCP3 in **a**. **c** The average spread of H3K4me3 showed periodicity along the normal direction to the central axis of SYCP3. The average cluster diameter in *white box* (**a**) was found to be 45 nm. **d** shows the histogram of the tangential distances taken along the central axis of SYCP3 in the *white boxes*. **e** shows the periodicity of the clusters of H3K4me3 loops. The periodicity was found to occur at intervals of 209 nm. The *blue lines* in the plot correspond to 95% confidence bounds (+/−0.1613)

sis steps, it is worth mentioning that the images hint at a spiralization of chromosomes in pachytene stage, possibly for functional reasons. It was shown that H3K9me3 displays a helical wrapping around the SC (Fig. 4.11). DNA staining itself also shows a trend to form spirals, either only at the extremity (Fig. 4.6) or all along the body of the chromosome (Fig. B.6). One may object that the situation studied is not native, as the chromosomes have been processed through a rather harsh protocol. Nonetheless, evidences show that the helical structure of single chromosomes is preserved in pachytene chromosomes showing bouquet-like patterns close to native state (Fig. B.7, two pair of chromosomes on left).

I further show high-order patterns of H3K4me3 on certain chromosomes, showing clear helical patterns. As H3K4me3 is probably spanning most of the space occu-

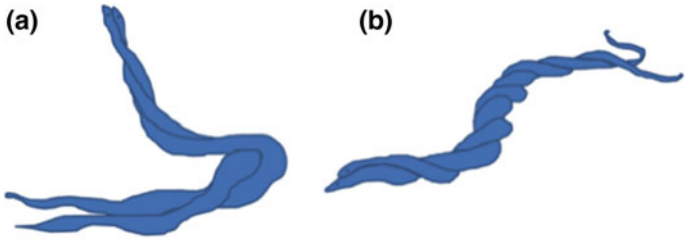

Fig. 4.16 A snake model for the formation of the synapsis. **a** Zygotene stage. The snakes represented on the cartoon start copulation by their enrolment close to the head. The heads of the snakes find each other at the telocentric ends of the zygotene chromosome by a yet unknown mechanism. **b** Pachytene stage. Starting from head, impulse is transmitted to the rest of the body. Attachment of the paired chromosomes at their telocentric end is followed by SC formation potentially followed by a twisting mechanism, which starts at the telocentric end to be loosely transmitted to the rest of the chromosome. I speculate that this process may facilitate recombination. Compare **b** with Fig. B.8

pied by chromatin, one can approximate the positions of the H3K4me3 for overall spatial occupancy of chromatin. To demonstrate the spiralization, I developed an algorithm to identify alternate patterns of H3K4me3 clusters on each side of the SC (Fig. 4.15b). Most of the neighbour clusters were found to be separated along the axis of SC, a pattern even more evident on the first image with the SYCP3 staining. Same type of alternative configuration was found using data from H3K27me3 imaging (Fig. B.5). Such chromosomes may role around each other in the fashion of mating snakes (see snake model, Fig. 4.16). Pairing of the two chromosomes could start by a tight enrolment of chromatin at the centromere, H3K9me3-rich (the spiral pattern of H3K9me3 in Fig. 4.11 ascertains this fact), to rapidly induce the wrapping of the rest of the chromosome. Recent data from 3D-SIM confirms a complete 3D twist of SYCP3 along the axis of the chromosome, as predicted by the snake model (David Fournier, personal communication, data not shown). Moreover, helical patterns are clearly identifiable in whole cell preparations of Xenopus oocytes from early studies on pachytene chromosomes (Gall and Pardue 1969), probably working as an anchor for the two chromosomes to start synapsis.

It is speculated that the helical patterns have a structural or a mechanistic function. Spiralisation is probably essential for pairing to happen, by inducing a wrapping of the two chromosomes around each other once pairing has started. Spiralisation may also help recombination events to form, following the initiation of synapsis to impose certain structural constraints that help crossing-overs to form.

4.6 A Model of Spatial Distribution of Chromatin Around the SC

Finally, I summarize the composition of high-order chromatin into lower-order histone modification clusters using distance profiles (Fig. 4.17, left). One can observe that while chromatin has the broadest extension, H3K9me3 follows the same shape

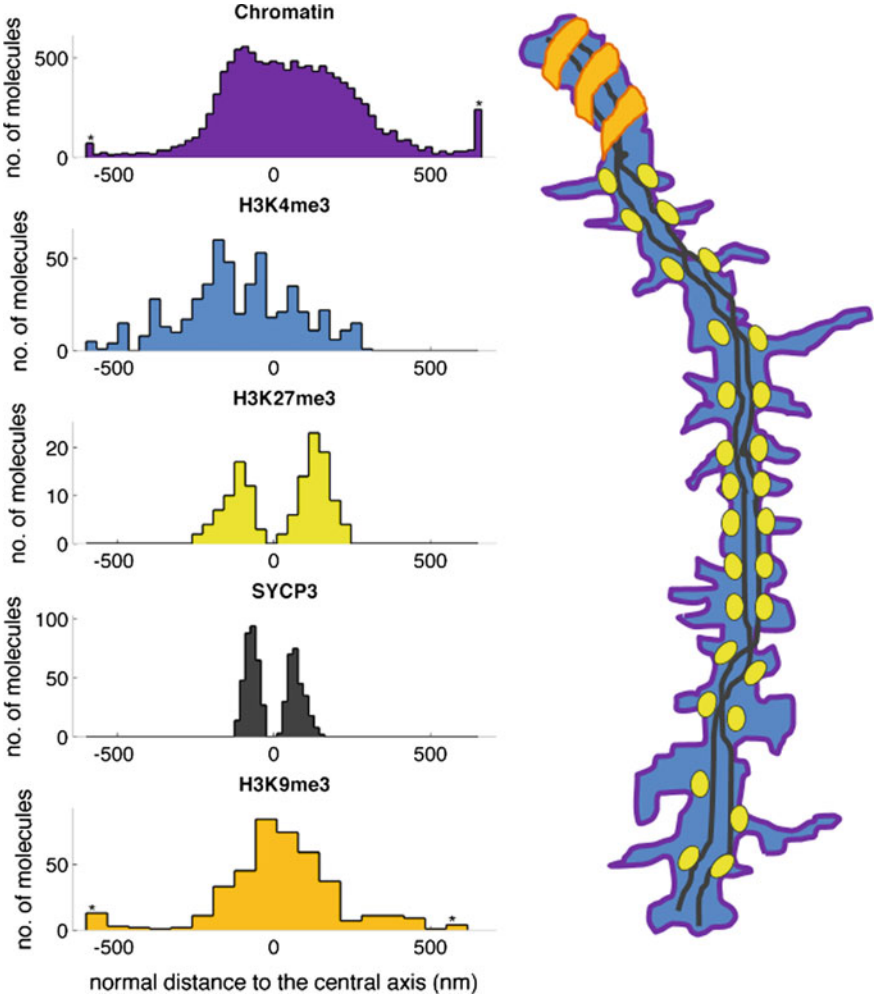

Fig. 4.17 Symmetric and periodic organisation of pachytene chromsomes: The two strands of the synaptonemal complex are displayed in *black*. In *purple*, chromatin covers the entire surface and is thought to be ubiquitously marked by tangential mark H3K4me3, shown in *blue*. Tangential, symmetrical and periodic H3K27me3 clusters are displayed with *yellow spots*. Polar chromatin associated to H3K9me3 is shown as an orange spiral pattern

as the chromatin profile and is normally distributed along the central axis of SC, hinting that the telocentric region is mostly covered by the H3K9me3 cluster, while other regions that extended laterally are deprived of this centromeric mark. Differently, H3K27me3 cluster follows the shape of the synaptonemal complex, hinting for its tangential localization. H3K4me3 profile is asymmetrically distributed and comparison with chromatin profiles shows a level of complexity that chromatin alone cannot capture, as possibly most of the DNA is not active. Most of the profiles are slightly lopsided, that I speculate to be mostly due to chromosome not being in the sample plane and the angle creating the asymmetry.

4.6.1 A 'Cluster-on-a-String' Model for Spatial Distribution of Pachytene Chromosomes

The different clusters observed (H3K4me3, H3K27me3 and H3K9me3) are obviously of much higher order than basic bead-on-a-string structures of DNA and histone complexes. As a result, I hypothesize that the patterns observed in the pachytene chromosomes are rather a large chunk of those beads, possibly of a state close to chromatin fibres. I describe them as 'clusters-on-a-string', to point that they are likely bulky regions epigenetically regulated, surrounded by disorganized DNA fibres. These structures are probably to relate to chromatin domains found in interphase (see Sect. 3.2.3 and Fig. 3.16). More has to be explored in order to see what is the structure of the clusters and the regions in between. For this, more informational staining will have to be performed, using either polymerases, splicing machinery or other enzymes.

Finally, I summarize our findings in a model of the pachytene chromosome, which displays roughly three epigenetic compartments, capturing most of the epigenetic information in chromatin according to the histone code table (Fig. 4.17, right). While H3K4me3 is covering the entire chromatin landscape, including lateral extensions, synaptonemal complex region and telocentric end of the chromosome, H3K27me3 is confined to the SC, a fact confirmed by a trend on distribution plots in Fig. 4.17, left. I speculate that the two marks anti-correlate in the SC. H3K4me3-rich spots being prone to recombination, following binding of PRDM9. H3K27me3-rich spots focused on repressing intermediate regions, either to silent undesirable elements such as repeated elements, which may strengthen its integrity by over-twisting.

4.7 Summary and Conclusion

Different variations of DNA and histone modifications staining, at single molecule resolution, have revealed two orders of chromatin in the meiotic chromosomes that were unknown before. The analysis shows that histone modifications can be useful

not only to add functional information but also to study the chromatin organisation in more details. It also shows that the level of resolution of histone modification is highly useful to characterize very fine regions such as loops; H3K4me3 staining revealed loop-patterns not observable with the DNA staining while H3K9me3 hints toward spiralization of DNA at telocentric end, a pattern less visible on DNA images.

The above results confirm the predicted anti-correlation from the genomic data of the three histone modifications. H3K9me3 and H3K27me3 clusters anti-correlate, as shown by Liu et al. (2014) using ChIP-seq data. Similarly to genomic data from ChIP-seq (Hammoud et al. 2014), H3K27me3 and H3K4me3 are shown to anti-correlate genome-wide, with lateral H3K4me3 marks being devoid of H3K27me3 mark, while axial H3K4me3 clusters show possible partial overlap with H3K27me3 clusters. Additional co-immunostaining of pairs of histone modifications should further reveal dependency and correlation with other marks.

Spreading technique can question the reliability of the patterns observed and one can wonder if they would be observed in intact nuclei. Though this is unlikely for two reasons; one is that in virtue of thermodynamics, a passive system will only loose complexity with time. Spreading chromosomes can at worst destroy clusters, but unlikely create ones, and moreover these patterns are reproducible across several samples. Second reason is that close to native states are sometimes observed (Fig B.7), with chromosomes bound by pairs via their centromeres, a pattern reminiscent from the native attachment of all chromosomes to the rRNA center (Gall and Pardue 1969). The helical structure of single chromosomes is preserved in these pairs (Fig B.7).

Study of the epigenetic regulation of the pachytene chromosome has left one with several important results. It was shown for the first time a high resolution map of pachytene chromosome using both a DNA dye and histone modifications, which when combined helped to have a comprehensible view of functional chromatin (Fig. 4.17). This can easily be pursued in different contexts, especially the one of disease phenotype, to see the implication of epigenetics in disease.

Moreover, this is also the first study to show that mammalian chromosomes display lateral loops, similar to one observed in yeast or amphibians. Finally, this study was the first to show high degree periodicity in chromatin organisation at multiple length scales. More importantly, I show here clusters of DNA and various post-translational histone modifications in a very comprehensive way for the first time, demonstrating the importance of the meiotic chromosome as a model to study chromatin organization. The clusters are arranged according to their functional position, and provide the extend of chromatin compartmentalisation. As such, I at least identify a new type of functional compartment of 50 nm size (using H3K4me3) and another one of about 120 nm (using H3K27me3).

The three histone modifications summarising the clustering generated from the histone code table have different functionalities for the cell activity and exhibit a higher degree of specialization during meiosis. During development, H3K4me3 and H3K27me3 histone marks are present at promoters and have the capacity to turn on and off genes, respectively. As a result, these genes are in a bivalent state. Genes which become activated loose the H3K27me3 mark and start to get transcribed. In more differentiated stages of development, H3K4me3 guides transcription, while

genes having only the H3K27me3 mark become totally repressed, eventually being rendered inaccessible via extreme compaction of chromatin (Pauler et al. 2009). A histone modification associated to this kind of dense chromatin is H3K9me3, mainly associated with telomeric, repeats and satellite sequences (Mikkelsen et al. 2007). The final picture of the epigenetic landscape of histone modifications can be simplified with a division between active genes displaying H3K4me3, inactive genes displaying H3K27me3 and inaccessible regions (rich in repeated elements) which bare a high density of H3K9me3 mark (Fig. 4.10).

In highly differentiated cells such as non-renewable adult tissues, the relationship between epigenetic marks and gene expression is less pronounced, with many genes either up-regulated or down-regulated, which do not seem to exhibit any H3K27me3 or H3K4me3 modulation (Wu et al. 2012), Epithelial-mesenchymal transition (EMT) data from David Fournier, not published), while many genes are kept totally silent during the entire life of the cell, with H3K27me3 spread all along the gene body (Pauler et al. 2009). As a result, the modulation of histone modification amplitude may play a special role in meiosis and possibly guide the structure of the chromosome.

As meiosis is the type of cell division that provides the basis for sexual reproduction and genetic variability, defects in synapsis and/or recombination of meiotic chromosome can lead to aneuploid syndromes and infertility. It is likely that the SC driven chromosomes have structurally distinct histone modifications patterns and a unique chromatin landscape compared to those identified here in the native state. This work also demonstrates the link between the structural hierarchy of chromatin organization in meiosis and epigenetic regulation of transcription.

I urge the scientists to use this model as a platform to study the epigenetic make-up of genomic regions of interest, and the basics of gene expression and epigenetic regulation. The meiotic chromosome, while being very specialized toward one goal, recombination, happens to be a promising candidate to study the fundamental principles that guide chromatin architecture.

References

Bannister AJ, Kouzarides T (2011) Regulation of chromatin by histone modifications. Cell Res 21(3):381–395

Barski A, Cuddapah S, Cui K, Roh TY, Schones DE, Wang Z, Wei G, Chepelev I, Zhao K (2007) High-resolution profiling of histone methylations in the human genome. Cell 129(4):823–837

Baudat F, Imai Y, de Massy B (2013) Meiotic recombination in mammals: localization and regulation. Nat Rev Genet 14(11):794–806

Berríos S, Manieu C, López-Fenner J, Ayarza E, Page J, González M, Manterola M, Fernández-Donoso R (2014) Robertsonian chromosomes and the nuclear architecture of mouse meiotic prophase spermatocytes. Biol Res 47(1):1

Bohn M, Diesinger P, Kaufmann R, Weiland Y, Müller P, Gunkel M, Von Ketteler A, Lemmer P, Hausmann M, Heermann DW et al (2010) Localization microscopy reveals expression-dependent parameters of chromatin nanostructure. Biophys J 99(5):1358–1367

Buard J, Barthès P, Grey C, de Massy B (2009) Distinct histone modifications define initiation and repair of meiotic recombination in the mouse. EMBO J 28(17):2616–2624

Callan HG (2012) Lampbrush chromosomes, vol 36. Springer Science & Business Media, New York

Clément Y (2012) The evolution of base composition in mammalian genomes. PhD thesis, Freie Universität Berlin

Gall JG (2012) Are lampbrush chromosomes unique to meiotic cells? Chromosom Res 20(8):905–909

Gall JG, Pardue ML (1969) Formation and detection of rna-dna hybrid molecules in cytological preparations. Proc Natl Acad Sci 63(2):378–383

Gustafsson MGL, Shao L, Carlton PM, Rachel Wang CJ, Golubovskaya IN, Zacheus Cande W, Agard DA, Sedat JW (2008) Three-dimensional resolution doubling in wide-field fluorescence microscopy by structured illumination. Biophys J 94(12):4957–4970

Heng HH, Chamberlain JW, Shi X-M, Spyropoulos B, Tsui L-C, Moens PB (1996) Regulation of meiotic chromatin loop size by chromosomal position. Proc Natl Acad Sci 93(7):2795–2800

Hernández-Hernández A, Ortiz R, Ubaldo E, Echeverría Martínez OM, Vázquez-Nin GH, Recillas-Targa F (2010) Synaptonemal complex stability depends on repressive histone marks of the lateral element-associated repeat sequences. Chromosoma 119(1):41–58

Hernández-Hernández A, Vázquez-Nin GH, Hernádez RO (2012) INTECH Open Access Publisher, Epigenetics of the Synaptonemal Complex

Kaufmann R, Piontek J, Grüll F, Kirchgessner M, Rossa J, Wolburg H, Blasig IE, Cremer C (2012) Visualization and quantitative analysis of reconstituted tight junctions using localization microscopy. PloS One 7(2):e31128

Lichten M (2001) Meiotic recombination: breaking the genome to save it. Curr Biol 11(7):R253–R256

Lippincott-Schwartz J, Patterson GH (2009) Photoactivatable fluorescent proteins for diffraction-limited and super-resolution imaging. Trends in Cell Biol 19(11):555–565

Liu N, Fromm M, Avramova Z (2014) H3k27me3 and h3k4me3 chromatin environment at super-induced dehydration stress memory genes of arabidopsis thaliana. Mol Plant 7(3):502–513

Mihola O, Trachtulec Z, Vlcek C, Schimenti JC, Forejt J (2009) A mouse speciation gene encodes a meiotic histone h3 methyltransferase. Science 323(5912):373–375

Mikkelsen TS, Ku M, Jaffe DB, Issac B, Lieberman E, Giannoukos G, Alvarez P, Brockman W, Kim T-K, Koche RP et al (2007) Genome-wide maps of chromatin state in pluripotent and lineage-committed cells. Nature 448(7153):553–560

Montrose J, Moses MJ, Russel LB, Cacheiro NL (1977) Mouse chromosome translocations: visualization and analysis by electron microscopy of the synaptonemal complex. Science 196(4292):892–894

Pauler FM, Sloane MA, Huang R, Regha K, Koerner MV, Tamir I, Sommer A, Aszodi A, Jenuwein T, Barlow DP (2009) H3k27me3 forms blocs over silent genes and intergenic regions and specifies a histone banding pattern on a mouse autosomal chromosome. Genome Res 19(2):221–233

Petronczki M, Siomos MF, Nasmyth K (2003) Un menage a quatre: the molecular biology of chromosome segregation in meiosis. Cell 112(4):423–440

Prakash K (2012) A binary combinatorial histone code. Master thesis, Aalto University

Prakash K, Fournier D, Redl S, Best G, Borsos M, Tiwari VK, Tachibana-Konwalski K, Ketting RF, Parekh SH, Cremer C et al (2015) Superresolution imaging reveals structurally distinct periodic patterns of chromatin along pachytene chromosomes. Proc Natl Acad Sci 112(47):14635–14640

Pratto F, Brick K, Khil P, Smagulova F, Petukhova GV, Daniel Camerini-Otero R (2014) Recombination initiation maps of individual human genomes. Science 346(6211):1256442

Rattner JB, Goldsmith M, Hamkalo BA (1980) Chromatin organization during meiotic prophase ofbombyx mori. Chromosoma 79(2):215–224

Sato A, Isaac B, Phillips CM, Rillo R, Carlton PM, Wynne DJ, Kasad RA, Dernburg AF (2009) Cytoskeletal forces span the nuclear envelope to coordinate meiotic chromosome pairing and synapsis. Cell 139(5):907–919

Schücker K, Holm T, Franke C, Sauer M, Benavente R (2015) Elucidation of synaptonemal complex organization by super-resolution imaging with isotropic resolution. Proc Natl Acad Sci 112(7):2029–2033

Sommermeyer V, Béneut C, Chaplais E, Serrentino ME, Borde V (2013) Spp1, a member of the set1 complex, promotes meiotic dsb formation in promoters by tethering histone h3k4 methylation sites to chromosome axes. Mol Cell 49(1):43–54

Sue Hammoud S, Low DHP, Yi C, Carrell DT, Guccione E, Cairns BR (2014) Chromatin and transcription transitions of mammalian adult germline stem cells and spermatogenesis. Cell Stem Cell 15(2):239–253

Syrjänen JL, Pellegrini L, Davies OR (2014) A molecular model for the role of sycp3 in meiotic chromosome organisation. Elife 3:e02963

Szczurek AT, Prakash K, Lee H-K, Żurek-Biesiada DJ, Best G, Hagmann M, Dobrucki JW, Cremer C, Birk U (2014) Single molecule localization microscopy of the distribution of chromatin using hoechst and dapi fluorescent probes. Nucleus 5(4):331–340

Wang Z, Zang C, Rosenfeld JA, Schones DE, Barski A, Cuddapah S, Cui K, Roh TY, Peng W, Zhang MQ et al (2008) Combinatorial patterns of histone acetylations and methylations in the human genome. Nat Genet 40(7):897–903

Wu C-Y, Tsai Y-P, Wu M-Z, Teng S-C, Wu K-J (2012) Epigenetic reprogramming and post-transcriptional regulation during the epithelial-mesenchymal transition. Trends Genet 28(9):454–463

Żurek-Biesiada D, Szczurek AT, Prakash K, Mohana GK, Lee H-K, Roignant J-Y, Birk U, Dobrucki JW, Cremer C (2015) Localization microscopy of dna in situ using vybrant dyecycle violet fluorescent probe: a new approach to study nuclear nanostructure at single molecule resolution. Exp Cell Res

Chapter 5
Conclusions

5.1 Originality of the Work Presented Here

In this thesis, I have shown the potential of single-molecule imaging to study chromatin architecture. The primary challenge was to systematically identify and characterise different building blocks of the chromatin organisation. Some elements were known since long, for example, the nucleosomes at the lowest level and the metaphase X-shaped chromosomes at the highest level of DNA compaction. In between these two extreme levels, a vast spectrum of structures remained mostly unexplored due to resolution limitation of light microscopy and lack of specificity in electron microscopy. Furthermore, an effort to combine and synchronise observations from different studies on chromatin organisation was lacking. This thesis is an attempt to combine old and new evidence to understand various structure-function conundrums of chromatin organisation and understand how chromatin structure affects gene regulation.

For genes to function properly, some fundamental structures must exist in a finite number. I speculate that these structures should be in a restricted size range and diversity. For instance, I found structural elements of about 100–400 nm probably corresponding to functional domains involved in activation or repression of transcription. After studying chromatin organisation at different phases of cell cycle, the following new patterns were described to refine the overall description of chromatin:

- patterns of chromatin in interphase: territories, subchromosomal domains (scale: 500 to 1000 nm), fundamental chromatin domains (scale: 100 to 500 nm) and chromatin fibres (scale: 30 to 100 nm).
- patterns of condensation during differentiation of cells, and more interestingly during stress: deprivation of oxygen and nutrients induces a characteristic ring/rod-like shape of chromosomes (scale: 40 to 700 nm).
- patterns of functional chromatin during meiosis (scale: 40 to 600 nm). Active chromatin localises laterally towards the exterior of pachytene chromosomes, likely facilitating transcription while inactive chromatin locates toward the interior showing a high level of periodicity and symmetry.

K. Prakash, *Chromatin Architecture*, Springer Theses,
DOI 10.1007/978-3-319-52183-1_5

5.2 A General Methodology to Study Chromatin Architecture

Further imaging at different scales should clearly identify patterns found to be associated with various nuclear phenotypes. Toward this, it will be more relevant to focus first on the strongest signals (Barr bodies, nucleolus) to generate certain rules and then go for the data of lower signals (autosomal chromosome territories, low-scale chromatin domains). Similarly to what has been used here, combined staining of DNA molecules and functional proteins, such as histone modifications, will help to characterise these structures in more depth. For instance, characterization of transcription during interphase will be essential. How many genes are transcribed during interphase and which structure chromatin is adopting? Model cells such as mesenchymal stem cells, whose chromocenters are associated to significant transcription, will be useful in these cases. For comparison, functional transcription machinery could be described in other interphase cells of lower transcription. Furthermore, information regarding building blocks of chromatin and the interplay between different hierarchical levels should be summarised in models to better understand the system under consideration. Dynamics of patterns should be determined in the light of various cell processes (either interphase steady state, cells in embryonic development, reaction to a stimulus). The SMLM method can be applied to many questions regarding chromatin organisation, for instance, it could investigate the difference of chromatin shape between the micronucleus and the macronucleus of the Tetrahymena.

The different findings are summarised in a model of chromatin architecture (Fig. 5.1). The various cartoons represent different stages of the cell cycle. In each of them, two kinds of chromatin organisation are distinguished, one condensed and particularly folded, usually associated with gene silencing, and the other being loose chromatin, often related to active transcription. Interphase stage shows most of the condensed chromatin at the periphery of the nucleus, while active chromatin is in the centre. Upon stress (the cartoon on the top right), chromatin starts to condense in the shape of elongated patterns at the periphery of the nucleus while progressively, an extreme compact pattern of chromatin appears toward the centre, forming intriguing ring-shaped structures (middle right cartoon). Before beginning any cell division, whether mitosis or meiosis, cells have to double their genetic material. As a result, to maximise transcription, late S phase to G2 phase is associated with a pattern where the nucleus is made of islands of condensed chromatin (the chromocenters) and shows loose active chromatin located at the periphery of the chromocenters, maximising the surface of transcription. Prophase stage of cell division starts by the recruitment of chromocenters to the lamina, in order chromosomes to find more easily each other in the next steps of mitosis or meiosis (central cartoon). The chromocenters drag the active chromatin behind them, displaying a hair like pattern. Mitosis is the product of attachment of chromatin domains with the aid of condensing polymers (bottom left cartoon). Meiosis is both a condensation process of chromatin (with the help of epigenetic regulators) and a polymerization process of synaptonemal complex pro-

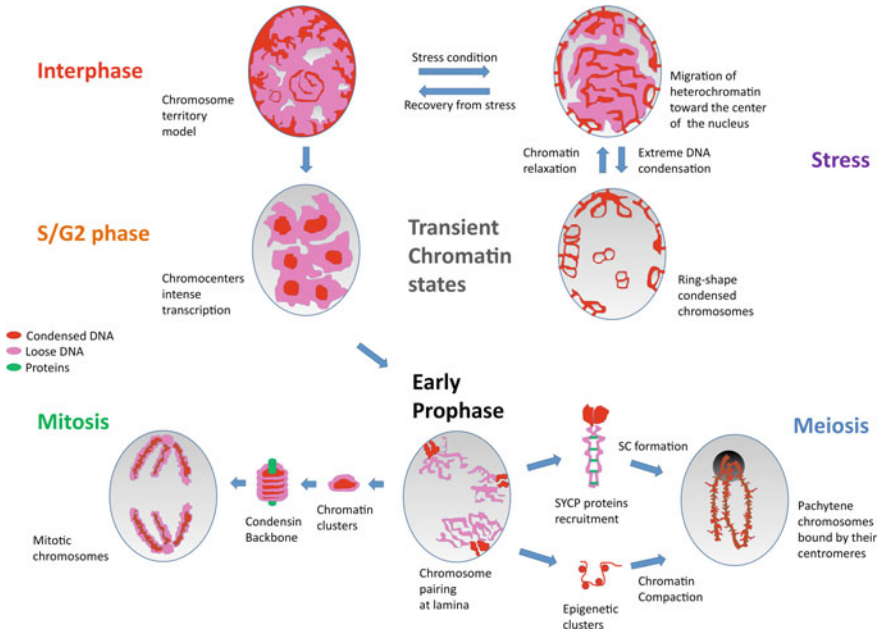

Fig. 5.1 Dynamic architecture of chromatin across the various stages of cell cycle. Image courtesy: David Fournier

teins, which leads to the typical structure necessary for recombination (bottom right cartoon).

5.3 Limitations of the Method and Possible Improvements

Many interrogations are brought by these findings. First of all, the exact physical mechanism for the powerful combination of 405/491 nm laser combination is unknown. The Jablonski diagram of such mechanism should be established based on appropriate physics methods. Improvement of imaging buffer should also follow a more thorough analysis. Usage of different redox agents, susceptible to improve the blinking of the fluorochrome molecules, should also be considered. Proper benchmarks between the DNA dyes and various combinations of fluorophore are still lacking and need to be set up. Most importantly is the comparison between the images generated by the SMLM methodology and other available high-resolution technologies on the same kinds of cells.

The randomness of some patterns at the lower level is still to be investigated (for instance in the case of DNA imaging of interphase nuclei). This can be achieved by combining DNA staining with EdU for the detection of new synthesised DNA in the same cell to see if the worm-like patterns follow the elongated EdU clusters. Finally,

different ways of analysing individual molecules could be done. For instance, what are the signals that blink exactly at the same position several times? How much blinking does one has per molecule for each DNA dye? Finally, a more thorough comparison between the different DNA dyes will be relevant for the community.

5.4 New Avenues for the Study of Chromatin Patterns During Meiosis

Complementary techniques should determine which molecules provoke the epigenetic patterns found in meiotic chromosomes. Inhibition or genetic invalidation should confirm their structural roles. The functionality of the clusters observed during meiosis should be explored by association to functional components. For instance, double strand break positions could be characterised on the meiotic chromosome to see which epigenetic mark co- or anti-localize. Complementary biochemical analyses will strengthen the functionality. Mutation of enzymes depositing the marks will provide more information regarding the assembly of epigenetically regulated clusters. Finally, the different stages of meiosis shall be characterised to have a dynamic picture of the epigenetic regulation and the way different patterns are formed.

5.5 Enlarging the Spectrum of Questions: Chromatin Organisation as a Fundamental Principle of Nucleus Formation

How do chromatin clusters form? Do sequences follow a pre-labelling, for instance via histone modifications, before being put together in a single cluster? Meiotic chromosomes seem to be an example platform to test this structure-to-function relationship. Contrary to interphase chromatin, meiotic chromatin is so well defined that there is potentially little overlap between different epigenetic domains and so a significant potential for isolating domains in further analyses. I also ask the following questions: How does chromatin shape changes during development? Are there defined chromosome territories positions in early phases of embryogenesis? How epigenetics relate to gene expression? All these dynamics are crucial to the understanding of fundamental genomic processes and will benefit from an unbiased, naive and structural analysis such as the ones presented in this work.

Appendices

Appendix A

See Figs. A.1, A.2, A.3, A.4, A.5 and A.6.

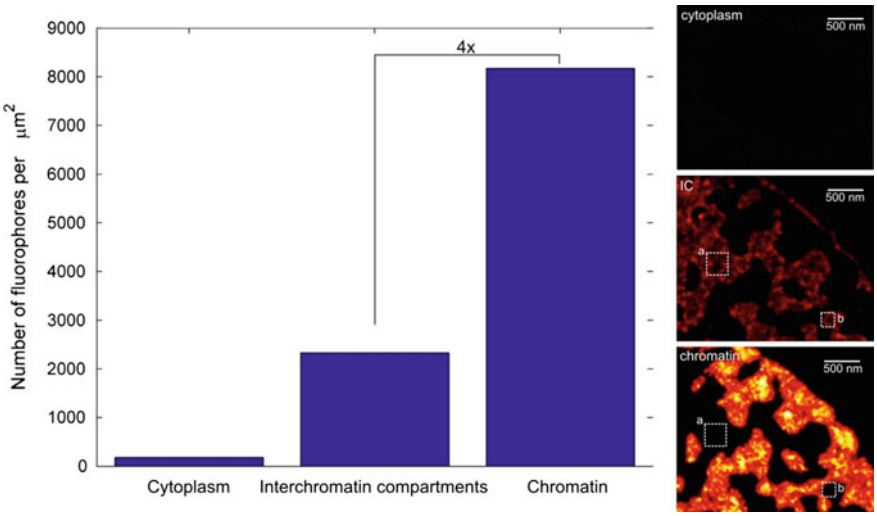

Fig. A.1 Areas and single molecule localisation of inter-chromosomal territories. Chromatin data have been arbitrarily thresholded based on the density of SM localizations and divided into two classes: interchromatin compartments (*IC*) and chromatin occupied regions. Then the areas and single molecule localization density were quantified. On average, IC displayed about 4 times less DNA-associated signals. However, some regions within IC displayed much lower DNA-associated signal (indicated with squared regions) (Żurek-Biesiada et al. 2015)

K. Prakash, *Chromatin Architecture*, Springer Theses,
DOI 10.1007/978-3-319-52183-1

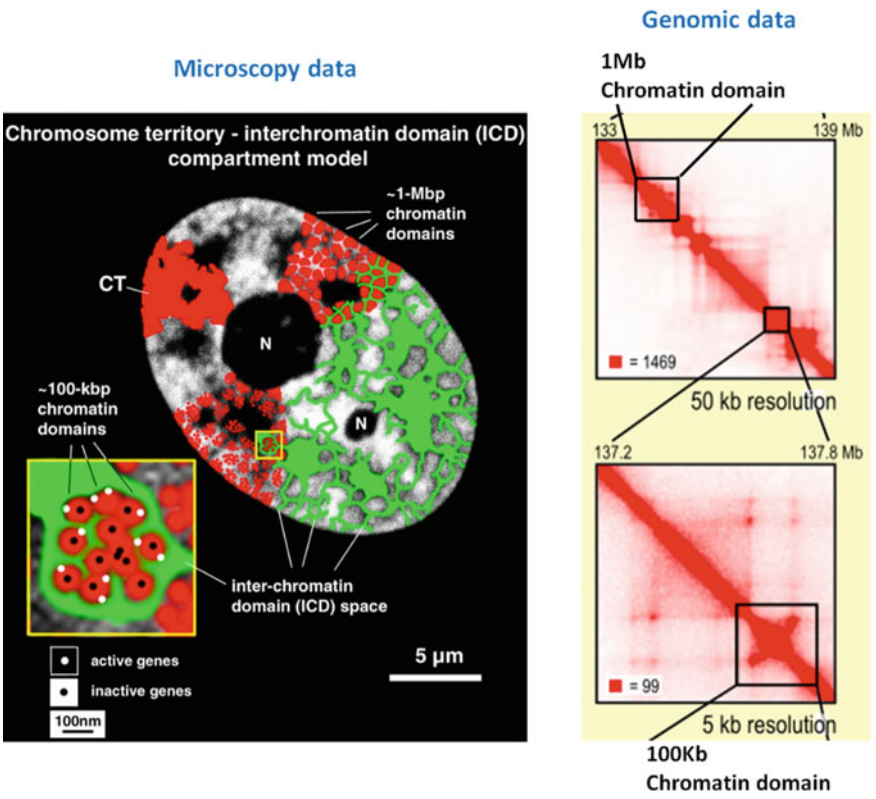

Fig. A.2 Comparison between objects found in microscopy and genomics. *Left panel* model of chromosome territories and their sub-domain, from Cremer and Cremer (2001), using information from a conventional light microscope. *Right panel* size of functional regions of the genome (chromatin domains), modified from Rao et al. (2014), generated after analysis of data from HiC

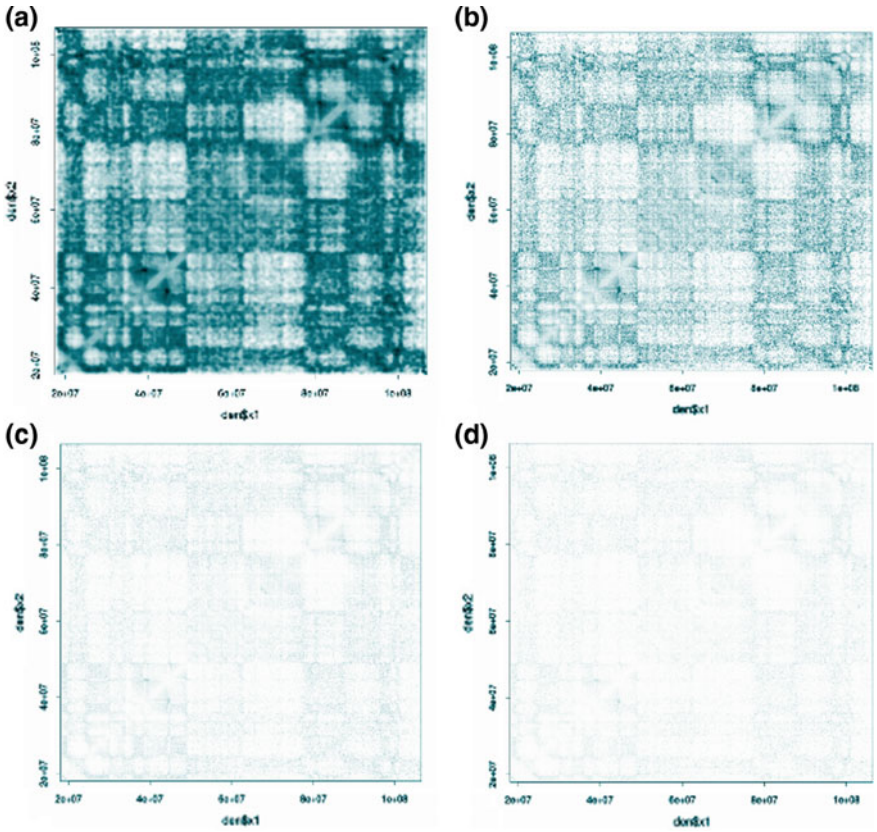

Fig. A.3 HiC data at various levels of resolution. The chromosome 14 (approx 10^8) is partitioned into bins of 10,000 (**a**), 40,000 (**b**), 66,000 (**c**), 100,000 (**d**) pixels. The figure shows that at a higher order or scale there is a large number of intra-chromosomal interactions on the chromosome 14, however when we start to bin the chromosome into pixels of smaller size these interactions start to vanish

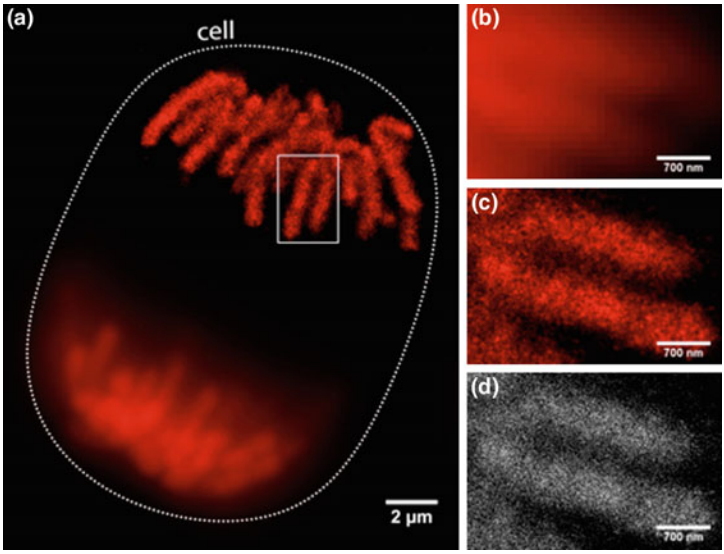

Fig. A.4 A comparison between images of mitotic chromosome DNA recorded using wide field or high-resolution condition. **a** chromosomes in anaphase, imaged by wide-field (*bottom*) and super-resolution localization microscopy (*top*). **b** An *inset* presenting chromosomes visualized with wide-field. **c** chromosomes shown in panel (**b**) imaged by super-resolution localization microscopy. Data points were blurred with using the value of their respective localization precisions (see Chap. 2). **d** Point representation of single molecules blurred in (**c**)

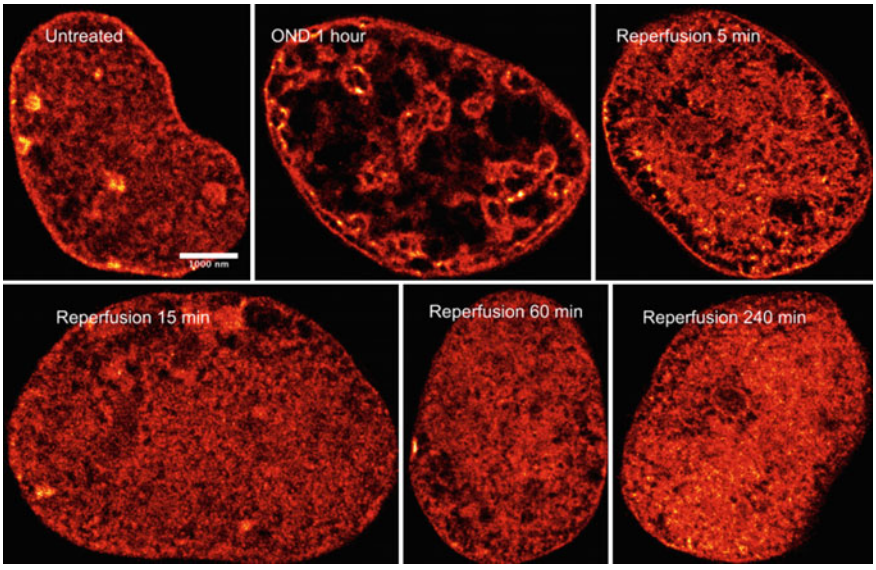

Fig. A.5 Replicates of the results presented in Fig. 1.21

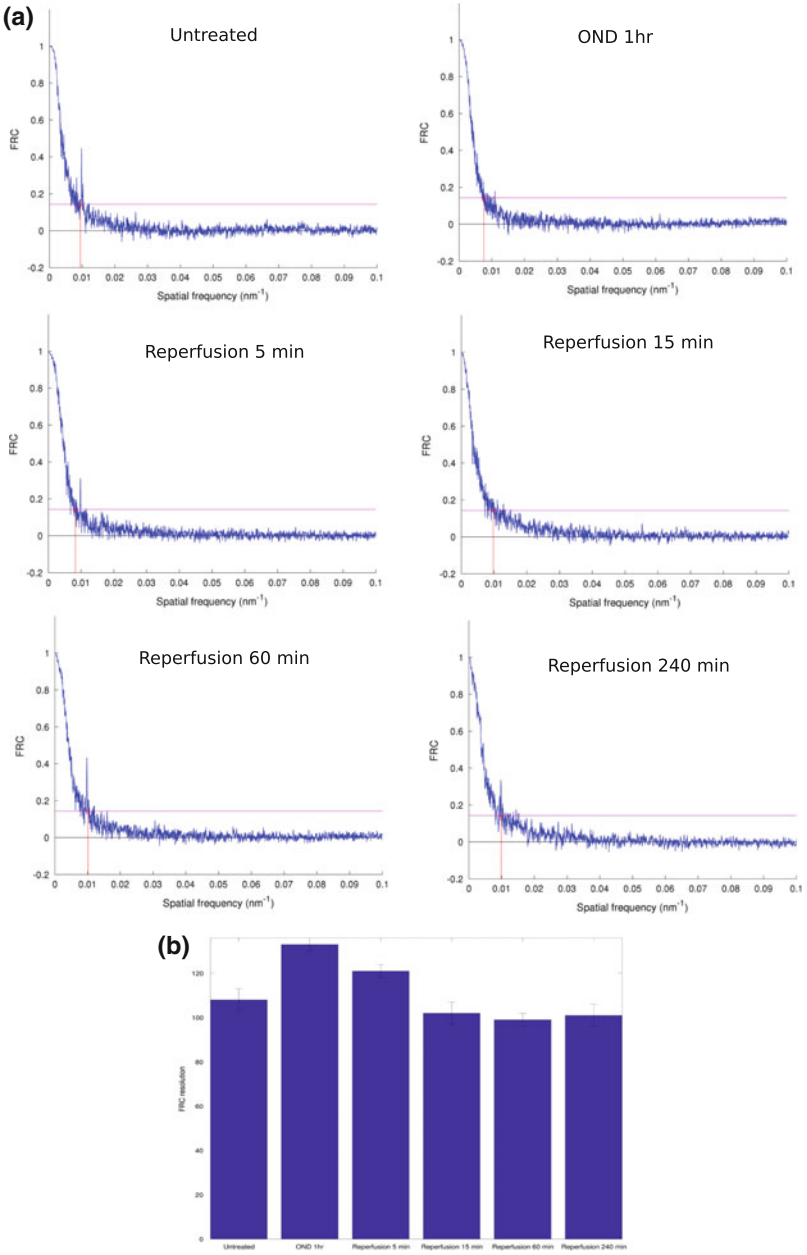

Fig. A.6 Fourier Ring Correlation (FRC) analysis of DNA/SMLM data (figure and caption modified from Kirmes et al. 2015). **a** Representative normalised FRC curves for untreated, OND, and in recovering cells. The *red horizontal line* designates the 1/7 threshold of the radially integrated Fourier frequencies in accordance with (Nieuwenhuizen et al. 2013). **b** Resolution estimates across all experimental conditions based on the threshold determined in (**a**)

References

Cremer T, Cremer C (2001) Chromosome territories, nuclear architecture and gene regulation in mammalian cells. Nat Rev Genet 2(4):292–301

Kirmes I, Szczurek A, Prakash K, Charapitsa I, Heiser C, Musheev M, Schock F, Fornalczyk K, Ma D, Birk U et al (2015) A transient ischemic environment induces reversible compaction of chromatin. Gen Biol 16(1):1–19

Nieuwenhuizen RPJ, Lidke KA, Bates M, Puig DL, Grünwald D, Stallinga S, Rieger B (2013) Measuring image resolution in optical nanoscopy. Nat Methods 10(6): 557–562

Rao SSP, Huntley MH, Durand NC, Stamenova EK, Bochkov ID, Robinson JT, Sanborn AL, Machol I, Omer AD, Lander ES et al (2014) A 3D map of the human genome at kilobase resolution reveals principles of chromatin looping. Cell 159(7):1665–1680

Żurek-Biesiada D, Szczurek AT, Prakash K, Mohana GK, Lee H-K, Roignant J-Y, Birk U, Dobrucki JW, Cremer C (2015) Localization microscopy of DNA in situ using vybrant dyecycle violet fluorescent probe: a new approach to study nuclear nanostructure at single molecule resolution. Exp Cell Res 343(2):97–106

Appendix B

See Figs. B.1, B.2, B.3, B.4, B.5, B.6, B.7, B.8 and B.9.

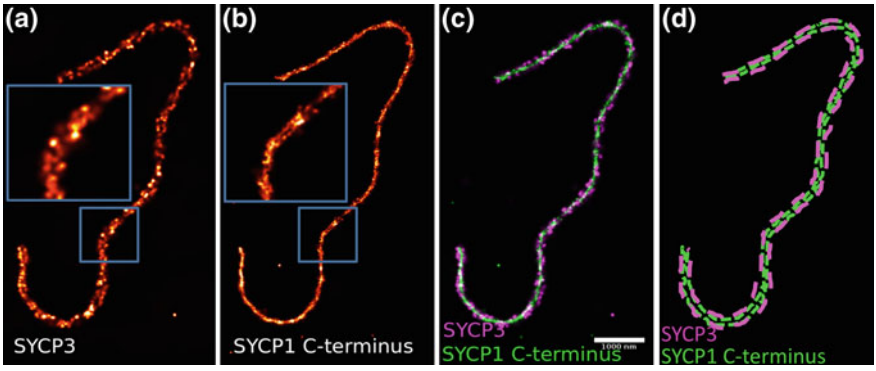

Fig. B.1 Relative localization of SYCP1 and SYCP3 within the synaptonemal complex. Single molecule localization images of SYCP3 labelled with Alexa 488 (**a**) and SYCP1 C-terminus labelled with Alexa 555 (**b**). **c** Dual color image of SYCP3 and SYCP1. Insets in **a** and **b** highlight the double strand nature of SYCP3 and SYCP1, respectively. **d** Shows an relative outline structure of SYCP3 and SYCP1

K. Prakash, *Chromatin Architecture*, Springer Theses,
DOI 10.1007/978-3-319-52183-1

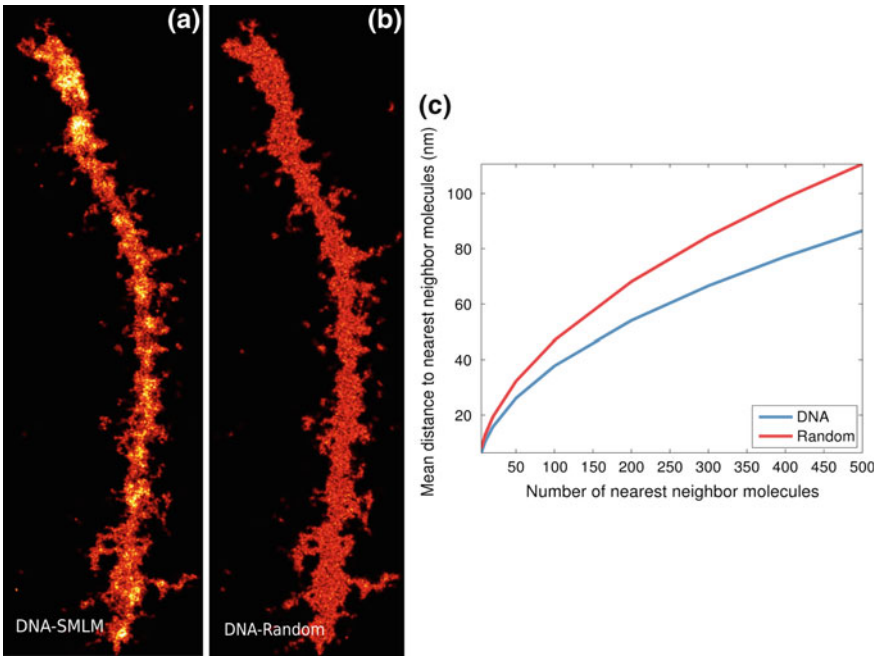

Fig. B.2 Validation of the chromatin clusters (figure and caption modified from Prakash et al. 2015). In order to validate the clusters found in the SMLM image of DNA (**a**), I compared it to a randomly simulated dataset (**b**). I generated a binary mask of the nearest neighbour blurred image and then randomly generated a number of points identical to the SMLM image. **c** The local condensation in SMLM and random images was characterised by detecting the 20–500 nearest neighbours. In each case the mean nearest neighbour distance was found to be significantly shorter than in the random simulated data-set. The mean distance to the 500 nearest neighbour was 86 nm for chromatin and 110 nm for the random data

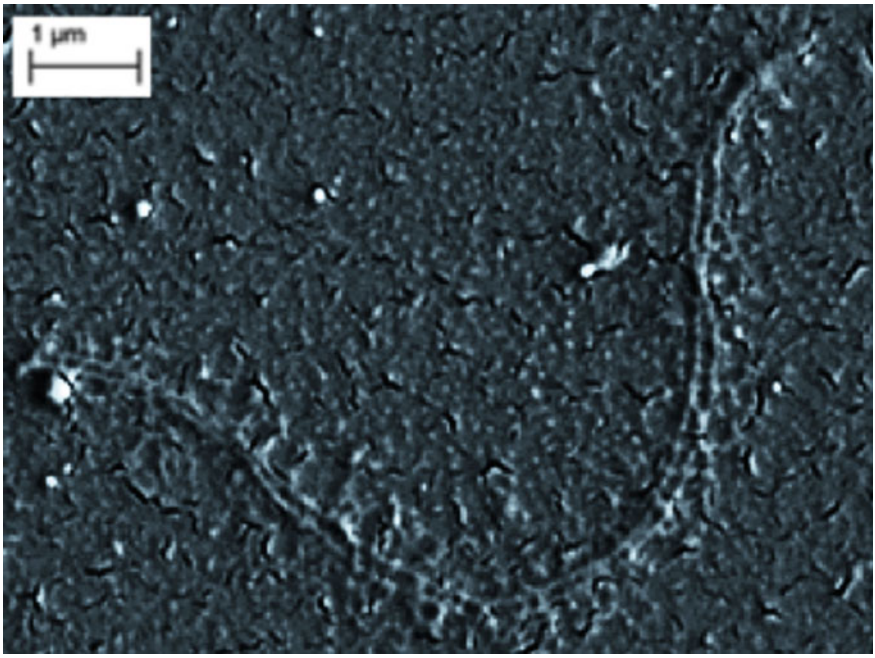

Fig. B.3 SEM data validate the pattern of chromatin found with SMLM. Chromatin shows a caterpillar-shape, with several ring-shape clusters found successively along the SC, similar to Fig. 4.6b. Courtesy Wioleta Dudka

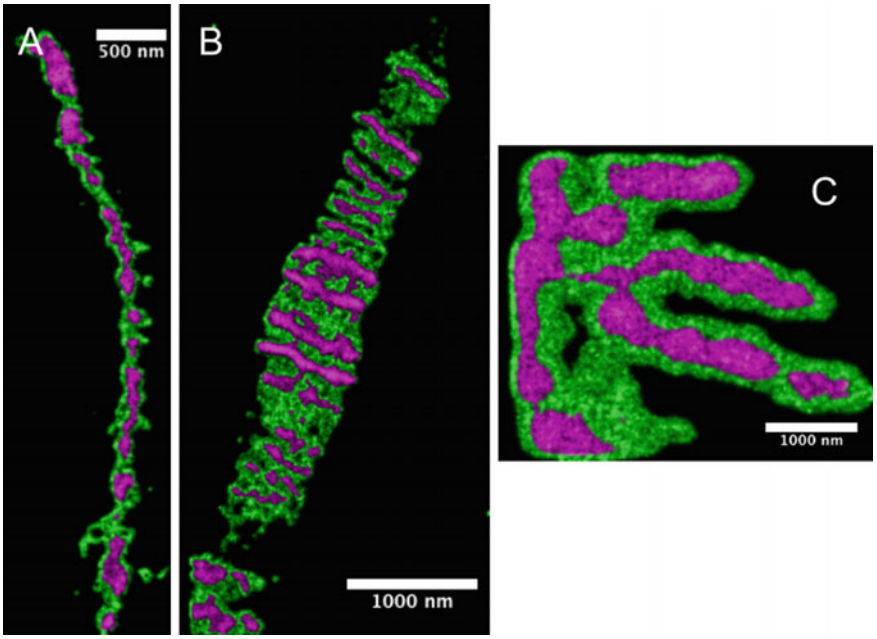

Fig. B.4 Chromatin rearrangement upon condensation. After G2 phase chromatin starts to condense around a scaffold of proteins and to achieve a maximal compaction. This moves the silent and inaccessible regions toward the interior while the loose and active chromatin goes toward the exterior, making chromatin accessible for transcription. Three different scenarios exemplifying this transition is shown in (**a**) meiotic chromatin at the pachytene stage in mouse, **b** organisation of polytene chromosomes in Drosophila and **c** organisation of mitotic chromosomes in anaphase

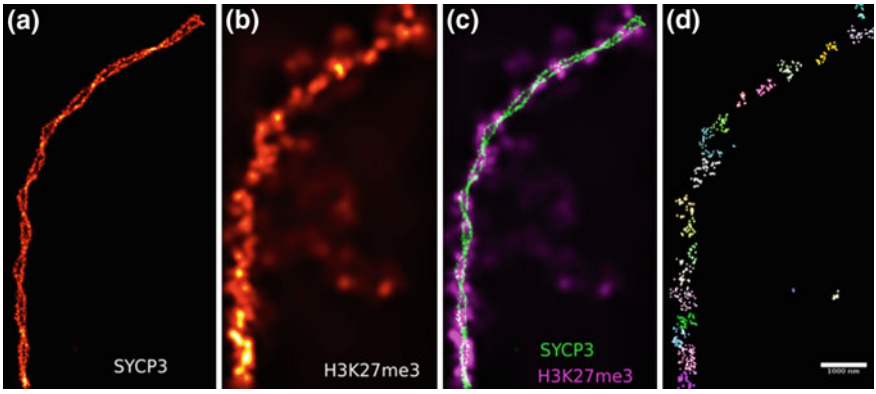

Fig. B.5 Helical structure of the pachytene chromosomes using information from H3K27me3 clusters. **a** SMLM image of H3K27me3 labelled with Alexa 488. **b** SMLM image of SYCP3 labelled with Alexa 555. **c** Two color SMLM image of H3K27me3 and SYCP3. **d** Clusters of H3K27me3 are highlighted in different colours to reveal an helicoidal structure. Twists of SYCP3 of same order as the H3K27me3 clusters are also observed (**c**). The size of clusters follows the trend found computationally. Periodicity of twists is close to 500 nm. Scale bar: 1000 nm

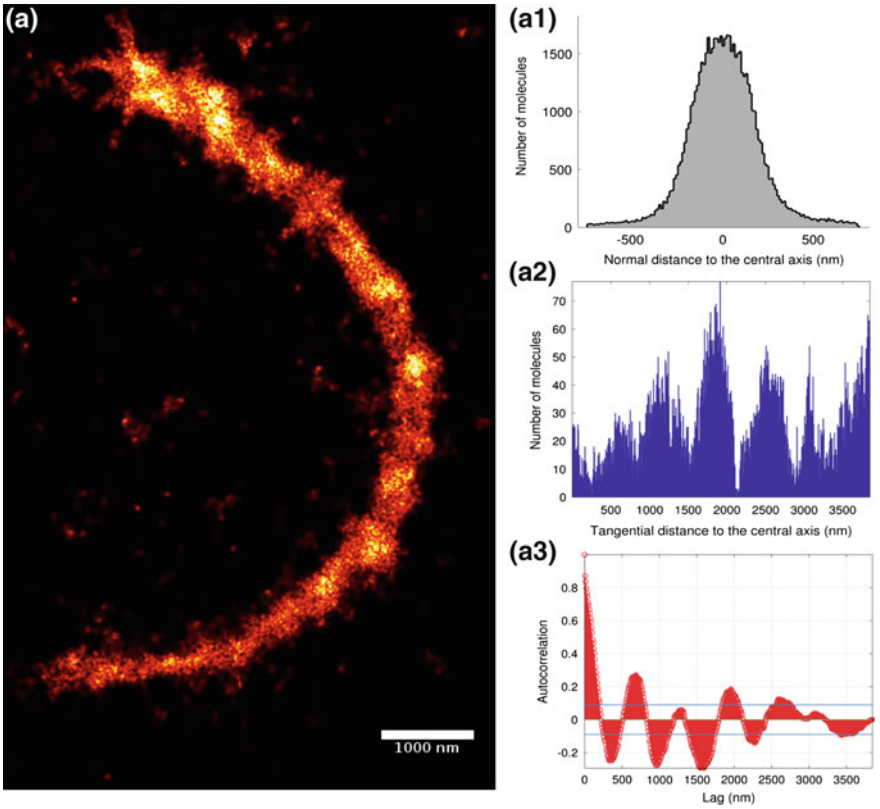

Fig. B.6 Spiralization of H3K9me3 confirmed by patterns of DNA (figure and caption modified from Prakash et al. 2015). Dense DNA clusters seem to spiral at one of the ends of the SC, confirming the specialization patterns of H3K9me3 found in Fig. 4.11. The average spread of DNA (**a1**) is around 500 nm. The cluster diameter in (**a**) was found to be 223 nm. **a2** Shows the histogram of the tangential distances taken along the central axis of SYCP3. Chromatin clusters were found to occur with a periodicity of 685 nm (**a3**). The *blue lines* in the plot correspond to the 95% confidence bounds (+/− 0.08) of the autocorrelation function

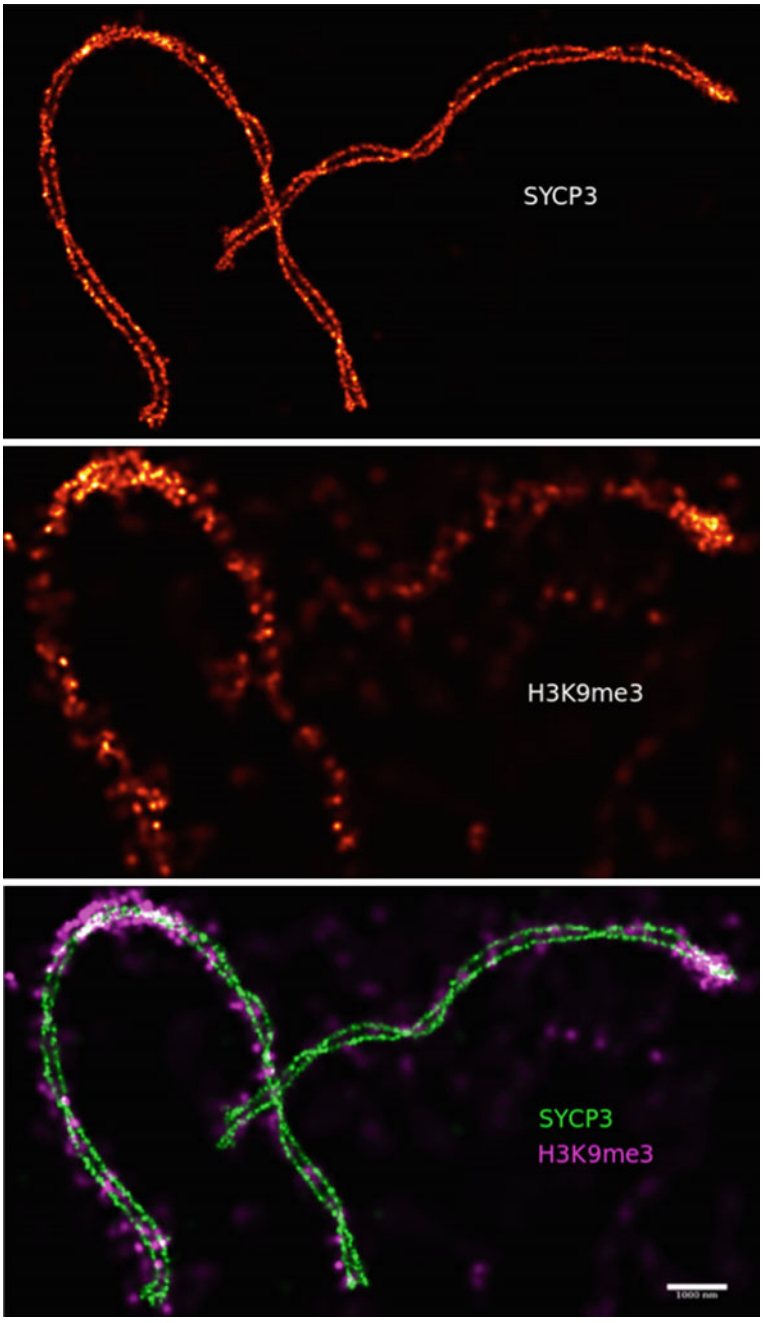

Fig. B.7 Helicoidal nature of the pachytene chromosomes. Pairs of pachytene chromosomes reminiscent from the in situ state of chromatin are displayed. Note that the helicoidal aspect of the paired chromosomes (*left*) are similar to the one of the solitary chromosome (*right*)

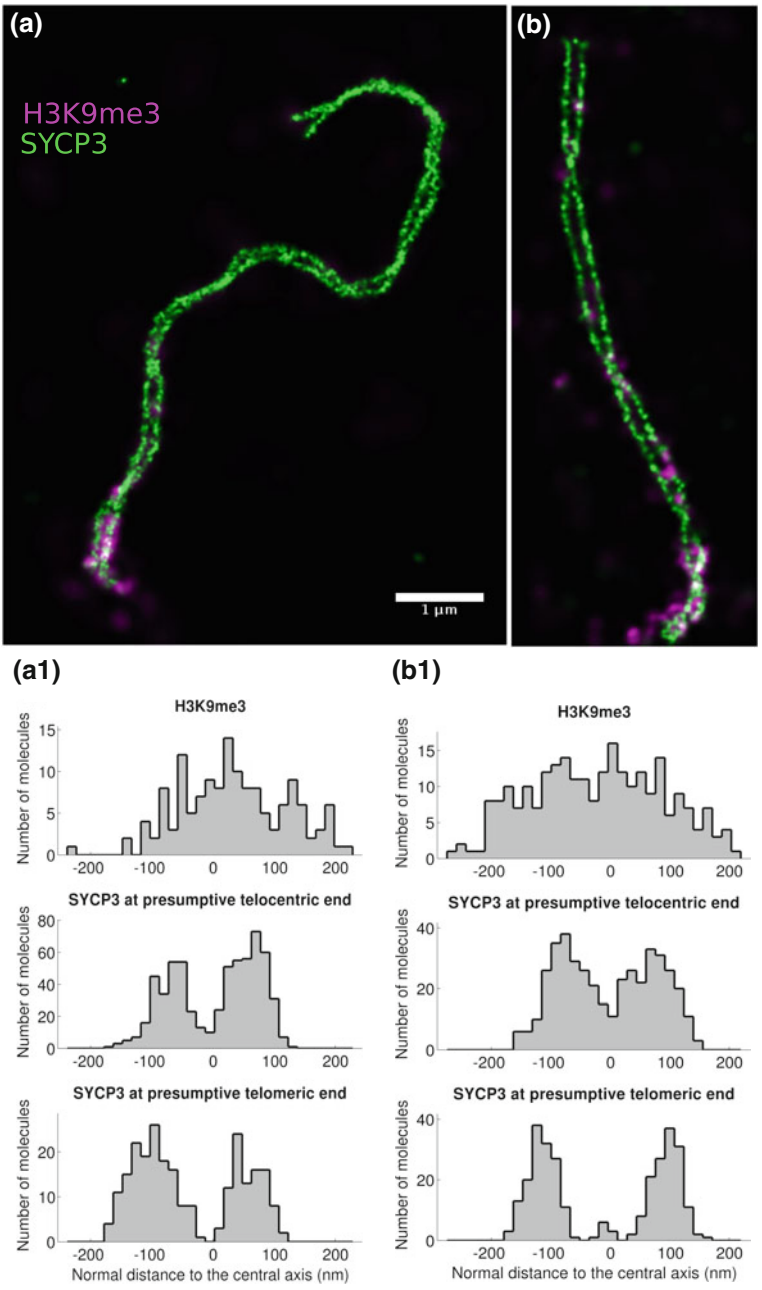

Fig. B.8 SYCP3 strands move apart at non-centromeric end of the SC. The centromeric ends of SYCP3 seem to be closer to each other than the non-centromeric end of SYCP3 (**a** and **b**). The average distance at the centromeric end in **a** and **b** is found to be 142 and 130 nm respectively, while the average distance at the non-centromeric end is 171 and 190 nm respectively (**a1** and **b1**). H3K9me3 is normally distributed at the centromeric end (figure and caption modified from Prakash et al. 2015)

DNA	cluster diameter	inter-cluster distance
Replicate 1	170	605
Replicate 2	223	685
Replicate 3	184	558

H3K27me3	cluster diameter	inter-cluster distance
Replicate 1	88	466
Replicate 2	128	480
Replicate 3	111	640

H3K4me3	cluster diameter	inter-cluster distance
Replicate 1	45	209
Replicate 2	47	216
Replicate 3	52	213

H3K9me3	Telocentric end	Telomeric end
Replicate 1	142	171
Replicate 2	130	190
Replicate 3	128	176

Fig. B.9 Characteristics of the epigenetic clusters identified to regulate pachytene chromosomes

Reference

Prakash K, Fournier D, Redl S, Best G, Borsos M, Tiwari VK, Tachibana-Konwalski K, Ketting RF, Parekh SH, Cremer C et al (2015) Superresolution imaging reveals structurally distinct periodic patterns of chromatin along pachytene chromosomes. Proc Natl Acad Sci 112(47):14635–14640